2017

Beach morphodynamics in the lee of a wave farm: synergies with coastal defence

Abanades Tercero, Javier

Beach morphodynamics in the lee of a wave farm: synergies with coastal defence

by

Javier Abanades Tercero

A thesis submitted to Plymouth University

in partial fulfilment for the degree of

Doctor of Philosophy

School of Marine Science and Engineering

Faculty of Science and Technology

Plymouth University

March 2016

Para Marcelina y María,
como pequeño homenaje
a todo lo que me
enseñasteis.

ACKNOWLEDGMENT

First and foremost, to Natalia, for proving your unconditionally love, support and encouragement. I could not have done this without you supporting me every single day during the last three years.

I would also like to thank my family for their support, and particularly, to my parents who taught me to fight for my dreams and never give up.

I am indebted to Prof. Gregorio Iglesias, who gave me the opportunity to come to Plymouth and make possible this thesis. Thank you for the confidence place in me, but also for infusing me with your passion for coastal engineering.

Thank you as well to Prof Deborah Greaves for giving me this opportunity at Plymouth University and providing her feedback that considerably improved the quality of the thesis.

I thank to all my colleagues of the COAST and CPRG research group, with whom I shared not only the day-to-day work, but also the ups and downs during all this time. Particular mention to Davide and Rob for all the great moments we had during lunch times, and to Carlos, with whom we shared a small family at Plymouth.

Last but not least, I would like to express my gratitude to all the anonymous reviewers of Coastal Engineering, Marine Geology and Renewable Energy, whose valuable comments have helped to improve this work.

En primer lugar, gracias a Natalia por proporcionarme su incondicional amor, apoyo y aliento. No podría haberlo hecho sin tu apoyo durante cada uno de los días de los últimos tres años.

Me gustaría también agradecer a mi familia su apoyo, y en particular a mis padres por haberme enseñado a pelear por mis sueños y nunca abandonar.

Estoy en deuda con el Profesor Gregorio Iglesias, quien me dio la oportunidad de venir a Plymouth y hacer esta tesis posible. Gracias por la confianza que me has dado, pero sobre todo por transmitirme tu pasión por la ingeniería de costas.

Gracias también a la Profesora Deborah Greaves por darme esta oportunidad en la Universidad de Plymouth y proporcionarme consejo que ayudó a mejorar la calidad de la tesis.

Quiero agradecer a todos mis compañeros de los grupos de investigación COAST y CPRG, con los cuales no sólo trabajé día a día, sino también compartí la montaña rusa de emociones que es el doctorado. Mención especial para Davide y Rob, por esos grandes momentos que pasamos durante la hora de la comida, y para Carlos, con el cual "creamos" nuestra pequeña familia en Plymouth.

Finalmente, mencionar mi gratitud a todos los revisores anónimos de las revistas Coastal Engineering, Marine Geology y Renewable Energy, cuyos comentarios me ayudaron a mejorar la calidad de mi tesis.

AUTHOR'S DECLARATION

At no time during the registration for the degree of Doctor of Philosophy has the author been registered for any other University award without prior agreement of the Graduate Sub-Committee.

Work submitted for this research degree at the Plymouth University has not formed part of any other degree either at Plymouth University or at another establishment.

This study was financed with the aid of a studentship form the School of Marine Science and Technology of Plymouth University.

The material presented in this thesis has been published in five journal papers, one of them under review, a book chapter and two conference proceedings. Relevant scientific conferences were attended at which work was often presented.

Journal Papers:

- Abanades, J., Greaves, D. & Iglesias, G. (2014a) 'Wave farm impact on the beach profile: A case study'. *Coastal Engineering*, 86 (0). pp 36-44.
- Abanades, J., Greaves, D. & Iglesias, G. (2014b) 'Coastal defence through wave farms'. *Coastal Engineering*, 91 (0). pp 299-307.
- Abanades, J., Greaves, D. & Iglesias, G. (2015a) 'Coastal defence using wave farms: The role of farm-to-coast distance'. *Renewable Energy*, 75 (0). pp 572-582.
- Abanades, J., Greaves, D. & Iglesias, G. (2015b) 'Wave farm impact on beach modal state'. *Marine Geology*, 361 pp 126-135.
- Abanades, J., Flor-Blanco, G; Greaves, D, Flor, G. & Iglesias, G. ' Mitigating dune erosion through wave farms'. *Coastal Engineering Journal* (under revision).

Book chapter:

- Abanades, J., and Iglesias, I., (2016) 'Chapter 9: Environmental Impacts'. Wave and Tidal Energy. Publisher: Wiley (under revision).

Conference Papers:

- Abanades, J., Greaves, D. and Iglesias, I., (2015) 'Synergies between wave energy and coastal protection'. EWTEC 15 Nantes
- Abanades, J., Greaves, D. and Iglesias, I., (2014) 'Using wave farms for coastal protection'. COASTLAB 14 Varna.

Word count of main body of thesis: 51.157

Signed……

Date……...29 of March 2016

ABSTRACT

Name: Javier Abanades Tercero

Title: Impacts of wave energy exploitation

Wave energy has a great potential in many coastal areas thanks to a number of advantages: the abundant resource, the highest energy density of all renewables, the greater availability factors than e.g. wind or solar energy; and the low environmental and particularly visual impact. In addition, a novel advantage will be investigated in this work: the possibility of a synergetic use for carbon-free energy production and coastal protection.

In this context, wave energy can contribute not only to decarbonising the energy supply and reducing greenhouse emissions, but also to mitigating coastal erosion. In effect, wave farms will be deployed nearshore to generate electricity from wave energy, and therefore the leeward coast will be exposed to a milder wave climate, which can potentially mitigate coastal erosion.

This thesis aims to determine the effectiveness of wave farms for combating coastal erosion by means of a suite of state-of-the-art process-based numerical models that are applied in several case studies (Perranporth Beach,UK; and Xago Beach, Spain) and at different time scales (from the short-term to the long-term). A wave propagation model, SWAN, is used to establish the effects of the wave farm on the wave conditions. The outcomes of SWAN will be coupled to XBeach, a costal processes model that is applied to analyse the effects of the milder wave conditions on the coast. In addition to these models, empirical classifications and analytical solutions are used as well to characterise the alteration of the beach morphology due to the presence of a wave farm.

The analysis of the wave farm impacts on the wave conditions and the beach morphology will be carried out through a set of *ad hoc* impact indicators. Parameters such as the reduction in the significant wave height, the performance of the wave farm, the effects on the seabed level and the erosion in the beach face area are defined to characterise these impacts. Moreover, the role played by the key design parameters of wave farms, e.g. farm-to-coast distance or layout, is also examined.

The results from this analysis demonstrate that wave farms, in addition to their main purpose of generating carbon-free energy, are capable of reducing erosion at the coast. Storm-induced erosion is significantly reduced due to the presence of wave farms in the areas most at risk from this phenomenon. However, the effects of wave farms on the coast do not lend themselves to general statements, for they will depend on the wave farm design (WEC type, layout and farm-to-coast distance) and the characteristics of the area in question, as shown in this document for Perranporth and Xago.

In summary, this synergy will improve the economic viability of wave farm projects through savings in conventional coastal defence measures, thereby fostering the development of this nascent renewable, reducing greenhouse gas emission and converging towards a more sustainable energy model. Thus, wave energy contributes to mitigating climate change by two means, one acting on the cause, the other on the effect: (i) by bringing down carbon emissions (cause) through its production of renewable energy, and (ii) by reducing coastal erosion (effect).

LIST OF CONTENTS

LIST OF ABBREVIATIONS

1DH – One dimensional horizontal

2D – Two-dimensional

2DH – Two dimensional horizontal

3D – Two-dimensional

BEM – Boundary Element Method

BLI – Bed Level Impact

CEA_b – mean Cumulative Eroded Area in the baseline scenario

CEA_f – mean Cumulative Eroded Area in the wave farm scenario

CFD – Computational Fluid Dynamics

CS – Case Study

EU – European Union

FEA_b – beach Face Eroded Area in the baseline scenario

FEA_f – beach Face Eroded Area in the wave farm scenario

LCD – Local Chart Datum

LCoE – Levelised Cost of Energy

MRE – Marine Renewable Energy

MSR – Mean Spring tide Range

NER – Non-dimensional Erosion Reduction in the wave farm scenario

OWC – Oscillating Water Column

PTO – Power Take Off

RMSE – Root Mean Square Error,

RSH – Reduction of the significant wave height

RTR – Relative Tide Range

WEC – Wave Energy Converter

LIST OF SYMBOLS

m_n – spectral moment of order n

f – frequency

f_p – peak frequency

$S\ (f, \theta)$ – wave energy density

H_s – significant wave height

T_p – wave peak period

c_g – group celerity

b – width of a wave energy converter

T_{m01} – wave energy period

ρ – water density

g – gravity acceleration

h – water depth

θ – wave direction

K_t – wave transmission coefficient

K_D – wave absorption coefficient

t – time

ϕ – velocity potential function

D – distance between the twin bows of a WEC

J – wave power

$N(\omega,\theta)$ – directional spectral density

ω – angular wave frequency

c_x and c_y – velocity propagation in the x- and y-space, respectively

c_θ and c_σ – velocity propagation in the direction and σ the relative frequency space, respectively

S – source term

H_{rms} – root mean square wave height

T_{m01} – mean absolute wave period

θ_m – mean wave direction

s – directional spreading coefficient

C – wave group varying depth averaged

D_s – sediment diffusion coefficient

u^E and v^E – depth-averaged velocities

C_{eq} – equilibrium concentration

ζ – seabed level

D_{50} – mean diameter of grain

$tan\ \beta$ – beach gradient

$u_{10,}$ – mean wind speed at a height of 10 m above the sea surface,

R^2 – coefficient of determination

$\bar{J}_{WEC}$ – average wave power in front of a generic WEC of the wave farm

H_b – breaking wave height

w_s – sediment fall velocity

v – fluid kinematic viscosity

γ_s – density of the sediment

m – beach slope

L_{bp} – breaking wave length

d_b – breaking water depth

LIST OF FIGURES

LIST OF TABLES

Chapter 1

Introduction

1. INTRODUCTION

This chapter deals with the foundation for the thesis and the work that is presented in the following sections. The framework of the thesis is introduced starting with the motivation; following this, the overarching aims and objectives are presented defining the main lines of the research; and finally, a summary of key research and relevant literature is provided, highlighting the principal areas relevant to the present study.

1.1 MOTIVATION

The adverse effects brought about by the world's reliance on fossil fuels are well known: (i) greenhouse gas emissions that exacerbate climate change, (ii) diminished reserves of carbon fuels, and (iii) geopolitical wrangling over the control of the oil and gas reserves, which has led to many conflicts and all-out wars in the last decades. In addition, the variability in oil and gas prices has a deleterious effect on the global economy. These arguments, and the international treaties and protocols signed to foster the efforts against climate change, call for the development of renewable energy sources.

Among renewable energies, the potential for development of Marine Renewable Energy[1] (MRE) is widely recognised (Bahaj, 2011; Iglesias & Carballo, 2009), so much so that it is poised to become a fundamental pillar in the EU energy policy, cf. the European Strategic Energy Technology Plan (SET-Plan) described in European Commission (2007). In fact, the MRE industry has established for ocean energy (wave and tidal) and offshore wind a target of installed capacity for 2050 of 188 GW and 460 GW respectively (EU-OEA, 2010; Jeffrey & Sedgwick, 2011; Moccia et al., 2011), which are ambitious goals given that the figures for 2020 are 3.6 GW and 40 GW

[1] Marine renewable energies include both ocean energy and offshore wind energy. Ocean energy comprises essentially wave and tidal energy, but also Ocean Thermal Energy Conversion (OTEC) and salinity gradient energy.

(EWEA et al., 2012). In the UK's perspective, the Low Carbon Innovation Co-Ordination Group (LCICG) signalled that wave energy could make a meaningful contribution to the energy mix from around 2025, with the potential to deliver over 50 TWh per year, i.e. around 10% of the UKs forecast electricity needs in 2050 (LCICG, 2012).

Furthermore, wave energy exploitation presents a number of advantages in relation to other renewable energies (Drew, Plummer & Sahinkaya, 2009a):

1. The resource: Sea waves offer the highest average energy density among renewable energy sources (Clément et al., 2002a) and the resource is very abundant in many coastal areas.
2. Availability: Wave can generate power up to 90 % of the time, compared to ∼20–30 % for wind and solar devices (Pelc & Fujita, 2002).
3. No losses in depth water: Waves are propagated from large distance without any losses in depth water.
4. The environmental impact: A wave farm operating nearshore causes a limited negative environmental impact (Halcrow, 2006). In general, offshore devices have the lowest environmental impact. The impact on the biodiversity is quite low, and just the species that reside near the surface could be slightly affected by the deployment of wave farms. Although the main advantage in this aspect is the negligible visual impact as wave farms are deployed far away from the coastline (generally between 5 and 10 km), especially in comparison with offshore wind parks.
5. Seasonality: Wave energy resource varies according to the electricity demand in temperate climates.

However, and despite of all the advantages of wave energy, the viability of wave energy projects needs to be enhanced in order to achieve the aforementioned goals. For this purpose, it is necessary to reduce the Levelised Cost of Energy (LCoE), which defines a unit cost for electricity by dividing the total energy production by the costs involved in developing projects. Wave energy's LCoE may be expected to fall in the years to come given the relatively immature stage of the technology. The process whereby the development of an incipient technology, improvements by practice and economies of scale lead to savings is exemplified by the so-called *learning curve.* The greatest opportunities for cost reduction in wave energy as a stand-alone energy source at present are related to the installation and construction processes (Astariz & Iglesias, 2015a) and the optimisation of the design.

In addition to the previous options, two "strategic" approaches for reducing the cost are: (i) combining wave energy with other forms of marine renewable – notably, offshore wind (Astariz et al., 2015a; Astariz et al., 2015b; Astariz et al., 2015c; Perez Collazo et al., 2014; Stoutenburg, Jenkins & Jacobson, 2010), and (ii) using wave farms for coastal defence in synergy with their main function of generating carbon-free energy (Abanades, Greaves & Iglesias, 2014a; 2014b; 2015b; 2015a).

Regarding the former, the author of this thesis has collaborated in the investigation of the advantages that combining wave and offshore wind energy present, which are detailed in Astariz *et al.* (2015a); (2015b; 2015c). In sum, combined wave-offshore wind energy brings down costs through shared electrical infrastructure (cables, substation, grid connection), foundations and substructures (hybrid systems) or moorings, and maintenance (crews, boats and other equipment). These items represent a substantial portion of the total cost, and therefore sharing them with an offshore wind farm would be effective in improving the economic viability of wave energy. Additional

advantages of combined offshore wind and wave energy are: (i) optimised use of the scarce marine space, with an enhanced energy yield per unit area; (ii) smoother power output; and (iii) a less energetic wave climate within the offshore wind farm, which will reduce the loads on foundations and, importantly, increase the weather windows for maintenance, which will in turn reduce downtime (Astariz *et al.*, 2015b; Pérez-Collazo, Greaves & Iglesias, 2015).

Regarding the latter, determining the effectiveness of wave farms to protect the coast is the main objective of this document. As waves propagate through the Wave Energy Converters (WECs) that form a wave farm, the wave height is reduced. Then, the coast in the lee of the farm is exposed to a milder wave climate, which in turn may result in a modification of the coastal processes that occur nearshore. Whether this modification can lead to a reduction of the erosion needs to be investigated given that the potential application of wave farms as a complement, or in certain locations as an alternative, to coastal defence presents numerous advantages, not least in the current transition environment.

The conventional approach to defending the coast against flooding and erosion involves coastal structures – this is the so-called "hard engineering" approach. The downsides of this approach are well known, particularly in the context of transition coasts, owing to the inability of structures to adapt to sea-level rise. Indeed, there have been recently many cases of coastal structures failing to cope with the increased pressures of climate change (Castelle et al., 2015; Kendon & McCarthy, 2015; Senechal et al., 2015; Sibley, Cox & Titley, 2015; Slingo et al., 2014; Spencer et al., 2015). These examples of failures of coastal structures – due to either structural collapse or excessive overtopping – expose the dramatic consequences of the inadequacy of many of the existing structures in the current transition scenario. The conventional approach to

solving this problem entails upgrading the existing structures or building new ones, in both cases at a large cost.

On these grounds, nearshore wave farms present three main advantages relative to conventional coastal structures. First, by providing renewable, carbon-free energy, wave farms contribute to decarbonising the energy supply and thereby combatting the man-made causes of climate change. Second, the environmental impact of wave farms on the littoral – the single most sensitive environment in the planet – is considerably lower than that of coastal structures. Last, but not least, wave farms consisting of floating WECs (e.g. WaveCat, WaveDragon, DEXA – see Section 2.3.2 WEC technologies) adapt naturally to sea level rise, and therefore can cope well with the main impact on the littoral of climate change.

Thus, rather than resorting to the conventional approach (more structures) to fix obsolete, underperforming structures, deploying wave farms to generate carbon-free energy as their main purpose and, in synergy with it, defending the coastline against erosion and flooding is a new alternative that warrants consideration. Incidentally, their application to coastal defence would enhance their economic viability through the savings achieved in conventional defence schemes.

This alternative to conventional coastal defence schemes (based on structures such as groynes, detached breakwaters, etc.) is in fact a new paradigm to mitigating climate change and confronting two global challenges: the environmental repercussions of the current energy model and the risks to properties and infrastructure posed by coastal erosion. As explained, these two challenges are connected, for climate change is set to exacerbate coastal erosion through its effects of sea level rise and increased storminess.

1.2 AIMS AND OBJECTIVES

The advent of wave energy warrants the investigation of using wave farms as an alternative to coastal defence, not least in this climate change scenario. In this sense, the overarching objective of this document is to analyse the effects of wave farms on the coast, and subsequently, to determine their effectiveness as part of a coastal protection scheme.

The fundamental objectives of this thesis are:

- Determination of the impacts of wave farms on the nearshore wave conditions. The manner in which the extraction of wave energy by the WECs that form the wave farm affects the wave patterns in the lee of the farm will be investigated.
- Quantification of the wave farm impacts on the beach profile (1DH or 2D) and on the beach morphology (2DH or 3D) based on the modified wave conditions in the lee of the farm.
- Evaluation of the modal state of the beach (e.g. dissipative, reflective and intermediate beach) in the presence and in the absence of a wave farm operating nearshore.
- Establishment of the effectiveness of wave farms to protect the coast. In view of the results from the points above, the degree of coastal protection offered by nearshore wave farms will be determined.
- Assessment of the effects at different time scales from the short (days) to the medium (months). The former allows primary the assessment of storm-induced erosion, while with the latter the morphological changes in beaches, such as profile erosion and accretion; and the modal state of the beach can be examined (Cowell & Thom, 1994).

- Identification of the role played by the key parameters of the design of wave farms, e.g. farm-to-coast distance and layout, in the synergetic application of wave farms.

The novelty of this thesis lies in the quantification of the wave farm effects on the beach. For the first time, the response of the beach with a wave farm operating nearshore will be analysed through the application of state-of-the-art process-based numerical models: a third-generation spectral wave model (SWAN) and a coastal process model (XBeach). Thus, this study will answer a fundamental scientific question: the response of the coastal environment under different wave conditions, in this case associated with the wave energy extraction by wave farms; bearing in mind that coastal environments are the most rapidly changing environments in the planet and wave energy is their main driving agent.

For this purpose, two case studies representative of the effects of climate change on the coast are considered: Perranporth Beach (UK) and Xago Beach (Spain). Perranporth Beach has experienced significant erosion over the last years, not least during the harsh winter 2013/14. Indeed, the Shoreline Management Plan has identified the area as subject to significant erosion risk, and a number of options are being assessed to confront this challenge (CISCAG, 2011). For its part, Xago has also experienced increased erosion on its dune system – evidenced by the recession of the dune toe, between 3.1 m and 11.5 m – under the heightened storminess of recent years (Flor-Blanco, Flor & Pando, 2013; Flor, Flor-Blanco & Flores-Soriano, 2015). In view of these risks, these areas constitute a prime location for using such wave farms for coastal protection.

A set of *ad hoc* indicators is developed in the frame of this work to quantify the effects of wave energy absorption by the farm on the wave conditions and the coastal

morphology and, subsequently, the degree of protection afforded by the wave farm in the different scenarios.

1.3 THESIS STRUCTURE

The structure of this thesis is as follows. First, in the following section the main aspects of wave energy and its current state-of-the-art will be included in order to identify the gaps in the knowledge and select the best methods to accomplish the objectives of this thesis. On this basis, the methodology will be presented in Section 3, which will be consisted of: (i) a description of the numerical models applied and their advantages against other state-of-the-art models; and (ii) the development of a set of *ad hoc* indicators to quantify the impacts of wave farms on the wave conditions and the beach morphology. Following this, the main characteristics of the two case studies considered: Perranporth and Xago Beach will be described in Section 4. The results of the wave farm impacts on the coast will be described in the following sections: in Section 5 the evolution of the beach profile at Perranporth Beach (2D) in the medium term, in Section 6 the response of the beach (3D) at Perranporth and Xago Beach in the short term, the role played at Perranporth by the farm-to-coast distance and the layout will be analysed in Section 7 and 8, respectively; and finally the evolution of the modal state of a beach at Perranporth will be studied in Section 9. To summarise and conclude, in Section 10 the main results will be synthesised, the future directions for wave energy outlined and conclusions drawn as to the effectiveness of wave power to combat climate change, with a focus on the mitigation of its effects on the double front of its roots (greenhouse gas emissions) and its consequences (sea-level rise and increased storminess).

Chapter 2

State-of-the-art

2. STATE-OF-THE ART

Marine Renewable Energy (MRE) can substantially contribute to increasing the proportion of renewables in the energy mix, and subsequently, reducing the carbon footprint. The great potential of marine renewable energies has been addressed in different studies (Bahaj, 2011; Clément *et al.*, 2002a; Pelc & Fujita, 2002; Thorpe, 1999; Twidell, 2005) and lies in the large variety of methods to harness the resource, including (i) tidal barrage power, using potential energy (head) difference; (ii) tidal stream power, using the kinetic energy in tidal flows; (iii) wave power, which captures the energy in wave motion; (iv) ocean circulation; (v) salinity or (vi) thermal gradients.

Among them, wave energy is one of the most promising renewable since it presents a large number of advantages: the abundance and high density of the resource in many coastal areas, leading to high availability values (approx. 90% vs. 30% in the case of wind or solar energy) and, importantly, the low environmental impacts and, in particular, the visual impact of wave energy converters, not least in the case of offshore floating WECs. However, on the downside, the levelised cost of wave energy conversion is high. On this basis, this thesis will analyse the effectiveness of applying wave farms for protecting the coast in synergy with their primary role, generating electricity; which would enhance the economic viability of wave energy. The following sections will focus on the main aspects of wave energy, which will be of relevance for the aim of this work.

2.1 FUNDAMENTALS OF WAVE ENERGY

In the following ocean waves and the wave resource are presented, followed by a brief summary of their mathematical treatment.

2.1.1 WAVES AND THE WAVE RESOURCE

The process of wind wave generation, whereby energy is transferred from the wind to the sea surface, is controlled by the wind speed under a quadratic relationship – meaning that, although *stricto sensu* any wind is capable of generating waves, in practice it is only the strong (storm) winds that generate wave fields of relevant power for energy conversion. This occurs primarily in the high seas, far from the coast. The waves thus generated travel over thousands of miles of open ocean in an extraordinarily efficient process of energy transmission – with very small energy losses – until they eventually reach a coastline. In approaching the shoreline waves leave deep water, propagating over intermediate and, subsequently, shallow water. Whereas waves in deep water do not interact with the seabed, in intermediate water they start interacting ("feeling") the seabed, and this interaction intensifies as water depths decrease, consisting of two fundamental processes, refraction and shoaling, which modify wave properties (Holthuijsen, 2007).

Ultimately, waves reach the shoreline, where they are extinguished, being their energy in part dissipated through breaking and in part reflected back. In areas sheltered by natural or man-made structures (headlands or breakwaters and groynes, respectively), another process is to be added to the former: diffraction. As a result of these nearshore processes, wave patterns in intermediate and shallow water are generally more complex than offshore – all the more so where the bottom contours are irregular. Indeed, an uneven bathymetry typically leads to wave energy concentrations in certain areas (Figure 2.1) – the so-called nearshore hotspots (Iglesias & Carballo, 2010a), and areas where the resource is comparatively very weak (e.g. bays). The typical spatial extent of nearshore hotspots is $O(10^2 – 10^3$ m), and therefore a detailed study (usually involving numerical modelling) must be carried out to determine the

optimum locations for a wave farm (Carballo & Iglesias, 2012; Veigas, López & Iglesias, 2014).

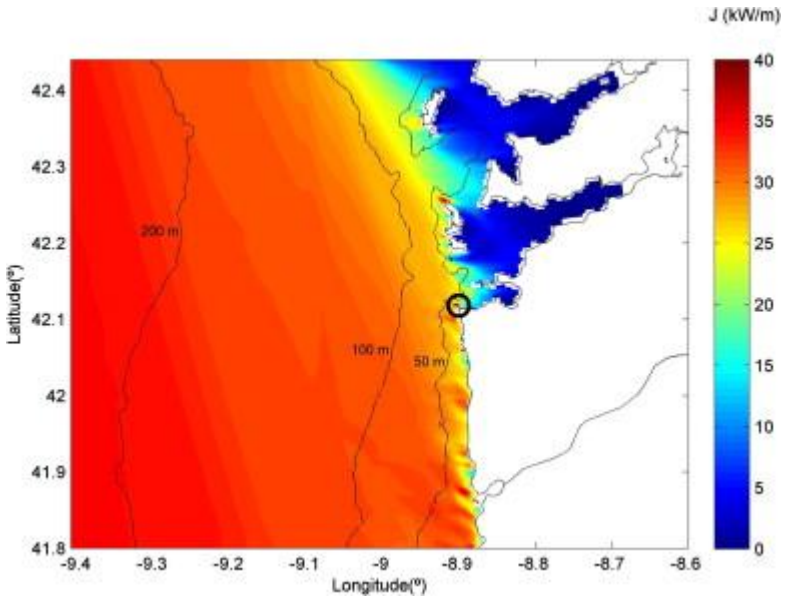

Figure 2.1 Annual mean wave energy concentration of NW Spain (Iglesias & Carballo, 2009).

The complexity of the wave energy resource stems not only from its spatial variability but also from its temporal fluctuations, which occur at different time scales (Carballo et al., 2015). At the shortest (wave) time scale, an individual wave is generally different from the next, only some seconds later; at longer time scales (monthly, seasonal) the wave resource will typically differ markedly, with values in winter bearing little resemblance to those in summer (Figure 2.2); at even longer time scales (hyperannual) oscillations (Iglesias & Abanades, 2014; Neill et al., 2009; Neill et al., 2014) such as ENSO (El Niño-Southern Oscillation) or NAO (North-Atlantic Oscillation). This remarks the importance of studying the wave farm impacts not just in the short-term scale (days), but also in longer time scales, such as medium (months) to large (years). In this sense this document will consider time scales ranged from hours (24 hours in the analysis of frequent storms – Section 7 and 8), to days (7 days in the study of storm clustering – Section 6), to months (6 months to analyse the medium-term

impacts – Section 5), to a year (to analyse the evolution of the modal state of the beach – Section 9).

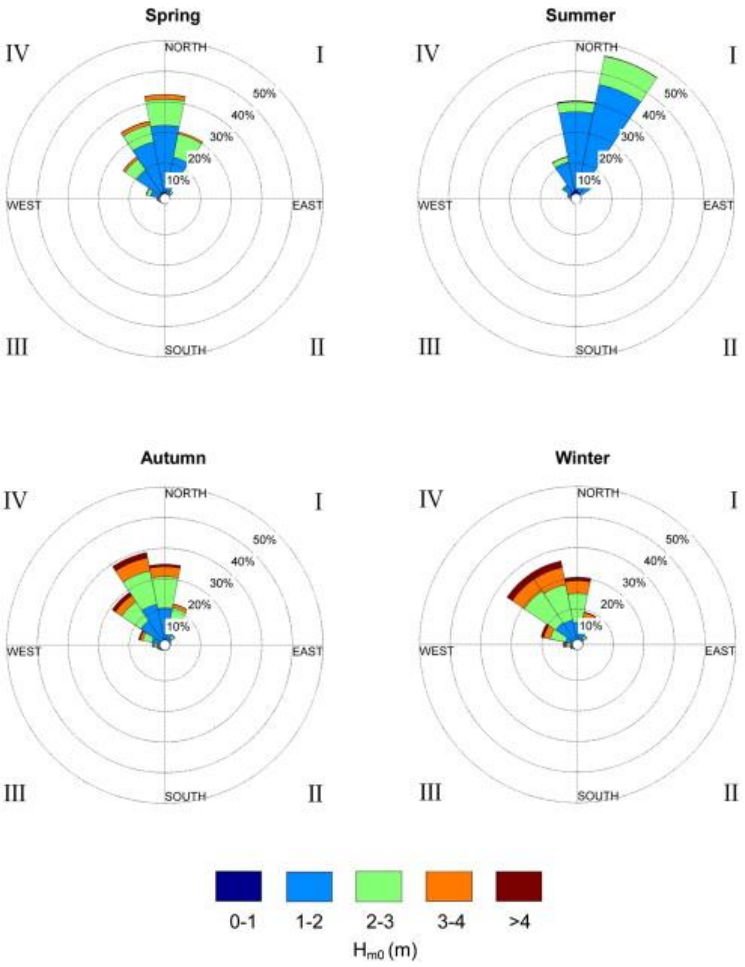

Figure 2.2 Seasonal wave height roses at La Isla Bonita in the Island of La Palma (Iglesias & Carballo, 2010c) [H_{m0}, significant wave height].

In view of the variability of the wave resource – spatial and temporal – a fundamental requirement for its exploitation is a detailed assessment of this variability in the areas or regions of interest. The variability of the wave climate has long been investigated for other purposes, including navigation, port and coastal engineering, offshore engineering and naval architecture – incidentally, fields in which wave energy is a source of concern (of loading, in technical terms) rather than a benefit. For this reason, the outcome of previous work, albeit informative, is often insufficient for purposes of assessing the wave resource, and an *ad hoc* characterisation of the wave resource is necessary.

The areas with realistic potential for the development of wave energy present average power values above 20 kWm^{-1}, and tend to be located in the Ecuador and high latitudes owing to the global atmospheric circulation. Furthermore, the seasonal variability of the wave resource is typically lower in the Southern Hemisphere than in the Northern. On this basis, many coastal areas of South America, Africa and Australia would be particularly attractive for wave energy exploitation – with the downside of their distance to the energy consumption centres. The characterisation of the wave resource has been undertaken recently in a number of areas with potential for the deployment of wave farms, and will be described in more detailed in Section 2.2 Wave energy resource characterisation.

2.1.2 MATHEMATICAL ASPECTS OF OCEAN WAVES

Ocean waves consist of a superposition of a very large number of individual sinusoidal (harmonic) waves, each with its own amplitude, frequency and direction. This superposition is expressed mathematically as a Fourier series, which can represent any sea state (Holthuijsen, 2007). The Fourier series, a time domain concept, has its counterpart in the frequency domain in the wave energy density spectrum, usually referred to for brevity as the wave spectrum, which quantifies the distribution of wave energy over the different frequencies. Often, the directional information is contained in the spectrum, which is then a directional spectrum.

On the basis of the directional wave energy spectrum it is possible to compute the wave parameters of interest, some of which are presented below (Dalrymple & Dean, 1991).

If the directional wave energy density is denoted by $S(f,\theta)$, with f the wave frequency, the spectral moments may be defined as

$$m_n = \int_0^{2\pi}\int_0^{\infty} f^n S(f,\theta)\, df\, d\theta, \quad n = 0,1,2... \tag{2.1}$$

The significant wave height is then given by

$$H_s = 4m_0^{1/2} \tag{2.2}$$

and the peak wave period may be computed as the inverse of the frequency at the spectral peak (f_p),

$$T_p = \left(f_p\right)^{-1} \tag{2.3}$$

The mean wave direction may be obtained from the directional wave energy spectrum through

$$\theta_m = \arctan \frac{\int_0^{2\pi}\int_0^{\infty} S(f,\theta)\sin\theta\, df\, d\theta}{\int_0^{2\pi}\int_0^{\infty} S(f,\theta)\cos\theta\, df\, d\theta} \tag{2.4}$$

The wave power, or wave energy flux, is given by

$$J = \rho g \int_0^{2\pi}\int_0^{\infty} c_g(f,h)\, S(f,\theta)\, df\, d\theta \tag{2.5}$$

where ρ is the seawater density, g is the gravitational acceleration, and c_g is the group celerity, i.e. the velocity at which wave energy propagates, which is a function of the wave frequency and water depth. Seawater density depends on salinity and temperature, which vary in time and space; an average value was taken for this work, ρ = 1025 kg/m^3.

Naturally the actual power output will depend on the converter efficiency, equation (1.6) yields the wave power per unit width of wave front; if a certain wave energy

converter (WEC) captures the energy of a width b of wave front, the corresponding power is

$$P_{WEC} = Jb \tag{2.6}$$

In many cases, the detailed shape of the spectrum is unknown, and only some of the characteristic wave parameters are given. In this case, the wave power, also known as wave energy flux, can be computed from the following approximation:

$$J = \frac{\rho g^2}{64\pi} T_{m01} H_s^{\,2} \ , \tag{2.7}$$

where ρ is the water density, g is the acceleration due to gravity, H_s is the significant wave height (m) and T_{m01} (s^{-1}) the wave energy period, defined as

$$T_{m01} = \frac{m_0}{m_1} . \tag{2.8}$$

Further analysis describing the equations that govern the extraction for specific devices can be found in the literature, e.g. Falcão (2010b); however this is not the aim of the present study.

2.2 WAVE ENERGY RESOURCE CHARACTERISATION

The generation of wave energy resource, as explained in Section 2.1.1 Waves and the wave resource, depends directly on wind and indirectly on sun, which characterise this resource as stochastic. Then, the characterisation of the resource is essential to assess the economic viability of a wave farm at a selected location. Most of the wave climate characterisations conducted so far have focussed on extreme conditions corresponding to return period of interest for the design of structures, and do not comprise the information required for the resource characterisation.

The lack of onsite wave buoy data limits the assessment of the wave energy resource characterisation; however, this shortcoming can be overcome through the application of numerical models, ideally calibrated and validated with wave data from wave buoys or other sources.

The offshore wave resource must be properly characterised as a prerequisite, for offshore wave conditions are required to prescribe the boundary conditions. The offshore wave resource can be described through: (i) deep water wave buoy data, where available; (ii) numerical models that account for wave generation and propagation in deep water (e.g., WAVEWATCH III); (iii) remote sensing (satellite, HF-RADAR, etc.); (iv) hindcast datasets; or a combination of the above. A detailed guide for characterising the resource can be found in Iglesias and Abanades (2014), which will not be presented in this document as it is out of its scope. The objective of this section is to identify the case studies for the analysis of the wave farm impacts where the resource is sufficiently large to justify the deployment of a wave farm.

The resource characterisation has been established at different scales: global, continental, national and regional, being the last one recommended for determining the best location for a wave farm. Regarding the global scale, Cornett (2008) assessed the global wave energy resource during 10 years, from 1997 to 2006, using the hindcast generated by the offshore third generation wave model WAVEWATCH-III (Tolman, 2002a; Tolman, 2002b), which consists of global and regional nested grids with a resolution of approx. 50 km. A weather model Global Forecast System (GFS) is coupled to implement wind data. The seasonality and variability of wave resource was quantified by means of several indicators, finding January and July with the greatest values of resource for the North and South Hemisphere respectively. Although the resolution of the study did not allow the identification of the best location for a wave

farm, the relevance of this work lies in the first approximation to determine the areas with greatest potential for wave energy exploitation (Figure 2.3).

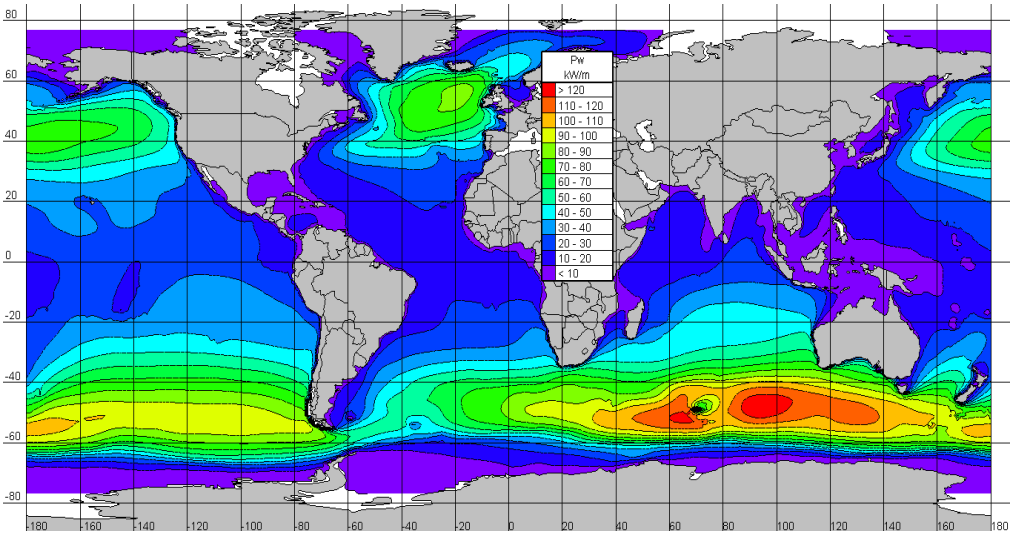

Figure 2.3 Global distribution of annual mean wave power (Cornett, 2008)

The greatest resource (over 120 kW/m) was found in the South Hemisphere, but in areas remote from the population. The coastal areas with the highest values of resource (over 70 kW/m) were the following: (i) the Atlantic façade of Europe, (ii) the Patagonia Coast (south of Chile); and (iii) the south of Australia Coast and New Zealand. While a significant proportion of the population live near the Atlantic Coast in Europe, the population density of the other two areas is very low, particularly in the Patagonia, which is practically uninhabited. To a less extent, with a mean value of the annual resource between 40-70 kW/m, the areas of South Africa and North Pacific Coast (United States and Canada) could be included.

According to these results and the population of the above areas, the Atlantic façade of Europe constitutes a prime area for wave energy exploitation. This has been corroborated by a number of studies focussed on the resource characterisation in Europe, which are described in the following paragraphs.

As regards the European scale, Pontes et al. (1996) presented WERATLAS (Wave Energy Resource Atlas), which is a user-friendly software that contains wave climate information of offshore locations in the North-Eastern Atlantic Ocean and the North, Norwegian, Barents and Mediterranean Sea. These data were extracted from the numerical wind-wave WAM model (Günther, Hasselmann & Janssen, 1992) in conjunction with the European Centre for Medium-Range Weather Forecast (ECMWF). This large area is divided into 5 smaller regions and consists of information recorded at 85 locations. The atlas results are in line with the results presented above for the global assessment, highlighting the predictions for the Atlantic Ocean façade.

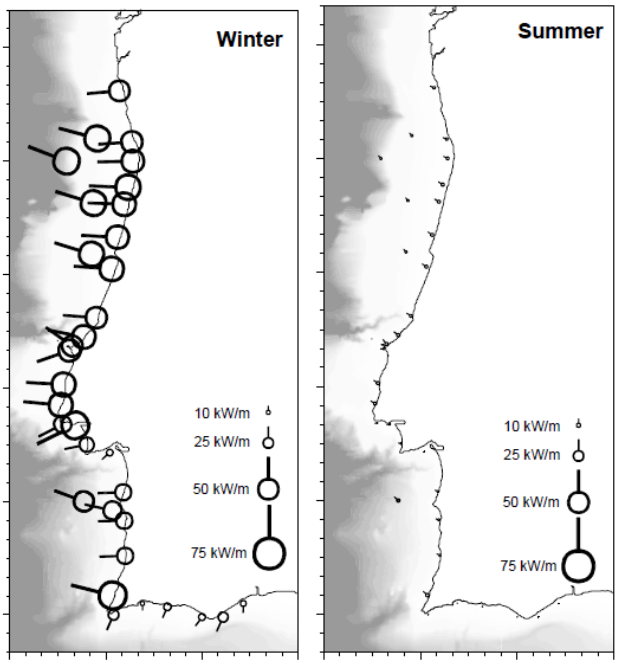

Figure 2.4 ONDATLAS in the Portuguese coast showing the mean winter resource and the summer resource (Pontes, Aguiar & Pires, 2005)

In a national scale, the ONDATLAS is a detailed nearshore wave energy atlas for Portugal (Pontes, Aguiar & Pires, 2005), which followed the same approach applied in WERATLAS, but in this case studying the nearshore area in Portugal. Figure 2.4 shows the seasonal variability of the wave resource along the coast, remarking the resource in the North Coast of Portugal. In the case of UK, ABPmer (2008) produced an atlas for

the characterisation of all renewable energies in UK (wave, wind and tidal). The wave energy resource atlas was conducted applying the UK Waters Wave Model with a resolution of 12 km and a Global Wave Model with a resolution of 60 km. These 2nd generation models are valid offshore since they are not able to calculate the coastal processes influenced by the bottom friction. Hindcast wave data were implemented in the model to provide wave datasets (and associated analysis) of up to 30 years temporal length along the UK coast.

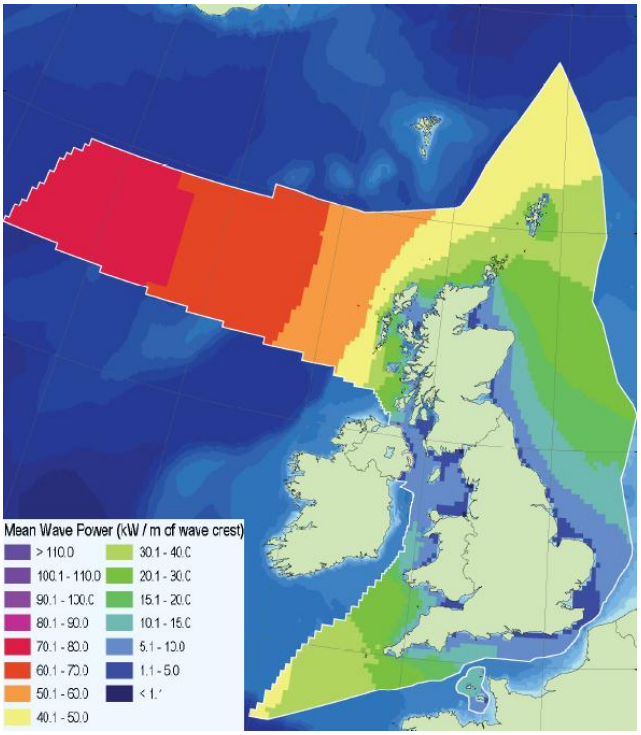

Figure 2.5 Annual mean wave power in the UK (ABPmer, 2008)

Figure 2.5 shows the annual mean wave power considering the contributions of the wind-wave and swell components. The wave energy resource was found to be of relevance in two main areas (Neill *et al.*, 2014; Reeve et al., 2011a; Smith, Pearce & Millar, 2012): Orkney (N Scotland) and Cornwall (SW England). In the former, numerous tests of marine renewable energies (both tidal and wave) have been conducted by the European Marine Energy Centre (EMEC). In the latter, the Wave Hub, a testing

facility for wave, tidal and offshore wind technologies, was installed and presents the advantage of being closer to a more populated area.

Finally, the characterisation of the resource at regional scales was generally carried out using finer resolutions. For this purpose, spectral wave models, e.g. in Iglesias and Carballo (2010c) and Rusu and Guedes Soares (2012), and less frequently Boussinesq-type wave models, e.g. in Vicinanza, Contestabile and Ferrante (2013), are generally applied in lieu of the hindcast models (WAM, WWWIII, etc.) that were used in the global, continental and national scales. A review of the different numerical models to study wave energy will be presented in Section 3.

These regional studies were conducted worldwide, from areas in the Pacific Coast (Lenee-Bluhm, Paasch & Özkan-Haller, 2011; Stopa, Cheung & Chen, 2011), to Islands in the Atlantic Coast (Gonçalves, Martinho & Guedes Soares, 2014a; Iglesias & Carballo, 2011; Veigas & Iglesias, 2013), to sheltered coasts such as the Mediterranean and Baltic ones (Bernhoff, Sjöstedt & Leijon, 2006; Liberti, Carillo & Sannino, 2013) to the Atlantic Coast in Europe and America (Defne, Haas & Fritz, 2009; Gonçalves, Martinho & Guedes Soares, 2014b; Iglesias et al., 2009). Between these areas, it is noteworthy to mention the north coast of Spain, which was well characterised from Galicia (NW) to the Basque Country (N) by Iglesias and Carballo (2009); (2010b; 2010a).

Figure 2.6 shows the wave energy resource in Asturias at two locations. The characterisation was carried out using a 44-year data series. The most likely scenarios were found around the isoline of 50 kW/m, and the mean annual wave power in these nearshore points was found to be over 30 kW/m. This constituted Asturias as a prime location for the deployment of a wave farm, as was corroborated by the Asturian Institution for Energy Development (Flor-Blanco et al., 2011).

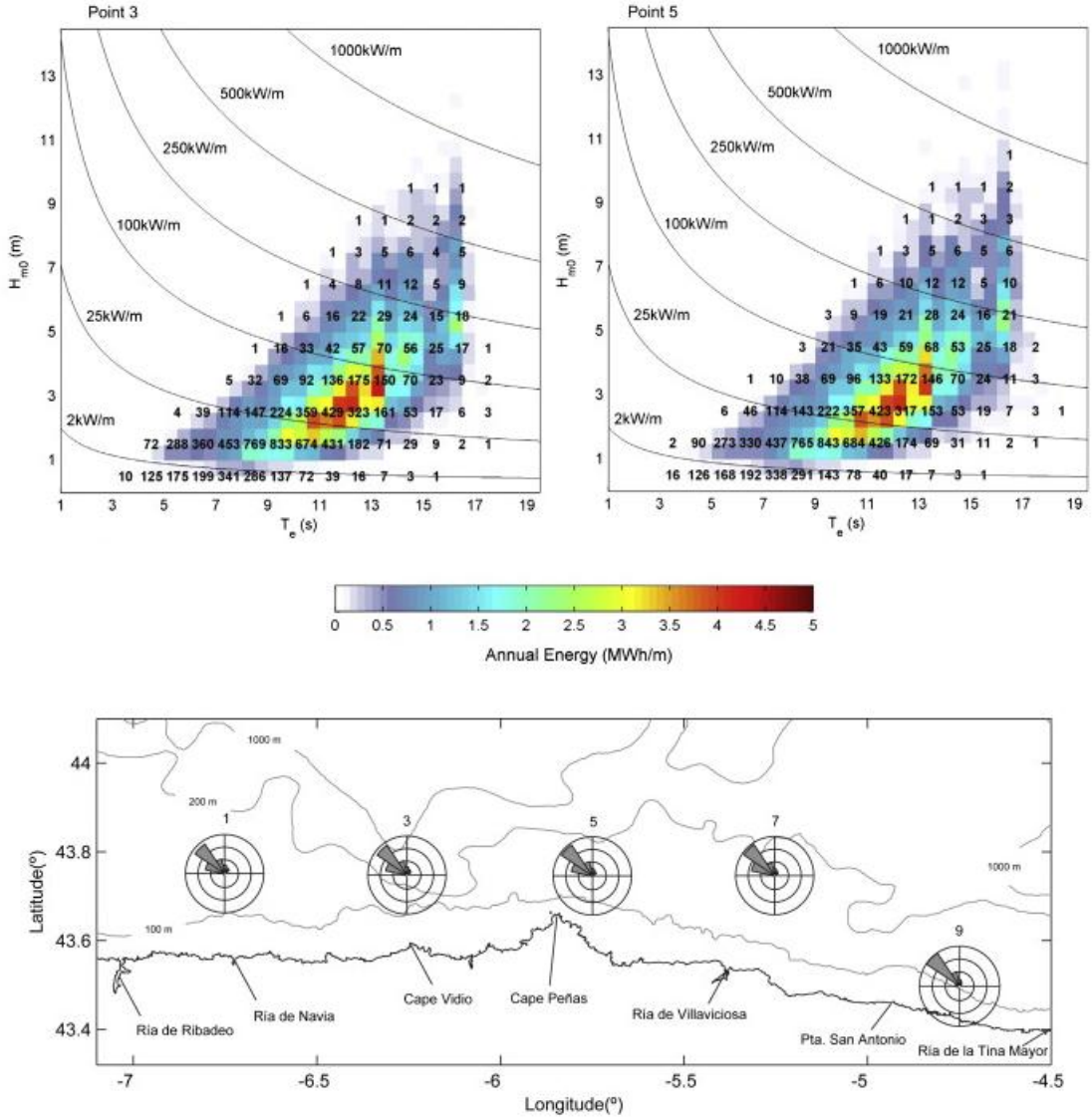

Figure 2.6 Combined scatter and energy diagrams in terms of significant wave height (H_{m0}) and energy period (T_e) at points 3 and 5 using 44 years of data (1958-2001). The colour scale represents annual wave energy, and the numbers the occurrence of the different sea states in hours per year (Iglesias & Carballo, 2010b).

Finally, several studies focused on determining the optimum location for a wave farm. As explained in Section 2.1, during the propagation of the waves to the coast their properties change as a result of the bottom friction experiencing refraction and shoaling. In the presence of irregular bottoms this interaction increases and results in areas of high energy concentration (*hot spots* – Figure 2.7) and, on the other side, areas of relatively low energy (*cold spots*). The relevance of this concept will be shown alongside this

thesis, in particular, in the comparison of the wave energy resource between the two case studies analysed – Section 10.

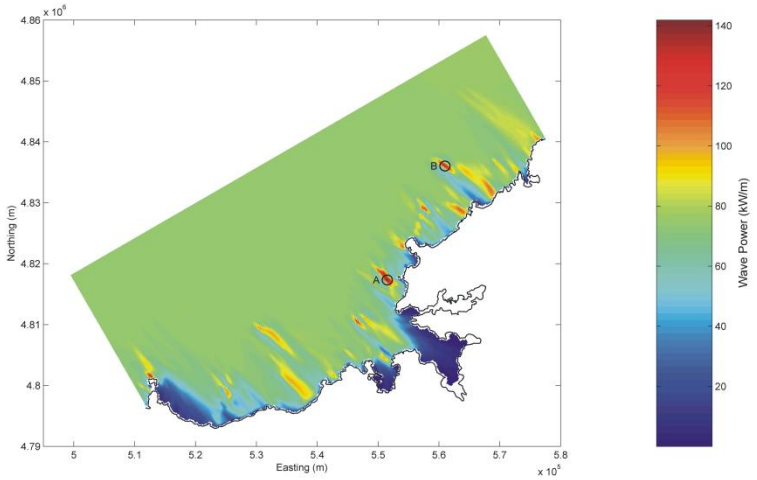

Figure 2.7 Nearshore hot spots off the coast of NW Spain (Iglesias & Carballo, 2009).

Based on the characterisation of the resource in conjunction with the distance to populated areas, the availability of data (both wave and bathymetric), and importantly, the erosion threat in the adjacent beaches, two case studies are selected along the Atlantic façade of Europe: Perranporth Beach in the SW of England and Xago Beach in the N of Spain. Therefore, these locations are primer areas for investigating the synergetic application of wave farms: carbon free energy generation and the mitigation of the climate change impacts.

2.3 WAVE ENERGY CONVERSION

At this time, wave energy is regarded as expensive – which can only be considered as natural at this point in time given its early stage of development and the difficulties posed by the harsh marine environment. It is clear, however, that for wave energy to truly take off, its costs must decrease. Over time it may be expected that, as the technology develops and larger investments are made, economies of scale will be

achieved, which will eventually lead to reductions in costs, especially related to the fabrication and optimisation of WECs.

The objective of this section is to identify and classify the different technologies to harness the wave motion; and based on this technology review, a Wave Energy Converter will be selected for the study of the wave farm impacts. At present no single technology can be deemed to be the definitive technology. A number of crucial aspects – from the energy performance to survivability under storm conditions – require further investigation. In addition to the existing technologies, new patents continue to appear. This interest in the sector is driven by the fact that the global wave resource is vast, and more than sufficient to set wave energy on a par with other renewables such as hydropower or wind energy.

Research and development of wave energy conversion, as many other renewables, gained momentum after the oil crisis in the 1973; however, the failure of several technologies during their testing resulted in a partial vanishing of the interest. The aspects that limited the development of wave energy at the time were (Kerr, 2007): (i) the low performance of the devices, (ii) the large electrical losses; and (iii) the lack of studies characterising the wave energy resource, which led to the installation of devices in areas with energetic resource but remote to the population. Then the high cost for the grid connection and the fabrication costs brought about the interruption of the wave energy development until the new century.

In this century, the appearance of new technologies that improved the efficiency and feasibility of the devices, a better understanding of the wave resource and the reduction of the grid connection costs increased the interest in wave energy. In 2000, Islay LIMPET, deployed in Scotland, was the first WEC prototype connected to the national grid of United Kingdom. In that decade, the Pelamis device was strongly

developed through numerical modelling and laboratory tests under extreme conditions to assess its reliability. Between 2004 and 2007, full-scale prototype tests were carried out at the European Marine Energy Centre (EMEC) in Scotland. After this testing phase, the first wave farm operating nearshore was installed in the northwest coast of Portugal at Aguçadoura, although after some problems the wave farm was decommissioned. Other projects conducted at different locations with different technologies can be seen in Table 2.1.

Wave Farm Name	Country	MW	Commissioned
Mutriku Breakwater Wave Plant	Spain	0.3	2009
Agucadoura Wave Farm	Portugal	2.25	2008
Islay Limpet	UK	0.5	2000
Orkney Wave Power Station	UK	2.4	2011
SDE Sea Waves Power Plant	Israel	0.04	2009
Siadar Wave Power Station	UK	4	2011

Table 2.1 List of wave farms, the country, the power installed and the commissioned year (European Commission, 2009)

The following subsection classifies the different WEC technologies according to different criteria: (i) installation site, (ii) dimensions relative to the wave length, and (iii) principle of operation. The latter is arguably the most usual, and will be developed in more detail. After, a review of the most relevant technologies will be presented in order to select the most appropriate WEC for the analysis of the wave farm impacts on the coast.

2.3.1 Classification of WECs

Classification according to the installation site: Three types of WECs can be distinguished according to this criterion:

- Onshore WECs, located entirely on land.
- Onshore-offshore WECs, which capture wave energy in the nearshore and transform it into electricity in an onshore facility.

- Offshore WECs, which are deployed in the sea. This group may be further divided according to whether the WECs are floating or resting on the seabed.

The most common location for WECs is offshore despite of the higher costs for the grid connection. The onshore technologies are characterised by their relatively simple and inexpensive maintenance, a result of both their good accessibility as onshore devices and the fact that they are less exposed to the harsh marine environment than the other categories. Another substantial advantage is the absence of a submarine cable – unlike offshore devices. On the downside, the wave resource that onshore WECs can exploit is smaller due to bottom friction and depth-induced wave breaking. A further disadvantage is the occupation of land and the corresponding environmental impact on the coastline, which can be more or less significant depending on the type of shoreline and the actual design of the device.

Classification according to the dimensions relative to wave length: This criterion distinguishes between two types of WECs: point absorbers and line absorbers. The dimensions of point absorbers are at least one order of magnitude smaller than the wave length, whereas the predominant dimension of line absorbers is of the same order of magnitude as the wave length. Line absorbers can be orientated transversally or longitudinally to the incoming wave direction.

Classification according to the principle of operation: There are three categories within this classification:

- Overtopping devices, based on waves overtopping a barrier, and the overtopping flowrate being stored at a reservoir and subsequently used to drive a turbine.

- Wave-activated bodies, which capture wave energy through the heaving motion of a floater.
- Oscillating Water Columns (OWCs), which – as indicated above – use a water column as a piston to create an air flow, which in turn drives a turbine-generator group.

2.3.2 WEC TECHNOLOGIES

A wave energy converter is a technology that uses the motion of ocean surface waves to create electricity. Energy capture is achieved by means of a Power Take Off (PTO) incorporated in the device that converts the mechanical energy into electricity. The PTO is different according to the WEC technology and its principle of operation. These technologies were reviewed by a large number of authors (Clément et al., 2002b; Drew, Plummer & Sahinkaya, 2009b; Falcão, 2010a; Falnes, 2007; Iglesias, Alvarez & García, 2010; McCormick, 1981; Thorpe, 1999).

Having put forward different criteria on which WEC technologies can be classified, in this section the state-of-the-art is reviewed through notable WECs. The last criterion of classification (principle of operation) is followed to systematise the review (Figure 2.8).

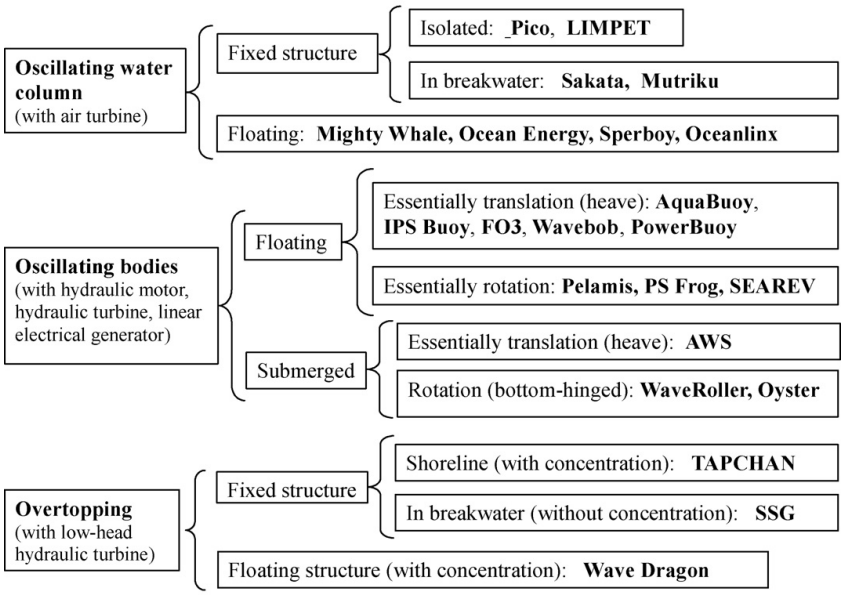

Figure 2.8 Classification of wave energy technologies in function of the location and the method of absorption (Falcão, 2010b)

Oscillating water columns (OWCs): The water column is housed in a semisubmerged concrete or less commonly steel chamber connected to the sea by an underwater opening. The lower part of the chamber is flooded with sea water, and its upper part contains air. The oscillation of the water inside the chamber (the "water column") induced by the waves outside causes the alternate compression and decompression of the air above, which is used to drive a bidirectional air turbine coupled to an electrical generator.

Onshore OWC is the most advanced technology. Figure 2.9 shows two devices that are currently in operation: Mutriku (Spain) or Pico (Acores, Portugal). Although the principle is very similar in both devices, the main difference lies in the installation of the chamber. While Mutriku is mounted on a breakwater, LIMPET is a fixed structure. Following a similar approach, floating OWCs are also installed offshore, e.g. Oceanlinx MK1 and Sperboy, but their level of development is lower compared to onshore WECs.

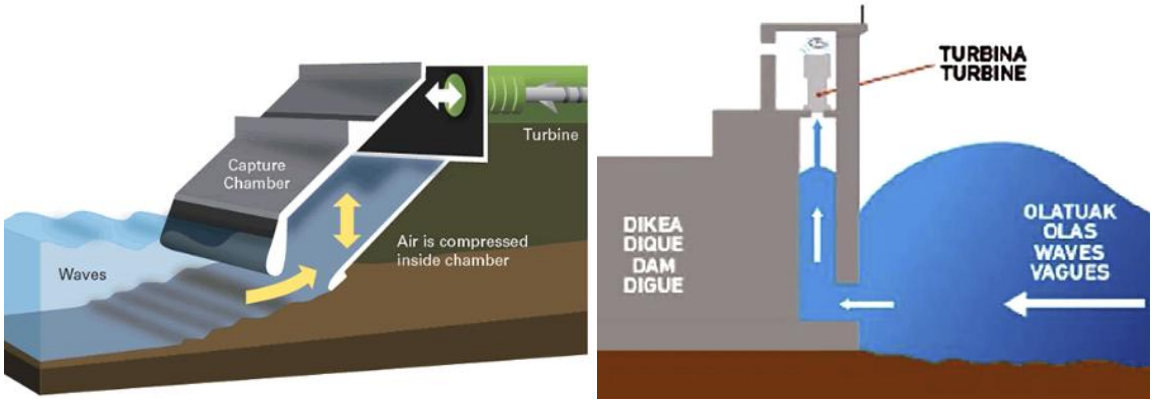

Figure 2.9 Schematic of the LIMPET WEC (left) and Mutriku breakwater-mounted OWC (right). Sources: EVE (2014) and Wavegen

In this context, this technology will not be considered for the study as the technology has been mostly developed onshore and therefore they could not be used in synergy for coastal protection.

Wave-activated bodies, also known as body system, are offshore devices generally comprised of a one or several floating bodies equipped with a power take-off (PTO) mechanism. The method of energy conversion is based on the body motion (in one or more degrees of freedom) as a response to the incoming waves. They can be either floating or fully submerged.

One example of a floating wave-activated body is the Pelamis device, which consists of a semi-submerged device composed of five cylindrical sections held together by cardan joints. As waves pass, the cylinders are displaced up and down by the buoyancy force, thereby activating the joints (Figure 2.10). They are usually located at water depths over 50 m at distances between 2 and 10 km from the coast.

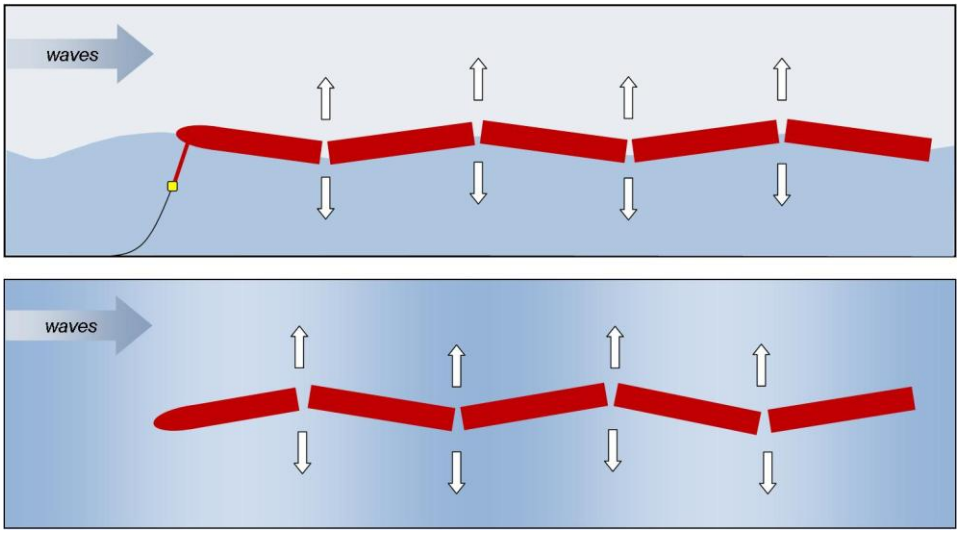

Figure 2.10 Scheme of Pelamis WEC. Source: (Pelamis Wave Power Ltd)

Other group of devices in this category are those composed of floatation elements oscillating on the sea surface. Among these is PowerBuoy (Figure 2.11), a point absorber consisting of a floating element that reacts against a submerged cylindrical body, terminated at its bottom end by a large horizontal damper plate that aims at increasing the inertia through the added mass of the surrounding water. The relative heaving motion between the two bodies is converted into electrical energy by means of a hydraulic PTO.

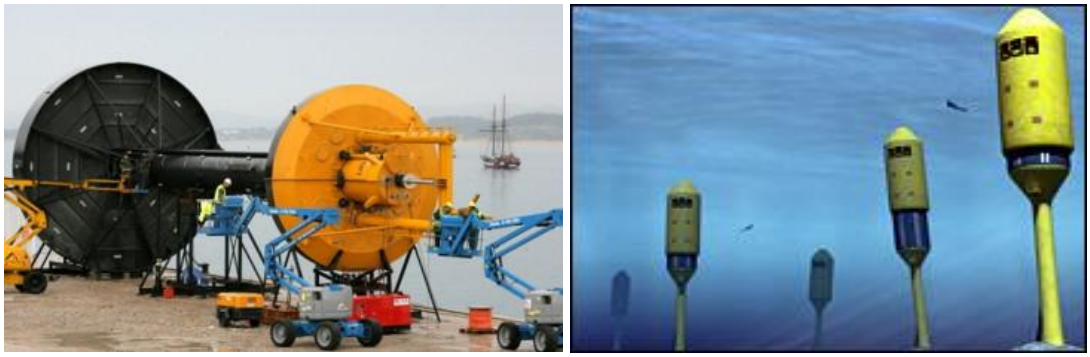

Figure 2.11 The floating PowerBuoy prototype (left) and submerged Archimedes Wave Swing (right). Sources: Ocean Power Technologies Inc (2014) and AWS Ocean Energy (2015)

Submerged offshore WECs are less common than floating ones, the reason being that underwater components add a new level of complexity. Designs are mostly at an early stage of development. The most developed device might be the Archimedes Wave

Swing (Figure 2.11). These devices cannot be seen on the surface of the sea, for it is located at a depth of 6 m – which reduces its visual impact. However, the maintenance of this device is relatively complex, as all the equipment is underwater.

In sum, the technology of these devices is more developed than the offshore OWC, however, although the performance of these devices can justify their deployment in wave farms, their principle of operation, either translation or rotation, does not bring about sufficient reductions of wave height in their lee to protect the coast. Therefore, these WECs will not be selected for studying their impacts on the coast.

Overtopping devices: An overtopping device captures sea water of incident waves in a reservoir above the sea level. This difference in elevation between the water in the reservoir and the sea surface is used to drive the PTO, generally a turbine. Overtopping devices have been designed and tested for both onshore and floating offshore.

Among the onshore devices, the Seawave Slot-Cone Generator harnesses the wave run-up over a sloping ramp, in principle on a rubble-mound breakwater. The water is captured through horizontal slots at three different levels, each connected with a reservoir. Nevertheless, these devices will not be considered in this thesis as its purpose is to investigate the impacts of an offshore wave farm on the coast in its lee.

However, the principle of operation allows the production of large amounts of energy and, at the same time, reduces significantly the wave height in the lee of the device. Therefore, offshore overtopping converters are suitable for the purpose of this thesis. In this context, two WECs should be outlined: the Wave Dragon (Kofoed et al., 2006; Tedd & Kofoed, 2009) and WaveCat (Fernandez et al., 2012; Iglesias et al., 2008). These devices are installed in relatively deep water, between 25 m and 40 m, to take advantage of the ocean waves.

In the case of Wave Dragon (Figure 2.12), overtopping occurs at a ramp perpendicular to the direction of the incoming waves. In order to capture a wave front length larger than the ramp itself, two deflectors protrude from the ramp sides; they focus the waves towards the ramp, thereby enhancing wave height. Overtopping water is collected in a reservoir above the sea level; the difference in elevation between the water in the reservoir and the outside (sea) water is used to propel an ultra-low head Kaplan turbine. Freeboard and draft are varied according to the wave conditions. Wave Dragon is one of the heaviest WECs, with a structure around 30,000 tons, which would require a substantial mooring system. The first prototype connected to the grid is currently deployed in Nissum Bredning, Denmark. Long term testing is carried out to determine system performance; i.e. availability and power production in different sea states.

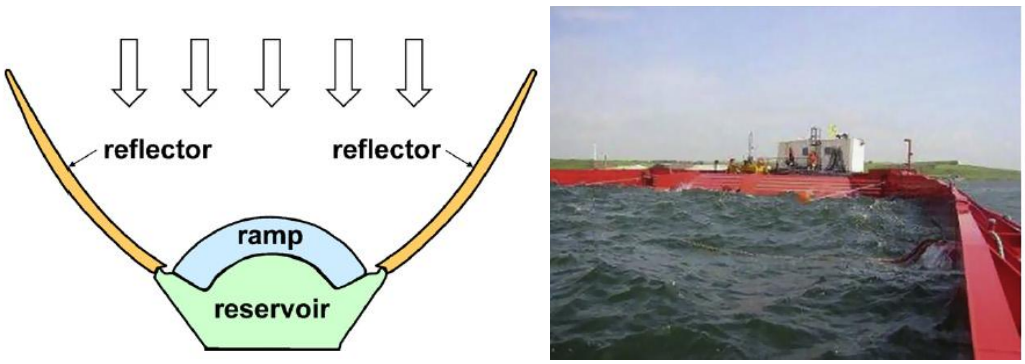

Figure 2.12 Scheme of Wave Dragon device (left) and the prototype installed in Nissum Bredning. Courtesy of Wave Dragon AS (2005),

The WaveCat (Figure 2.13) differs from the Wave Dragon in its structure and in the way overtopping occurs. Like a catamaran – from which it takes its name – WaveCat consists of two hulls. Unlike a catamaran, however, the hulls are convergent rather than parallel, so that from above they form a wedge. With a single-point mooring system (e.g., CALM, catenary anchor leg mooring) WaveCat swings so that it is always orientated in the direction of the incoming waves, which propagate into the wedge. As a wave crest advances between the two hulls, the wave height is enhanced by the tapering

channel until, eventually, the inner hull sides are overtopped. Unlike Wave Dragon, in which the overtopping wave crest impinges normally on a ramp, in the case of WaveCat the overtopping crest impinges obliquely on the hull side. Overtopping water is collected in three reservoirs on each hull, at different levels – all above the mean sea level. The difference in elevation with respect to the exterior (sea) level is used to drive a turbine for each reservoir as the water is let out back to sea. Freeboard and draft, as well as the wedge angle, can be varied according to the sea state.

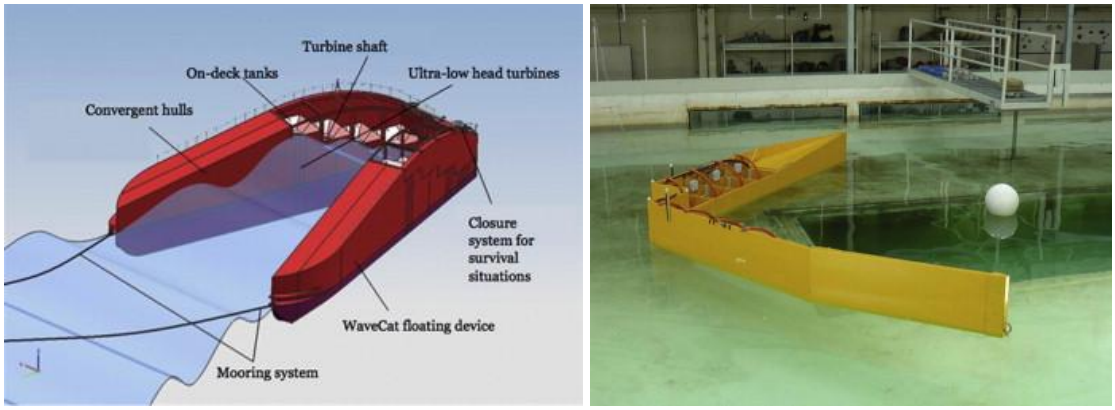

Figure 2.13 WaveCat scheme (left) and the tests conducted at the laboratory of Porto (right) at a scale of 1:50 (Fernandez *et al.*, 2012).

The advantages of WaveCat are threefold. First, overtopping occurs along the hull sides, so the WEC motions do not significantly affect the overtopping volumes but merely shift the point along the hull where overtopping starts. Second, the oblique overtopping signifies that the wave loads on the structure are considerably lower than in the case of normally incident waves. Last, but not least, the wedge between the hulls can be closed so WaveCat becomes a conventional (monohull) ship – a useful survivability strategy. Maintenance costs are expected to be low, similar to those of a ship, and the fact that it can be towed to a dry dock in its closed configuration (monohull) and repaired using the same installations is an added advantage. On these grounds, the WaveCat WEC is selected for studying the impacts of wave energy on the coast.

2.4 WAVE FARM IMPACTS

Wave Energy Converters (WECs) will be deployed forming arrays, also known as wave farms, because single devices will not be able to provide the amounts of energy that are required. Within the farm, the incident waves are reflected, transmitted and absorbed by the WECs, which in turn, may affect the overall performance of the farm as the wave resource is altered. In other words, the incident wave power is partly absorbed and redistributed around the WECs that form the wave farm, and this can result in a positive or negative effect on the power absorption of the neighbouring WECs.

Subsequently, as the wave is partially absorbed by the WEC, the wave height in the lee of the farm is considerably reduced and this modification of the wave conditions can affect positively or negatively the morphodynamics and morphology of the beach. This is particularly relevant in wave farms formed by offshore overtopping devices (e.g. WaveCat and Wave Dragon), which are based on waves overtopping a barrier.

In this heading the studies focused on assessing the impacts of the wave farms will be presented. The review will be divided in 3 sub-sections: first, the studies focussed on the WEC-wave interaction in the wave farm scale; second, those that assessed the wave farm impacts on the wave conditions; and, thirdly, the works that outlined the idea of using wave farms for coastal protection.

2.4.1 WEC-WAVE INTERACTION

The primary objective of most of the studies that analysed the WEC-wave interaction was to determine the optimal array configuration in order to minimise the negative interactions between WECs, and therefore maximise the overall performance of the wave farm. For this purpose, sensitivity analyses were carried out applying different numerical models. However, an optimum layout cannot be generalised as it will vary as a function of: (i) the boundary conditions of the wave farm, i.e. wave

climate, (ii) the location of the wave farm, e.g. distance to the coast and the water depth, and (iii) the type of wave energy converter.

The type of WEC is likely the most important aspect since the processes that govern the WEC-wave interaction vary as a function of the WEC. For instance, in the case of Oscillating Water Column (OWC) systems (e.g. Sperboy, Ocean Energy) or oscillating bodies (e.g. PELAMIS, AquaBouy), the incident wave is partly diffracted, also called scattered, and partly absorbed due to the destructive interference with the generated (also called radiated) wave. Consequently, the performance of the adjacent WECs in the farm is influenced by the scattered incident wave and the radiated wave from the oscillating device. For its part, absorption is the prevalent process that governs the interaction between overtopping WECs and the wave field, as the devices absorb wave energy by capturing the water volume of overtopped waves in a reservoir, and then, creating a hydraulic head. This generates a shadow in the lee of the devices, which can affect the performance of the WECs installed in the next rows. In sum, the redistribution of wave energy in the farm will vary according to the type of WEC deployed (Beels et al., 2010a).

Child and Venugopal (2010), on the basis of their first work (Child & Venugopal, 2007), pioneered the optimisation of wave farm layouts. They analysed different array configurations under different wave conditions. The optimisation process is accomplished with arrays of five wave-activated floating devices, identical in geometry and power take-off characteristics. The interaction of each array was determined applying a numerical model that accounted for the incident, the scattered and the radiated wave in conjunction with the motion of the device. In addition, a genetic algorithm (G) and the parabola intersection (PI) method were used to obtain the optimal

configurations. The results showed that the staggered formations maximised the resource of the wave farm (Figure 2.14).

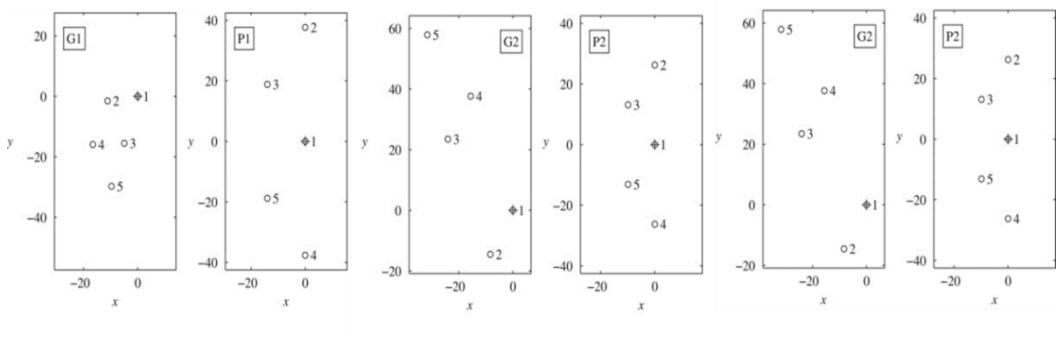

Figure 2.14 Optimum array configuration (units: m). The G and P denote the method applied to optimise the layout and correspond to general algorithm and parábola intersection, respectively. The number signify the objective pursued: (1) to maximise power in an array of real-tuned devices, (2) to maximise power in an array of reactively tuned devices, and (3) to minimise power in an array of reactively tuned devices.(Child & Venugopal, 2010)

Babarit (2010) studied the WEC-wave interaction as a function of the distance between devices. For practical reasons, e.g. grid connection and moorings costs, distances between devices around hundreds of meters were considered. The different array configurations were studied at deep water to simplify the problem, by means of a Boundary Element Model (BEM) based on the linear potential flow theory under regular and irregular wave conditions. Based on the results presented, locating wave devices at distances shorter than 100 m is not recommended due to the negative interaction between devices. For greater distances, between 100 and 500 m, recommendations are difficult to establish since the wave interaction varied depending on the array configuration, particularly when the direction of the incident waves were not aligned with the array. This is one of the main disadvantages of oscillating devices in relation to overtopping devices since the latter have a degree of liberty to move in order to be always aligned with the wave direction and then maximise their performance.

Similarly, Borgarino, Babarit and Ferrant (2012) assessed the influence of the interactions between WECs in the energy production of the array. Two WECs were

considered: heaving cylinder and surging barge, which were arranged in 9-body arrays with regular patterns, forming either square or triangular grids. This study revealed that locating WECs in wave farms forming square configurations is not appropriate, particularly for short spacing between devices, as the masking effect is exacerbated. In this line, the study corroborates that the triangle-based arrays, also called staggered formations, may be the most suitable configuration, as they minimise the destructive interactions between WECs.

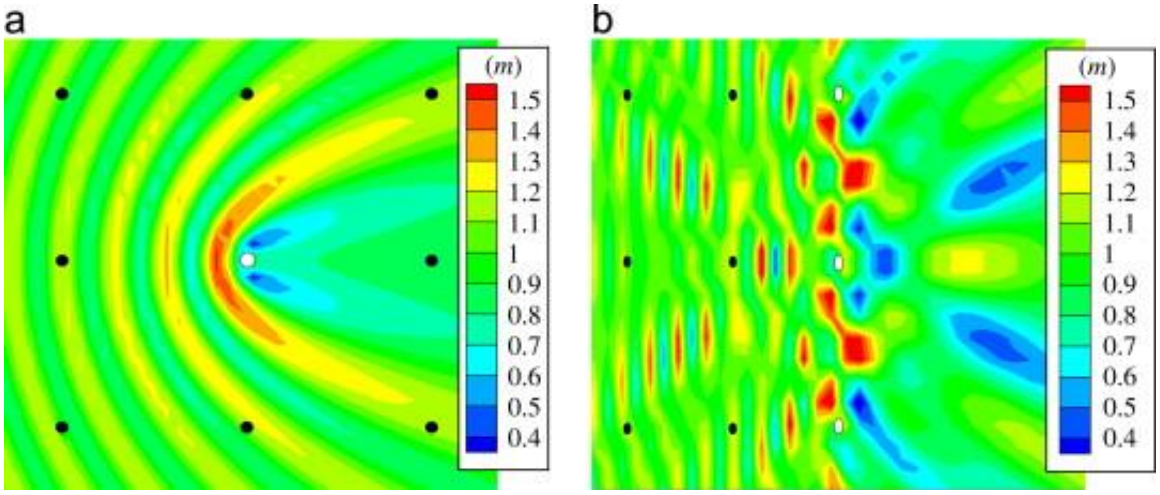

Figure 2.15 Wave amplitude around a set of 1 (a) or 3 (b) heaving cylinders in a view of a 9-body array. The figure a shows the wave amplitude around the white cylinder; and the figure b, the wave amplitude around the three white cylinders in interaction. (Borgarino, Babarit & Ferrant, 2012)

To complement the result from the numerical models, physical modelling has also been conducted to determine the interaction between converters. Stratigaki et al. (2014) analysed the effects in large arrays of up to 25 heaving point absorber WECs for a range of configurations and wave conditions. Although all the configurations have not been analysed, the results of the 5 × 5-WEC rectilinear array showed the wave height attenuation in the lee of the WEC array. Figure 2.16 illustrates the modification of the wave field with the devices for large-crested waves. While in the first rows of devices the wave height increased, in the lee of the device attenuation, up to 18.10% at a distance of 30D – with D indicating the diameter of the device – was found. The future analysis of the other

array configurations will allow the determination of the best layout to minimise the destructive interaction between devices.

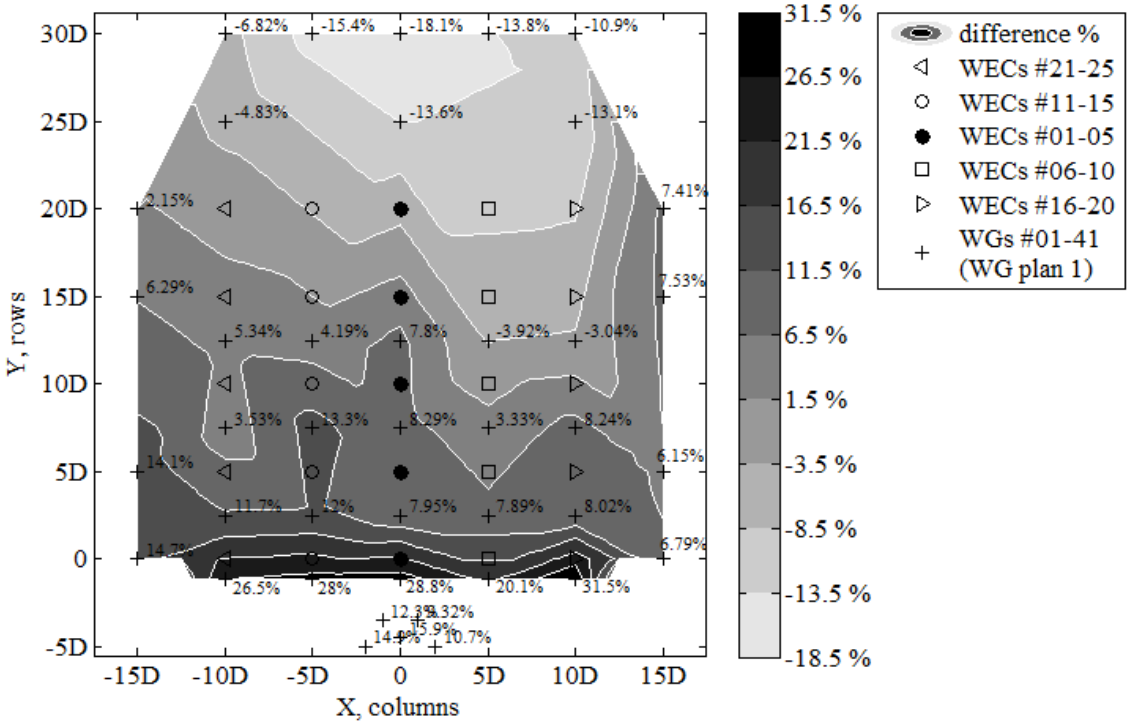

Figure 2.16 Perturbed wave field normalized by recorded undisturbed wave field for the 5 x 5 WEC array configuration (Stratigaki *et al.*, 2014). The basin width (X, columns) and length (Y, rows) are expressed in number of WEC unit diameters, D = 0.315 m.

Regarding offshore overtopping converters, the studies have been mainly focused on the aforementioned devices: Wave Dragon and WaveCat WECs. Beels *et al.* (2010a); (2010b) implemented the Wave Dragon WEC in a time-dependent mild-slope equation model (MILDwave) to establish the optimum wave farm. To model the combined effects of reflection, transmission and consequently absorption of a WEC, laboratory tests of a single device were conducted to determine the wave transmission coefficient.

The optimisation of the layout was carried out by means of the assessment of two key parameters: (i) the distribution of the WECs and (ii) the spacing between WECs. Regarding the former, both staggered and aligned (also called square) were studied in a 9-WECs array arranged in 3 lines. The representation of the effects on the wave height

in the adjacent WECs and the lee of the devices was carried out by means of an absorption coefficient, K_D, which represented the ratio between the disturbed significant wave height and the incident significant wave height at the wave generation boundary.

Figure 2.17 illustrates that the reduction of the significant wave height is higher in front of the devices situated in the second and third row in the case of the aligned formation, and therefore the staggered formation presents better performance than the square grid. While, the capture ratio in the second and third row of devices was 45% and 35%, respectively for the staggered grid, in the case of the aligned grid both rows presented ratios of 30% (Beels *et al.*, 2010a). However, it is noteworthy to highlight that this finding does not imply that the attenuation of the wave height in the lee of the wave farm formed by staggered grids is less than with aligned grids.

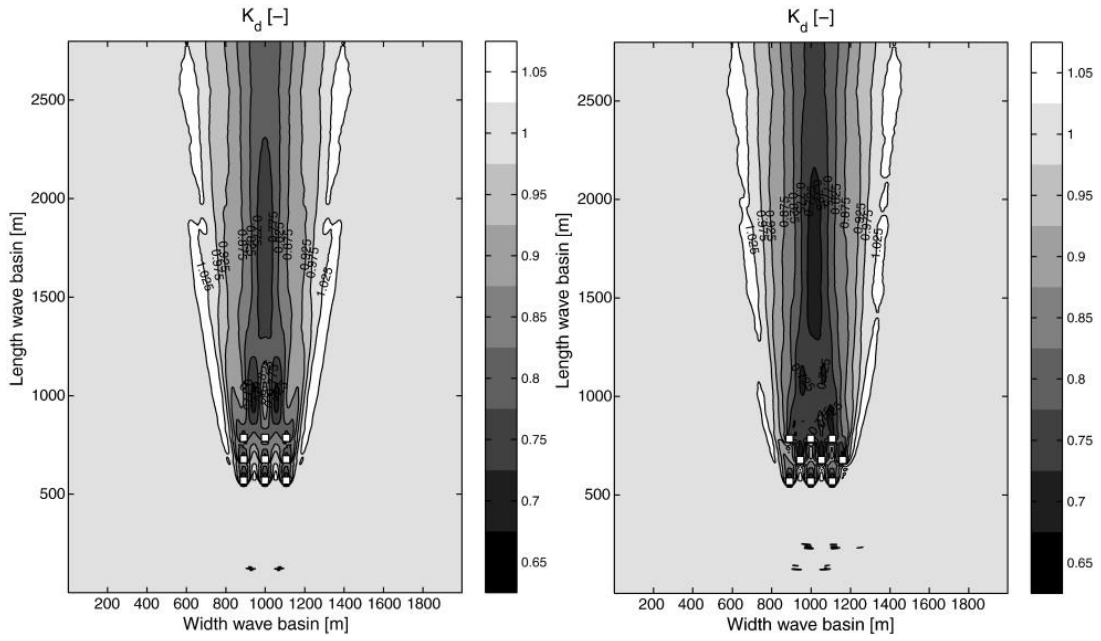

Figure 2.17 Calculated disturbance coefficient, K_D, of an aligned (left) and staggered (right) array formed by 9 Wave Dragon WECs for irregular long-crested waves (Beels *et al.*, 2010a)

Secondly, and considering a staggered formation, the influence of the distance between devices is analysed. A 5 Wave Dragon farm was studied with three spacings: D, 2D and 3D, with D = 260 m, i.e. the distance between the twin bows of the device. For overtopping converters, the greater the spacing, the lesser the interaction; however,

it also needs to take into account that the smaller the distance, the cheaper the cost of the farm. The results showed that the layout with a distance between devices of 2D was the optimal farm layout (Figure 2.18), taking cost and spatial considerations into account. Furthermore, it was observed that five Wave Dragon WECs installed in a staggered grid at a distance of 2D, would produce practically five times more than a single Wave Dragon WEC, as the incident wave power in the second row is barely affected by the first row (Beels *et al.*, 2010b).

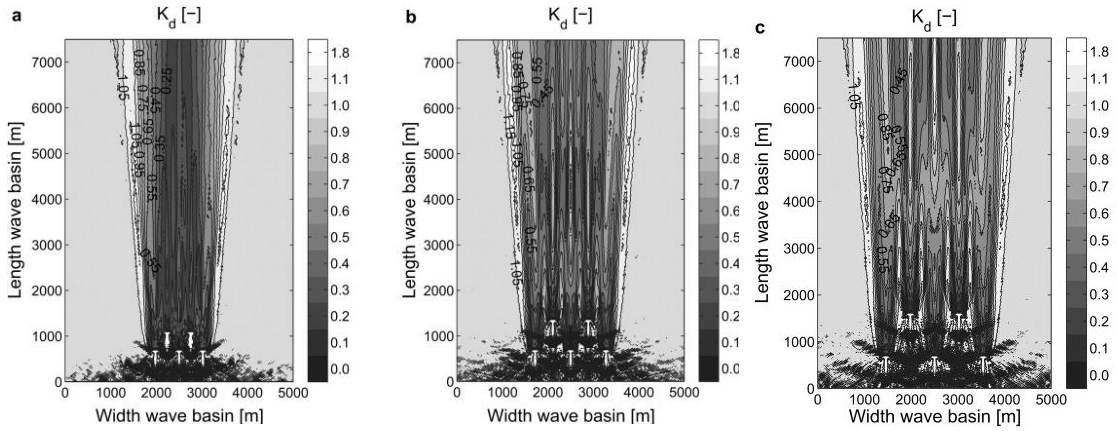

Figure 2.18 Calculated disturbance coefficient, K_D, of a 5 Wave Dragon array arranged in two rows with a spacing of D (left – a), 2D (middle – b) and 3D (right -- c), with D = 260 m, for irregular long-crested waves (Beels *et al.*, 2010b).

As regards the WaveCat, Carballo and Iglesias (2013) studied two different 12-WaveCat array configurations, the first with the WECs arranged in just one row, and the second with the devices in two rows in a staggered formation. This work aimed at proving that the performance of the wave farm is not drastically affected by the absorption of the first row of devices. For this purpose, the phase-averaged spectral model SWAN (Booij, Holthuijsen & Ris, 1996) was applied using the values gathered in the experimental campaign carried out to determine the WaveCat WEC-wave interaction under different wave conditions (Fernandez *et al.*, 2012).

Based on previous studies, a separation of 2.2D – with D equal to 90 m and corresponding to the distance between the twin bows of the device – was considered. In

this case, the results (Figure 2.19) showed that the wave height in front of the devices in the second row was lower than the first, and therefore the overall performance of the wave farm was greater with just one line. On the other hand, the one-row layout is less appropriate than the two-rows given that its greater performance does not justify the increase of the costs (maintenance, cable, space occupied, among others).

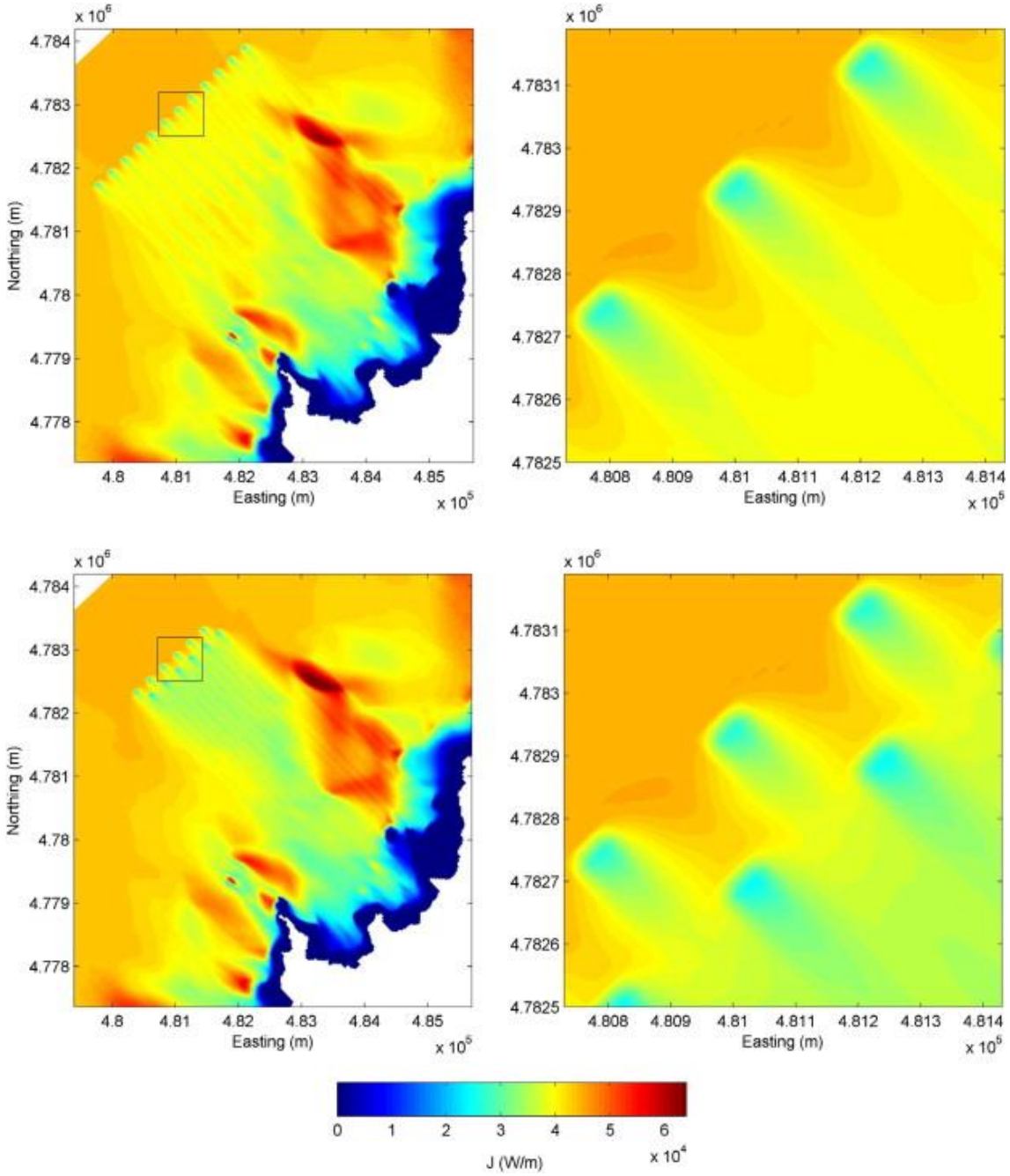

Figure 2.19 Spatial distribution of the wave power in a row (above) and two rows (below) configuration with H_s = 3m, T_e = 10.8s and Direction = NW (Carballo & Iglesias, 2013).

In sum, although there is no prevailing layout, which is in line with the absence of a prevailing WEC, a number of recommendations can be extracted from this section. Spacing between devices below 100 m are completely inappropriate, especially for overtopping devices, in which the absorption by the WEC is the most relevant process. The works reviewed showed that avoiding the destructive interference between devices is essential in the design of the wave farm layouts in order to not decrease their performance and, therefore, their economic viability. On the other hand, distances between WECs over 300 - 400 m, are not recommended since they would increase significantly the costs of the wave farm.

2.4.2 WAVE FARM IMPACTS ON THE WAVE CONDITIONS

The knowledge of the impacts of wave farms is a fundamental prerequisite for the development of wave energy and this is reflected in the number of studies investigating the effects of wave farms on the wave conditions in their lee.

First, Millar, Smith and Reeve (2007) used the spectral wave model SWAN to investigate the effects of a wave farm in the Wave Hub project (UK). A fine grid was nested in a coarse computational grid with a resolution of 200 and 5000 m, respectively. The wave field-wave farm interaction was studied by means of different notional energy absorption coefficients: (i) 0% that represents complete absorption of all incoming wave energy at the obstacle (an unachievable scenario); (ii) 70% that corresponds to an array of densely spaced with high-efficiency WECs, (iii) 90% that represents lower efficiency, widely spaced WECs, and (iv) 40%, included in the study to enable the establishment of trends. The study analysed the reduction of the wave height brought about by the Wave Hub along the 300 km of shoreline in the SW Coast of England under different wave conditions.

The results (Figure 2.20) showed that the reduction of the significant wave height on the coastline reached values around 5% in the case of the scenario with a transmission coefficient of 40%; while in the scenarios with lower efficiencies (e.g. 90%), the changes were practically negligible.

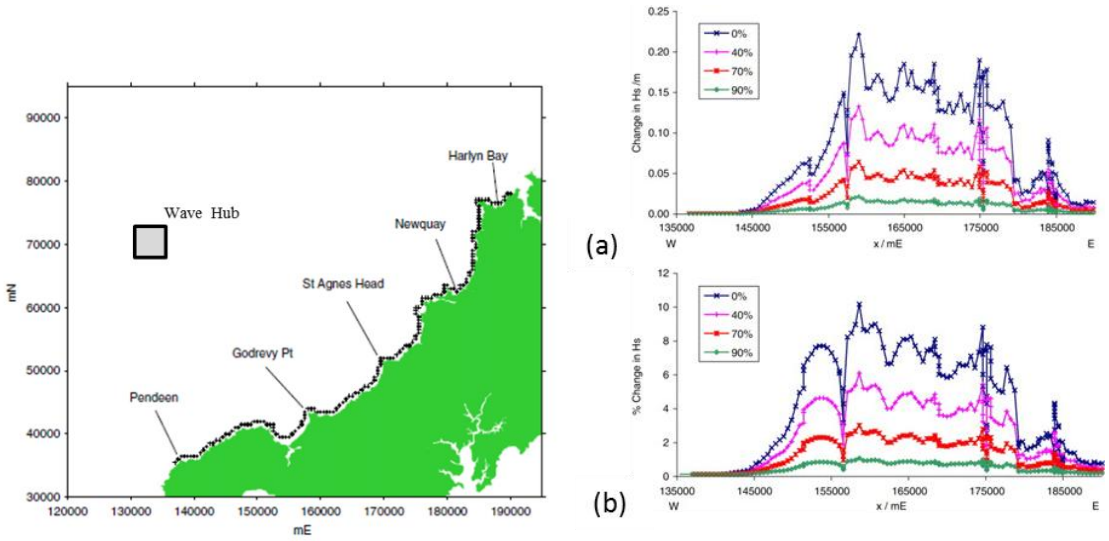

Figure 2.20 On the left hand, location of the Wave Hub and the points studied along the coastline, from Pendeen (W) to Harlyn Bay (E). On the right hand, (a) ΔH_s and (b) $\Delta H_s/H_s$ along the coastline varying wave energy transmission percentages for the reference sea state: H_s = 3.3 m, T_m = 11 s and Direction = N.

This work pioneered the analysis of the impacts of the wave farm on the wave conditions, but the validity of the results warrants discussion. Three shortcomings of the model are detected: (i) the resolution of the model limited the accuracy of the results as the assessment was carried out with a grid of 200 m, (ii) the wave farm was modelled as a single element, and finally (iii) the values of the wave absorption coefficient were notional. In spite of that, this work represented a scientific breakthrough in the study of the wave farm impacts.

Smith, Pearce and Millar (2012) followed a similar procedure, although some changes were adopted to obtain more realistic results. The most relevant upgrade was the use of a wave absorption coefficient that varies as a function of the frequency. The SWAN source code was modified to apply an individual transmission coefficient to

each of the frequency bins of the spectrum, thus allowing variation in energy absorption across the spectrum.

Every WEC has its own response function (Power Transfer Function, PTF) that defines the proportion of power extracted from the waves as a function of the wave frequency. The wave farm was represented in three configurations: (1) a continuous barrier of 4 km as it was defined by Millar, Smith and Reeve (2007), (2) a series of smaller 100 m width barriers with 200 m spacing between them, and (3) two staggered rows of 100 m barriers with an inter- and intra-row spacing of 200 m and 500 m, respectively (Figure 2.21).

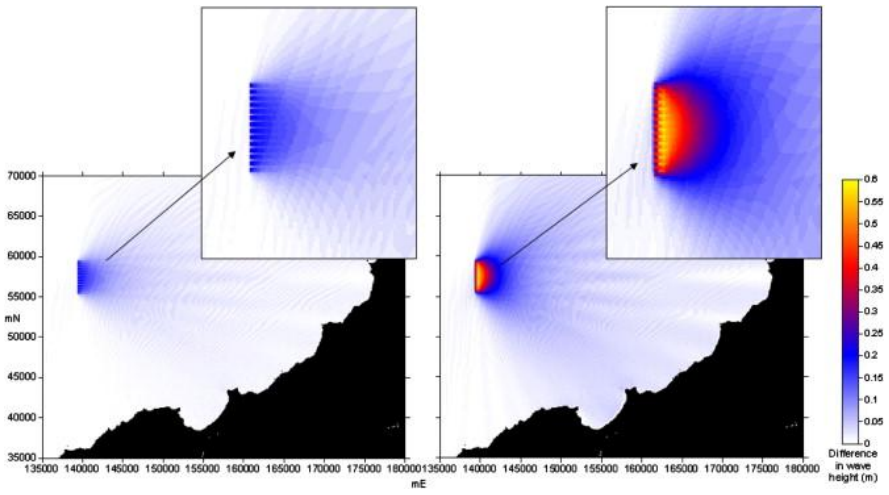

Figure 2.21 Impacts of a wave farm on the wave conditions with a series of smaller 100 m barriers arranged in a row (left) and two staggered rows of 100 m barriers (Smith, Pearce & Millar, 2012).

The results were analysed at different distances from the wave farm: 1, 5 and 10 km with a grid spacing of 100 m across the grids (Figure 2.22). Two scenarios were considered: low-efficient (narrow PTF) and high-efficient (wide PTF) WECs. Whereas, a wide bandwidth PTF captured power across a wider range of the spectrum but, potentially, with a lower maximum absorption; a narrow bandwidth PTF, captured higher power at the peak, but which can only convert the power of the waves across a narrow section of the spectrum.

Figure 2.22 shows that the low-efficient scenario presented negligible reductions of the wave height in the lee of the farm, with values around 1% at a distance of 10 km from the farm. On the other hand, the attenuation of wave energy for the high-efficient case cannot be overstated, with reductions over 5% at distances of 5 km in the lee of the farm. However, this work did not overcome the main shortcomings of the previous paper: the absorption in the farm was still modelled with notional values (motivated by the lack of data at that time), and the resolution of the grid.

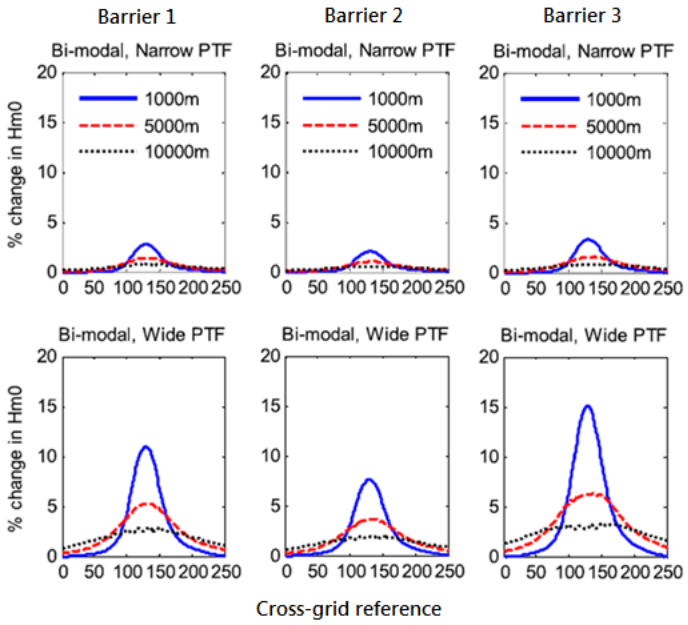

Figure 2.22 Results along the grid transect at 100 m intervals at distances of 1, 5 and 10 km in the lee of the wave farm for the different array layouts: continuous barrier (left – barrier 1), single row of 100 m barriers (middle – barrier 2) and two staggered rows of 100 m barriers (right – barrier 3) (Smith, Pearce & Millar, 2010).

Following a different approach, Venugopal and Smith (2007) applied a nonlinear Boussinesq wave model (MIKE 21) to assess the manner in which the modification of the wave absorption coefficient affected the wave conditions in the Orkney Islands (Scotland). The devices were modelled as solid structures and porous structures. As for the former, the devices mainly reflected waves (as a vertical breakwater) and did not allow any wave energy absorption or transmission through them. As for the latter, the modification of the porosity values enabled the representation of different degrees of

reflection, absorption and transmission. The wave farm was modelled with 5 WECs, whose dimensions were 160 m length and 10 m width, with a spacing of 160 m.

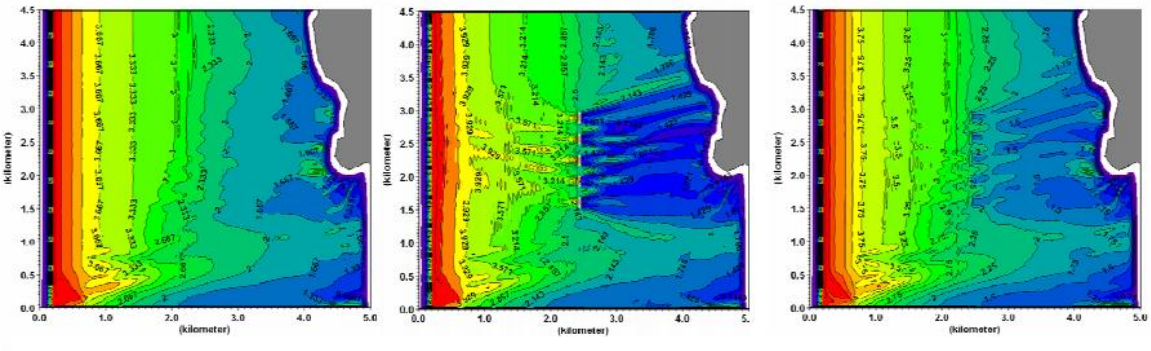

Figure 2.23 Modification of the significant wave height in the following scenarios: (a) no structure placed, (b) solid structure and (c) structure with porosity = 0.7 (Venugopal & Smith, 2007).

Figure 2.23 shows the comparison between the baseline scenario (no farm) and the wave farm scenarios. While the devices 'non-absorbent' (i.e., solid structure, n = 0) presented results that are unachievable, with reductions of wave height of up to 70%, the devices modelled with a porosity coefficient of 0.7 significantly reduced the wave height in the lee of the coast, with reductions of over 10% at the shoreline. The disturbance coefficient, $K_{D,}$ is illustrated in Figure 2.24 along the line that crossed the device 3 from offshore to the coast for different porosities. The highest reductions were found for values of porosity equal to 0.5 and 0.6; as the non-porous or solid scenario led to an increase of the reflection and diffraction. For its part, with higher values of porosity the device acted like a transparent structure, resulting in less reflection and less absorption as indicated by a maximum reduction of only about 13% in wave height behind the device for n = 0.9.

However, although the model represented better the impacts as high-resolution grids were implemented, the approach to model the wave energy extraction caused by the WECs was very poor. Furthermore, the variation of the results as a function of the

absorption was not clear, with smaller porosities providing greater reductions in the lee of the device than solid structures.

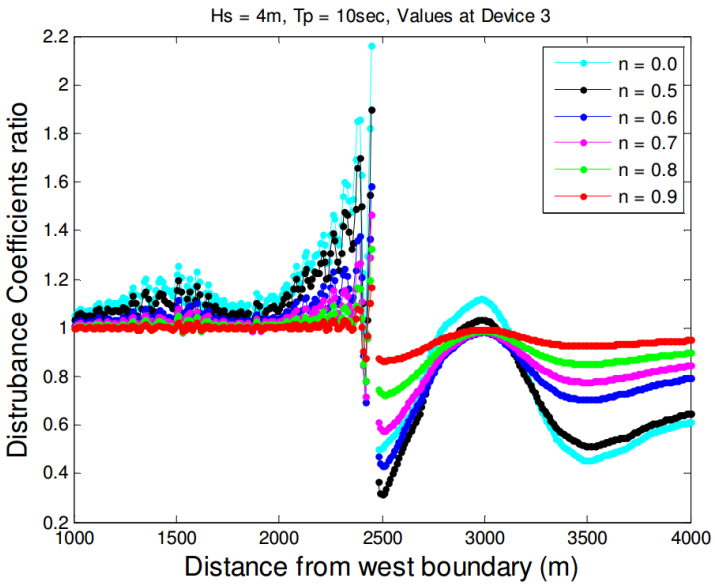

Figure 2.24 Disturbance coefficient ratio for the different porosity values along the line from offshore to the coast crossing the device 3 (Venugopal & Smith, 2007).

Palha et al. (2010) used the parabolic mild slope wave model REFDIF to accomplish a sensitivity analysis of different array configurations formed by Pelamis WECs to analyse their impact on the wave conditions at the West coast of Portugal. The main difference from the previous works was the approach taken in modelling the energy absorption. Instead of using notional values of wave energy extraction by the WEC, estimated coefficients were provided by the developer. The REFDIF model was adapted to consider the effects of the WECs, but the model could only be run under monochromatic wave conditions.

Five wave farm configurations were tested, named A to E (cases b to f in Figure 2.25). In configurations A to C, the wave farms were positioned along a single row perpendicular to the wave propagation direction. In D and E the WECs were arranged in three and two staggered rows, respectively. Values of up to 23% of wave energy extraction were found within the wave farm. The configurations A to C and E presented

the lower variation on the significant wave height in points near the coast in relation to the array configuration D. Along the contour of 10 m water depth it was found that the E configuration, despite its less reduction of wave height (~15%) in the lee of the farm than the D layout (~20%), extended its impact along a wider area (Figure 2.26). This work revealed that the attenuation of wave height is very significant in the lee of the farm, especially considering that the PELAMIS device is a wave-activated body and the main process that govern its interaction with the wave field is not the wave absorption, as it is in the case of overtopping wave converters (which leads to greater reductions of wave height in the lee of the devices).

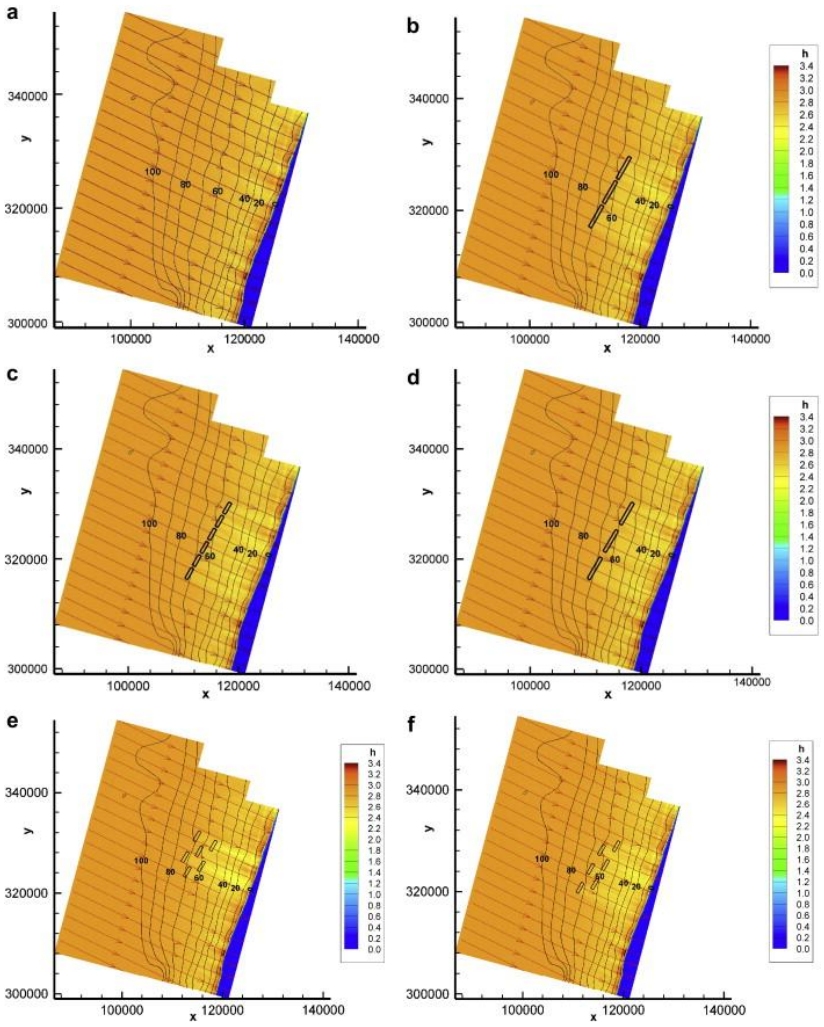

Figure 2.25 Values of the significant wave height and wave direction on the domain for the different configurations under January offshore wave condition: H_s = 2.9 m, T_e = 11.1 s, Direction = NW (Palha *et al.*, 2010).

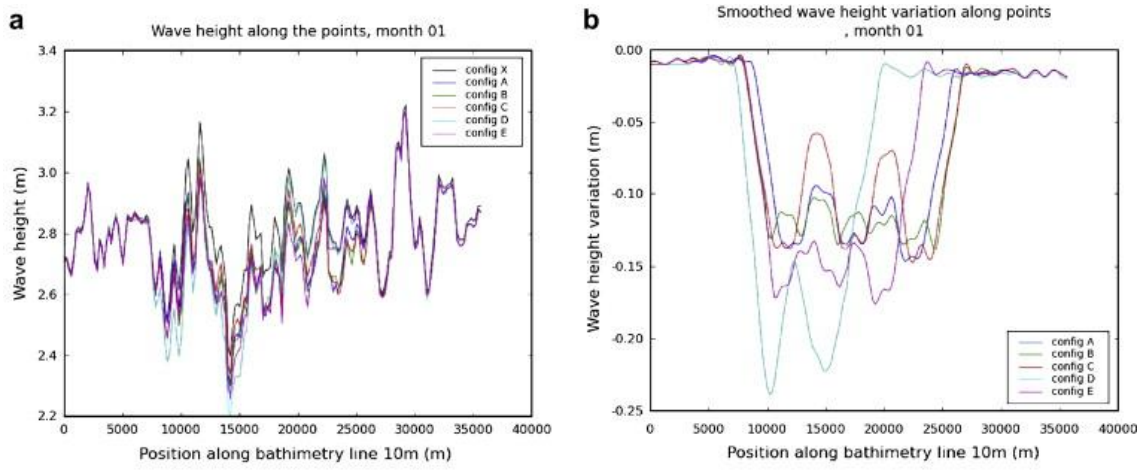

Figure 2.26 Wave height (left) and variation of the wave height (right) along the contour of 10 m for the following scenarios: without (configuration X) and with wave farms (configurations A to E) (Palha *et al.*, 2010).

Iglesias and Carballo (2014) analysed the influence of another key design parameter: the farm-to-coast distance. Based on the layout presented by Carballo and Iglesias (2013), the wave farm was located at three farm-to-coast distances: 2, 4 and 6 km from the 10 m contour (Figure 2.27), at water depths of 30, 50 and 80 m, respectively. The aforementioned shortcomings were overcome with the implementation of the wave farm in a high-resolution grid and modelling the wave-WEC interaction with the wave transmission coefficient obtained in laboratory tests.

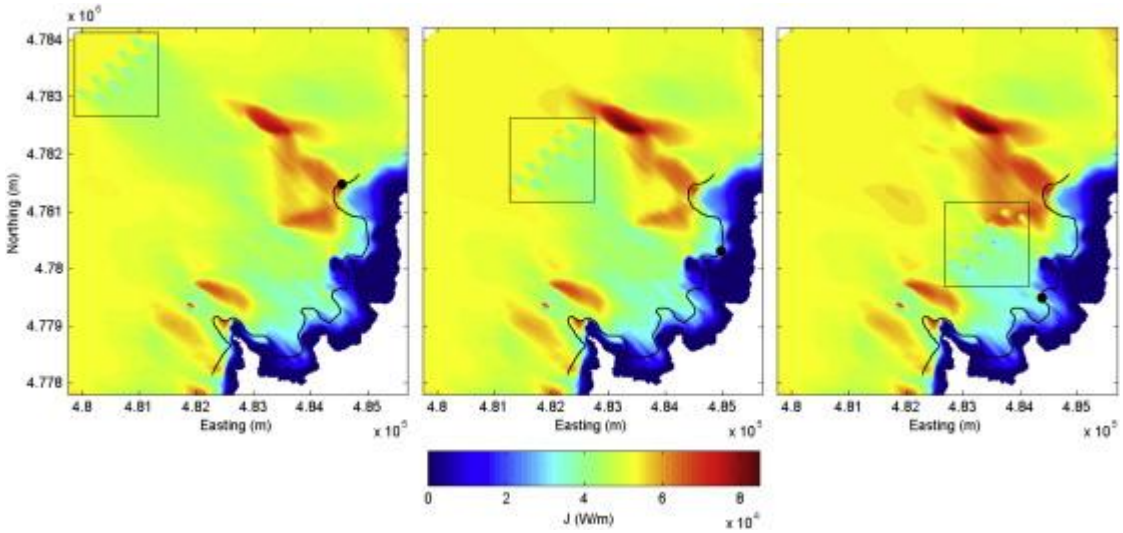

Figure 2.27 Wave power pattern with the farm located at a distance from the 10 m water depth contour of 6 km (left), 4 km (middle) and 2 km (right) under winter conditions. The wave farm area is marked with a box (Iglesias & Carballo, 2014).

The results showed that the greatest attenuation of wave energy was found with the closest wave farm to the coast, with values over 20%. The farm at an intermediate distance also reduced significantly the wave height (~18%) and the furthest wave farm presented the lowest attenuation (~10%). On the other hand, the resource for the furthest wave farm was larger than the other two scenarios. This work demonstrated the important role played by the distance to the coast, and that a detailed impact assessment must be carried out for any wave farm project to determine the optimum location based on a series of parameters: resource, impact, costs (the greater the distance the greater the cost due to moorings and cables, among others), etc.

In summary, two main recommendations can be extracted from these works: (i) the necessity of using high-resolution grids to define correctly the position of the WEC in the farm, and to resolve the individual wakes caused by the devices and their interaction each other; and (ii) the use of data obtained from real models, prototypes or laboratory tests to predict the wave-WEC interaction with accuracy.

2.4.3 WAVE FARMS FOR COASTAL PROTECTION?

In view of the effectiveness of wave farms to reduce the wave energy in their lee, the possibility of protecting the coast through wave farms has attracted the interest of a number of studies. One of the first works on this issue was conducted by Vidal et al. (2007) and analysed the impacts of a wave farm formed by 10 OPT PB150 buoys located at Santona (N Spain) at a water depth of 50 m. The wave propagation was conducted by means of the OLUCA-SP model, that solves the parabolic version of the mild slope equation, and the results were coupled to the EROS-SP, which was applied to determine the sediment transport.

The results of the wave height attenuation in the lee of the farm (Figure 2.28) were not in line with the results presented above; with reductions either in the lee of the farm

or at the coastline found to be practically negligible (as sediment transport is driven by wave energy). Thus, the modification of the sediment transport was insignificant. In any case, the results of the study cannot be generalised, considering that the wave farm was composed of buoy-type WECs, whose interaction with the waves is not governed by the absorption, and therefore, the degree of protection afforded is less than in the case of overtopping devices.

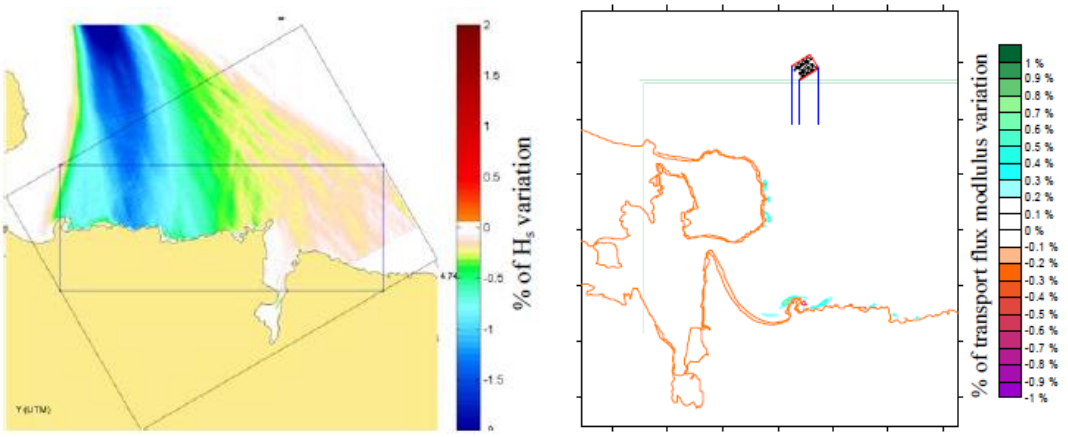

Figure 2.28 Variation of the wave height (left) and the transport flux (right) under the following wave conditions: H_S = 6 m, T_p = 15 s and Direction = NW (Vidal *et al.*, 2007).

Ruol et al. (2011) studied the impacts of a wave farm consisting of one line of DEXA WECs (wave activated bodies) at a distance to the coast of 650 m in Milano Marittima (Italy), a beach that is maintained periodically by beach nourishment. For this purpose, experimental tests of the device were carried out in order to determine the wave transmission coefficient (K_T) as a function of the length of the device and the length of the incident wave. On this basis, the variations in the longshore sediment transport were assessed using the CERC formula (US Army Corps Of Engineers, 1984).

For the wave conditions analysed the wave transmission coefficient was approx. 0.8, and this resulted in a decrease of the sediment transport of 43%. Figure 2.29 shows the evolution of the sediment along the coastline in the presence and in the absence of the wave farm. The green lines (right image) show the net sediment transport, north

(positive) minus south (negative). It is interesting to notice that the reduction of the two components (North and South) is not proportional, and the distribution of the net transport in presence and in absence of the WEC is quite different. These results are very promising but need to be corroborated with more accurate studies. Furthermore, the distance of the farm to the coast contributed to reaching this degree of coastal protection.

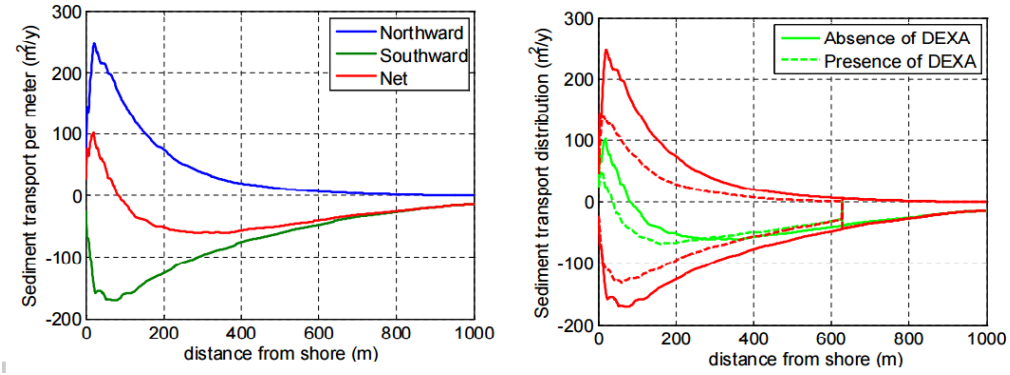

Figure 2.29 On the left hand, the distribution of sediment transport with the presence of the wave farm. On the right hand, the results with the farm (dashed line) are shown alongside the baseline scenario (solid line), with the green lines showing the net sediment transport, northward minus southward contribution (Ruol *et al.*, 2011).

Nørgaard, Andersen and Kofoed (2011) analysed the possibility of using a 3-Wave Dragon wave farm for coastal protection in the North Coast of Spain. For this purpose, a Boussineq-type wave model, MIKE21, was applied to analyse the impact of the wave farm using the transmission values obtained in the laboratory tests of a single Wave Dragon WEC. The impact of the wave farm was significant (Figure 2.30), corroborating the great potential of wave farms to reduce the wave height in their lee; with reductions by up to 21%. However, although the study outlined the possibility of using wave farms for protecting the coast, the effects on the coast were not assessed.

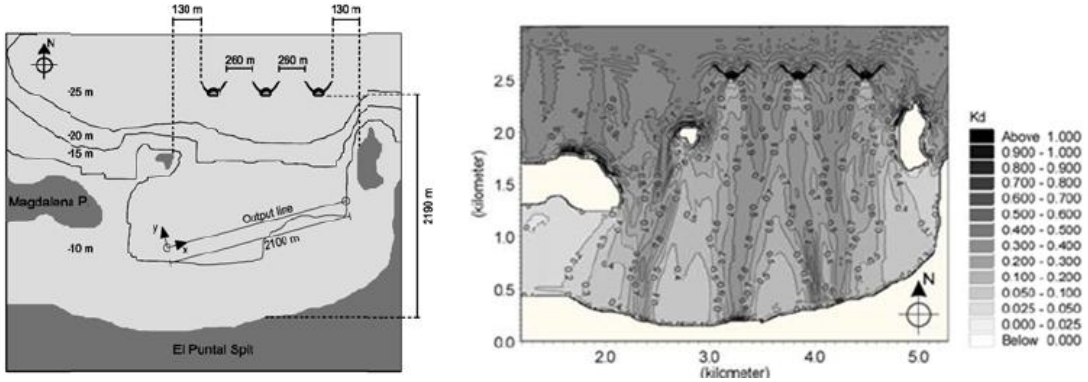

Figure 2.30 3-Wave Dragon wave farm layout (left) and effects on the wave conditions by means of the disturbance coefficient, K_D, under the following wave conditions: H_s = 5m, T_e = 10s and Direction = N (Nørgaard, Andersen & Kofoed, 2011)

Similarly, Zanuttigh and Angelelli (2013) studied the synergetic application of wave farms analysing the impacts of a wave farm formed by floating DEXA WECs in Santander (Spain). The investigation consisted of physical and numerical modelling. Regarding the former, tests of a single device (in a scale of 1:30) and a 3-WEC array (in a scale of 1:60) were carried out to determine the transmission coefficients. As for the latter, the impacts on the wave conditions were assessed applying MIKE21.

The results showed that the transmission coefficient of a single device was approx. 0.8, while in the case of the array the transmission coefficients in the lee of the device located in the second row varied from 0.6 to 0.9 as a function of the wave conditions. Based on these coefficients, the analysis of the wave farm impacts through numerical modelling showed a reduction of the wave height of up to 20% in some sections of the coastline (Figure 2.31). These results were of relevance as a wave-activated body was considered to protect the coast (as mentioned above, overtopping WECs are generally the most effective for this purpose) and their efficiency to attenuate the wave height in the lee of the farm was proven by means of physical and numerical modelling; however, the effects of the wave energy extraction on the coast were not quantified.

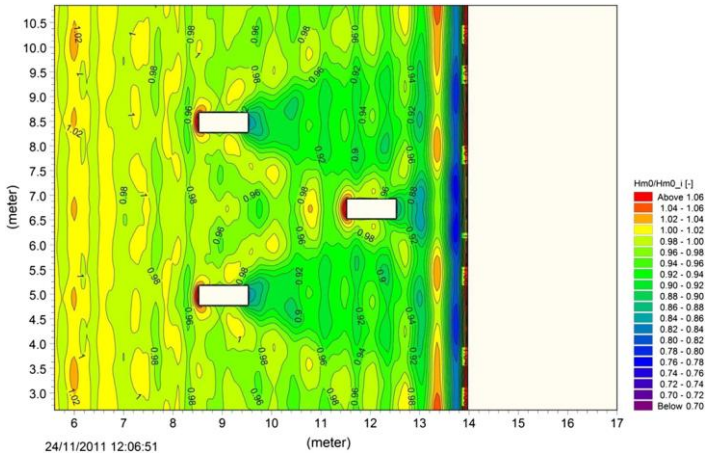

Figure 2.31 Ratio between local and incoming (target) wave height in presence of the wave farm. The white area represents the emerged beach extension (Zanuttigh & Angelelli, 2013).

Neill and Iglesias (2012) applied the cross-shore profile model, UNIBEST-TC, to analyse the impacts of extracting wave energy on the beach profile. Energy was extracted from the model boundary considering a 10% reduction in wave energy due to WEC array operation. Although this was a relatively simple approach to account for WEC array operation at the model boundary, it was sufficient to enable a first order examination of the environmental impact on nearshore processes.

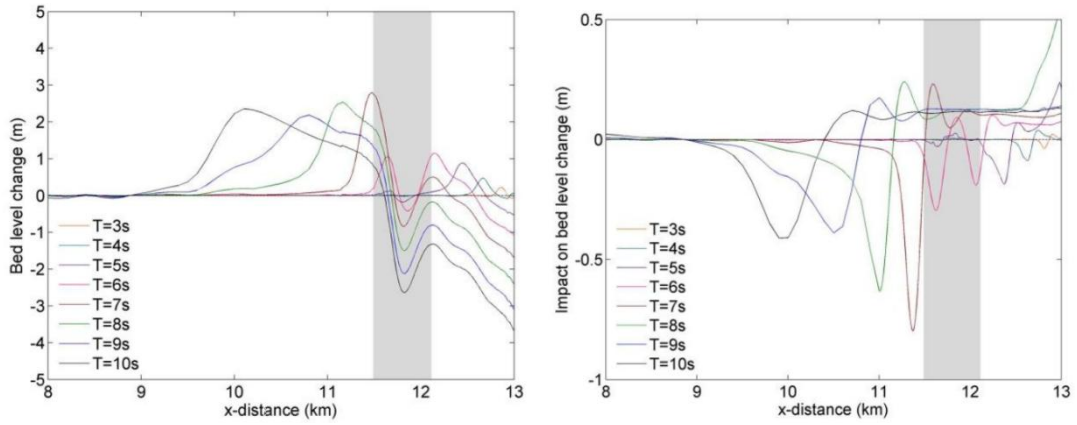

Figure 2.32 Natural change in bed level after 6 months of simulation (left) and considering the 10% reduction of wave energy due to the operation of a wave farm (right). Grey shading indicates position of sand bar at the beginning of each simulation.

The results shown above outline the capability of a wave farm to protect the coast by means of enhancing the sand bar formation. Since reduced water depth over the bar enhances depth-induced wave breaking, WEC array operation could provide enhanced coastal protection from storm waves. However, this statement needed to be tested for

variable wave forcing over seasonal timescales, and for more realistic WEC array energy extraction scenario.

Finally, Mendoza et al. (2014) investigated the effects of 4 different wave farms composed of 3 Wave Dragons arranged in 2 rows (overtopping), 8 Blow jets arranged in one row (hybrid system, whose main principle is overtopping), 45 DEXA arranged in 5 rows (wave-activated body) and 18 Seabreathe arranged in 2 rows (offshore OWC). The first two wave farms were located at Santander Bay (Spain) and the other two at Las Glorias Beach (Mexico). The impacts on the wave conditions were analysed by means of a 2D elliptic modified mild-slope model, WAPOQP; and the effects on the coast by applying the analytical solution presented in Kamphuis (1991b) for calculating Long-Shore Sediment Transport (LST). According to the type of WEC, the wave farms were located at different farm-to-coast distances, and consequently, water depths. Figure 2.33 shows the results at Santander bay, and can be readily observed the different effects on the wave patterns as a function of the WEC. The greater dimensions of the Wave Dragon resulted in a greater shadow in the lee of the farm.

Based on these results, the impact of the wave farm was analysed by means of the LST formula. In the case of Santander the beach studied was Somo (on the right hand of Figure 2.33). Using the rates of longshore sediment transport, an index was developed to compare the impact between the baseline and wave farm scenarios, x_p/x_u, which indicates the accretion (positive) or the erosion (negative) induced by the wave farm. Figure 2.34 shows the longshore sediment transport rates and the results for the index x_p/x_u, finding that the Wave Dragon and the DEXA WECs offered the greatest degree of coastal protection. However, if their effectiveness to protect the coast is analysed in terms of number of devices, it is clear that the overtopping device is the most appropriate for this purpose, as the array of DEXA WECs consisted of 45 devices,

while the Wave Dragon was formed by only 3. In any case, although these results were very promising they were based on the longshore sediment transport and the storm-induced erosion was not quantified. For this purpose, a coastal process model is needed.

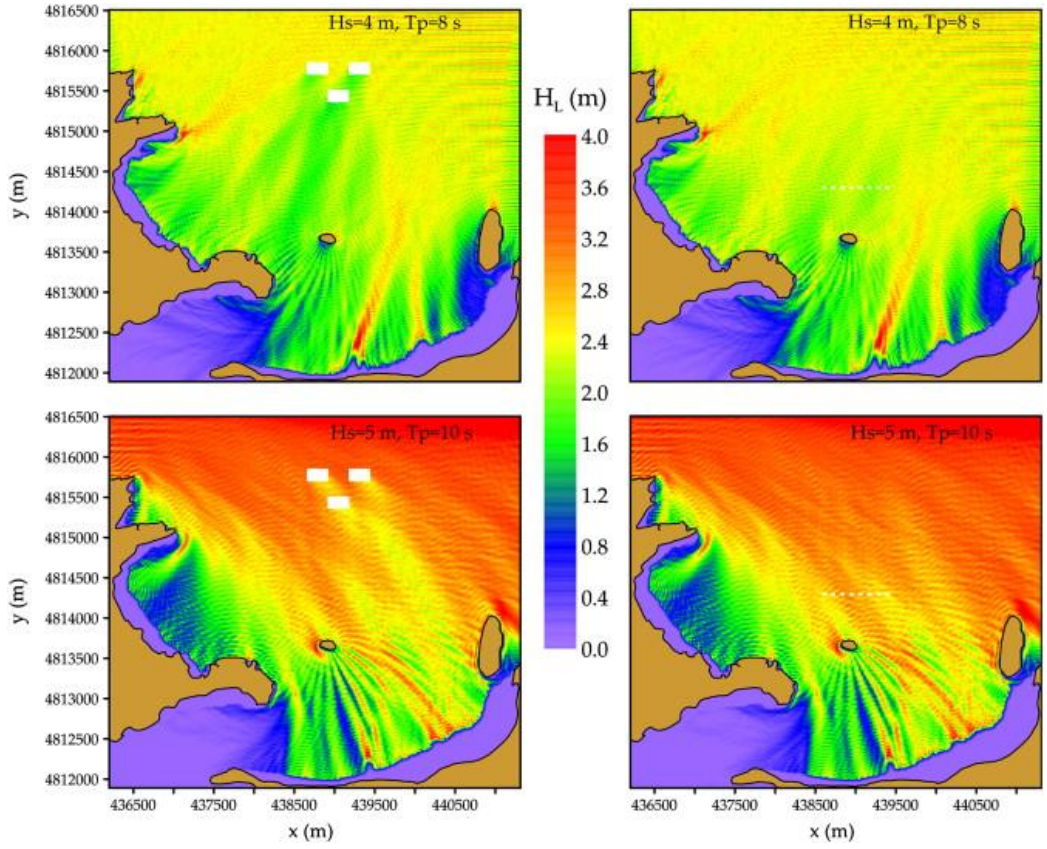

Figure 2.33 Wave farm effects on the wave conditions at Santander Bay: in the left column, a 3-Wave Dragon wave farm and in the right column a 8-Blow-Jet wave farm (right column). The wave conditions are indicated in the upper line (Mendoza *et al.*, 2014)

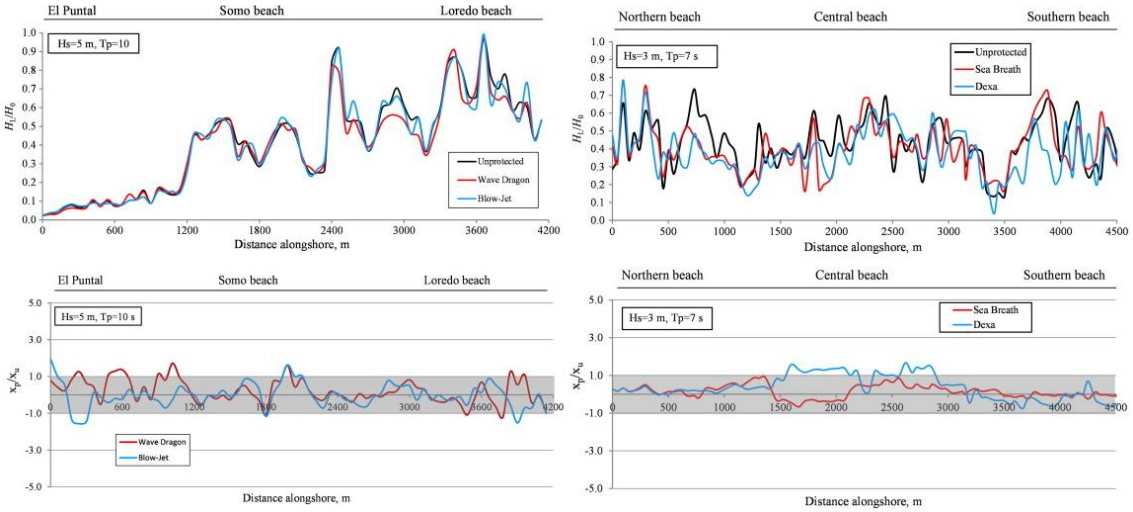

Figure 2.34 Coastline evolution trends for Santander and Las Glorias beaches under different wave farm scenarios (Mendoza *et al.*, 2014)

In summary, even though most of the works presented praised the effectiveness of wave farms for protecting the coast, this has not been deeply analysed so far. A clear attenuation of the wave height in the lee of the device was observed in practically all cases, which decreased towards the coastline, but was still significant at water depths below 10 m. Furthermore, analytical solutions have demonstrated that wave farms would reduce the longshore sediment transport in sandy beaches, which in turn, would result in savings from beach nourishment. However, the manner in which wave energy extraction by WECs affects the coastal processes, and in particular storm-induced erosion, have not been analysed yet, and this aspect is crucial, not least for being required for any Environmental Impact Assessment, but also to establish the degree of coastal protection that a wave farm can offer. On this basis, assessing wave farm impacts, both on the wave conditions and on the coastal processes, is the main focus of the present thesis.

Chapter 3

Methodology

Chapter 3

3. METHODOLOGY

This section presents the methods followed to bridge the gap in the knowledge of the wave farm impacts on the coast, and subsequently to establish the degree of coastal protection offered by wave farms. It will be divided in three sections: the first two will describe the numerical models applied to analyse the impacts on the wave conditions (Section 3.1) and the beach morphology (Section 3.2) and will be followed by the definition of a series of *ad hoc* impact indicators, most of them developed in the frame of this thesis to analyse the impacts of wave farms (Section 3.3). The numerical modelling sections will include a review of the main techniques and models to determine the optimum models for the purpose of the thesis.

3.1 MODELLING WAVE FARM IMPACTS ON THE WAVE CONDITIONS

Numerical modelling, in conjunction with laboratory tests, is one of the pillars to study the effects of wave farms. The wave farm-wave field interaction can be studied by means of phase-resolving or phase-averaged models. Phase-resolving techniques include potential flow models and those that resolve equations such as Navier-Stokes, Boussinesq and mild slope. On the other hand, phase-averaged methods are spectral wave models that resolve the wave action balance equation. In this context, a brief review of the different methods to model wave energy exploitation will be presented, illustrating with examples the applicability of the different models. The different methods and the main equations will be presented; nevertheless, a full description of the models will not be accomplished as it is out of the scope of this section, which actually aims to select the proper tool for studying the wave farm impacts on the wave conditions.

3.1.1 NAVIER-STOKE SOLVERS (CFD)

The term CFD stands for Computational Fluid Dynamics (CFD), and therefore, would encompass any model that resolves fluid mechanics; however, it is well known that this term is used to refer non-linear Navier-Stoke Solvers. The Navier-Stoke equations are based on the mass and momemtum conservation, accounting for processes as turbulence of viscous effects. They can be classified into two categories: (i) direct numerical simulation and (ii) CFD codes, in which some of the processes are resolved through parameterisation rather than being directly resolved.

CFD models present a large number of advantages, e.g. accounting for turbulence and two-phase flow, which indicate the model as the most appropriate for assessing breaking conditions or flows containing gas. For instance, these models are particularly relevant to study OWC WECs (López et al., 2014). On the downside, the main disadvantage of these models is their computational demand even in reduced scales due to the very fine mesh required for these models. As a consequence, CFD models were applied to determine the response of single WECs, and, therefore, their utilisation for investigating the effects of wave extraction in the lee of the devices is not suitable.

3.1.2 POTENTIAL FLOW MODELS

Among potential flow models, Boundary Element Method (BEM) has been the method most applied for marine renewable energy. They are primary based on the following assumptions:

- The fluid is invicid (i.e. frictionless)
- The flow is irrotational (i.e. the fluid particles are not rotating). Then, if $\phi(x,y,z,t)$ is the velocity potential function, the velocity can be derived at any point of the fluid domain as:

$$\vec{V}(x,y,z,t) = \vec{\nabla}\phi(x,y,z,t) \tag{3.1}$$

- The flow is incompressible, which leads to

$$\nabla^2 \phi(x, y, z, t) = 0, \tag{3.2}$$

in order to satisfy the Laplace's equation.

Nonetheless as the flow is irrotational, processes such as wave breaking cannot be accounted for. Furthermore, water depth is usually assumed constant along the array to simplify the problem, as the accurate representation of the bottom friction effects would increase considerably the computational time. In this line, BEM models have been generally applied to determine the WEC-wave field interaction within the wave farm (Babarit, 2010; Borgarino, Babarit & Ferrant, 2012; Child & Venugopal, 2007; Child & Venugopal, 2010), in most of them with the purpose of identifying the optimal layout for wave farms, as seen in Section 2.4 Wave farm impacts.

In sum, these models despite of numerous advantages are not recommended to describe the impacts of wave energy extraction on the coast in the lee of the farm, especially in shallow waters when coastal processes such as wave breaking, shoaling and refraction occur.

3.1.3 BOUSSINESQ MODELS

Boussinesq-type wave models are based on the classic Boussinesq equations (Peregrine, 1967), which basically do not account for the vertical component of velocity, assume the horizontal velocity constant along the depth, the fluid incompressible and the flow irrotational, in order to approximate wave propagation. This approximation is not accurate in shallow waters due to the non-linearity and dispersion properties of waves. Therefore, the depth averaging limits their application to water depths of up to 0.25 times the deep water wave length.

In view to improving the applicability of these equations in both shallow water and deep water the classic Boussinesq equations were enhanced to account for the effects of deeper water depths, varying bathymetries, frequency dispersion, wave breaking, among others. Then, one of the most representative models, MIKE21BW, is based on the enhanced Boussinesq equations and calculates the free surface elevation from the flux density, rather velocities as potential flow models do. The model accounts for the most important wave transformation such as shoaling, refraction, diffraction, wave breaking and non-linear wave-wave interaction. On the other hand, the complexity of Boussinesq models limit their application for running time series of several hours and the model can become unstable under some circumstances.

Regarding their applicability to marine renewable energy, the model has been applied to determine the impact of wave farms on the wave conditions in their lee under different wave conditions (Nørgaard, Andersen & Kofoed, 2011; Venugopal & Smith, 2007; Vidal *et al.*, 2007; Zanuttigh & Angelelli, 2013), but its applicability for time series is not recommended due to the computational costs associated.

3.1.4 MILD SLOPE WAVE MODELS

Mild-slope models receive their name as were developed to describe the propagation of the waves over low gradient bathymetries. They are based on the Mild-slope equations (Berkhoff, 1974), which are a type of depth-averaged equation derived from the potential flow theory. The simplicity of the original equation presented several limitations given that only linear and monochromatic waves were propagated over mildly varying bathymetries; nonetheless the recent enhanced forms of the equation allow the consideration of processes such as wave breaking, diffraction, nonlinearity of waves and bottom friction. The equation can be presented in its fully-fledged elliptical version (the most complex) or in its parabolic and hyperbolic incarnations.

Several models based on the different forms of the equation (MILDwave, OLUCA-SP, WAPOQP, REFDIF) have been used to study the effects of wave farms within the wave farm as well as in its lee (Beels *et al.*, 2010a; Beels *et al.*, 2010b; Mendoza *et al.*, 2014; Palha *et al.*, 2010). The model is considerably faster solving wave propagation than the aforementioned ones; nonetheless, as it depends on the potential wave theory, it has insufficient theoretical foundation to deal with physical processes as reflection and diffraction.

3.1.5 SPECTRAL MODELS

Finally, spectral wave models are phase-average models, which rather than predicting the surface elevation of the waves through a suite of equations, resolve the evolution of the directional spectrum as waves propagate over varying water depths by means of the energy conservation equation (Hasselmann, 1971; Longuet-Higgins & Stewart, 1961). Hence, these models compute the wave action, which consists of the spectral energy density divided by the intrinsic frequency. The new third-generation of wave models (which refers to those that account for all the physics relevant for the development of the sea state) predicts accurately the growth, decay and transformation of wind-generated waves and swells in the deep waters and shelf-seas. Thus, spectral models are capable of representing most of the wave transformation processes: shoaling, depth- and current-induced refraction, wind forcing, whitecapping, bottom friction dissipation, depth-induced breaking and non-linear quadruplet and triad wave-wave interactions. On the downside, as phase-averaged models, the diffraction cannot be calculated explicitly; nevertheless, in the case of SWAN (one of the most used wave propagation models) it can be modelled through a phase-decoupled refraction-diffraction approximation.

Regarding their applicability to study wave farm impacts, wave spectral models, and particularly SWAN, have been the most used numerical method (Carballo &

Iglesias, 2013; Gonzalez, Zou & Pan, 2012; Iglesias & Carballo, 2014; Millar, Smith & Reeve, 2007; Reeve et al., 2011b; Rusu & Guedes Soares, 2013; Smith, Millar & Reeve, 2007; Smith, Pearce & Millar, 2010). As they solve the energy conservation equation, the implementation of the wave farms into the model is carried out by means of transmission coefficients that represent the absorption of wave energy brought about by the WECs. This approach does not account for the energy radiated, which will be of relevance in the case of wave-activated bodies. However, for overtopping devices, it can be assumed negligible, especially to study the effects of a wave farm on the coast.

Hence, in view of the aims and objectives of this thesis (Section 1.2) and considering the efficiency of wave spectral models to propagate long time series, the use of these models, in this case SWAN, is the most appropriate approach. A brief introduction of the model will be presented in the following section.

3.1.5.1 SWAN

Mathematical model

Simulating WAves Nearshore, SWAN (Booij, Ris & Holthuijsen, 1999), is a third-generation wave model that estimates the characteristics of the waves (significant wave height, peak period, mean direction, etc., or even more accurately, the directional wave spectrum) in coastal areas, lakes and estuaries from given wind, bottom and current conditions.

The model solves the spectral wave action balance equation without a priori assumptions on the shape of the wave spectrum. The wave field is described by the two-dimensional wave action density spectrum, $N(\omega,\theta)$, where ω is the angular wave frequency and θ is the wave direction. The wave action density spectrum is used in lieu of the energy density spectrum, for action density is conserved in the presence of currents whereas energy density is not; in any case, the wave energy spectrum may be

computed from the wave action spectrum. The wave action balance equation is discretised by means of the finite difference method in time, geographic space (x,y), and spectral space (ω,θ).

The spectral wave action balance equation reads

$$\frac{\partial N}{\partial t}+\frac{\partial(c_x N)}{\partial x}+\frac{\partial(c_y N)}{\partial y}+\frac{\partial(c_\omega N)}{\partial \omega}+\frac{\partial(c_\theta N)}{\partial \theta}=\frac{S}{\omega} \tag{3.3}$$

The first term on the left-hand side represents the local rate of change of wave action density in time; the second and third terms stand for the propagation of wave action over geographical space, with propagation velocities c_x and c_y in the x and y directions respectively; the fourth term quantifies the shifting of the relative frequency due to variations in depths and currents, with propagation velocity c_ω in the ω direction; finally, the fifth term represents the effects of refraction induced either by depth variations or by currents, with propagation velocity c_θ in the θ direction. The expressions of the above propagation velocities are derived from linear wave theory. As for the right-hand side of the equation, S includes the source and sink terms of physical processes which generate, dissipate or redistribute wave energy:

$$S=S_{nl4}+S_{nl3}+S_{in}+S_{wc}+S_{bot}+S_{brk} \tag{3.4}$$

where S_{nl4} refers to the redistribution of energy by nonlinear quadruplet wave–wave interactions, S_{nl3} the non-linear triad redistribution of wave energy, S_{in} the transfer of energy from the wind to the waves and the dissipation of wave energy due to whitecapping, S_{bot} the sink term of energy dissipation by bottom friction and S_{brk} the energy dissipation in random waves due to depth-induced breaking.

The wave energy flux, also called wave power, is computed on its $x-$ and $y-$ components with the two following expressions:

$$J_x = \int_0^{2\pi} \int_0^{360} \rho g c_x E(\sigma,\theta)\, d\sigma\, d\theta \tag{3.5}$$

$$J_y = \int_0^{2\pi} \int_0^{360} \rho g c_y E(\sigma,\theta)\, d\sigma\, d\theta \tag{3.6}$$

where $E(\sigma,\theta)$ is the directional spectral density, which specifies how the energy is distributed over frequencies (σ) and directions (θ). The wave power magnitude is then calculated as

$$J = \left(J_x^2 + J_y^2\right)^{\frac{1}{2}} . \tag{3.7}$$

The whole set of the governing equations regarding the spectral description of wind waves, the propagation of wave energy, the source and sinks, the influence of ambient current on waves, the modelling of obstacles and the wave-induced set-up can be found at SWAN's manual (SWAN, 2007).

Numerical model application

SWAN has been developed to simulate coastal wave condition, and for this purpose the essential input data consists in a detailed bathymetry and the incident wave and wind field. The wave and wind data can be prescribed offshore coupling SWAN with larger scale models. In the case of the present document, the wave data is obtained with a three-hourly frequency from WaveWatch III, a third-generation offshore wave model consisting of global and regional nested grids with a resolution of approx. 50 km (Tolman, 2002b). In the same line, the wind data was provided from the Global Forecast System (GFS) weather model.

The best practice to apply the model efficiently is through various grids, refining the grid towards the area of interest. In this line, the nesting concept is a very important implementation in order to reduce computational time and enhance accuracy, and it refers to computations conducted first on a coarse grid for a larger region and using the results as boundary conditions for a finer grid in the region of interest. The same types of coordinates (cartesian or spherical) have to be used in order to apply nesting. It is important to mention that curvilinear grids can be used for nested computations, but the boundaries should always be rectangular. Moreover, SWAN can also simulate unstructured grids, also called irregular grids and consists of triangles or tetrahedrons in an irregular pattern. This is relevant for complex bottom topographies in shallow areas and irregular shorelines.

Hence, as calculations are performed on a grid, SWAN is an Eulerian model that accounts for refractive propagation over varying bathymetries and current fields by solving the discrete balance equation. SWAN provides a representation of directional and non-directional spectrum at any point of the computational grids through spectral and time-dependant parameters of waves, e.g. wave height, peak or mean period, wave direction and energy transport.

On these grounds, the application of SWAN in this thesis will be conducted using two computational grids, a coarse grid from offshore to the coast and a high-resolution nested grid in the area of interest. The resolution of the nested grid allows the precise definition of the WEC position in the array and the simulation of their individual wakes with accuracy. This is a prerequisite to a detailed assessment of the wave farm effects (Carballo & Iglesias, 2013). The device that will be considered for the study is the WaveCat Overtopping WEC, as explained in Section 2.3.2 WEC technologies. The WEC-wave field interaction will be modelled by means of the wave transmission

coefficients obtained in the laboratory tests (Figure 2.13) conducted at the laboratory of Porto by Fernandez *et al.* (2012). The transmission coefficients were calculated as the ratio between the wave heights measured in the lee and in front of the device under different wave conditions. The results showed that the wave transmission coefficient presented very small variability ($K_t \sim 0.76$), and therefore a constant value will be used in the medium- and long-term analysis. The limited range of wave conditions impeded the development of a frequency-dependant model; however, this is included in the future lines of research as part of the European WAVEIMPACT project lead by Prof Gregorio Iglesias and that is focussed on the interaction between a wave farm and the ocean through laboratory tests and numerical modelling (vid Section 10.2 Future Research lines)

3.2 MODELLING WAVE FARM IMPACTS ON THE BEACH MORPHOLOGY

The results of the wave propagation model will be coupled to a coastal processes model for the first time for this purpose. Applying a coastal processes model, the natural coastal response during time-varying storm conditions can be assessed. In this sense, the effects on the coast of the modification of the wave conditions caused by the wave farm will be studied in this thesis in order to establish the effectiveness of wave farms to protect the coast.

While the number of wave models and theories is large, the number of models to describe the beach morphodynamics is limited. The coastal processes models could be classified in two categories: depth-averaged and depth-resolving models. The latter correspond with phase-resolving models, primarily Boussinesq models; which resolve the wave field on the time scale of individual waves and are capable to model the non-linear evolution of the wave field with accuracy. However, despite of their advantages to simulate the wave field, their representation of the coastal processes is less efficient.

Furthermore, depth-integrated models require higher computational costs and this make them not appropriate for simulating storm clustering.

On the other hand, depth-averaged models have evolved from 1DH (2D) to 2DH (3D). The Storm-induced BEAch Change, SBEACH (Larson & Kraus, 1989) model was one of the first numerical models to analyse beach erosion and is cross-shore beach numerical model to analyse berm, and dune storm-induced erosion. The model is limited to cross-shore given that to account for the landward transport, heuristic approaches can be adopted, but their application to analyse the beach morphology (3D) is very complicated. In this context, XBeach is a three-dimensional model for wave propagation, long waves and mean flow, sediment transport and morphological changes of the nearshore area, beaches, dunes and back barrier during storms.

Moreover, the model has been widely and successfully applied to simulate the beach response under storm conditions (Callaghan, Ranasinghe & Roelvink, 2013; McCall et al., 2010; Pender & Karunarathna, 2013; Roelvink et al., 2009; Splinter et al., 2014), so XBeach is the most appropriate coastal processes model to analyse the effects of wave energy extraction on the beach.

3.2.1 XBEACH

Model equations

The model solves coupled 2D horizontal equations for wave propagation, flow, sediment transport and bottom changes, for varying (spectral) wave and flow boundary conditions. Wave processes are solved with the time dependent wave action balance equation (2.4) coupled to the roller energy equations and the nonlinear shallow water equations of mass and momentum; and sediment transport are modelled with a depth-averaged advection diffusion equation on the scale of wave groups.

The wave group forcing is derived from the time-varying wave action balance with a dissipation model different to the presented for the wave propagation model and allows the combination with wave groups. A roller model is used to represent momentum stored in surface rollers which leads to a shoreward shift in wave forcing. The wave-group forcing drives infragravity motions and both longshore and cross-shore currents. To model these infragravity waves and unsteady wave-induced currents, in addition to surface elevations and flows, the shallow water momentum and mass balance equations are implemented by means of the Generalized Lagrangian Mean formulation. These equations are not presented given that are out of the scope of this thesis and can be found in the XBeach's manual (Roelvink et al., 2006), however the depth-averaged advection diffusion equation (Galappatti & Vreugdenhil, 1985) is presented below due to its importance in the erosion process,

$$\frac{\partial(hC)}{\partial t}+\frac{\partial(hCu^E)}{\partial x}+\frac{\partial}{\partial x}\left(D_s h\frac{\partial C}{\partial x}\right)+\frac{\partial(hCv^E)}{\partial y}+\frac{\partial}{\partial y}\left(D_s h\frac{\partial C}{\partial y}\right)=\frac{hC_{eq}-hC}{T_S} \tag{3.8}$$

where the *x*- and *y*-coordinate represent the cross-shore and longshore direction, respectively, C is the depth-averaged sediment concentration, D_s is the sediment diffusion coefficient, the terms u^E and v^E represent the Eulerian flow velocities, T_s is the sediment concentration adaptation time scale that depends on the local water depth and the sediment fall velocity, and C_{eq} is the equilibrium concentration according to the Van Rijn-Van Thiel formulation (Van Thiel de Vries, 2009), thus representing the source term in the sediment transport equation.

The novelty of this model lies in the computation of the sediment transport in the time-scale of wave groups since they dominate the flow during overwash in conjunction with a robust momentum conserving drying/flooding formulation regimes. Furthermore, as the model takes into account the variation in wave height in time it resolves the long

wave motions created by this variation, so-called ‘surf beat’, and is responsible for most of the swash waves that actually hit the dune. Hence, XBeach is more capable to model the development of the onshore/offshore sediment transport.

Numerical model application

Similarly to SWAN, the necessary data to simulate the beach response using XBeach is bathymetry data and wave and water level conditions. The bathymetric data, gathered during field campaigns, is interpolated onto the grids. In the case of coastal processes models, it is not common to use the concept of nested grids to study the response of beaches. Regarding the water levels and wave conditions, the model allows the implementation of water level time series to all four corners of the model domain and wave forcing on the offshore boundary. In this line, the definition of the grid should be aligned with the direction of the beach in order to cover with one of the contours the beach area, and with the opposite the offshore one. Thus, the offshore wave conditions, extracted from SWAN, will be prescribed in this offshore boundary. Finally, the results of the bed levels, water levels, water depths and concentrations are defined in the cell centres, and velocities and sediment transports are defined at the cell interfaces.

3.3 IMPACT INDICATORS

The wave farm impacts on the nearshore wave conditions and the beach morphology were analysed be means of a series of impact indicators.

3.3.1 WAVE CONDITION INDICATORS

The farm impacts on the nearshore wave conditions were analysed by means of the : (i) the Reduction in the Significant wave Height, *RSH*, and (ii) the average wave power of the wave farm, $\overline{J}_{WEC}$. These indicators are applied to the results of the wave propagation model.

The quantification of the attenuation of the wave height in the lee of the device is carried out by means of the Reduction in the Significant wave Height (*RSH*) index, defined by

$$RSH(x,y) = \frac{(H_{s,b}(x,y) - H_{s,f}(x,y))}{H_{s,b}(x,y)} \ , \tag{3.9}$$

where $H_{s,f}$ and $H_{s,b}$ are the significant wave height with and without the wave farm, respectively, at a point in the coast designated by its coordinates (*x*,*y*), with the *x*-coordinate referring to the easting and the *y*-coordinate to the northing of the computational grids of the wave propagation model.

The average wave power of a WEC, $\overline{J}_{WEC}$, quantifies the average resource available in front of a generic WEC of the wave farm. This indicator is defined to compare the resource found at different locations and varying the key design wave farm parameters, e.g. farm-to-coast distances and spacing between devices. $\overline{J}_{WEC}$, in units of Wm^{-1} in the SI, is defined as

$$\overline{J}_{WEC} = \frac{1}{M\,N} \sum_{n=1}^{N} \sum_{m=1}^{M} J_{n,m} \tag{3.10}$$

where the index $n = 1 \ldots N$ refers to the WEC, with N the total number of WECs in the farm, $m = 1 \ldots M$ refers to the point in time, based on the discretisation

$$t = m\Delta t \tag{3.11}$$

where t is time and M is the total number of time points studied and $J_{n,m}$ is the wave power incident on the n-th WEC at the m-th point in time, which is calculated applying the equation (2.7).

Finally, the total incident power in the device is calculated through the capture width, which computes the wave crest captured by the device. This factor varies according to the type of WEC and for the case of the WaveCat is the distance between its twin bows, equal to 90 m.

3.3.2 BEACH INDICATORS

The *ad hoc* impacts on the coastal morphodynamics were studied applying the impact indicators developed in the framework of this thesis: (i) Bed Level Impact (*BLI*), (ii) beach Face Eroded Area (*FEA*), (iii) Non-dimensional Erosion Reduction (*NER*), and (iv) mean Cumulative Eroded Area (*CEA*). These impact indicators are applied to the results of the coastal propagation model and allow the quantification of the offshore/onshore and alongshore sediment transport.

The bed level impact *(BLI)*, with units of m in the S.I., represents the change in bed level caused by the wave farm and is defined as

$$BLI\left(x,y\right)=\zeta_f\left(x,y\right)-\zeta_b\left(x,y\right), \tag{3.12}$$

where $\zeta_f(x,y)$ and $\zeta_b(x,y)$ are the seabed level with the farm and without it (baseline), respectively, at a generic point of the beach designated by its coordinates (x,y) in the computational grid of the coastal processes model. The y-coordinate axis follows the general coastline orientation, with the y-coordinate increasing towards the eastern end of the beach, and the x-coordinate represents the beach profiles with x-values increasing towards the landward end of the profile. A positive value of *BLI* signifies that the seabed level is higher with the farm than without it.

The storm-induced erosion in the beach face area, which corresponds to the seaward section of the beach exposed to and shaped by the action of waves, is quantified by the

beach face eroded area (*FEA*) indicator, with units of m^2 in the S.I., and it is defined in both scenarios, baseline (FEA_b) and with the wave farm (FEA_f):

$$FEA_b(y) = \int_{x_1}^{x_{max}} \left[\zeta_0(x,y) - \zeta_b(x,y)\right] dx, \tag{3.13}$$

$$FEA_f(y) = \int_{x_1}^{x_{max}} \left[\zeta_0(x,y) - \zeta_f(x,y)\right] dx, \tag{3.14}$$

where $\zeta_0(x,y)$ is the initial bed level at the point of coordinates (x,y), and x_1 and x_{max} are the values of the x-coordinate at the seaward end of the beach face and landward end of the profile, respectively. The *FEA* indicator is a profile function, and hence depends on only the y-coordinate.

The non-dimensional erosion reduction (*NER*) is also a profile function, in this case non-dimensional, defined as

$$NER(y) = \frac{FEA_b - FEA_f}{FEA_b}. \tag{3.15}$$

It expresses the variation in the eroded area of a generic profile (y) brought about by the wave farm as a fraction of the total eroded area of the same profile. A positive or negative value implies a reduction or increase in the eroded area as a result of the wave farm.

Finally, the mean cumulative eroded area (*CEA*), with units of m^2 (or m^3 per linear metre of beach) in the S.I., was also determined in the baseline (CEA_b) and with the wave farm (CEA_f) scenario. For its definition, three reference profiles were considered: P1, P2 and P3 (Figure 3.14). For each of these the beach was divided into two parts, to

the north (CEA_b^N and CEA_f^N) and south (CEA_b^S and CEA_f^S) of the reference profile, and the corresponding indicators were computed from

$$CEA_b^S(x) = \frac{\int_{y_0}^{y_P}\int_{x_0}^{x}[\zeta_0(\chi,y)-\zeta_b(\chi,y)]\,d\chi\,dy}{(y_P - y_0)}, \tag{3.16}$$

$$CEA_f^S(x) = \frac{\int_{y_0}^{y_P}\int_{x_0}^{x}[\zeta_0(\chi,y)-\zeta_f(\chi,y)]\,d\chi\,dy}{(y_P - y_0)} \tag{3.17}$$

$$CEA_b^N(x) = \frac{\int_{y_P}^{y_{\max}}\int_{x_0}^{x}[\zeta_0(\chi,y)-\zeta_b(\chi,y)]\,d\chi\,dy}{(y_{\max} - y_P)}, \tag{3.18}$$

$$CEA_f^N(x) = \frac{\int_{y_P}^{y_{\max}}\int_{x_0}^{x}[\zeta_0(\chi,y)-\zeta_f(\chi,y)]\,d\chi\,dy}{(y_{\max} - y_P)}, \tag{3.19}$$

where χ is the variable of integration representing the coordinate along the profile, and x and x_0, and y_0, y_{max} and y_P are the limits of integration along the profile and along the coast, respectively. x_0 is the value of the x-coordinate corresponding to the first point of the profile and x takes values from x_0 to x_{max}. Along the beach, y_0 is the value of the y-coordinate corresponding to the westernmost point of the beach, y_{max} the easternmost point and y_P the value corresponding to the reference profile. The factor represents the average cumulative eroded area of the two sections of the beach along the profile (x). A positive value signifies that the mean volume of material along the section of the beach is reduced compared with the initial situation (erosion).

Chapter 4
Case Studies

4. CASE STUDIES

A number of aspects are considered in the selection of the cases studies: the wave energy resource, the threat of coastal erosion in the adjacent beaches, the distance to populated areas and the availability of data (water level, wave field and bathymetric). Following this, two case studies are selected along the Atlantic façade of Europe: Perranporth and Xago Beach, located in the SW England and N Spain, respectively.

While at Xago Beach the location of the wave farm is delimited by the Asturian Institution for Energy Development (FAEN), at Perranporth Beach there is no defined area, which allows the study of the role played by several key design parameters, e.g. the farm-to-coast distance and the farm layout (vid Chapter 7, 8 and 9).

In this chapter, the main features and data of both beaches will be presented.

4.1 PERRANPORTH BEACH

Perranporth Beach is a 3.6 km sandy beach located in Cornwall, SW England (Figure 4.1). The selection of this case study is motivated by two main reasons: (i) the erosion experienced by the beach over the last years, and particularly under the storms of February 2014; and (ii) the interest of the area for wave energy development, as shown e.g. by the nearby Wave Hub – a grid-connected offshore facility for WEC testing.

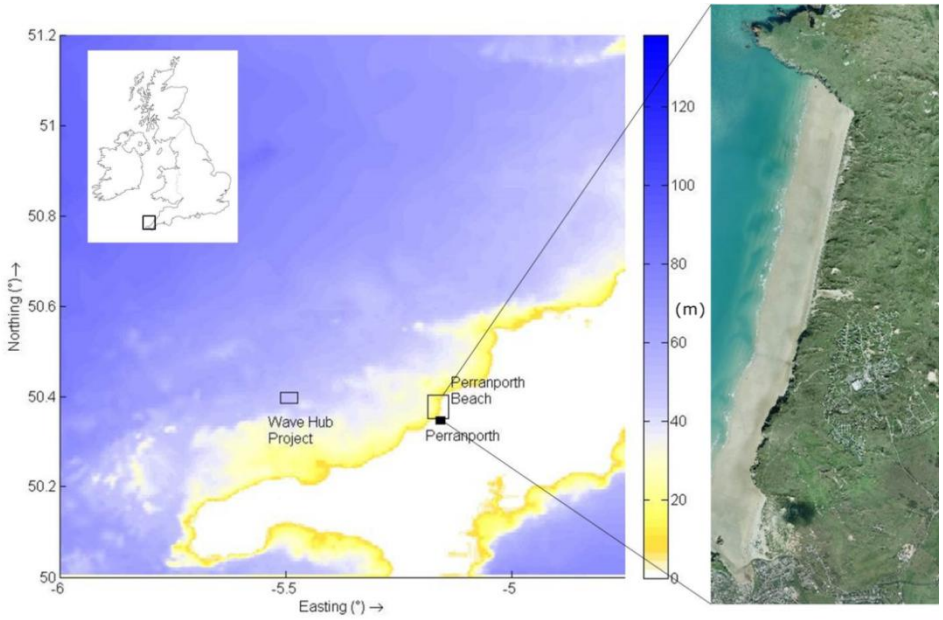

Figure 4.1 Location of Perranporth Beach and the Wave Hub in SW England [left; water depths in m], and aerial photo of the beach [right; courtesy of Coastal Channel Observatory].

Regarding the coastal erosion issues, the dune erosion during the storms of winter 13/14 threatened the foundations of many properties in the waterfront as can be seen in Figure 4.2. The Cornwall Council estimated that $1x10^6$ tonnes of sand were washed out at Perranporth Beach, i.e. 210.28 m^3/m (cubic metres per metre width of beach) were eroded during that winter (Watknis, 2014). Furthermore, these figures are set to increase as a result of sea-level rise and increased storminess due to climate change, e.g. Pugh (2004), Stocker et al. (2014) and Chini et al. (2010). Then, it is hard to overstate the economic and environmental consequences of coastal erosion: loss or damage to property and infrastructure, losses through decreased revenues in the tourist and recreational sectors, etc.

In this line, the Cornwall and the Isles of Scilly Coastal Advisory Group declared Perranporth subject to flooding and erosion in the latest Shoreline Management Plan (CISCAG, 2011) and, stated that, although it is not recommended to carry out any short-term action, it is necessary to monitor the beach as current erosive trends could risk many properties, and therefore intervention would be required in the near future. For

these purposes, a substantial investment (over £3.2 billion from April 2010 to March 2015) has been and will be undertaken by the Department for Environment, Food & Rural Affairs (DEFRA) to manage areas in flood and coastal erosion risk (DEFRA, 2015b).

Figure 4.2 Damages at Perranporth Beach after storms in winter 2013/14. Courtesy of West Briton.

Regarding the resource, the area has been identified as a prime region for the development of wave energy, as explained in Section 2, and has attracted research attention from the characterisation of the resource (Martinho & Soares, 2011; van Nieuwkoop et al., 2013) to the determination of the wave farm impacts on the wave conditions (Gonzalez-Santamaria, Zou & Pan, 2013; Millar, Smith & Reeve, 2007; Reeve *et al.*, 2011b; Smith, Pearce & Millar, 2010).

As for the beach, Perranporth is located on the north coast of Cornwall and faces the Atlantic Ocean and Perran Bay. It lies between two rocky headlands and is oriented northeast-southwest. The beach is backed by a sandy dune, which has been designated as a Special Area of Conservation by the European Union. The beach has a relatively flat intertidal area, tan $\beta = 0.015 - 0.025$, and a medium sand size, $D_{50} = 0.27 - 0.29$ mm, derived from the erosion of rocky shores and cliffs (Austin et al., 2010). The Mean Spring tidal Range (MSR) is 6.3 m (macro-tidal beach) and the tidal regime is semidiurnal.

The beach is characterised by the occasional presence of a submarine bar, at water depths between -5 and -10 m, particularly in winter, which forms part of the response mechanism of the natural system to protect the beach face from increased wave attack. It has a bearing on behaviour of the beach; under energetic waves and increased offshore sediment transport, it grows at the expense of the intertidal beach face. This causes that waves break over the bar and create rip circulation. These rip currents are anti-clockwise and are controlled by the gaps in the bar. In this sense, the beach has been described as dissipative (Butt, Russell & Turner, 2001; Masselink et al., 2005) and as a low-tide bar rip system (Scott, Masselink & Russell, 2011; Scott et al., 2007), with Austin *et al.* (2010) indicating that it is at the transition between the low tide bar/rip and dissipative beach.

The beach profiles used in this document were obtained through field surveys conducted by the Coastal Channel Observatory. The surveys conducted at the end of summer at Perranporth Beach, are generally associated with less energetic wave conditions. The beach profile evolution is characterised during the summer by an increase of the sediment transport onshore. In contrast, offshore movement of sediment is the predominant phenomenon during the winter owing to the more energetic wave conditions, which results in a lowering of the intertidal beach face. Indeed, most of the profile changes at Perranporth Beach occur in the lower intertidal to sub-tidal active regions (Scott, Masselink & Russell, 2011).

The wave conditions are described using half-hourly data from the directional wave buoy off Perranporth, in approximately 10 m of water, operated by the Coastal Channel Observatory. The analysis of these reflects the exposure of the area to heavy swells generated by the long Atlantic fetch, as well as to locally generated wind seas. The average significant wave height (H_s), peak period (T_p) and peak direction (θ_p) in the

period covered by the wave buoy data (2006 – 2014) were: 1.79 m, 10.36 s and 280°, respectively.

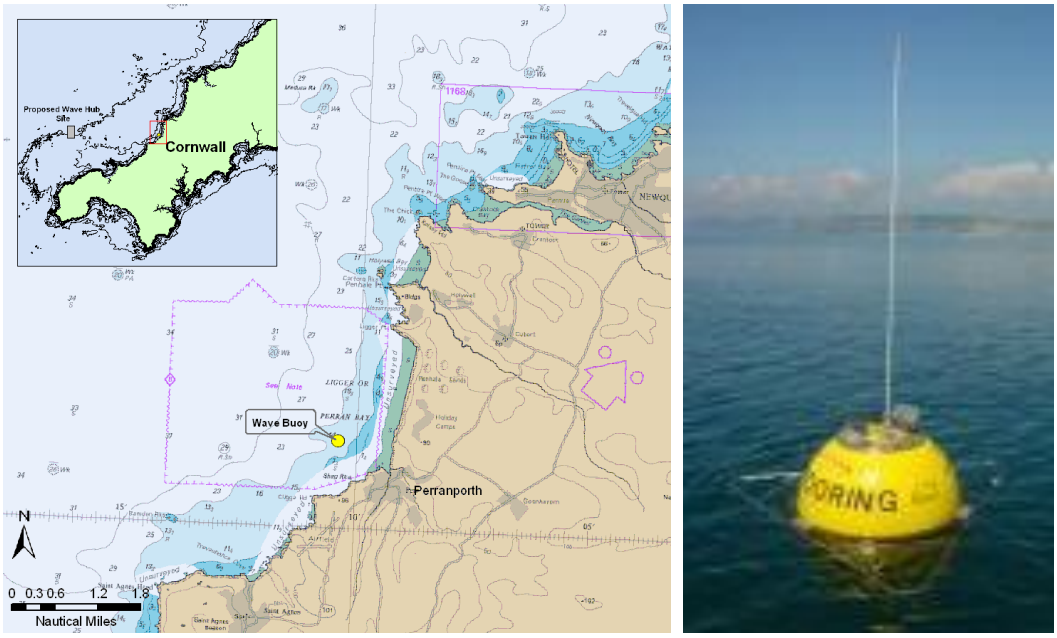

Figure 4.3 Location of the wave buoy deployed off Perranporth at a water depth of 10m. Chart (left) and photo (right) courtesy of Marine Digimap and Coastal Channel Observatory.

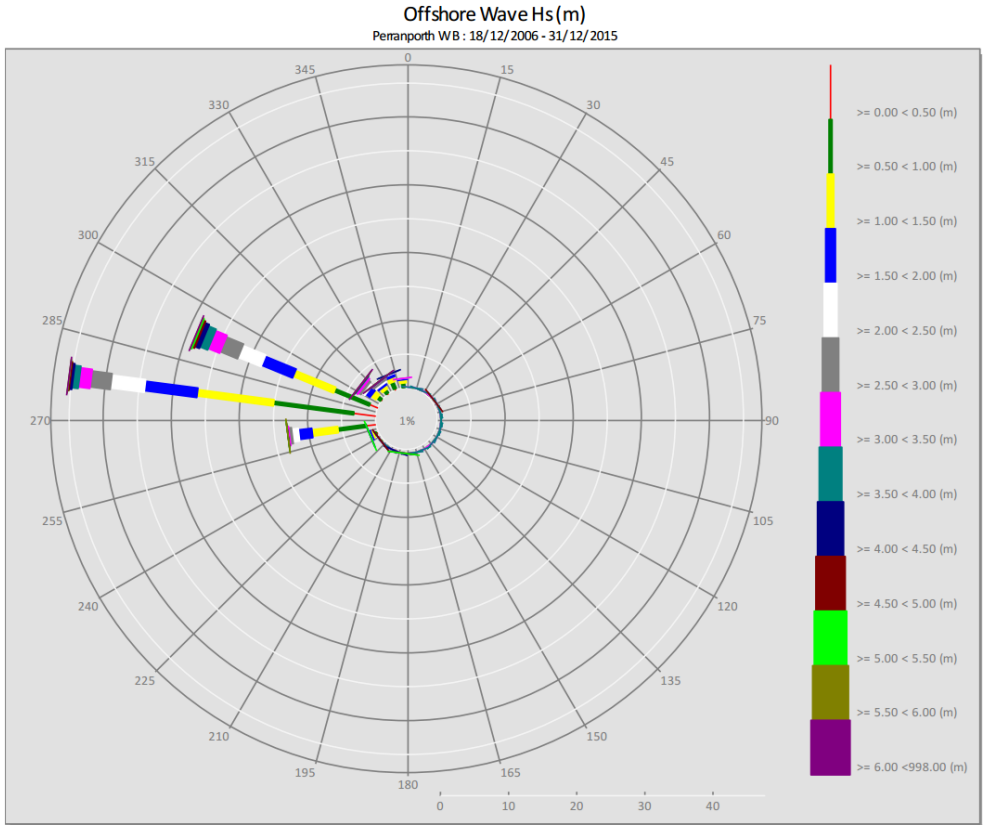

Figure 4.4 Significant wave height rose (m) at the offshore wave buoy off Perranporth from 18/12/2006 - 31/12/2015. Source: Coastal Channel Observatory

The wave rose off Perranporth (Figure 4.4) illustrates that waves come predominantly from the IV quarter (W-N). The mild waves (the most common) come from directions around the East, while the greatest waves are more likely from directions around the NW. This is also shown in Figure 4.5; where the wave heights over 4 m generally come from directions around 300°. Observing the period, the waves can be distinguished between swell and wind waves. The former and more frequent are associated to higher periods, in general peak periods over 10 s and are the result of the orientation of the coastline and its exposure to the long Atlantic fetch. Whereas the latter corresponds with periods around 5 s and are consequence of the strongest winds, usually from the NW, with the mean wind speed at a height of 10 m above the sea surface, $u_{10,}$ over 20 ms^{-1}.

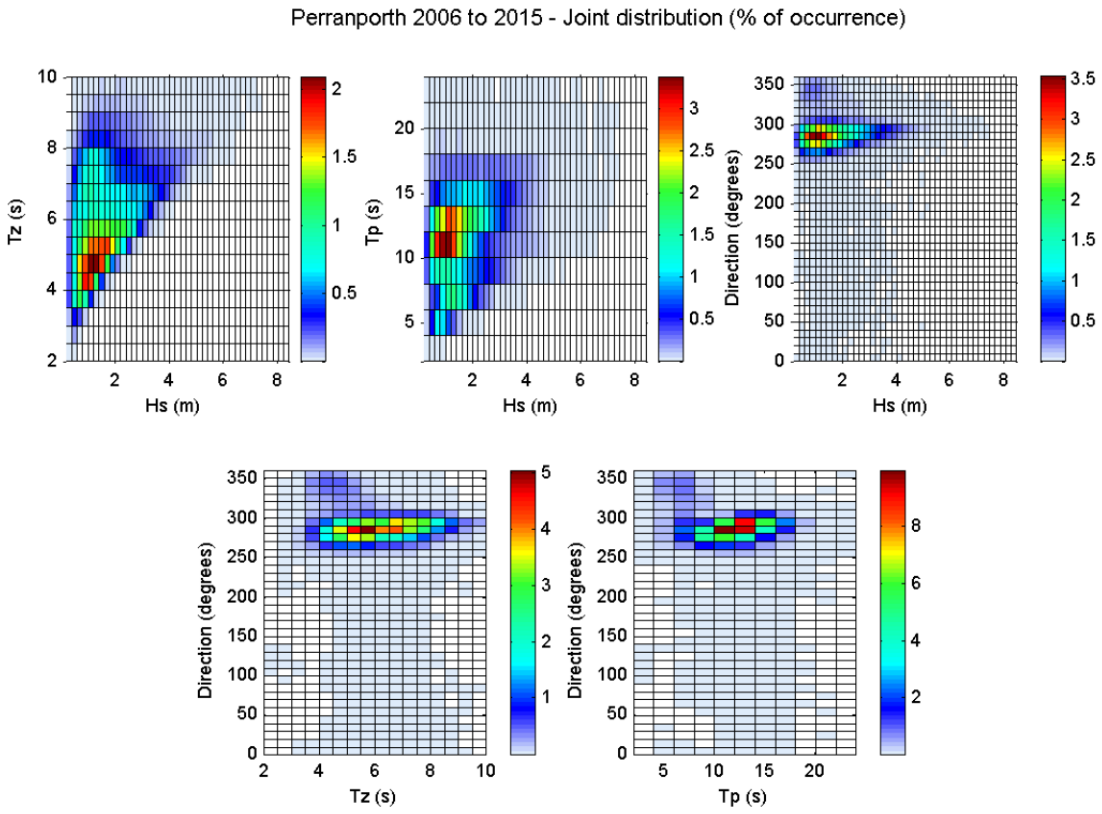

Figure 4.5 Joint distribution (% of occurrence) from 18/12/2006 - 31/12/2015 of the main wave parameters: Direction, Peak Period (T_p), Mean Period (T_Z) and Significant Wave Height (H_S). Source: Coastal Channel Observatory.

The wave data from the offshore buoy will be used to validate the results of the wave propagation model, which will be forced with the hindcast data from WaveWatch III, as explained in the Methodology (Section 3.1.5.1).

In addition, as the SW coast of England is characterised by a large tidal range, tide was included into the morphodynamic model with constituents obtained from the TPXO 7.2 global database, a global model of ocean tides that solves the Laplace equations using data from tide gauges and the TOPEX/Poseidon Satellite (Egbert, Bennett & Foreman, 1994) .

4.2 XAGO BEACH

Xago Beach, an approx. 2 km sandy beach located on the coast of Asturias (N Spain), was selected based on the studies of the Asturian Institution for Energy Development (FAEN), which defined two locations for the installation of the first offshore wave farm on the Spanish Coast (Figure 4.6): Xago and Llumeres Beach (Flor-Blanco *et al.*, 2011). The determination of these areas for wave energy exploitation were motivated by the large wave energy resource found in the characerisation of their resource (Iglesias & Carballo, 2010b) and the *ad hoc* morphologic and bathymetric study to select the adequate area for the deployment of a wave farm.

Xago was selected rather than Llumeres for three reasons: (i) the resource was greater in Xago than Llumeres, which is sheltered to the waves from the IV quarter by Cabo de Peñas; (ii) while the Xago area is located in front of Aviles, the third biggest city of Asturias with a population over one hundred thousand people, the population of the cities near Llumeres do not exceed ten thousand people; and finally (iii) in the lee of the area defined in Xago, it is found Xago Beach, a very touristic place that has

experienced significant erosion over the last lustrum, which may affect the economy of the area. In contrast, in the lee of the area defined in Llumeres, it is found Llumeres Beach, a 500 m gravel beach whose relevance is not as significant as Xago Beach.

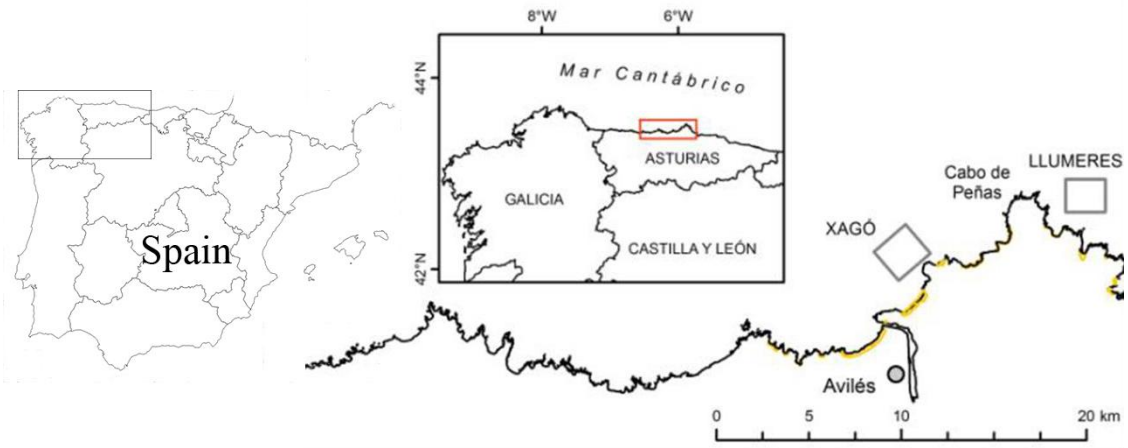

Figure 4.6 Location of Xago Beach in Asturias, N Spain. The squares on the right-hand side of the figure delimit the areas selected for the deployment of wave farms: Xago and Llumeres beaches.

Xago is a large, embayed and mostly dissipative beach, which is transformed into low-tide bar/rip channel systems at times of low wave conditions. The beach, characterised by a flat intertidal area, is practically rectilinear with an orientation southwest-northwest and a medium siliciclastic sand size. A number of samples were collected in the intertidal area to determine the grain size distribution – an essential prerequisite for the coastal processes model. The values of D_{50} (= 0.27 mm) and D_{90} (= 0.43 mm) and are obtained by means of the GRADISTAT model (Blott & Pye, 2001).

With a semidiurnal tidal regime and a Medium Spring tidal Range (MSR) of 2.66 m, Xago lies at the transition between a lower mesotidal and a macrotidal beach (Flor-Blanco, Flor & Pando, 2013). The wave conditions are analysed using the wave data from the SIMAR-44 dataset, a suite of hindcast points along the Spanish coast that analyse the wave conditions during the last 44 years. Particularly, the SIMAR point 3085039 located off Xago Beach is used for this purpose (Figure 4.7). The wave rose in

this point (Figure 4.8) shows that the beach is exposed primarily to waves from the IV quarter, particularly from the NW, with a probability of occurrence greater than 70%.

Finally, high-resolution bathymetric data of the study area, obtained in *ad hoc* surveys conducted by the University of Oviedo, are used as input for the coastal processes and wave propagation numerical models. Importantly, this dataset covered not only the submarine beach but also the subaerial, including the dune system, with elevation values ranging from –20 m to +15 m (relative to the Spanish National Geodetic Vertical Datum).

Figure 4.7 Location and relevant information of the SIMAR point 3085039. Courtesy of Google Earth.

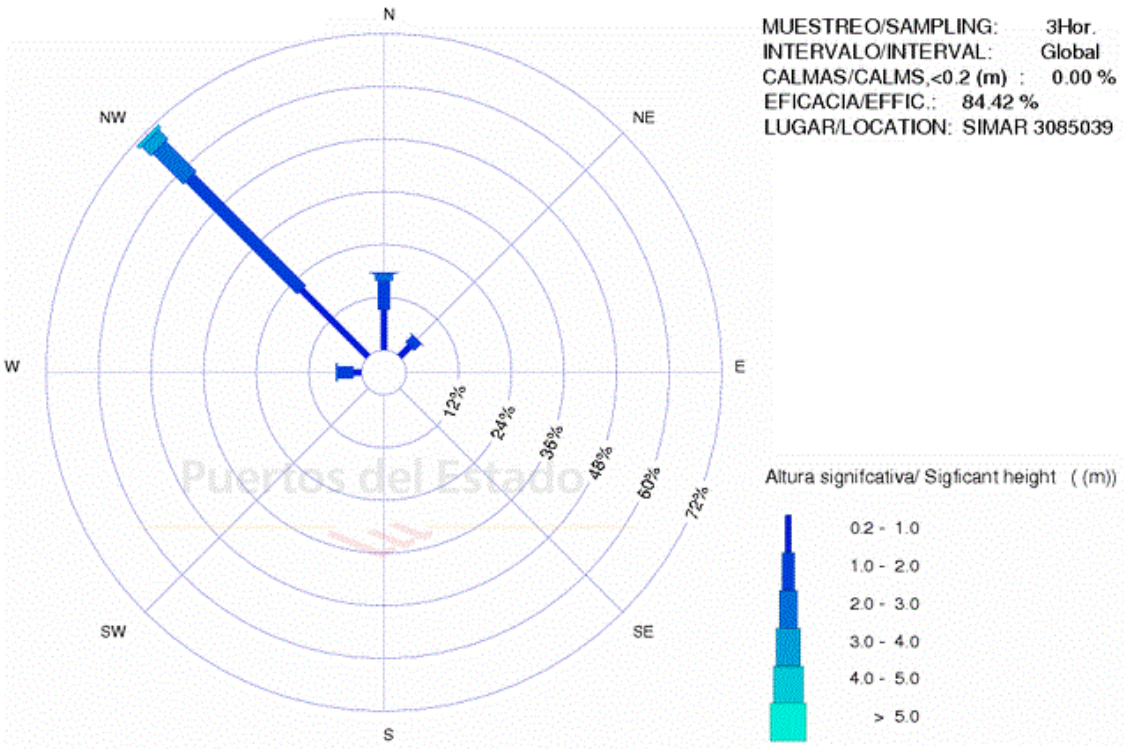

Figure 4.8 Wave rose of the SIMAR point 3085039. Courtesy of Puertos del Estado.

Chapter 5

Wave Farm Impacts on the Beach Profile

5. WAVE FARM IMPACTS ON THE BEACH PROFILE

If a wave farm is to be used for protecting the coast, in addition to its primary objective of generating free-carbon energy, it is essential to understand its impact on the beach profile – an aspect of great practical relevance that has not been investigated so far. This is the main objective of the present chapter, which is conducted through a case study: Perranporth Beach. The following contents are published in the paper of Coastal Engineering (5-year impact factor: 2.757): "**Wave farm impact on the beach profile: a case study**", which was accepted for publication on the 13 January 2014.

This chapter is structured as follows. In section 5.1, the specific methods and data used to study the impacts in the medium term are presented. This is followed by the results describing the impact of the wave farm on the wave conditions and the evolution of the beach profiles in Section 5.2. Finally, in Section 5.3, conclusions are drawn concerning the effects of a wave farm on the beach profile.

5.1 MATERIALS AND METHODS

The study covered the period from November 2007 to May 2008, corresponding to the part of the annual cycle with the highest frequency of storms based on the onsite wave buoy data. This time scale allows the assessment of the morphological changes in beaches, such as scarp formation, profile erosion and accretion, and bar evolution (Cowell & Thom, 1994).

The wave data used for this study were hindcast and onsite wave buoy data. The directional wave buoy of the Coastal Channel Observatory located in front of Perranporth beach, in approximately 10 m of water depth with reference to the local chart datum (LCD), provided half-hourly data. The wave buoy data were used in conjunction with hindcast data from WaveWatch III to validate the high-resolution

nearshore wave propagation model from November 2007 to November 2008. During the period studied, the mean values of significant wave height, H_s, and peak wave period, T_p, were 2.4 m and 13 s, respectively. Given the orientation of the coastline and its exposure to the long Atlantic fetch, the relevant wave directions come from the IV quarter (from W to N), prevailing NW.

Wind data with a three-hourly frequency obtained from the Global Forecast System (GFS) weather model were used as input of the wave model. In the period covered in the study the mean wind velocity magnitude at a height of 10 m above the sea surface was u_{10} = 9.5 ms^{-1}. The strongest winds came from the NW, with u_{10} values exceeding 20 ms^{-1}.

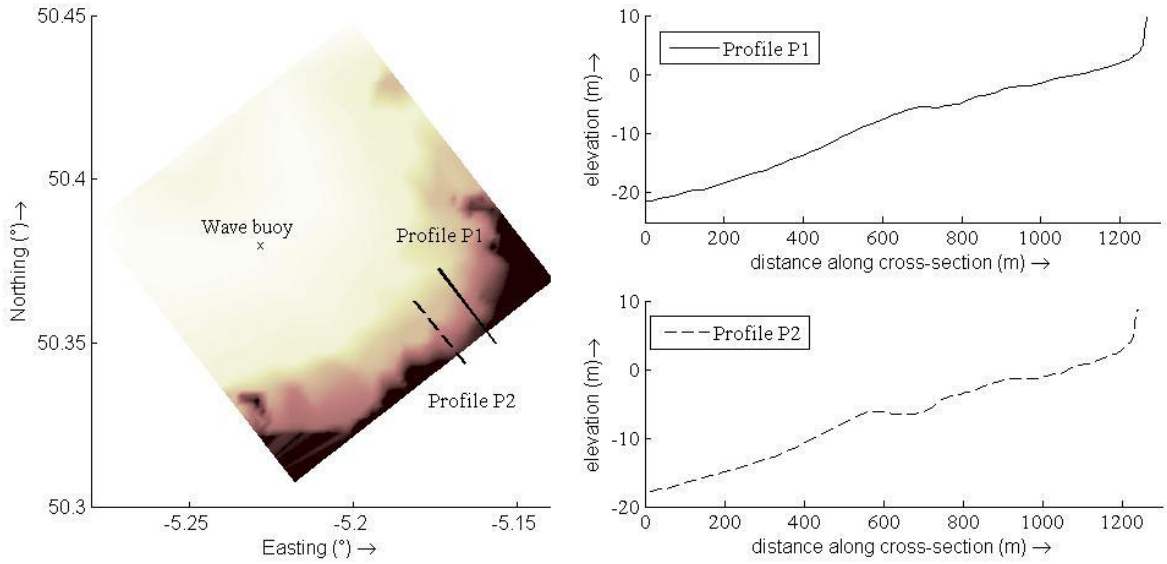

Figure 5.1 Initial beach profiles (P1 and P2) including their location and the position of the wave buoy. Water depth in relation to local chart datum

As mentioned in Section 3, the methodology is based on coupling two numerical models: a nearshore wave propagation model (SWAN) and a morphodynamic model (XBeach), which are run in two scenarios, both with and without the wave farm.

Regarding SWAN, a high-resolution grid is essential in this work in order to: (i) implement the WECs that formed the wave farm in their exact position, (ii) represent accurately the impact of the wave farm on the wave conditions in its lee, and (iii) determine the wave conditions to establish the morphodynamical state of the beach. On this basis, two computational grids are defined (Figure 5.2): (i) an offshore grid covering approx. 100 km × 50 km with a grid size of 400 × 200 m, and (ii) a high-resolution nearshore (nested) grid covering the study area, with dimensions of approx. 8 km × 6 km and a grid size of 16 m × 12 m.

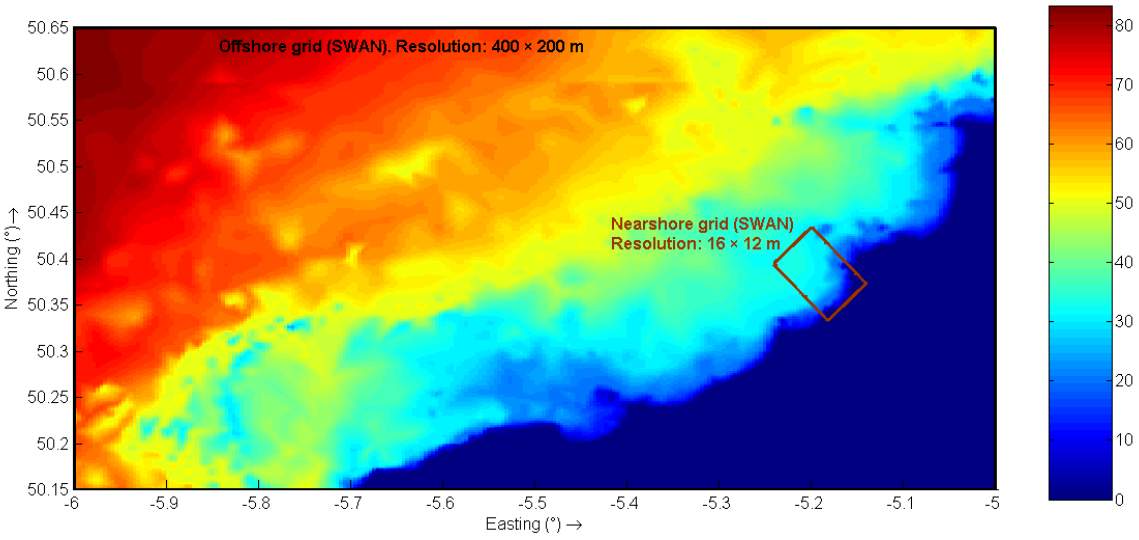

Figure 5.2 Computational grids of the wave propagation [water depths in m].

To study the effects of wave energy exploitation on the beach profile an array of 11 WaveCat WECs arranged in two rows was considered. Following Carballo and Iglesias (2013), the array was located in a water depth of 35-40 m (Figure 5.3). The distance between devices was 2.2*D*, where D = 90 m is the distance between the twin bows of a single WaveCat WEC. Finally, the wave transmission coefficient of the WECs, obtained from the laboratory tests carried out by Fernandez *et al.* (2012), was input into the coastal propagation model. Based on the results of these tests, which showed a very small variability in the wave transmission coefficient, the value K_t = 0.76 was adopted.

Regarding XBeach, this model is generally applied to analyse the response of the beach under storm conditions (Armaroli et al., 2013; McCall *et al.*, 2010), however in this case analyses the beach profile evolution in the medium term. For this purpose, the approach used in Pender and Karunarathna (2012, 2013) is followed, as they demonstrated that XBeach is capable of modelling the medium-term evolution of the beach profile of a sandy beach. Their results showed a good fit to the measured profiles after each storm period.

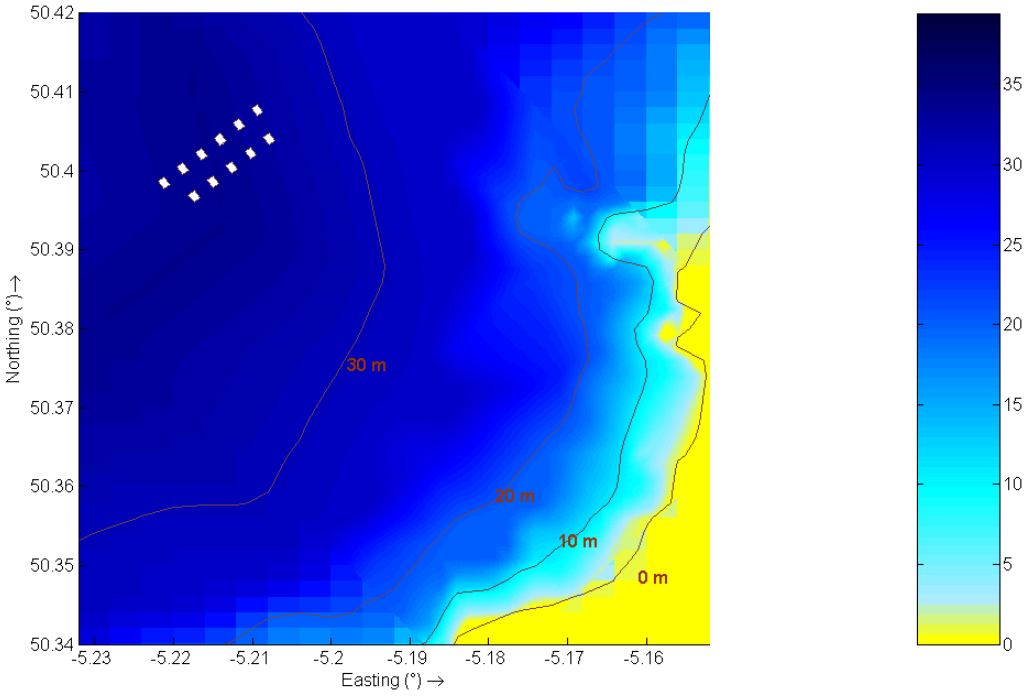

Figure 5.3 Schematic of the wave farm considered off Perranporth Beach, at a distance of 6 km from the 10 m water depth contour. Profiles P1 and P2 are shown.

From the results of the nearshore wave propagation model, spectra with a frequency of 6 hours are obtained with and without the wave farm to compare the impact on the coast. These spectra were the input of the morphodynamic model, which provided beach profile results every 6 minutes to compare their evolution in both cases.

A varying grid size was employed in the morphodynamic model: the resolution was defined as a function of the water depth and the offshore wave conditions, and subjected

to the grid size smoothness constraints. On these grounds, the Courant condition was applied to find the optimal grid size. The optimised grid was coarser in high water depths and finer in the intertidal zone, where a size of 1 m was adopted so as to accurately characterise the evolution of the profile.

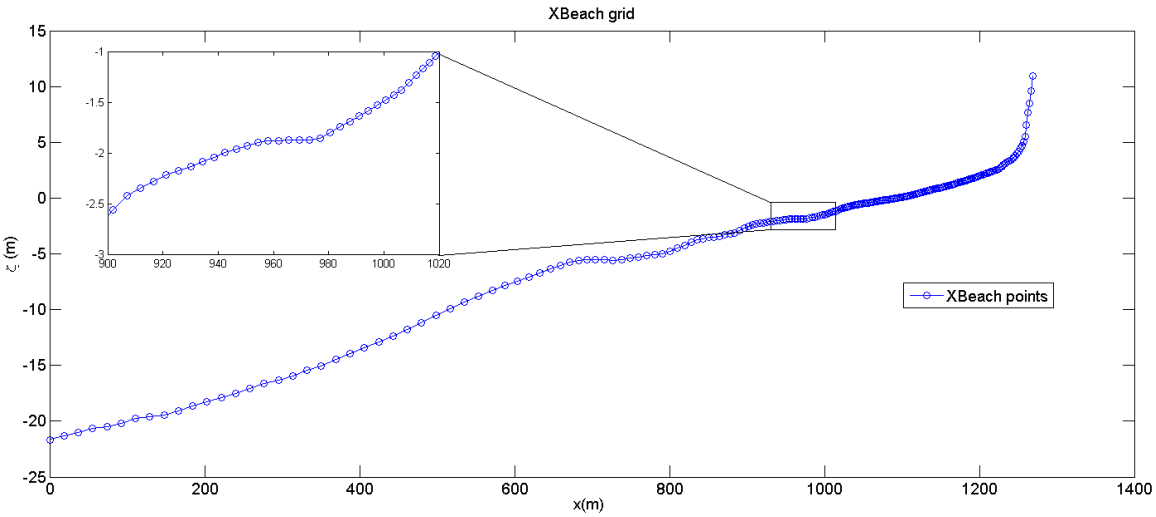

Figure 5.4 Optimised X-Beach grid

Finally, to describe properly the behaviour of the beach, the time series of wave data was broken down into a number of segments (Table 5.1). These segments were grouped into two types, Type A (Accretion) and Type E (Erosion), depending on the values of the wave parameters and the consequent nature of the beach profile changes, either accretionary or erosionary. Type A, associated with calm conditions, was set with a stationary constant wave energy distribution, based on given values of root mean square wave height *(H_{rms})*, mean absolute wave period *(T_{m01})*, mean wave direction *(θ_m)* and directional spreading coefficient *(s)*, obtained from the nearshore wave propagation model. Type E, associated with storm periods, used the parametric spectra as input to create time-varying wave amplitudes, i.e., the envelopes of wave groups (Van Dongeren, Battjes & Svendsen, 2003). The difference in approach between the two categories is the way that wave groups were treated. Type A segments included wave groups, as they are important to describe the behaviour of the beach during erosion

conditions. In contrast, wave groups were not taken into account in Type E segments because this would result in an overestimation of erosion (Baldock, Manoonvoravong & Pham, 2010).

Type	Period	Number of days	Wave conditions	
			$\overline{H_S}$ (m)	$\overline{T_P}$ (s)
Accretion	01/11/2007-30/11/2007	30	1.017	7.672
Erosion	31/11/2007-10/12/2007	10	3.918	11.444
Accretion	11/12/2007-23/12/2007	13	1.369	10.047
Erosion	23/12/2007-07/02/2008	44	2.563	10.257
Accretion	08/02/2007-23/02/2008	15	1.387	10.841
Erosion	24/02/2007-01/04/2008	38	2.359	9.838
Accretion	02/04/2007-30/04/2008	29	1.278	8.491

Table 5.1 Accretionary and erosionary periods with their corresponding average wave conditions

5.2 RESULTS

First, the model was validated using the wave buoy data at Perranporth Beach from November 2007 to October 2008, missing out January 2008 owing to the lack of data. Figure 5.5 and Figure 5.6 show the good fit achieved between the significant wave height computed by SWAN and the values from the wave buoy. The coefficient of determination, R^2, and the Root Mean Square Error, *RMSE*, confirm the goodness of the fit: $R^2 = 0.94$ and $RMSE = 0.38$ m.

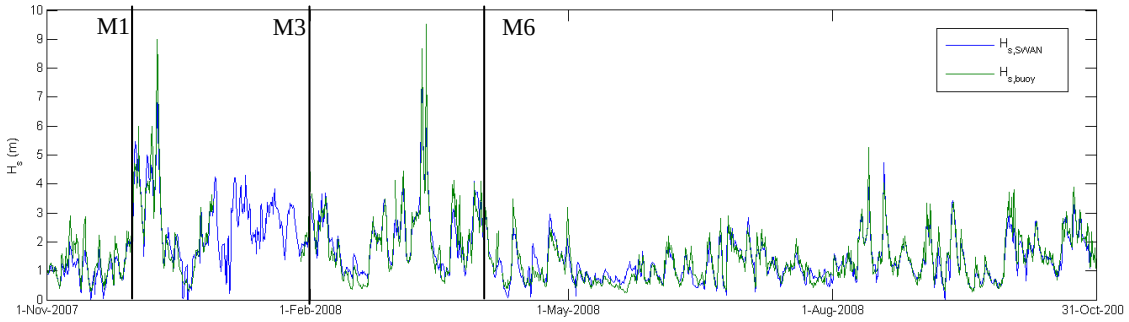

Figure 5.5 Time series of simulated ($H_{s,\,SWAN}$) and measured ($H_{s,\,buoy}$) significant wave height. The vertical lines depicted in the graph show the months 1, 3 and 6 after the first point of the simulation.

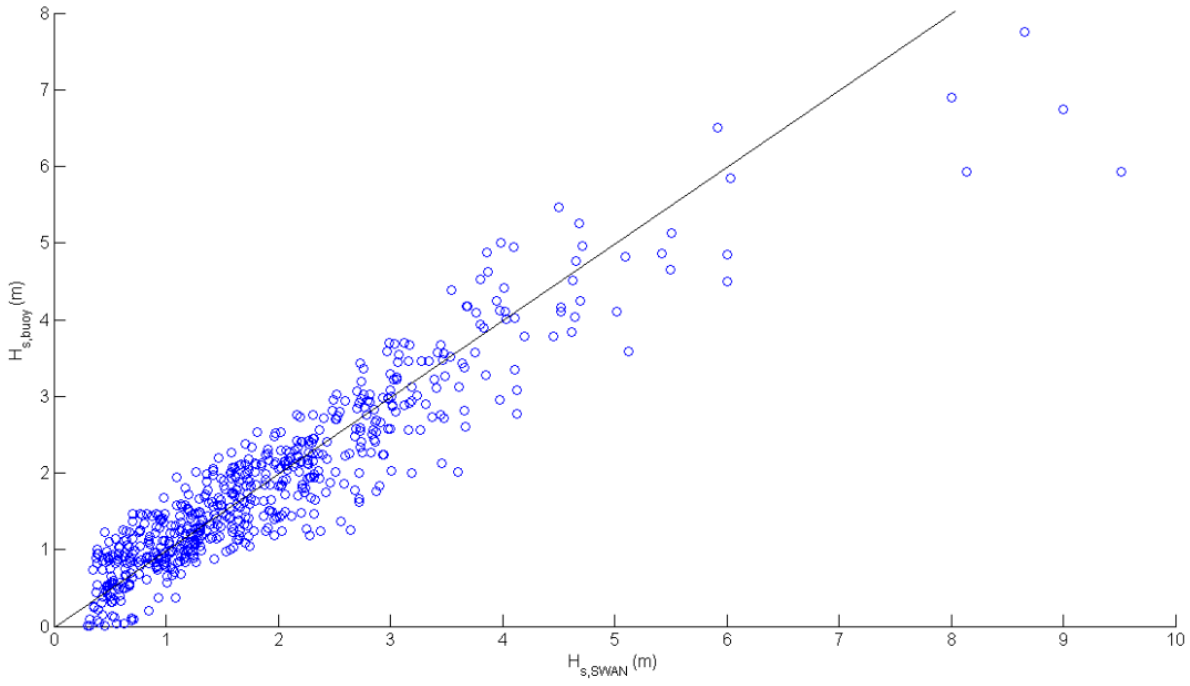

Figure 5.6 Scatter diagram: simulated ($H_{s,\,SWAN}$) vs. measured ($H_{s,\,buoy}$) significant wave height.

Second, having validated the numerical model, it was used to compare the wave patterns with and without the wave farm and to determine the wave conditions to be used as input to the morphodynamic model. As an example of the effects of the wave farm on the wave patterns, the wave propagation corresponding to the peak of a storm on 10 March 2008 is shown in Figure 5.7. The deep water wave conditions were: significant wave height, H_{s0} = 10.01 m; peak wave period, T_p = 15.12 s; and peak wave direction, θ_p = 296.38°. A substantial decrease of the significant wave height was

apparent in the lee of the wave farm. This decrease was less marked on the beach itself due to the wave energy diffracted from the edges into the shadow of the farm. In the northern section of the beach the reduction of wave height was more pronounced than elsewhere owing to the deep water wave direction (approx. WNW). For waves coming from northern direction the shadow brought about by the wave farm was expanded to southern sections of the beach, although the greatest impact was still found in the north part of the beach.

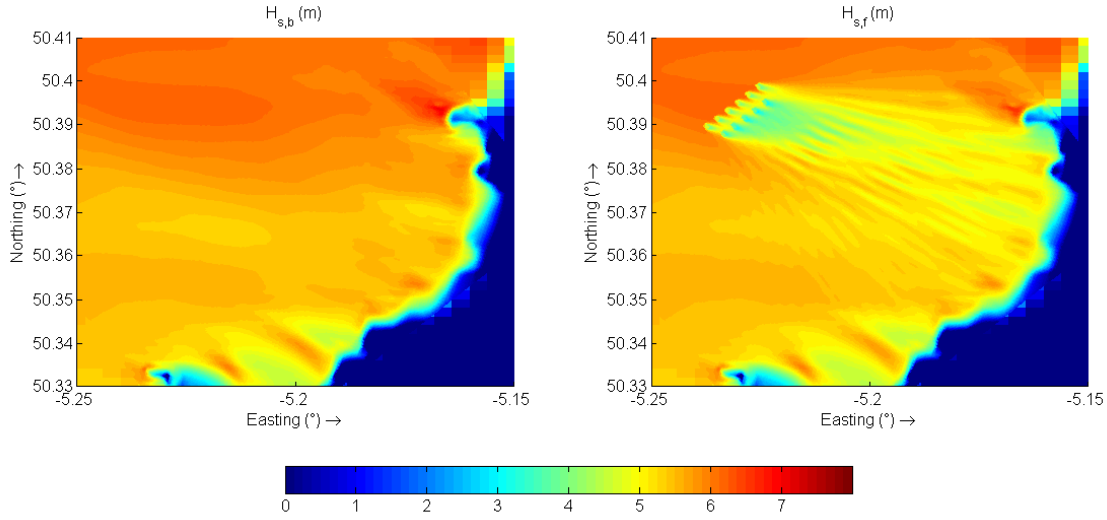

Figure 5.7 Significant wave height in the baseline scenario ($H_{s,b}$) and in the presence of the farm (Hs,f) at the peak of a storm (10 Mar 2008, 18:00 UTC) [Deep water wave conditions: H_{s0} = 10.01 m, T_p = 15.12 s, θ_p = 296.38 °].

For a better quantification of the impacts of the wave farm on the wave conditions, the *RSH* index is applied, which refers to the reduction of the significant wave height in the lee of the wave farm (Figure 5.8). The greatest impact was found in the lee of the second row of devices, with *RSH* values exceeding 0.5. The reduction reached another peak towards the coastline as a result of the merging of the wakes caused by the WECs, with values of approx. 0.4. As mentioned above, these values decreased towards the coastline, however the alteration of the wave conditions cannot be overlooked and have a significant bearing on the evolution of the beach profile.

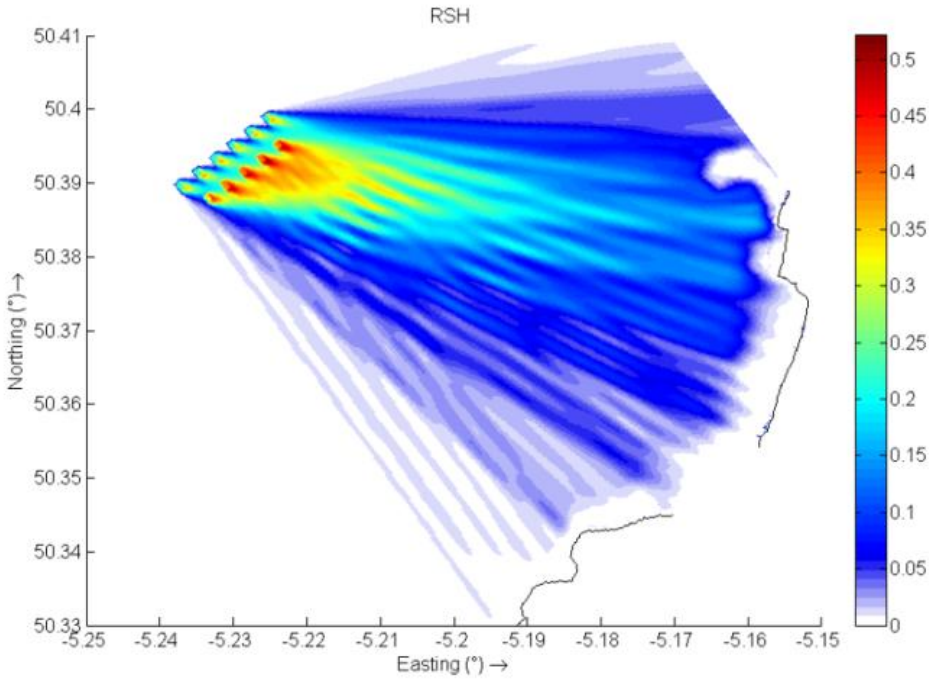

Figure 5.8 Reduction of the significant wave height (*RSH*) brought about by the wave farm at the peak of a storm (10 Mar 2008, 18:00 UTC) [Deep water wave conditions: H_{s0} = 10.01 m, T_p = 15.12 s, θ_p = 296.38 °].

The modification of the wave patterns in the lee of the wave farm could be affected by the division of the spectral space carried out by the wave propagation model, in which elementary bins with a constant directional resolution $\Delta\theta$ are employed *(Zijlema, 2010). A priori* this should not affect the accuracy of the results, as the number of directions used in this documents were 36; i.e. a directional resolution of 5 degrees. This value is recommended in the literature (SWAN, 2007), but even higher values (30 degrees) have been applied to conduct successfully wave propagations (Monbaliu et al., 2000). In addition, the wave energy is not just concentrated in one directional sector, as due to refraction and nonlinear interactions, wave energy shifts in the spectral space from one directional sector to another. Therefore, the results seem not to be altered by the spectral resolution, as can be seen in Figure 5.8, where the wakes caused by the WECs are smaller than the 5 degrees and are represented in the space domain.

Observing the effects on the wave power (*J*), similar patterns can be observed, with the greatest impact taking place in the north section of the beach (Figure 5.9). The

average reduction of the wave power during the period studied at different points along the 10 m contour is shown in Table 5.2. In line with the results previously presented, the areas most sheltered by the wave farm are the middle and, especially, the north section of the beach. On these grounds two profiles in the north and middle sections of Perranporth Beach are selected for the analysis of the impacts of the wave farm on the beach profile (Figure 5.1).

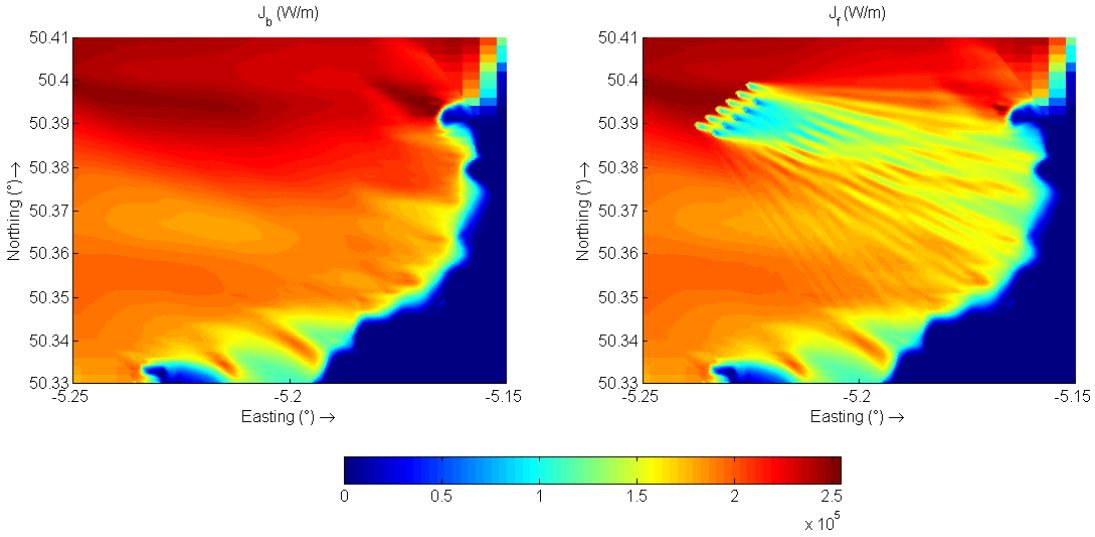

Figure 5.9 Wave power in the baseline scenario (J_b) and in the presence of the farm (J_f) at the peak of a storm (10 Mar 2008, 18:00 UTC) [Deep water wave conditions: H_{s0} = 10.01 m, T_p = 15.12 s, θ_p = 296.38 °].

Beach Point	Coordinates		ΔH_s (%)	ΔJ (%)
	Easting (°)	Northing (°)		
North	-5.17	50.36	3.26	12.82
Middle	-5.18	50.35	1.75	6.80
South	-5.21	50.34	0.70	1.52

Table 5.2 Significant wave height reduction (ΔH_s) and wave power reduction (ΔJ) caused by the wave farm at different points along the 10 m contour.

The evaluation of the resource in the wave farm was carried out by means of the $\overline{J}_{WEC}$ indicator, which represents the annual mean wave power incident on a generic WEC of the wave farm. The resource was evaluated during the year used for the validation purposes (Nov 2007 – Oct 2008) to consider both summer and winter period.

The average resource found in the case of locating the wave farm at a distance of 6 km from the coast was 17.26 kW/m. Considering the 11 WECs that form the wave farm and the capture width of the WaveCat (90 m), the annual mean of the total incident wave power at the wave farm was 17 MW. Applying the values obtained in Fernandez *et al.* (2012) for the efficiency of the WaveCat, the annual mean production of a wave farm of 11 WECs would be 4 MW. As this technology is in a nascent stage, the performance of wave farms would be further discussed further in Section 10.1.3, comparing the performance presented with other WECs.

Third, the impact of the wave power reduction on the beach was studied through the evolution of the two profiles of Perranporth Beach. This was carried out using the spectra generated by the wave propagation model with and without the wave farm in the morphodynamic model. The series were split, as explained in the methodology, to describe suitably the behaviour of the beach in different periods. The results showed that type E segments are mainly responsible for the erosion of the profiles.

Figure 5.10 shows the evolution of the beach profiles 1 (P1) and 2 (P2) after a storm. The graph compares the initial beach profiles with those after three months of operation of the wave farm. Both graphs illustrate that the erosion of the profiles is concentrated mainly in the beach face, which is the section of the profile exposed to wave uprush. The eroded material was moved to lower sections of the profile.

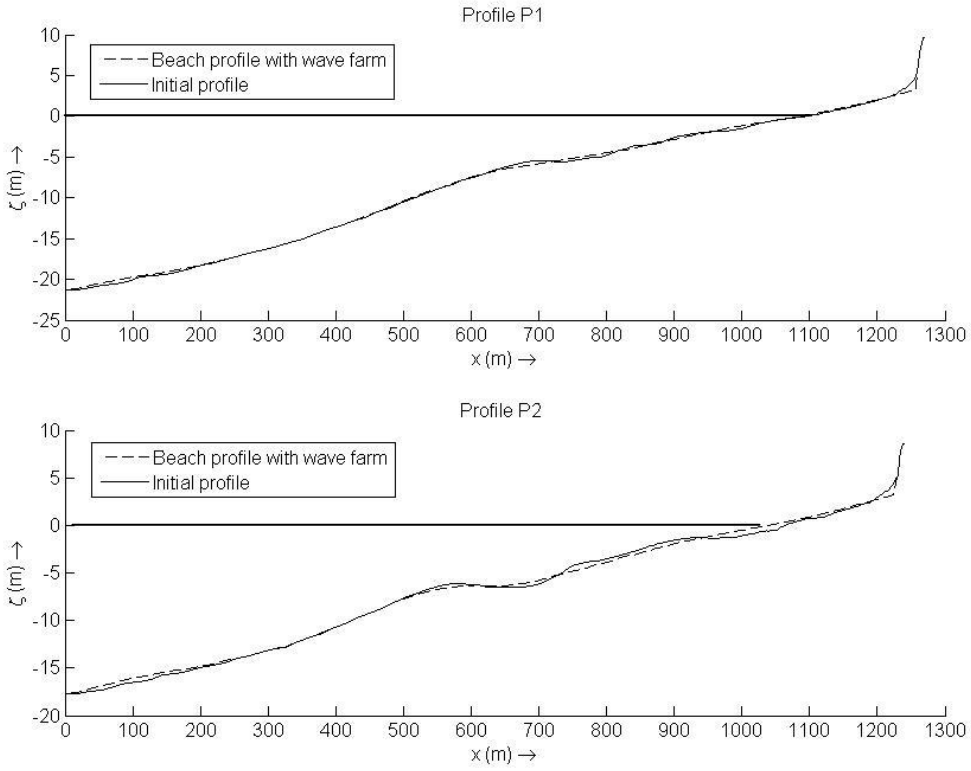

Figure 5.10 Bed level at beach profile P1 and P2: initial [1 Nov 2007, 0000 UTC] and after three months with and the wave farm [22 Jan 2008, 15:47 UTC]. The average wave conditions between these two points in time were: H_s = 2.02 m and T_z = 939 s.

To better visualise the effect of wave energy extraction, the situation of profile P2 with and without the farm is shown in Figure 5.11. The reduction of the significant wave height in the lee of the wave farm led to a substantial reduction (of the order of 3 m) in the erosion of the dune delineating the landward limit of the beach. It is also noteworthy that the wave farm not only reduced the volume of material eroded, but also altered the sediment transport patterns, displacing the landward end of erosion towards the sea around 10 m after 3 months of simulation.

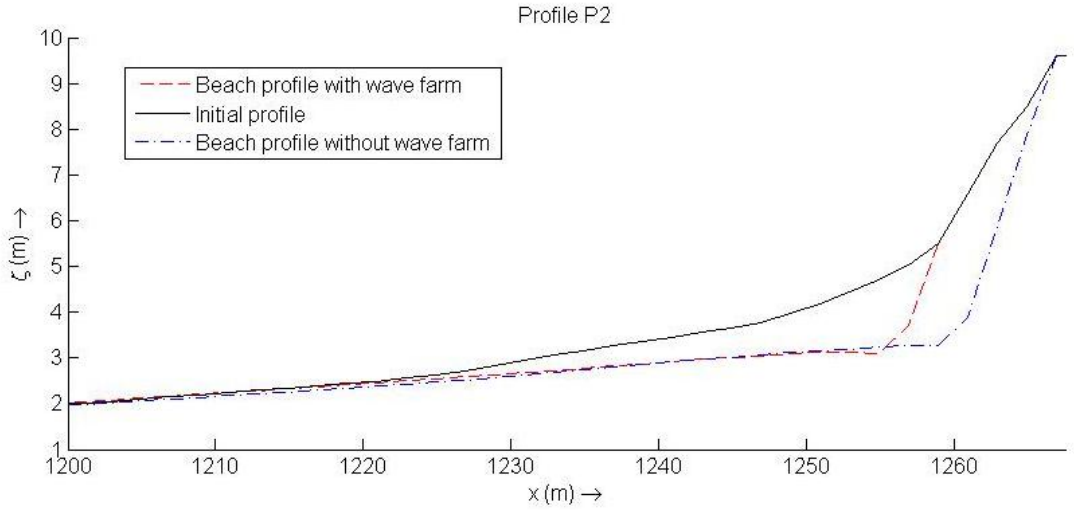

Figure 5.11 Beach face level at Profile P2: initial [1 Nov 2007, 0000 UTC] and after three months with and without the wave farm [22 Jan 2008, 15:47 UTC]. The average wave conditions between these two points in time were: H_s = 2.02 m and T_z = 939 s.

The impact of the wave farm on the beach profile was analysed through the parameters defined in Section 3.3.2. The Bed Level Indicator (*BLI*) along Profiles P1 and P2 is illustrated in Figure 5.12 for three different points in time: 1 month (*M1*), 3 months (*M3*) and 6 months (*M6*) after the beginning of the study period. The results for both profiles show a significant reduction of the erosion in the beach face and in the submarine bar (around x = 600 m). The bar forms part of the response mechanism of the natural system to protect the beach face from increased wave attack. Figure 5.12 proves that the effect of the wave farm was a reinforcement of the bar, and therefore enhanced protection for the beach face in storms. Advancing in time, the *BLI* values increased in the bar area, i.e., the aforementioned effect was intensified; results that go in line with the stated by (Neill & Iglesias, 2012).

Regarding the beach face area, the *BLI* values for both profiles were also significant and showed that the wave farm contributed to mitigating the erosion in that section. This is nowhere more apparent than on the dune at the landward end of the profile, where *BLI* values exceed 1 m. In view of the importance of erosion on the beach face the *FEA* and *NER* indicators are applied. Table 5.3 shows the values of the eroded areas

on the beach face (*FEA*) at the same points in time as in Figure 5.12. It is observed for both profiles, and particularly in Profile P1, that the erosion is higher at the first two points in time (*M1* and *M3*) than at the last one, which is associated with less energetic conditions (Figure 5.7). Although the points *M1* and *M3* were associated to erosionary periods, they did not coincide with the end of these periods, where generally the greatest values of storm-induced erosion were found. This is reflected in the values of erosion found on the beach face, with the greatest *FEA* values found at the end of the period studied.

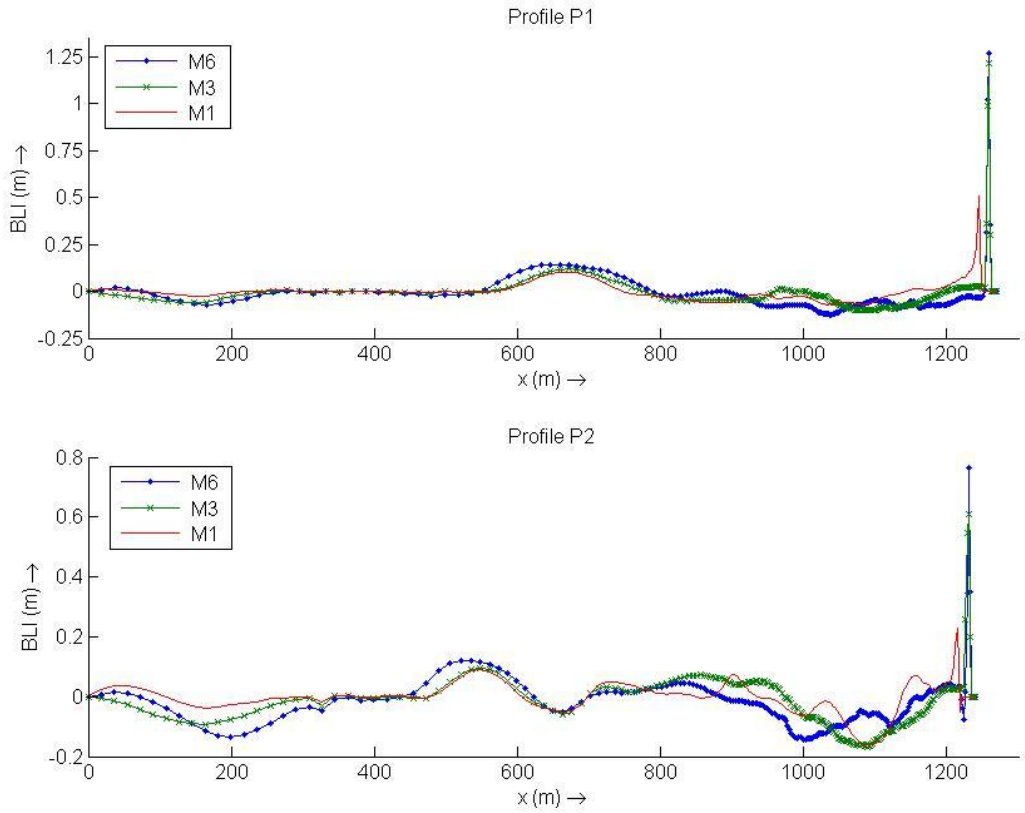

Figure 5.12 Evolution of *BLI* along Profiles P1 and P2 at different points in time: 1 month (*M1*), 3 months (*M3*) and 6 months (*M6*) after the beginning of the study period.

The reduction of the erosion brought about by the wave farm is studied by means of the *NER* indicator, which showed reductions over 30% in the profile P1 (located in the north section of the beach – the most sheltered by the farm) during the erosionary periods (*M1* and *M3*). It is also noted that the effect of the wave farm was more

significant in the north of the beach (Profile P1) than in the middle (Profile P2), as may be seen in Table 5.1. Analysing the evolution of the *NER* values over time, it is observed that the wave farm was more effective to mitigate storm-induced erosion during erosionary periods than accretionary, although still significant values (*NER* > 20% in the north section of the beach) are found at the end of the simulation for both profiles.

Profiles	*M1*			*M3*			*M6*		
	FEA_b (m^2)	FEA_f (m^2)	*NER* (%)	FEA_b (m^2)	FEA_f (m^2)	*NER* (%)	FEA_b (m^2)	FEA_f (m^2)	*NER* (%)
Profile P1	20.53	14.11	31.27	16.3	10.42	36.07	23.85	18.66	21.76
Profile P2	15.69	12.91	*17.72*	21.31	16.85	*20.93*	25.53	21.42	*16.10*

Table 5.3 Eroded area in the baseline scenario (*A*), in the presence of the farm (A_f), and Erosion Impact (*EI*) index for Profiles P1 and P2 at different points in time: 1 month (*M1*), 3 months (*M3*) and 6 months (*M6*) after the beginning of the study period

5.3 CONCLUSIONS

The results showed a significant reduction of the erosion along profiles P1 and P2, which may indicate some degree of coastal protection owing to the presence of the wave farm nearshore. The extraction of wave energy by the WECs resulted in significant reductions of erosion, with values in the north section of the beach varying from 36% during storm conditions, to 22% at the end of the simulation, which corresponded to accretionary conditions.

This substantial reduction in the erosion of the profiles constitutes an added benefit of the wave farm. However, this chapter was framed as the first step in the assessment of the impact of wave farms on the beach, and consequently to prove that a wave farm can be considered a complement to conventional forms of coastal protection, the response of the beach in 3D must be evaluated, which is the aim of the following chapter.

Chapter 6

Wave Farm Impacts on the Beach Morphology

6. WAVE FARM IMPACTS ON THE BEACH MORPHOLOGY

This chapter presents the impacts of wave farms on the beach morphology (3D) in the short-term. Two case studies are presented in this chapter: Perranporth Beach (SW England) and Xago Beach (N Spain). The following contents are published in the paper of Coastal Engineering: "**Coastal defence through wave farms**" in the case of Perranporth Beach (accepted for publication on 26 June 2014); and under review in the paper of Coastal Engineering Journal (2016): "**Mitigating dune erosion through wave farms**" in the case of Xago Beach.

In view of the promising results presented in the Chapter 4, this chapter goes a step further by transcending the cross-shore (2D) analysis and examining the impact of wave energy exploitation on beach morphology (3D) – an aspect whose importance can hardly be overstated. On this basis, the chapter has a threefold objective: (i) to compare the response of the beaches under storm conditions (short term) with and without a wave farm; (ii) to assess whether the nearshore attenuation of wave energy caused by the wave farm results in a reduction in the erosion on the beach; and, on these grounds, (iii) to establish whether a wave farm can contribute to coastal protection.

6.1 PERRANPORTH BEACH

6.1.1 MATERIALS AND METHODS

This section analyses the period from 5 December 2007 UTC 00:00 to 10 December 2007 UTC 18:00 (Figure 6.1), a stormy period with the following average wave conditions: H_s = 4.2 m, T_p = 12.1 s and θ_p = 295°.

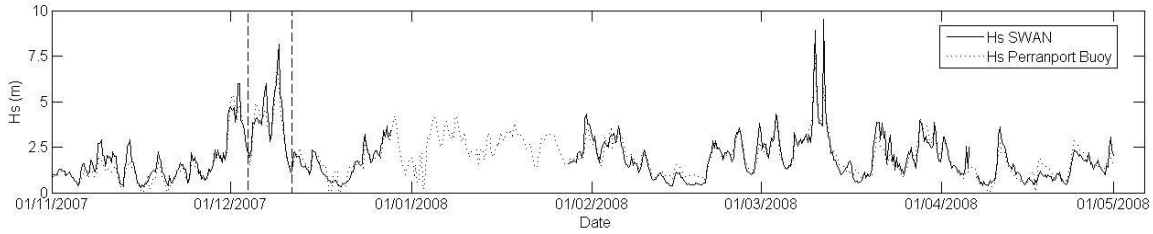

Figure 6.1 Time series of simulated (H_s*SWAN*) and measured (H_s*buoy*) significant wave height used to validate the wave propagation model. The storm conditions studied from 5 Dec 2007, 00:00 UTC; to 10 Dec 2007, 18:00 UTC are highlighted.

To determine the wave farm impacts on the wave conditions and the coastal processes, the wave propagation model (SWAN) is coupled to the coastal processes model. The response of the beach during the storm period studied was investigated in both scenarios: (i) in the baseline scenario (without the wave farm), and (ii) with the wave farm, to compare the evolution of the beach and establish the contribution of a wave farm to protect the coast.

Regarding the wave propagation model, the successfully validated high-resolution nested grids and model set up applied in the previous chapter were used. Likewise, the same wave farm configuration and distance to the coast (6 km from the 10 m water depth contour) was considered (Figure 5.3), which allows the comparison of the wave farm impacts between the short and middle term.

As for the coastal processes model, in this case it is applied in 2DH mode (*x*, *y*, *z*), with a grid extending 1250 m across shore and 3600 m alongshore with a resolution of 6.25 m and 18 m, respectively (Figure 6.2). The model used a number of spectral parameters obtained from the nearshore wave propagation model (the root-mean-square wave height, H_{rms}, mean absolute wave period, T_{m01}, mean wave direction, θ_{m}, and directional spreading coefficient, *s*) as input to create time-varying wave amplitudes, i.e., the envelopes of wave groups, which have crucial importance in describing the behaviour of a beach during erosion conditions (Baldock et al., 2011). The bathymetry of the beach was based on the data provided by the Coastal Channel Observatory. The

elevation values implemented in the model ranged between –20 m and 25 m (Figure 6.3) with reference to the local chart datum (LCD).

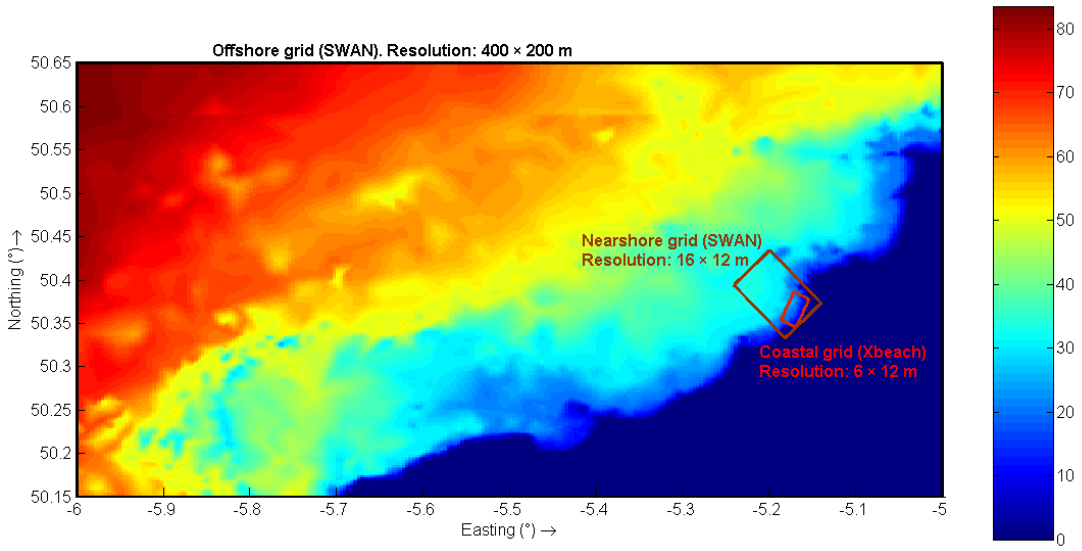

Figure 6.2 Computational grids of the wave propagation (SWAN) and coastal processes (XBeach) models [water depths in m]

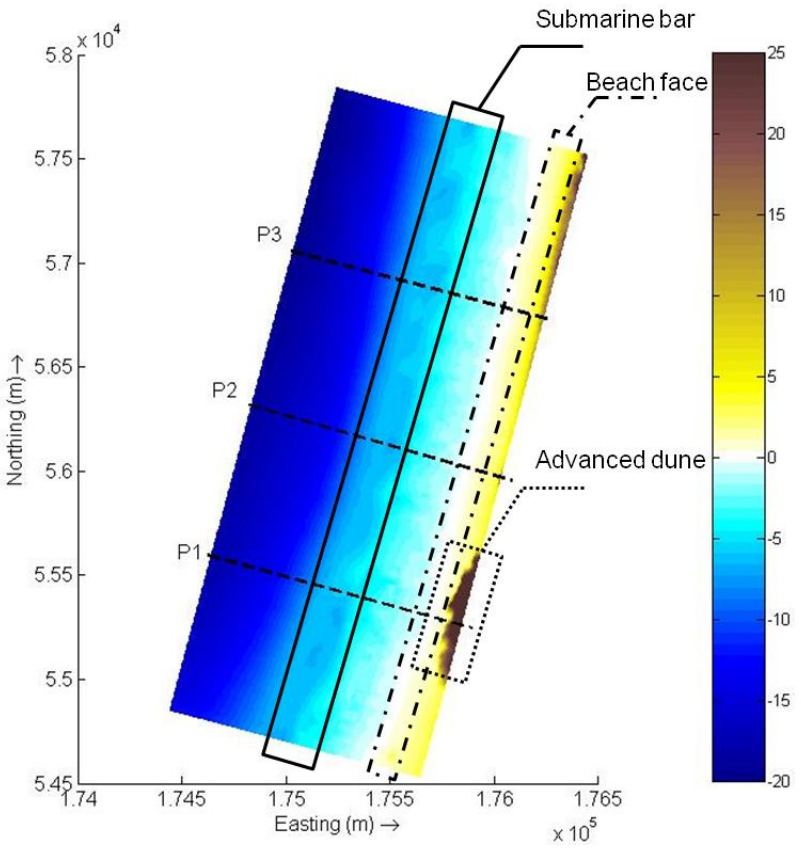

Figure 6.3 Bathymetry of Perranporth Beach for the coastal processes model. Profiles P1, P2 and P3 included. Water depth in relation to local chart datum [in m].

6.1.2 RESULTS

The results of the wave propagation model were studied in both scenarios: baseline and in the presence of the wave farm, to observe the impact of the wave farm on the wave conditions. The reduction of the significant wave height in the lee of the farm is shown in Figure 6.4, in which the shadow zone downstream of each WEC is apparent. The greatest impact occurred in the lee of the second row of devices. On the coast, the impact was mainly focused on the north section of the beach as the offshore wave direction was west (268 °).

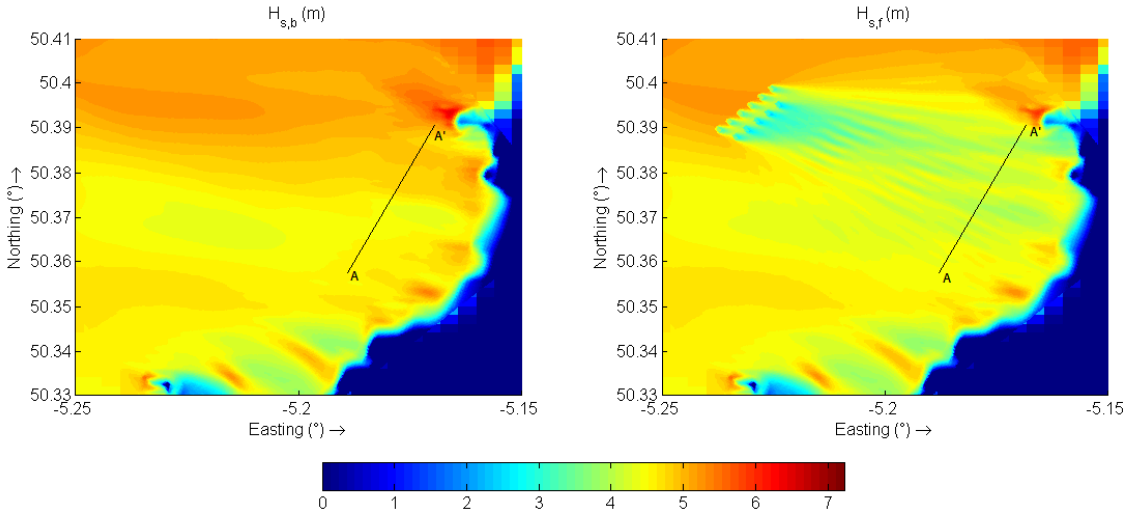

Figure 6.4 Significant wave height in the baseline scenario (H_s) and with the wave farm (H_{sf}) at the first peak of the stormy period studied (5 Dec 2007, 18:00 UTC). [Deep water wave conditions: H_{s0} = 6.89 m, T_p = 15.64 s, θ_p = 268.45 °]. The line AA' is shown.

This can be observed applying the reduction of the significant wave height (RSH) factor. The shadow in the lee of the farm with waves coming from the NW (Figure 5.8) was wider than waves from the W (Figure 6.5). However, on the other hand the reduction of the wave height with waves from the W was higher in certain sections of the beach, such as the north, with values over 10 % along the 20 m contour.

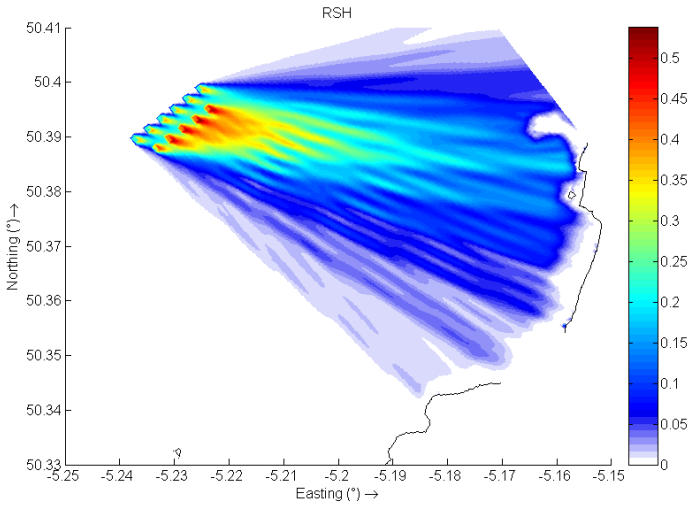

Figure 6.5 Reduction of the significant wave height (*RSH*) brought about by the wave farm at the first peak of the stormy period studied (5 Dec 2007, 18:00 UTC). [Deep water wave conditions: H_{s0} = 6.89 m, T_p = 15.64 s, θ_p = 268.45 °].

The wave conditions along the line AA' (Figure 6.4), in approximately 20 m of water depth, were input to the coastal processes model. The significant wave height (H_s) across AA' in both scenarios is shown in Figure 6.6, where the shadow due to the wave energy absorption of each device can be readily identified. It is also remarkable in which manner the reduction of the wave height increased towards the north section of the beach (A' in the figure).

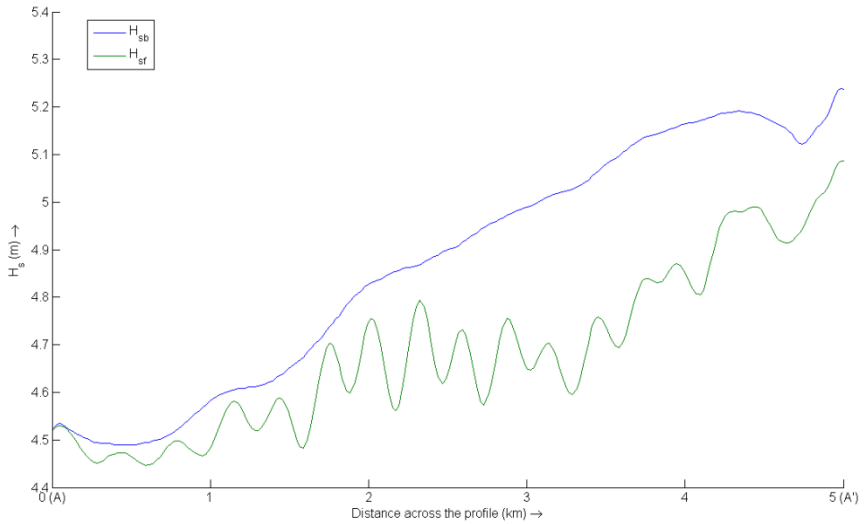

Figure 6.6 Significant wave height in the baseline scenario (H_s) and in the presence of the farm (H_{sf}) across the line AA' at the first peak of the storm studied (5 Dec 2007, 18:00 UTC). [Deep water wave conditions: H_{s0} = 6.89 m, T_p = 15.64 s, θ_p = 268.45 °].

Applying the suite of core impact indicators, defined in Section 3.3.2, to the results of the coastal processes model, the alteration caused by the wave farm on the longshore and offshore/onshore sediment transport was quantified. First, the response of the beach without the wave farm (baseline scenario) was analysed so as to understand in which manner the wave farm affects the beach. The sea bed level difference between the first and the last point of the simulation (Figure 6.7) shows that there are two main areas affected by the storm-induced erosion: the submarine bar and the beach face area. The greatest values were found at the toe of the dune in the central section of the beach, although these values were associated with the isolated response of some profiles. With less significant erosion rates, a long stretch of the beach was affected on the beach face in the north section of the beach. This response of the beach under storm conditions goes in line with the behaviour observed at Perranporth in previous studies (Scott et al., 2008).

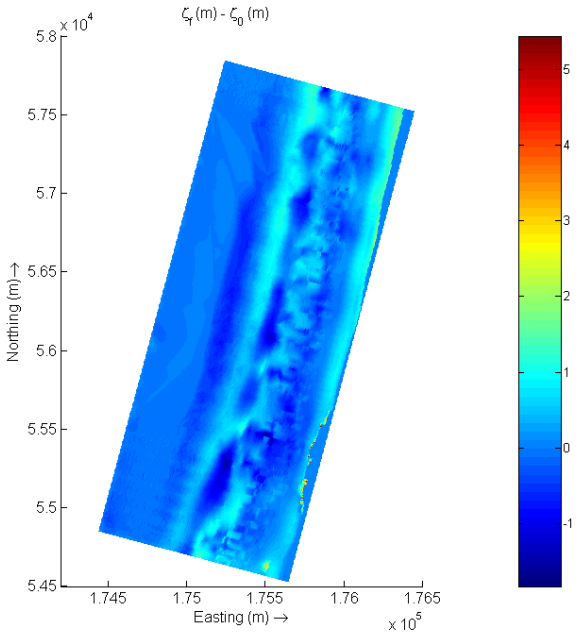

Figure 6.7 Bed level difference between the first (ζ_b) and the last point (ζ_0) of the simulation.

The alteration of the sea bed level by the wave farm was analysed through the BLI factor (Figure 6.8). The reduction of the erosion was observed mainly in the dune at the

back of the beach, reaching values greater than 4 m in the middle section of the beach, as result of the wave energy extraction by the wave farm. A reduction of the erosion was also found along the bar, especially in the middle section of the beach where the *BLI* parameter reached values of 0.5 m. On the other hand, the material eroded from the dune was moved to lower sections of the profile, between the bar and the dune, which resulted in the *BLI* parameter taking negative values in the region of –0.5 m.

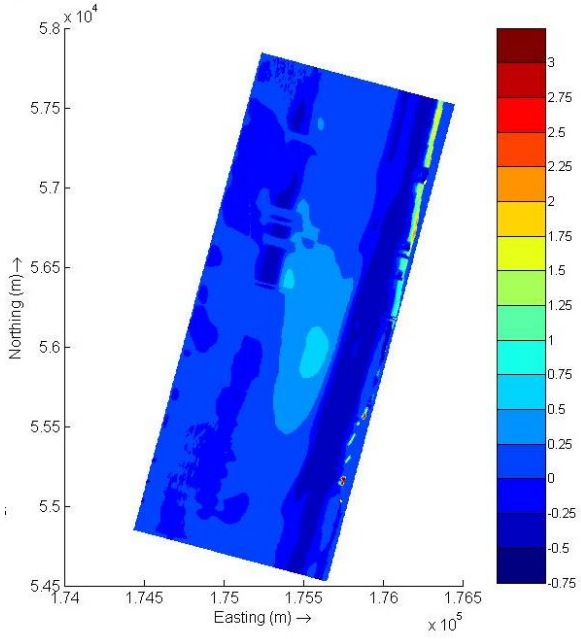

Figure 6.8 Bed level impact (*BLI*) at the end of the time period studied [10 Dec 2007, 06:00 UTC].

On this basis, the impact of the wave farm on the bed level is shown in Figure 6.9 along three profiles: P1 (south), P2 (middle) and P3 (north), located in Figure 6.3. The initial profile (ζ_0) was compared with the profiles at the end of the storm studied in both scenarios: the baseline (ζ_b) and in the presence of the farm (ζ_f). The results show a more significant effect on profiles P3 and P2 (northern and middle areas of the beach) than on P1, in accordance with the wave conditions shown in Figure 6.4. As may be observed in Figure 6.8, the effects of the wave farm are more pronounced in the intertidal area over the mean water level (at the landward end of the profiles) and over the bar. Furthermore, Profile P3 shows that the wave farm not only reduced the eroded area but also altered

the sediment transport pattern, moving the landward end of erosion by up to 30 m towards the sea in the case of the north of the beach.

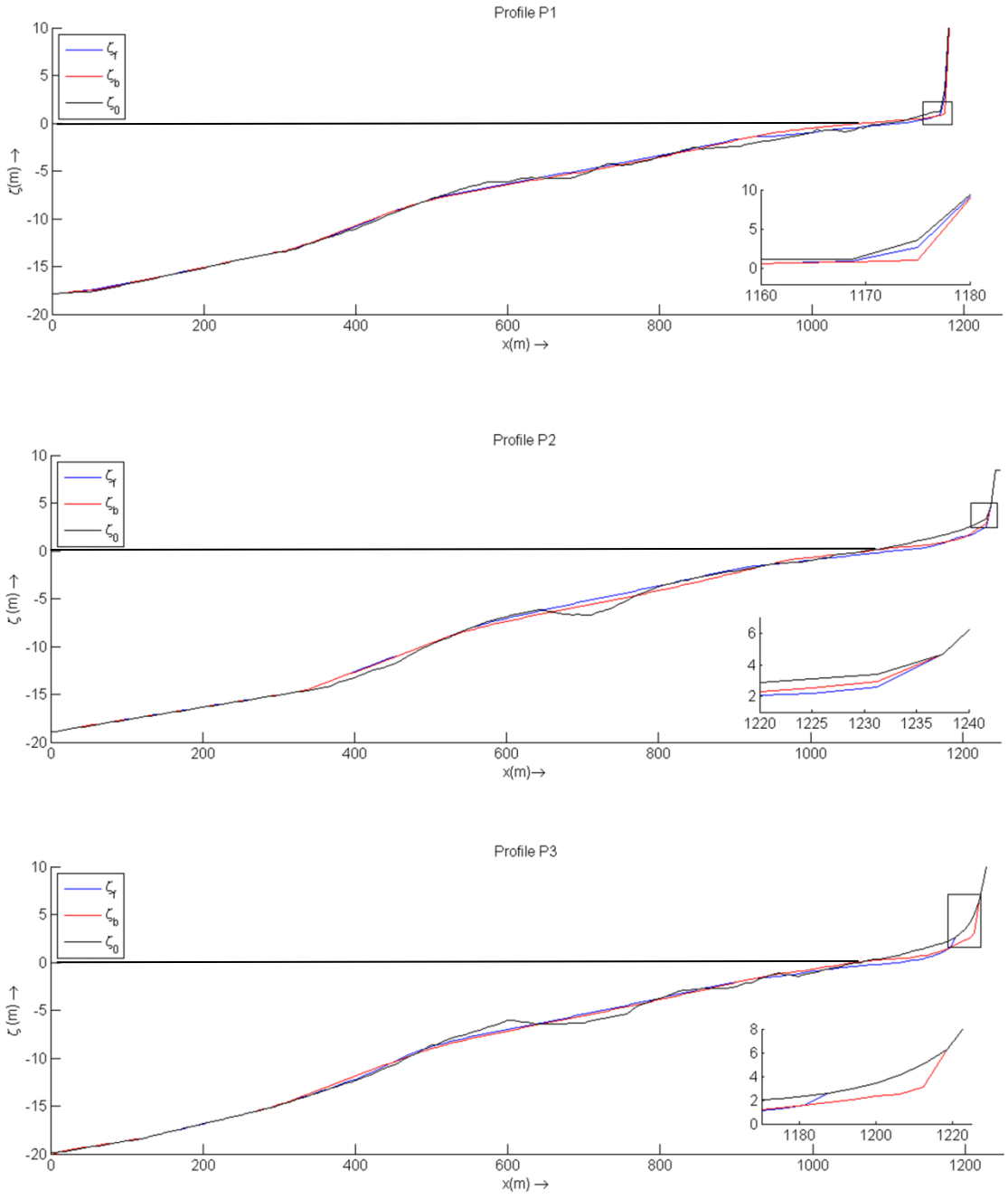

Figure 6.9 Bed level at Profiles P1, P2 and P3: initial (ζ_0) [05 Dec 2007, 00:00 UTC] and at the end of the simulation in the baseline scenario (ζ_b) and with the wave farm (ζ_f) [10 Dec 2007, 06:00 UTC].

The volume of material moved per linear metre along the beach (y) was studied through the mean Cumulative Eroded Area (CEA). This indicator showed the difference in material eroded along the profile (x) between the initial and final points of the time period studied in both scenarios: baseline (CEA_b) and with the wave farm (CEA_f).

Figure 6.10 shows the results in the southern and northern areas across the different reference profiles P1 (south), P2 (middle) and P3 (north). In the case of profile P2, the wave farm modified the sediment transport patterns significantly: whereas erosion was reduced in the northern area of the beach, in the southern area the material eroded increased for water depths below 5 m. As for profile P1, the northern area of the beach presented less sediment transport in the presence of the wave farm for water depths over 7 m, while accretion occurred for water depths below 7 m. In the case of profile P3, the sediment transport patterns were hardly affected by the wave farm for water depths over 5 m, but in water depths below 5 m erosion decreased in the southern area of the beach. In summary, in the baseline scenario (without the wave farm) accretion was found to occur in the deeper sections of the profile in the northern area owing to the offshore sediment transport from the beach face and the submarine bar. In the presence of the wave farm, however, the erosion of the beach face and submarine bar was significantly reduced. As a result of this, and of the increase of the southward sediment transport, the accretion of the deeper sections of the profile in the northern area that occurred in the baseline scenario was replaced by accretion in the southern area of the beach for values of the x coordinate greater than 600 m (as may be seen on profiles P2 and P3).

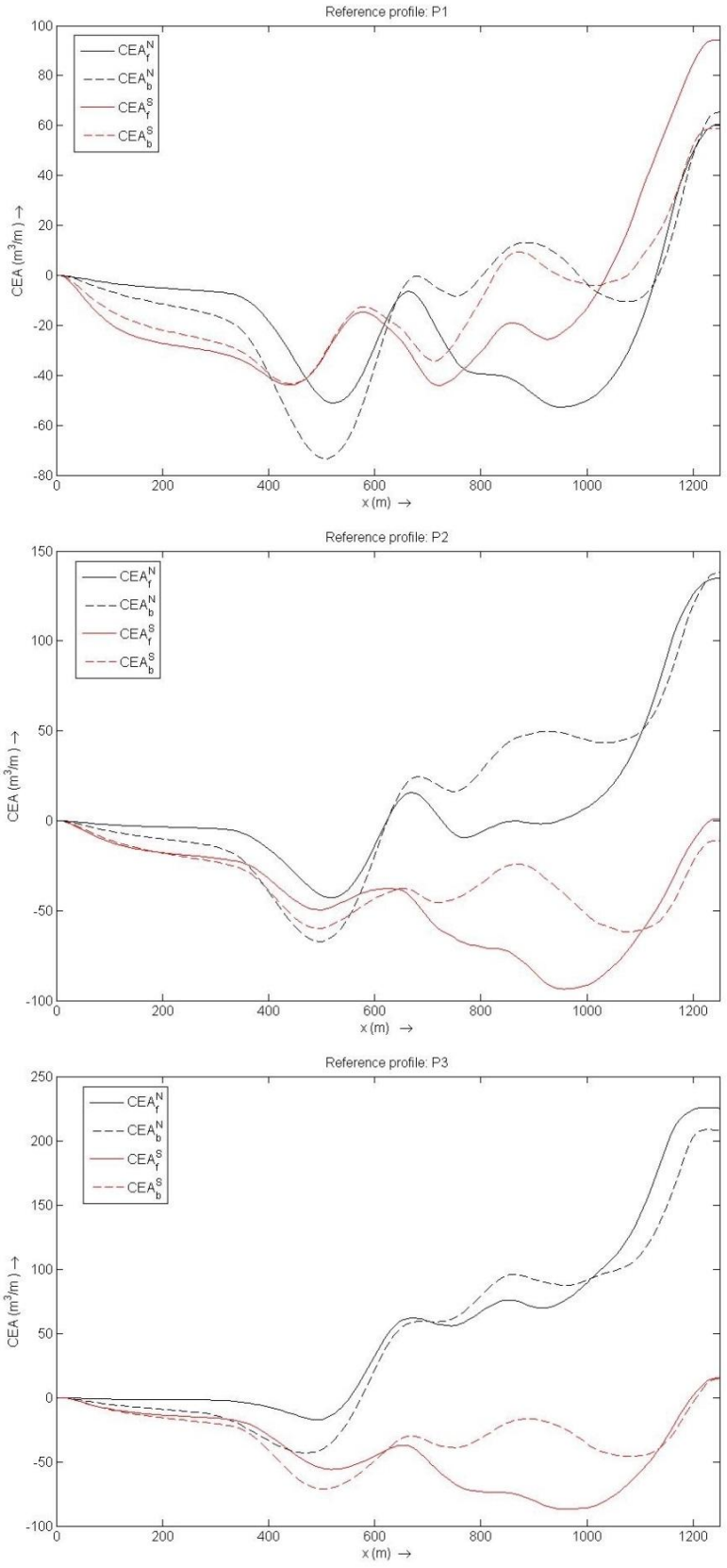

Figure 6.10 Mean cumulative eroded area in the baseline scenario (CEA_b) and in presence of the wave farm (CEA_f) in the southern area (in red) and northern area (in black) across each of the reference profiles P1, P2 and P3, at the end of the time period studied [10 Dec 2007, 06:00 UTC]. The *x*-coordinate represents the distance along the profile, with $x = 0$ the most offshore point.

Finally, the results of the beach face eroded area (*FEA*) confirmed the contribution of the wave farm to reducing erosion. Figure 6.11 shows the evolution of the erosion on the beach face along Perranporth Beach (*y = 0* corresponds to the southernmost point of the beach). The most severe erosion took place in the southernmost area of the beach, which is not backed by the dune system, and the northern area, where the waves were higher (Figure 6.3). As regards the efficacy of the wave farm for coastal protection, the reduction in erosion was more significant in the northern area of the beach than in the south and in the middle. In Figure 6.12, the non-dimensional erosion reduction (*NER*) is represented on the basis of the results of the eroded area in the beach face, confirming that the wave farm attenuated the erosion in the north of the beach, with values over 40% in a 1 km stretch of the beach. As regards the southern area of the beach, 500 m < *y* < 1500 m, the *NER* factor fluctuated strongly, due to isolated responses of different points of the profiles.

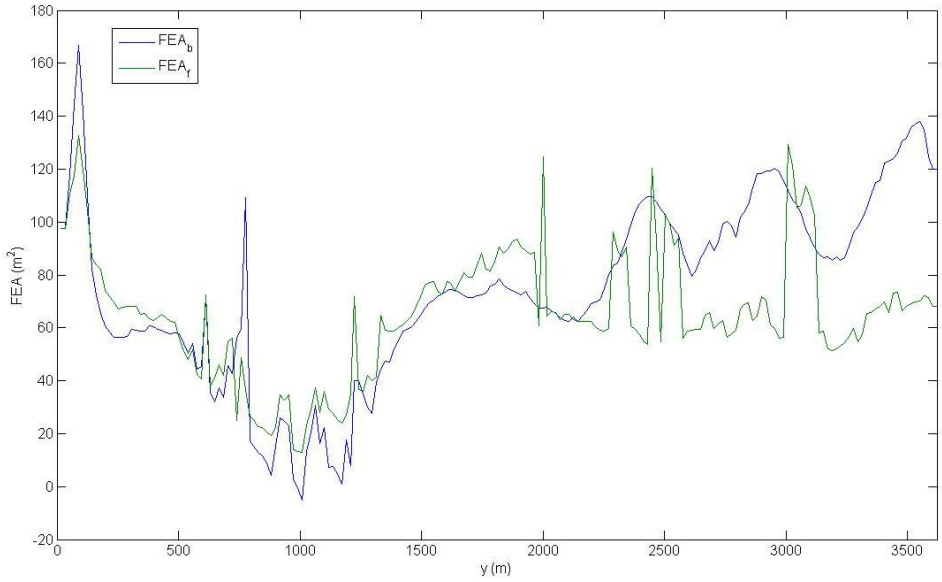

Figure 6.11 Beach face eroded area in two scenarios: baseline (FEA_b) and with the wave farm (FEA_f) along Perranporth Beach (*y* - coordinate, with *y* increasing towards the north of the beach) at the end of the time period studied [10 Dec 2007, 06:00 UTC].

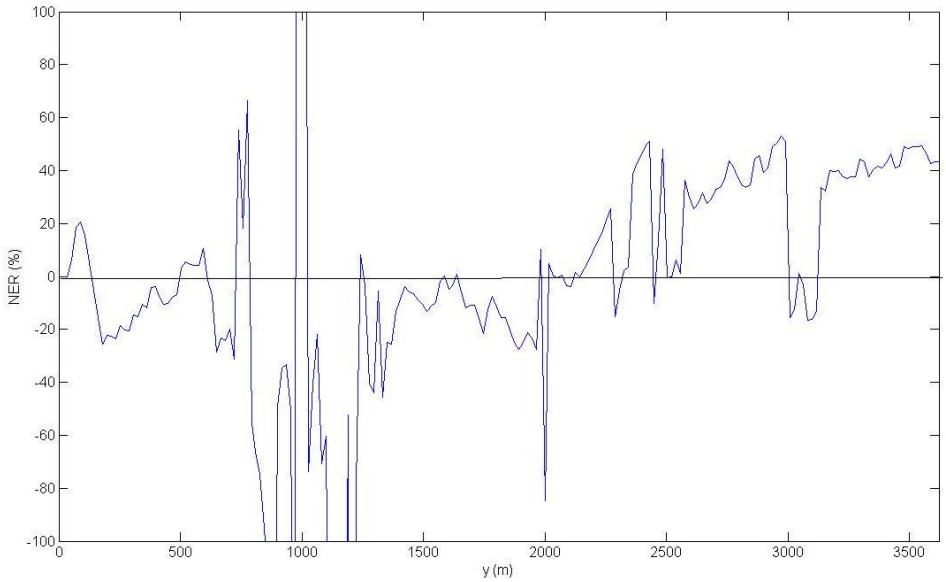

Figure 6.12 Non-dimensional erosion reduction (*NER*) at the beach face along Perranporth Beach (*y* - coordinate, with *y* increasing towards the north of the beach) at the end of the time period studied [10 Dec 2007, 06:00 UTC].

The results obtained in this work seem to lend credence to the hypothesis formulated at the outset, namely that a wave farm can serve as a coastal defence measure. It is important to bear in mind, however, that these results, and in particular their quantitative aspects, were derived for a specific case study: a beach with a bar between -5 m and -10 m backed by a well-developed dune system and under the attack of a storm of certain characteristics. On this basis, another case study with different characteristics (e.g. no presence of a submarine bar, different wave resource and grain size distribution) is presented in the following section to corroborate the degree of coastal protection afforded by wave farms.

6.2 XAGO BEACH

The case study of Xago Beach (Figure 4.6) is of particular relevance as this area was selected by the Asturian Institution for Energy Development (FAEN) for the deployment of the first offshore wave farm in Spain based on the characterisation of the wave energy resource, in conjunction with a morphologic and bathymetric study of the

area (Flor-Blanco *et al.*, 2011). Furthermore, Xago has experienced increased erosion on its dune system – evidenced by the recession of the dune toe, between 3.1 m and 11.5 m (Figure 6.13) – under the heightened storminess of recent years (Flor-Blanco, Flor & Pando, 2013; Flor, Flor-Blanco & Flores-Soriano, 2015). In this context, the possibility of protecting the coast through a nearshore wave farm is of great interest – and therein lies the motivation of this case study.

Figure 6.13 Dune toe recession at Xago Beach

6.2.1 MATERIALS AND METHODS

Xago is a lower mesotidal beach, with a semidiurnal tidal regime and a Medium Spring Range (MSR) of 2.66 m (Flor-Blanco, Flor & Pando, 2013). In the period considered for validation purposes (January 2010 - December 2010), the average values of significant wave height (H_s), mean period (T_m) and wave direction (θ) were: 1.40 m, 6.02 s and 317.1°, respectively. In the case of the stormy period considered for the assessment of the wave farm effects on the beach (7 November 2010 – 16 November 2010) the average wave conditions off Xago Beach were: H_s = 3.72 m, T_m = 7.49 s and

θ = 299.9°. Finally, three-hourly values of wind speed and direction obtained from the Global Forecast System (GFS) weather model are input into the wave propagation model. In the year studied there was no clearly prevailing wind direction – the highest probability of occurrence (22.4%) corresponded to S winds (from 157.5° to 202.5°). The strongest winds were associated with NW directions (from 292.5° to 337.5°), with wind speed values (u_{10}) exceeding 20 ms^{-1}.

The wave model is forced using the aforementioned data and validated during a year (January-December 2010) using the buoy data off Salinas Beach (Aviles Buoy located approx. 1 km to the west of Xago Beach) in conjunction with the SIMAR-3085039 point (off Xago Beach) from the SIMAR-44 dataset provided by Puertos del Estado (Spain).

In order to locate precisely the position of the WECs and simulate the wave farm impacts on the wave conditions in its lee, two computational grids with different resolutions were defined in SWAN (Figure 6.14): (i) the coarser grid with a spacing of 50 × 50 m extended 25 × 25 km, covering part of the Avilés canyon System (including the Avilés Canyon itself) with water depths over 900 m in the grid; and (ii) the finer (nested) grid with a spacing of 12 × 15 m extended 5.4 km offshore and 4.5 km from east to west, covering the area of interest. The wave farm was located in the area defined in the project at a water depth of ~30 m. The same layout than the one considered at Perranporth (consisting of 11 converters arranged in two rows) is studied in order to compare the results between the two case studies (Figure 6.15).

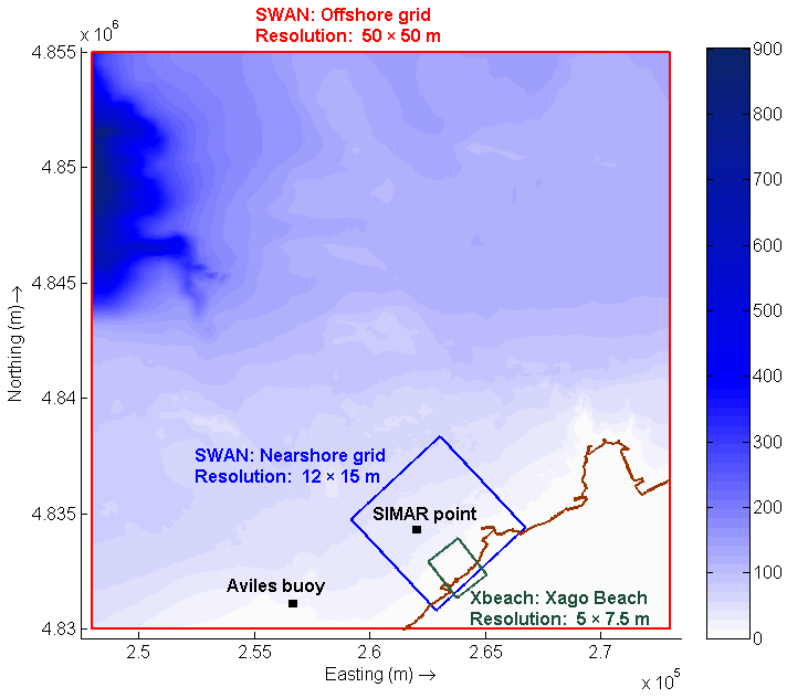

Figure 6.14 Computational grids for the SWAN and XBeach models, and wave buoy locations [Water depths in m].

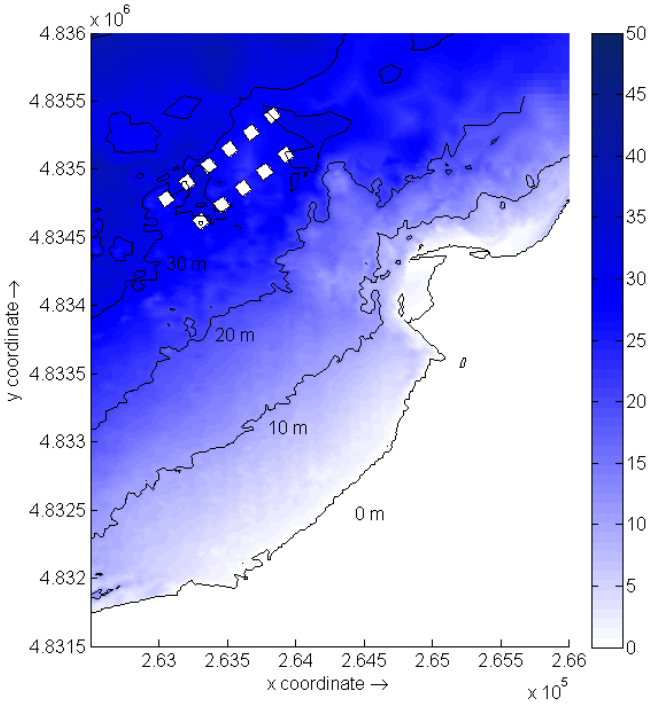

Figure 6.15 Wave farm layout off Xago Beach [Water depths in m].

The energy density output files (wave height, period, direction and spreading) from SWAN are used to prescribe the offshore boundary condition for XBeach. The grid in this model was extended approx. 1.7 km alongshore and 2 km offshore, from the dune system to water depths of 20 m, with a resolution of 7.5 and 5 m, respectively.

The high-resolution bathymetric data of the study area, obtained in *ad hoc* surveys by the University of Oviedo, were used as input for the coastal processes and wave propagation numerical models (Figure 6.16). Importantly, this dataset covered not only the submarine beach but also the subaerial, including the dune system, with elevation values ranging from –20 m to +15 m in the case of the coastal processes grid (relative to the Spanish National Geodetic Vertical Datum).

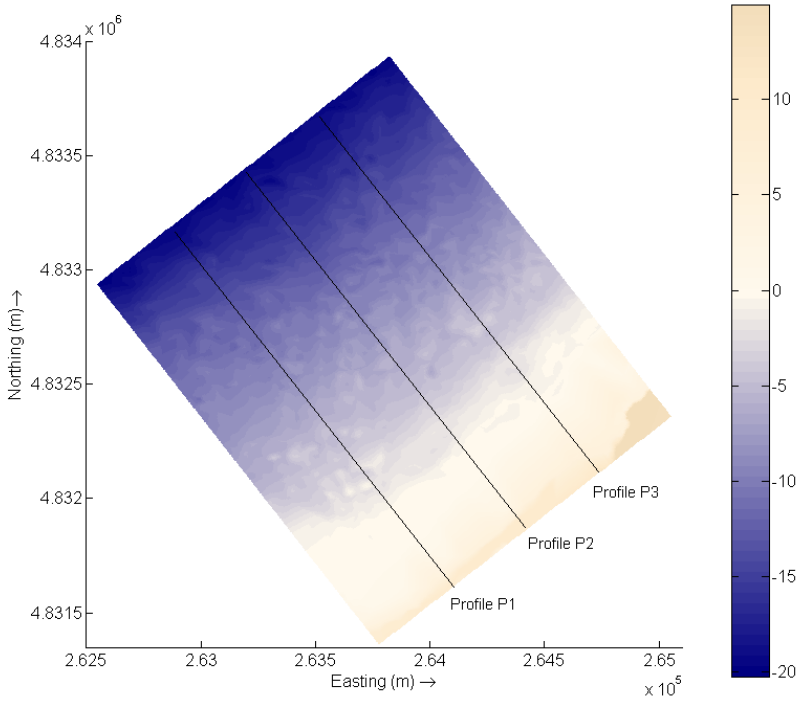

Figure 6.16 Bathymetry of Xago Beach for the coastal processes model with Profiles P1, P2 and P3. [Water depths in m].

6.2.2 RESULTS

First, the model was validated using the data from the wave buoy off Avilés (with available data from 1 March 2010 – 1 September 2010) and the point SIMAR44-3085039 (1 January 2010 – 31 December 2010). The model results were in excellent agreement with the observations (Figure 6.17 and Figure 6.18), as corroborated by the root mean square error and coefficient of determination (Table 6.1).

Data	Data available	Error statistics	
		Root Mean Square Error (*RMSE*) [in m]	Coefficient of determination (R^2) [-]
Buoy data off Avilés	1st March 2010 – 1st September 2010	0.33	0.89
SIMAR44-3085039	1st January 2010 – 1st January 2011	0.45	0.92

Table 6.1 Wave data used to validate the wave propagation model and values of the error statistics: Root Mean Square Error (*RMSE*) and the coefficient of determination (R^2).

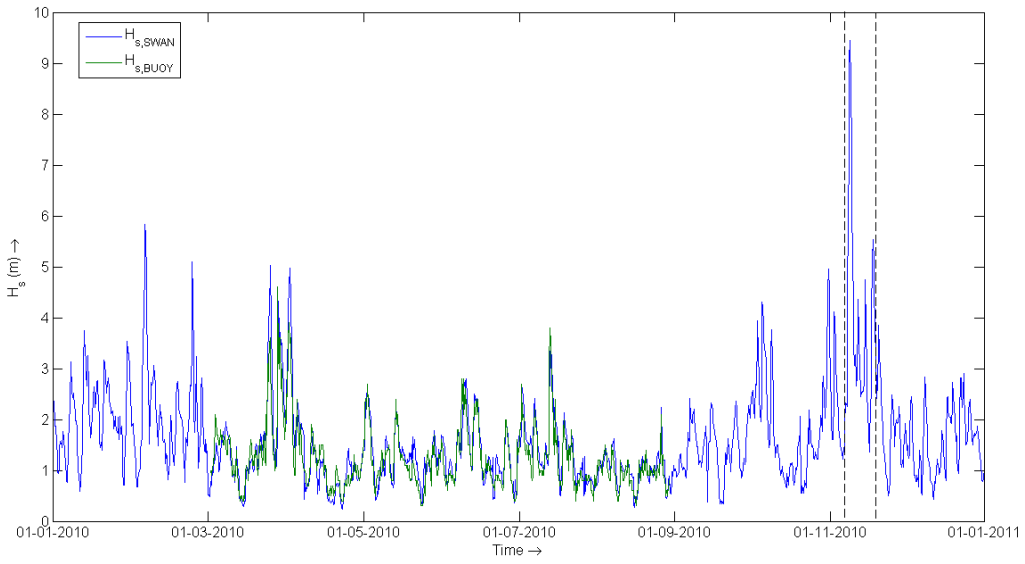

Figure 6.17 Validation of wave propagation model with the Aviles buoy data: observed ($H_{S,\,BUOY}$) *vs.* calculated ($H_{S,\,SWAN}$) time series of significant wave height. The dashed lines delimit the stormy period used for the study.

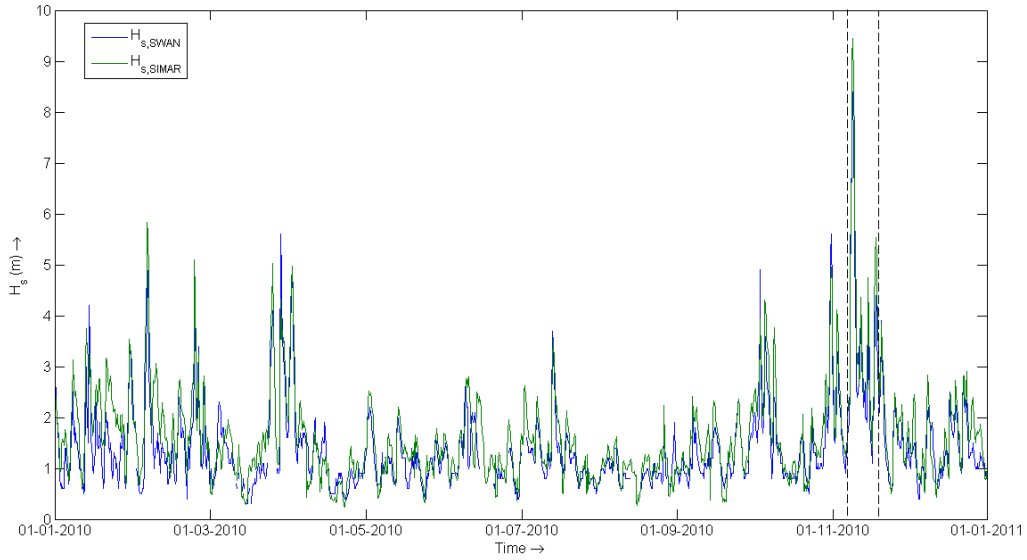

Figure 6.18 Validation of wave propagation model with the point SIMAR44-3085039 off Xago Beach: observed ($H_{S,\ SIMAR}$) vs. calculated ($H_{S,\ SWAN}$) time series of significant wave height. The dashed lines delimit the stormy period used for the study.

The impacts of the wave farm on the coast were analysed during the stormy period from 7 November 2010, 12:00 UTM to 16 November 2010, 06:00 UTM (delimited by dashed lines in Figure 6.17 and Figure 6.18). The significant wave height patterns at 18:00 on 9 November 2010 (Figure 6.19) display a conspicuous concentration of wave energy – indeed, the area defined in the project for the installation of the wave farm is a nearshore hotspot (Iglesias & Carballo, 2010a), i.e. an area with a concentration of wave energy due to wave interaction with the irregular bathymetry.

To put the area into perspective, it can be compared with the wave energy resource found at Perranporth. While the value of $\bar{J}_{WEC}$ .at Perranporth during a year was 17.26 kW/m, in the case of Xago it was 20.21 kW/m, albeit the wave farm was located at a smaller farm-to-coast distance (1.7 km) than at Perranporth (6 km). This difference (approx. 15%) in the wave energy resource reflects the large wave resource available in the area defined by the project.

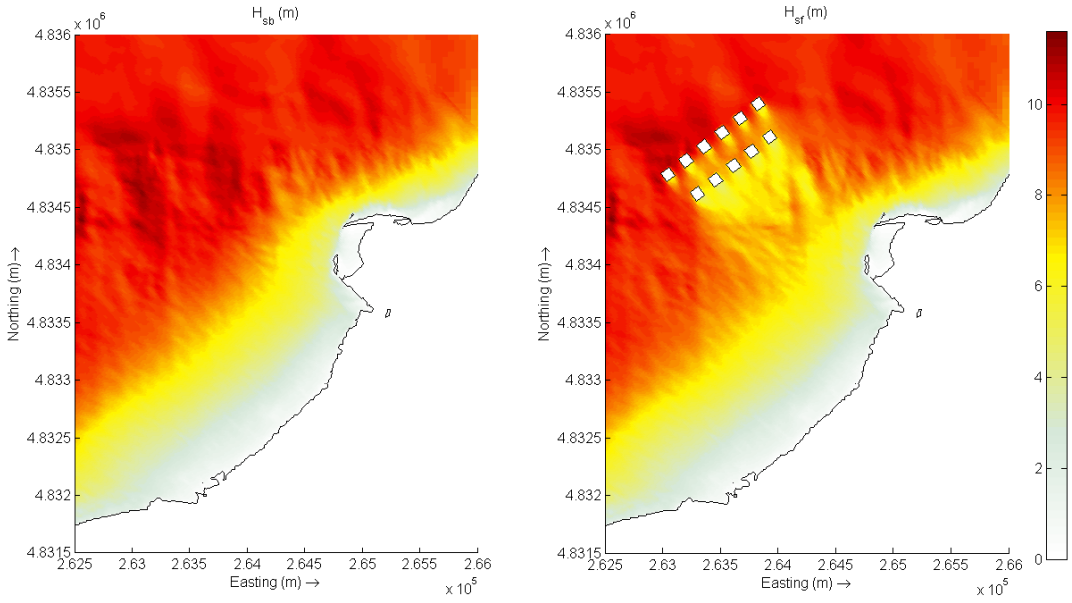

Figure 6.19 Significant wave height in the baseline scenario (H_{sb}) and with the wave farm (H_{sf}) on 9 Nov 2010, 18:00 UTC. [Deep water wave conditions: H_{s0}=10.28 m, T_p = 16.19 s, θ_p = 314.94 °].

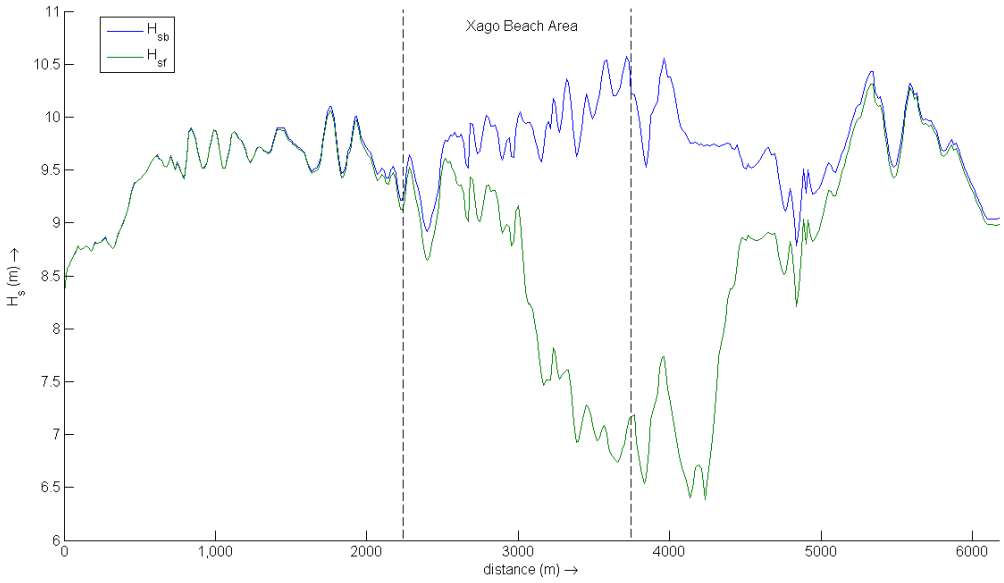

Figure 6.20 Significant wave height in the baseline scenario (H_{sb}) and with the wave farm (H_{sf}) along the 20 m water depth contour on 9 Nov 2010, 18:00 UTC. [Deep water wave conditions: H_{s0}=10.28 m, T_p = 16.19 s, θ_p = 314.94 °].

The impacts of the wave farm on the wave patterns were especially significant in the lee of the wave farm, where the reduction of the significant wave height (*RSH*) reached the greatest values (over 50%). This reduction decreased towards the coastline

due to the energy diffracted into the shadow of the WECs; however, the impact cannot be overlooked, with values exceeding 15% along the 10 m contour. The farm was not directly in front of the beach but displaced somewhat to the east, which reduced its impact on the west section of the beach. Figure 6.20 illustrates the reduction in the significant wave height along the 20 m contour depicted in Figure 6.15, which was used as input for the coastal processes model. The shadow caused by the farm extended over approx. 3 km (Figure 6.21), with an average *RSH* value exceeding 50% in the lee of the farm over. Owing to the position of the farm, this reduction in nearshore wave height extended some distance east of Xago Beach.

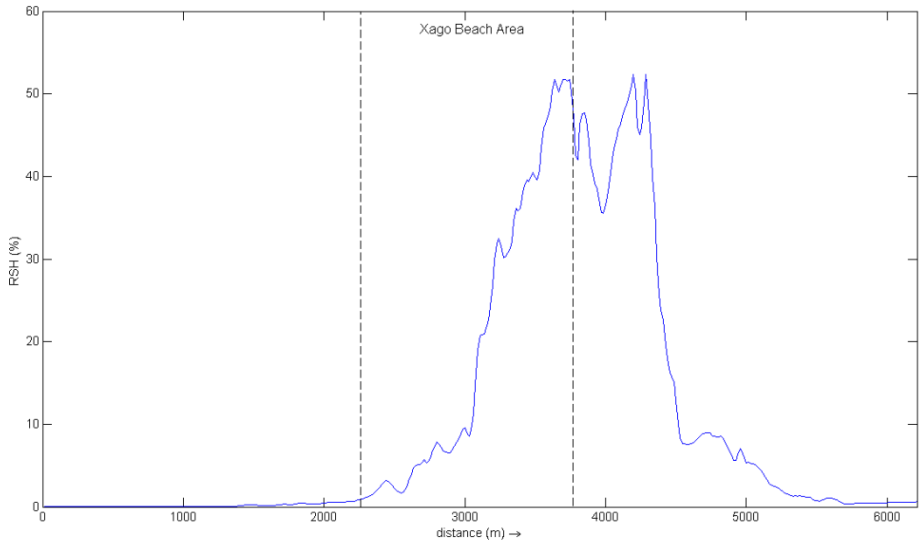

Figure 6.21 Reduction of the significant wave height (*RSH*) parameter along the 20 m water depth contour on 9 Nov 2010, 18:00 UTC. [Deep water wave conditions: H_{s0}=10.28 m, T_p = 16.19 s, θ_p = 314.94 °].

The spectral wave conditions along the 20 m contour were input into the coastal processes model by means of energy density output files to study the response of the beach under storm conditions with and without (baseline) the wave farm and, on these grounds, quantify the degree of coastal protection afforded by the wave farm. First, the erosion and accretion patterns at Xago Beach are analysed in the baseline scenario. Three main sections can be observed (Figure 6.22): (i) the west section, which experiences significant storm-induced erosion; (ii) the middle section, characterised by

deposition in the intertidal area of the material eroded in the previous section, and some erosion on the dune front; and (iii) the east section of the beach, characterised by intense erosion of the dune. It is also noteworthy how the evolution of the foredune front seems to have varied over the last years relative to the previous decades: whereas the dune limit advanced from 1970 to 2011 (Figure 6.22), it receded from 2011 to 2014 (Figure 6.13). This change from progradation to recession may well be related to the severe winter gales experienced in the 2011-2014 period (Flor-Blanco, Flor & Pando, 2013).

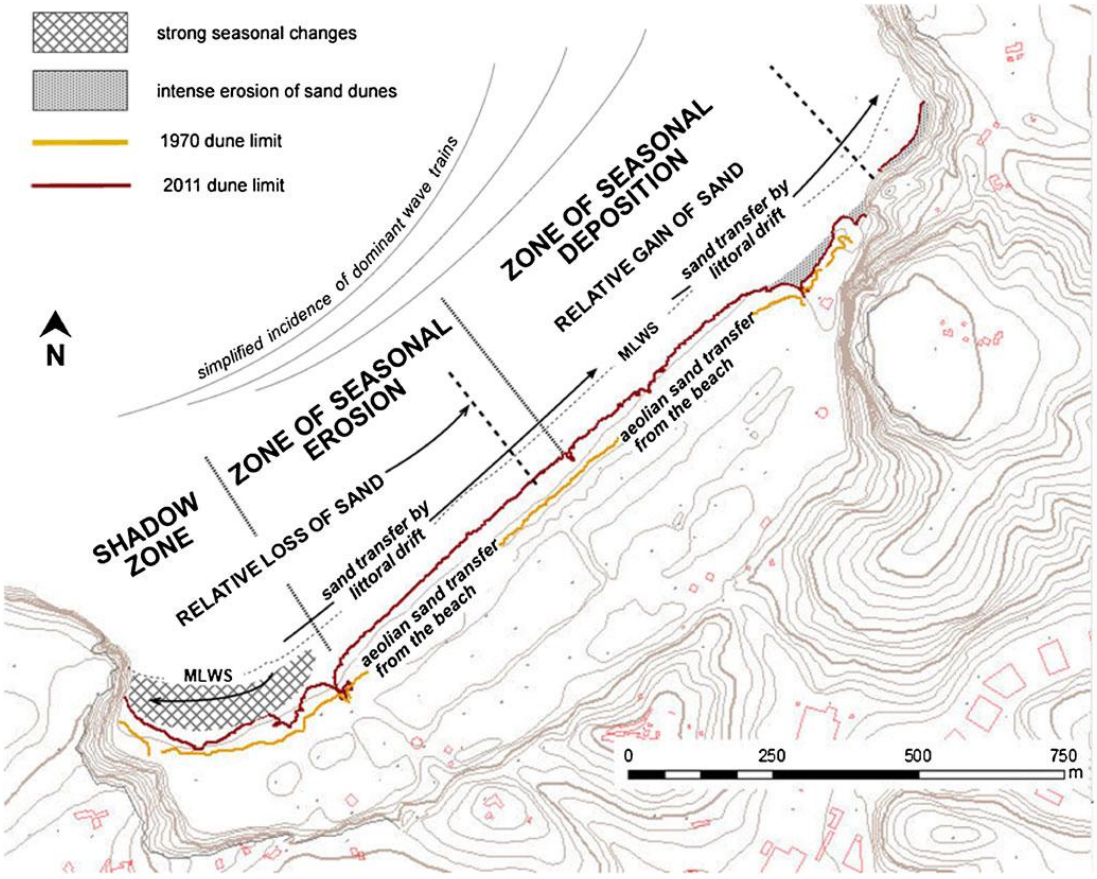

Figure 6.22 Simplified dynamic and sedimentary model of Xago Beach (Flor-Blanco, Flor & Pando, 2013)

The model results in the baseline scenario (Figure 6.23) are in good agreement with the general sedimentary dynamics of the beach. In effect, the difference in bed level elevation between the beginning and the end of the simulation period corresponds well with the sections previously identified (Figure 6.22). The most acute erosion occurs in

the east section of the beach, with bed level differences of up to 2.5 m. In the west section erosion was also considerable, in line with the general dynamics. For its part, in the middle section erosion of the dune was found to be less significant, and sediment deposition occurred in the intertidal area.

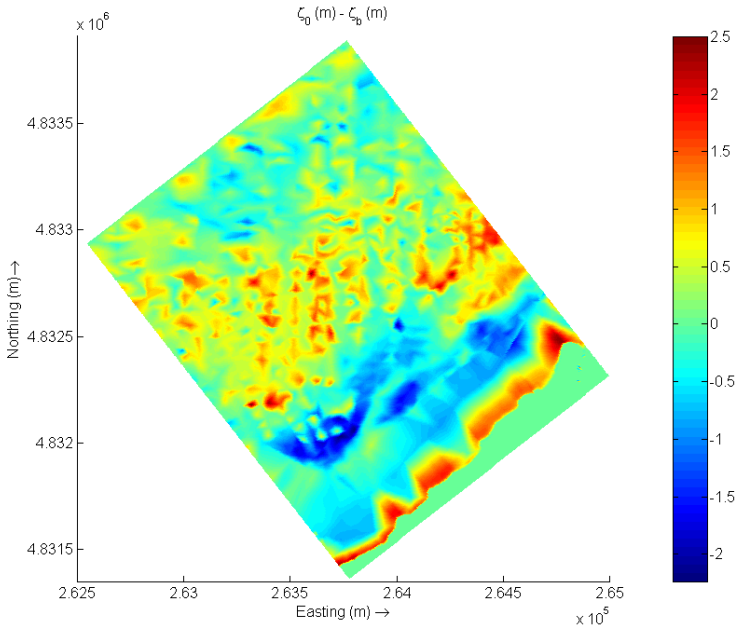

Figure 6.23 Bed level difference between the first (ζ_b) and the last point (ζ_0) of the simulation.

For the analysis of both scenarios with and without the wave farm, the impact indicators are applied. Figure 6.24 shows the *BLI* values (the bed level difference between the wave farm and the baseline scenarios) at the end of the storm period analysed. Three main areas can be distinguished: the first two, the dune front along the entire beach and the low tide terrace in the east section, with positive *BLI* values, i.e. reduction of erosion due to the wave farm; and the third area, the low tide terrace in the west and middle sections, with negative *BLI* values, i.e. reduction of accretion due to the wave farm.

The greatest *BLI* values (over 2 m) were found in the first area, the dune front, and especially in the east section of the beach, which experienced the greatest erosion in the baseline scenario. As regards the west section of the dune front, which also underwent

significant storm-induced erosion, the wave farm contributed to reducing the erosion by up to 1.5 m. Finally, in the middle section, with lower values of erosion in the baseline scenario, the reduction of the erosion on the dune front caused by the wave farm was also lower, below 1 m. In sum, the wave farm contributed significantly to reducing storm-induced erosion on the dune front.

In the second area, the low-tide terrace in the east section of the beach, the maximum *BLI* values were smaller than on the dune front but nevertheless relevant – with storm-induced erosion decreasing by up to 1 m over a large area. Thus, in the east section of the beach, both on the dune front and the low-tide terrace, erosion is significantly mitigated, which can be explained by the fact that this area is directly in the lee of the wave farm, with consequential reductions in significant wave heights – over 50% at the 20 m contour.

Finally, in the third area, the west and middle sections of the low-tide terrace, negative *BLI* values are found due to the greater volume of material eroded in the baseline scenario from the dune front and to the contributions of material eroded from the east section.

As mentioned above, the dune front experienced the greatest reductions of erosion, importantly the landward end of erosion was displaced seaward by over 10 m along the three profiles considered, representative of the three sections of the beach (Figure 6.25): P1 (west), P2 (middle) and P3 (east). In the east section this seaward displacement reached a very substantial 25 m, which is indicative of the efficiency of the wave farm in countering the storm-induced erosion that affected Xago in the last lustrum (Figure 6.13).

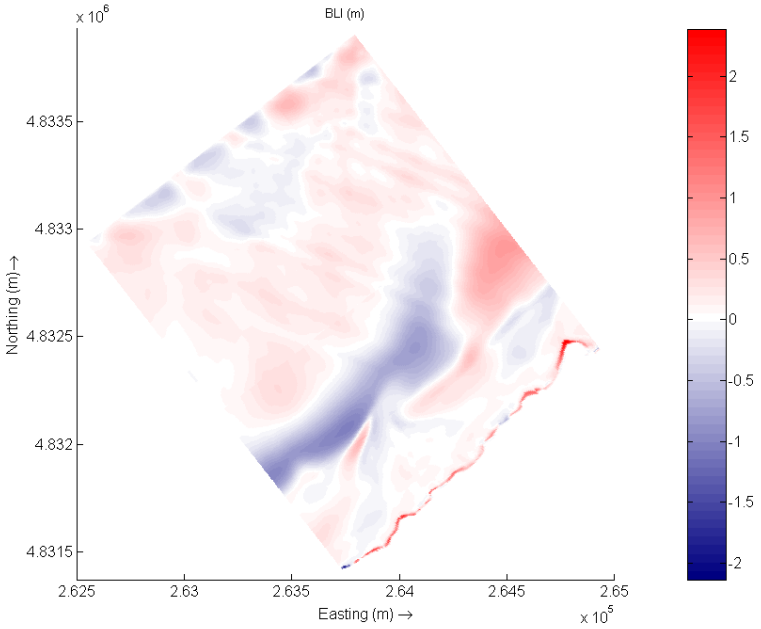

Figure 6.24 Bed level impact (*BLI*) in the area of interest at Xago Beach at the end of the time period studied [16 Nov 2007, 06:00 UTC].

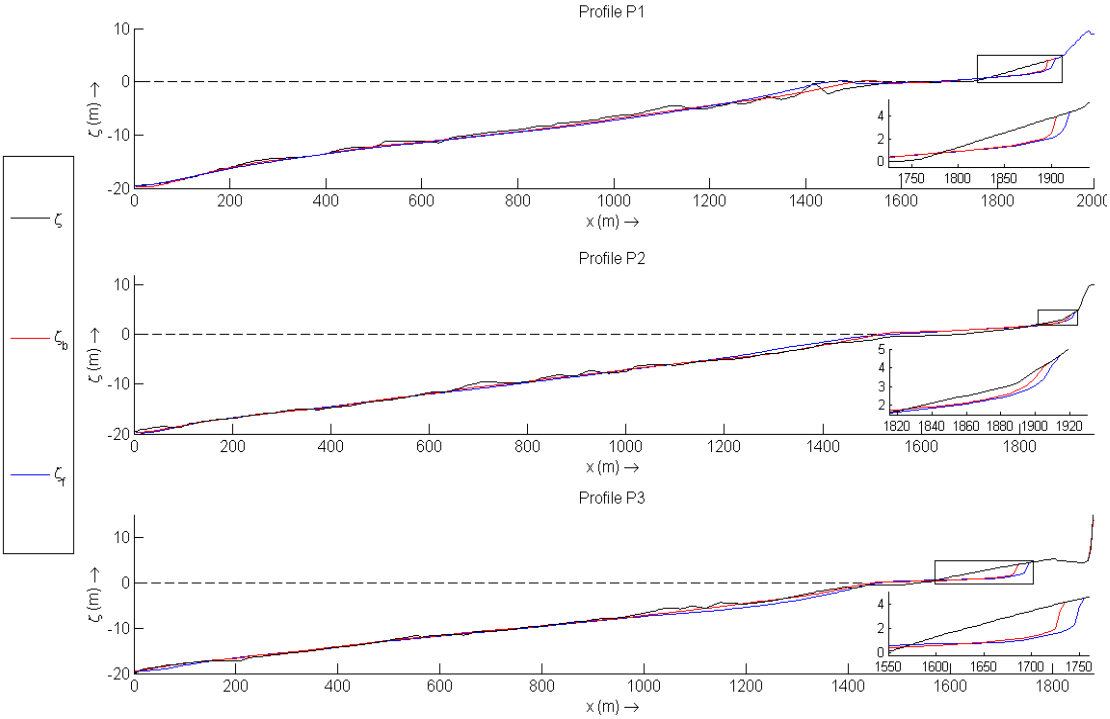

Figure 6.25 Bed level at profiles P1, P2 and P3: initial (ζ_0) [07 Dec 2007, 12:00 UTC] and at the end of the simulation in the baseline scenario (ζ_b) and with the wave farm (ζ_f) [16 Nov 2007, 06:00 UTC].

As regards the erosion on the beach face, two impact factors were applied: *FEA* and *NER*. The *FEA* values (Figure 6.26) confirmed that the most sensitive area to storm-induced erosion is the east section of the beach and consequently the greatest volumes

of material eroded occurred there. Significant erosion also occurred in the west section of the beach, although in the case of the westernmost section the area eroded in the beach face was less significant than on the front dune (Figure 6.24). On the other hand, in the central and east section of the beach, erosion was less pronounced on the front dune than on the beach face, where it reached values similar to the west part of the beach. This pattern can be observed in Figure 6.25, with profiles P1 (west) and P3 (east) more affected by the erosion at the toe of the dune than profile P2 (middle), but with similar impacts along the beach face.

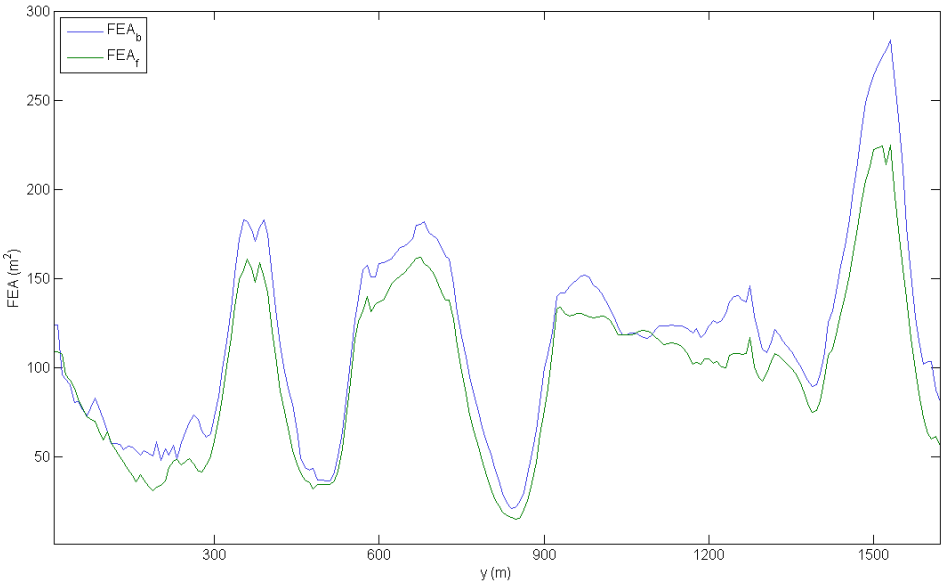

Figure 6.26 Beach face eroded area at the end of the time period studied [16 Nov 2007, 06:00 UTC] in two scenarios: baseline (FEA_b) and with the wave farm (FEA_f). The *y*- coordinate represents the beach profile, with y increasing eastwards.

In order to analyse globally the effects of the wave farm, the *NER* index is applied, which represents the change in the eroded area caused by the wave farm as a percentage (Figure 6.27). The wave farm was found to reduce erosion ($NER > 0$) in most of the beach, with the highest values in the east section ($NER > 60\%$). This is precisely the area where the erosion of the beach face was more pronounced; hence it is an excellent indicator of the effectiveness of wave farms to protect the coast in erosion-prone areas. This drastic decrease in erosion in the east section, for all its importance, must not

obscure the relevant effect reductions elsewhere, with an average *NER* value along the entire beach of 17.64%.

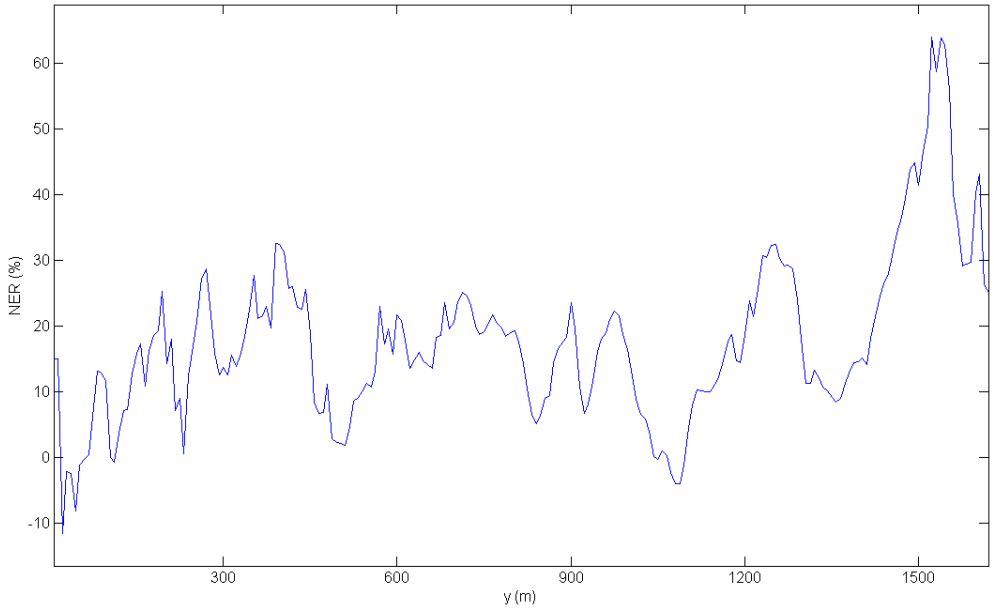

Figure 6.27 Non-dimensional erosion reduction (*NER*) on the beach face at the end of the time period studied [16 Nov 2007, 06:00 UTC]. The *y*- coordinate represents the beach profile, with y increasing eastwards.

6.3 CONCLUSIONS

Comparing the effects of the wave farm at Xago with those at Perranporth Beach, UK, (Abanades, Greaves & Iglesias, 2014a; 2014b; 2015b), significant differences were found; which reflects the need for site-specific assessment of the effects of wave farms on the beach. These differences lied in part to the presence of a submarine bar at Perranporth, which provided a degree of protection to the beach. This was not the case at Xago, where storm-induced erosion was consequently more pronounced. On these grounds, the wave farm was more effective to mitigate erosion on the dune front at Xago, as reflected by the very substantial seaward displacement of the landward end of erosion by up to 25 m in large sections of the beach. This shows a clear contribution of the farm to arresting the erosive trends affecting the dune system. Regarding the erosion patterns in the beach face, the reduction afforded by the wave farm was greater at

Perranporth, as a larger section of the beach was protected (*NER* > 40% in a section of 1500 m, nearly half of the beach), while in Xago greater values where found (*NER* > 60%) but in smaller sections of the beach. Therefore, in both cases, Xago and Perranporth, the results vindicate the initial hypothesis that wave farms can contribute to protecting the coast and, particularly, mitigating dune erosion.

Having determined the effectiveness of wave farms to protect the coast in the medium and the short term, the following chapters will investigate the wave farm impacts on the coast and on the wave conditions as a function of the key design parameters: the farm-to-coast distance in Chapter 7 and the wave farm layout in Chapter 8.

Chapter 7
Influence of the Farm-to-Coast Distance

7. INFLUENCE OF THE FARM-TO-COAST DISTANCE

The location of a wave farm, and, in particular, its distance to the coast is one of the key aspects in a wave energy project. In the selection of the location a number of variables are typically taken into account, from the wave resource to the maintenance and infrastructure costs; however, the effects of the farm on the coast, which can be instrumental in mitigating storm-induced erosion and thus contribute to coastal defence, are seldom, if ever, considered. Furthermore, these impacts can be controlled by locating the wave farm closer to or further from the coastline. In this context, the objective of this chapter is to establish the dependence of the degree of coastal protection offered by the farm on its distance from the coastline by means of a sensitivity analysis focused on Perranporth Beach (SW England). The following contents are published in the paper of Renewable Energy (5-year impact factor: 3.982) "**Coastal defence using wave farms: The role of farm-to-coast distance**", which was accepted for publication on the 20 October 2014.

7.1 MATERIALS AND METHODS

In this chapter, four scenarios were compared, corresponding to three locations of the wave farm at different distances from the coast, plus the baseline (no farm) scenario, under different wave conditions. Based on the work of Iglesias and Carballo (2014) that analysed the influence of the farm-to-coast distance in the impact of wave farms on the wave conditions, the following distances were considered in this chapter: 2 km, 4 km and 6 km from the reference (10 m water depth) contour – corresponding to water depths of approx. 25 m, 30 m and 35 m, respectively (Figure 7.1). These wave farms were implemented on the high-resolution grid of the wave propagation model described and validated in Section 5.1.

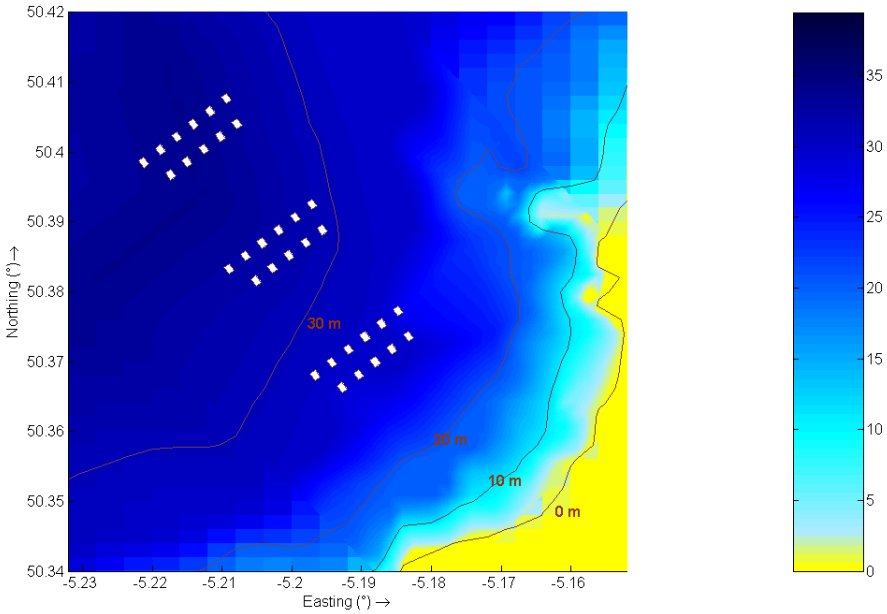

Figure 7.1 The three locations considered for the wave farm, at distances of 2 km, 4 km and 6 km from the reference (10 m water depth) contour [water depth in m].

In this chapter, following Kenney (2009) and based on the analysis of the offshore wave climate in the area, two frequent wave conditions (Table 7.1) were prescribed at the outer (ocean) boundary of the SWAN offshore grid. The results from this model were coupled to XBeach, which was used to analyse the response of the beach with and without the wave farm during 24 hours, the typical duration of these wave conditions at Perranporth.

Case study	H_s (m)	T_p (s)	θ (°)	s (°)	K_t
CS1	3	12	315 (NW)	26.50	0.76
CS2	3.5	11	315 (NW)	26.34	0.78

Table 7.1 Offshore wave conditions: significant wave height (H_s), peak period (T_p), mean direction (θ), spreading (s) and transmission coefficient (K_t) for the different case studies.

7.2 RESULTS

The results obtained from the nearshore wave propagation model were analysed to study the impact of the wave farm on the wave conditions. The nearshore significant wave height (H_s) for the different scenarios (baseline and with the wave farm at

distances of 2 km, 4 km and 6 km from the reference contour) is shown in Figure 7.2 for CS1 (Table 7.1). The reduction in the significant wave height in the lee of the farm caused by the energy extraction is apparent. This reduction was assessed by means of the impact indicator RSH_i (Figure 7.3). The maximum value of the indicator was achieved within the second row of WECs with values of up to 50%. At a distance of 1.5 km from the second row of devices, the reduction reached a peak of 40% due to the merging of the shadows caused by the first and the second row of devices. However, this reduction decreased moving towards the coast due to the redistribution of the energy from the edges into the shadow caused by the wave farm. At a water depth of 10 m, the average reduction caused by the wave farm closest to the coast (2 km) was approx. 25%, whereas for the wave farm at 4 and 6 km the average reduction was approx. 15% and 9%, respectively.

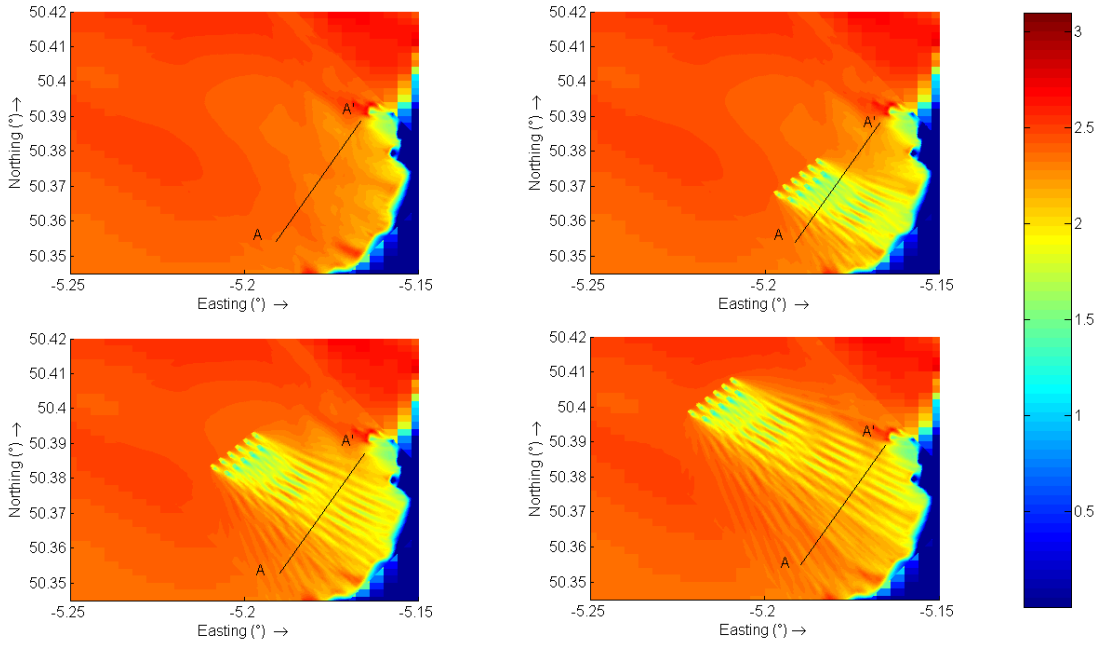

Figure 7.2 Significant wave height [m] in the baseline scenario and in the presence of the farm at distances of 2 km, 4 km and 6 km from the reference (10 m water depth) contour in CS1 (clockwise from above left).

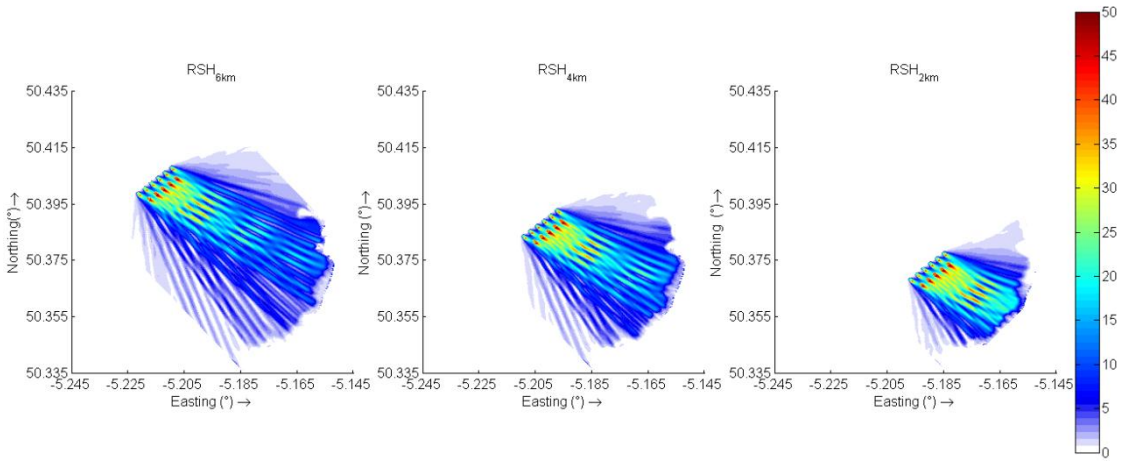

Figure 7.3 Reduction of the significant wave height (%) with the wave farm at a distance of: 2 km (*RSH2km*), 4 km (*RSH4km*) and 6 km (*RSH6km*) from the reference (10 m water depth) contour in study CS2 [in m].

The relevance of the farm-to-coast distance may be readily observed in the shadows caused by the wave farm at different distances. The area affected at the coastline by the wave farm furthest to the coast (6 km) was greater than 7 km, however the average reduction of the significant wave height in this area was less than 5%. On the other hand, the wave farm at 2 km affected a smaller area in the coastline, around 4 km, but the reduction exceeded 10%. Figure 7.4 shows this reduction for CS1 (above) and CS2 (below) along the line AA´, located in Figure 7.2, which corresponded to the area of interest at Perranporth Beach and was used as input for the coastal processes model. This figure confirmed the different shadow pattern brought about by the wave farm at a distance of 4 and 6 km compared with the 2 km. In the latter, the reduction mainly occurred in the central section of the beach, being less significant in the north area of the beach. However, for the other two scenarios, the reduction was found to be approx. constant along the line AA´.

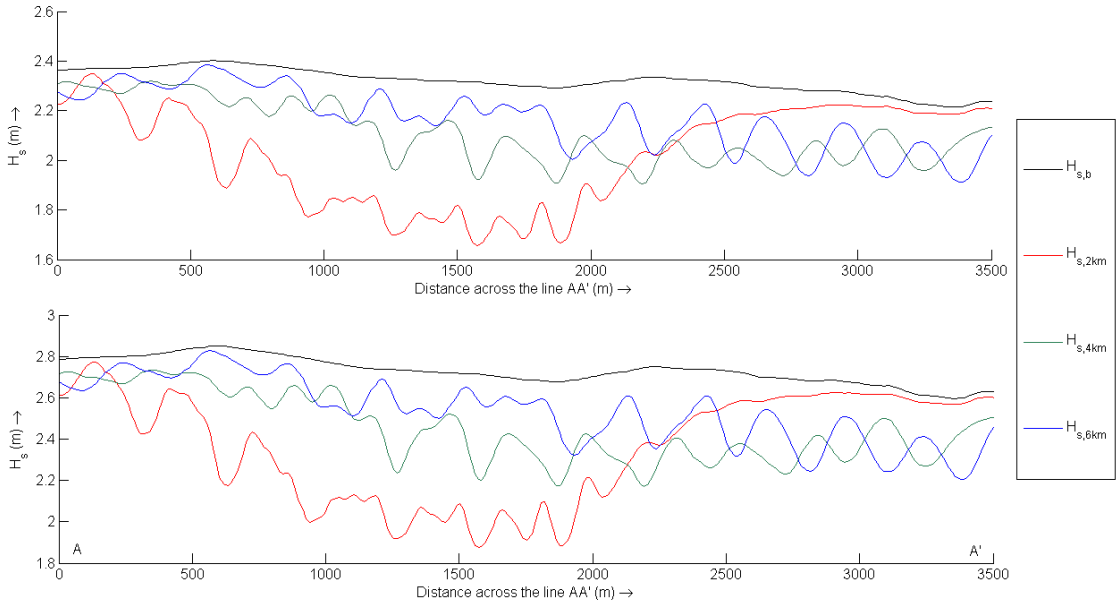

Figure 7.4 Significant wave height [in m] in the baseline scenario ($H_{s,\,b}$) and in the presence of the farm at a distance of: 2 km ($H_{s,2\,km}$), 4 km ($H_{s,4\,km}$) and 6 km ($H_{s,6\,km}$) from the reference (10 m water depth) contour across the line AA' in CS1 (above) and CS2 (below).

In terms of wave power, the resource was evaluated at the location of each of the WECs in the wave farm. Table 7.2 shows the average wave power incident on a generic WEC of the wave farm for the different distances, it was found that the closer the wave farm to the coast, the lesser the resource, due to the dissipation caused by the different coastal processes that occur in intermediate and shallow water. For the wave farm closest to the coast the reduction of the wave power compared to the scenario with the wave farm at a distance of 6 km was 10.5% and 8.7% for CS1 and CS2, respectively. In the case of the wave farm at 4 km the reduction compared with the scenario at 6 km is 5.7% and 7.3% for CS1 and CS2, respectively.

Case study (H_s)	$\bar{J}_{WEC}$		
	2 km	4 km	6 km
CS1: 3 m	17.95	18.91	20.07
CS2: 3.5 m	30.89	31.37	33.83

Table 7.2 Average wave power on a generic WEC of the wave farm ($\bar{J}_{WEC}$) for the different case studies [kW/m]

In order to obtained a better characterisation of the wave energy resource as a function of the farm to coast distance, the $\overline{J}_{WEC}$ values for the different wave farm scenarios were analysed during the time series used for validation purposes (Nov 2007 – Oct 2008). Similarly, the resource found for the wave farm at 2 km was 15% lower than that for the farm at 6 km (Table 7.3). The difference in terms of the available resource is less between the farm at 4 km and 6 km (5%). In summary, on the one hand the wave farm closest to the beach caused the greatest reduction in the significant wave height, but, on the other hand, the resource in that area was lower than in deeper areas, and, therefore, a comparative study of the response of the beach under storm conditions is necessary to determine the best location for a wave farm in terms of wave energy resource and coastal protection.

Wave farm scenario	$\overline{J}_{WEC}$ (kW/m)
2 km	14.46
4 km	16.44
6 km	17.26

Table 7.3 Average wave power on a generic WEC of the wave farm ($\overline{J}_{WEC}$) from Nov 2007 to Oct 2008 [kW/m]

The alteration of the beach morphology by the wave farm was quantified by means of the impact indicators. The first indicator was the bed level difference, *BLI*, which represented the difference of the bed level between the baseline and the wave farm scenarios at a point in time. Figure 7.5 shows *BLI* values at the end of the storm for CS1 with the wave farm at a distance of 2 km (left), 4 km (middle) and 6 km (right). It was observed that the main impact caused by the wave farm was located at the beach face, where reductions of the erosion up to 1.5 m were found.

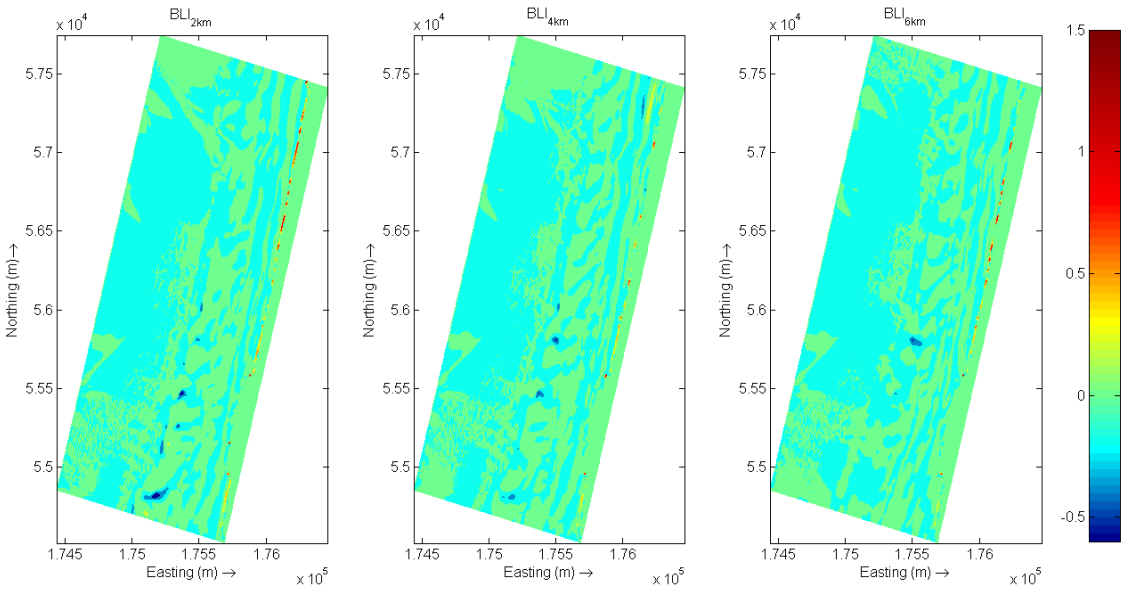

Figure 7.5 Bed level impact with the wave farm at a distance of 2 km (BLI_{2km}), 4 km (BLI_{4km}) and 6 km (BLI_{6km}) at the end of the storm in CS1.

Figure 7.6 illustrates the evolution of three profiles at the end of the storm for CS2, corresponding with three section of the beach that were identified by their different responses under the storms: (i) the southern section of the beach (P_1 in Figure 7.6) with a smooth slope in the intertidal area; (ii) the area backed by a very steep dune (P_2 in Figure 7.6) where the mean water level was close to the toe of the dune; and (iii) the northern section of the beach (P_3 in Figure 7.6) also backed by the dune, but with a greater distance from the toe of the dune to the mean water level. In the case of P_1 and P_3 the main erosion occurred on the beach face and this material was moved to lower sections of the beach, however in the case of P_2 accretion was detected in the intertidal area due to the material eroded in the steep dune for the proximity of the mean water level to it. In the area of P_3 were found the greatest values of the *BLI* indicator, with reductions greater than 1 m, while in the section P_1 the reduction took values of approx. 0.5 m.

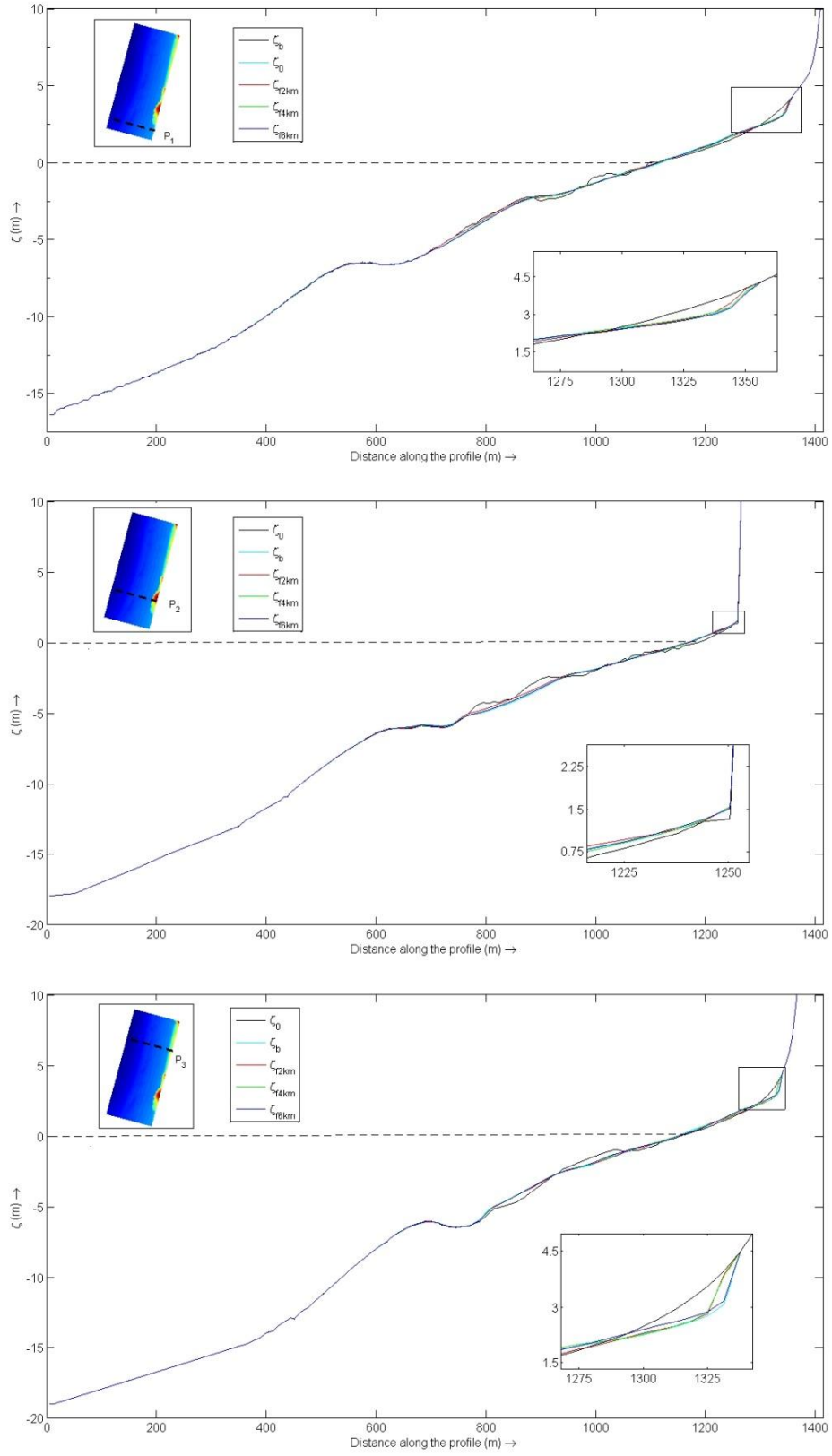

Figure 7.6 Bed level at Profiles P_1, P_2 and P_3: initial (ζ_0) and at the end of the storm in CS2 in the baseline scenario (ζ_b) and with the wave farm at a distance of 2 km (ζ_{f2km}), 4 km (ζ_{f4km}) and 6 km (ζ_{f6km}).

In the comparison between scenarios, the wave farm at a distance of 2 km caused greater reduction of the erosion in the beach along the beach than the other scenarios, in

which areas with significant reductions of erosion were combined with negligible values or even accretion. In the lower sections of the beach, accretion occurred due to the amount of material eroded in the beach face. In the scenario with the wave farm closest to the coast the *BLI* took negative values of -0.5 m in the southern area of the beach, which meant that the accretion without the farm was bigger than with it, due to the greater erosion produced in the intertidal area in the baseline scenario. This reduction of the accretion with the wave farm at a distance of 4 km and 6 km took place only in a few sections of the beach with *BLI* values less than 0.3 m.

The impact factor *FEA* was defined to quantify the erosion in the beach face along the beach (Figure 7.7). The greatest values of this indicator along the beach were focussed in the southern area because this section was not backed by the dune. The erosion in the baseline scenario was, in general, greater than the scenarios with the wave farm, especially in the middle and northern area of the beach, *y*–coordinate (along the beach) > 1250 m. To compare the reduction between the different wave farm scenarios the indicator *NER* was defined, which showed the variation of the erosion in terms of the eroded area in the baseline scenario (Figure 7.8). The *NER* values fluctuated considerably along the beach, but it was observed that the reduction using a wave farm at a distance of 2 km was greater than the other two scenarios.

In the area of the steep dune (500 m < *y*–coordinate < 1250 m), the erosion in the beach face was very low (negligible in some sections), and very few profiles presented an isolated response taking the NER factor negative values (greater erosion with the farm than without it). However, in terms of the average reduction of the beach face erosion along the whole beach, it was confirmed that the wave farm at 2 km offered a greater degree of coastal protection, around 15% in both case studies, than the scenario with the wave farm at 4 and 6 km, which presented an approximate reduction of approx.

10%. Considering particular sections of the beach, the impact was much more significant, for instance, the reduction exceeded 20% for the wave farm at 2 km for values of the *y* – coordinate between 1200 and 2000 m in CS2, which was the area most affected by the reduction of the significant wave height. The results for the wave farm at 4 and 6 km did not present large differences in terms of the reduction of the erosion along the whole beach; however the average reduction for the farm at 4 km was slightly greater (13%) than the farm at 6 km (11%) in the area backed by the dune (*y* > 1250 m).

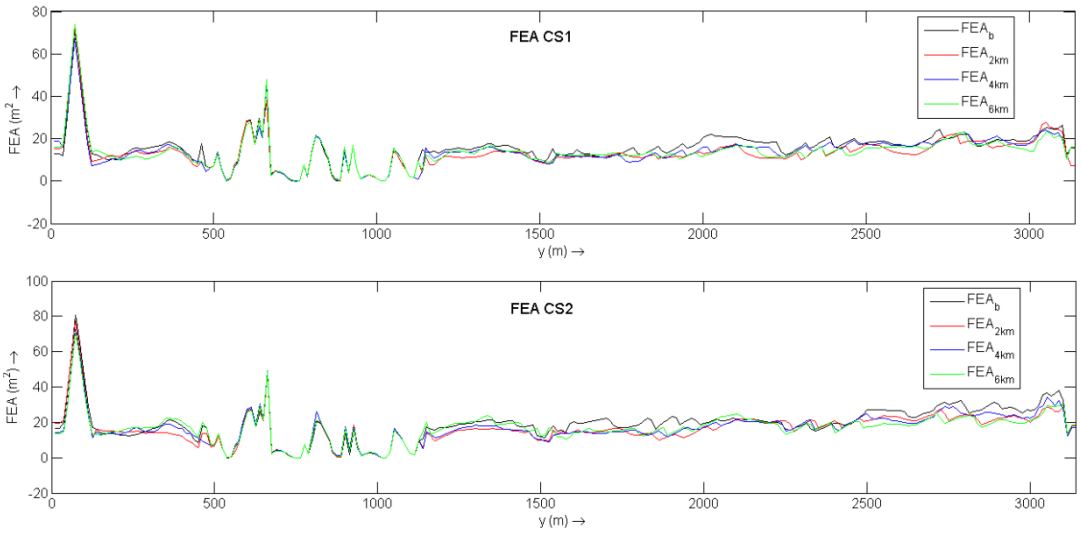

Figure 7.7 Beach face eroded area in the following scenarios: baseline (FEA_b) and with the wave farm at a distance of 2 km (FEA_{2km}), 4 km (FEA_{4km}) and 6 km (FEA_{6km}) along Perranporth Beach (*y* - coordinate, with *y* increasing towards the north of the beach) at the end of the storm in CS1 (above) and CS2 (below).

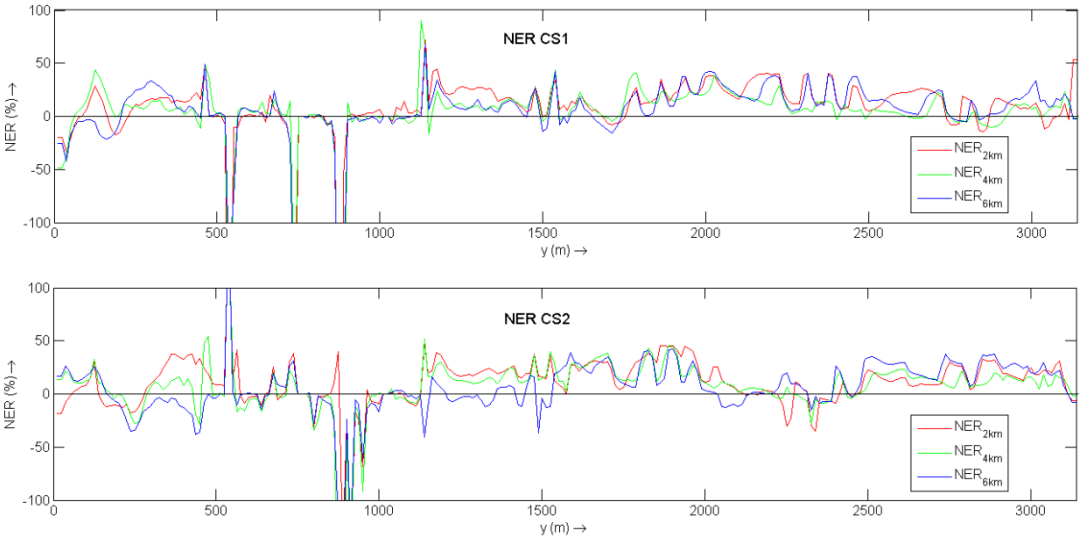

Figure 7.8 Non-dimensional erosion reduction (*NER*) at the beach face in the following scenarios: with the wave farm at a distance of 2 km (NER_{2km}), 4 km (NER_{4km}) and 6 km (NER_{6km}) along Perranporth Beach (*y*-coordinate, with *y* increasing towards the north of the beach) at the end of the storm in CS1 (above) and CS2 (below).

Finally, the *CEA* was applied to the northern (CEA^N) and southern (CEA^S) section of the beach taking as reference for each case the profiles considered in Section 6.1 (see Figure 6.3): P1 (south), P2 (middle) and P3 (north), which allowed the variations in the longshore sediment transport to be studied. Figure 12 shows the evolution of this factor along the profile (x) for CS1, where the negatives values represented an increase in the volume of material with respect to the initial conditions (accretion). In the lowest section of the profile, the volume of material for the scenarios studied was larger than the initial volume due to the material eroded, mainly from the following sections along the profile: (i) the beach face (1200 m < x-coordinate < 1300 m) and (ii) the area that faced the storms in low tide (800 m < x-coordinate < 1000 m), which was more significant in the southern area of the reference profiles. The geomorphological complexity of the southern section of the beach resulted in very different behaviour between the different scenarios.

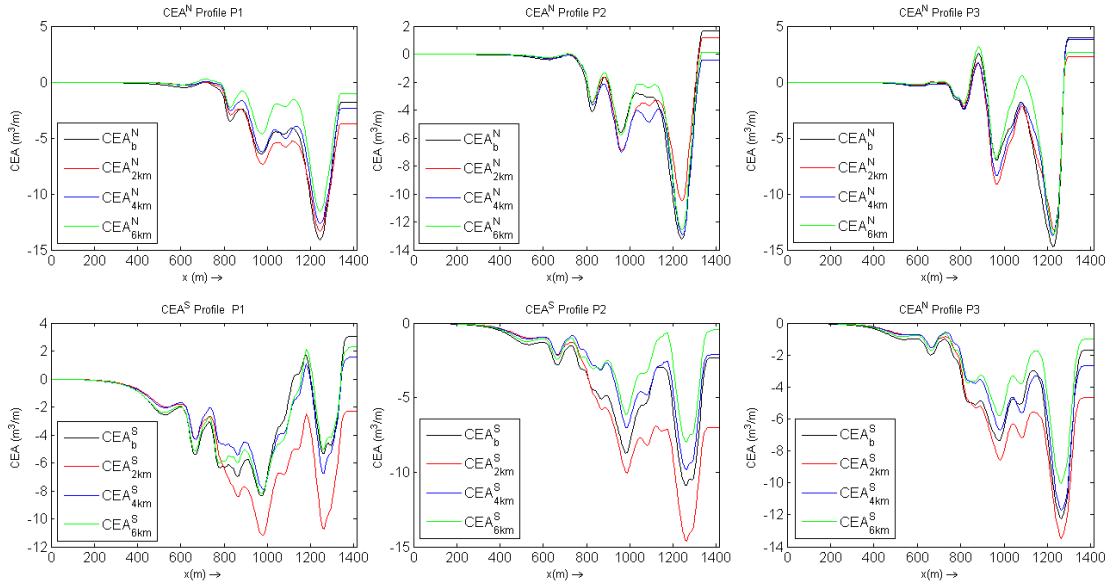

Figure 7.9 Mean cumulative eroded area in the baseline scenario (CEA_b) and in presence of the wave farm at a distance of 2 km (CEA_{2km}), 4 km (CEA_{4km}) and 6km (CEA_{6km}) from the reference (10 m water depth) contour in the northern area (above) and southern (below) across each of the reference profiles P1, P2 and P3 (Figure 6.3) at the end of the storm in CS1. The x- coordinate represents the distance along the profile, with x = 0 the most offshore point.

The wave farm at a distance of 2 km presented a significant rise in the volume of material in the southern area of the beach, especially taking as reference the profiles P1 and P2. This could be associated to the modification of the wave patterns brought about by the wave farm, given that the main reduction of the significant wave height occurred in the southern and middle area of the beach. Therefore, part of the material eroded in the northern section, where the reduction of the significant wave height was less, could be moved to the southern part of the beach, increasing the volume in this section. As for the wave farm at 4 and 6 km, they did not present significant differences compared with the baseline scenario, nonetheless the erosion caused in the absence of the farm was greater. For instance, in the northern area of the different profiles, it is observed that the greatest accretion at x = 1250 m occurred in the baseline scenario due to the largest amount of material eroded at the beach face. In the case of the profile P1, this was followed by the scenario with the wave farm at a distance of 2 km, associated with the material moved from the north of the beach, but for the profiles P2 and P3, the greatest values of accretion, after the baseline scenario, occurred with the wave farm at 4 and 6 km given that the farm at these distances reduced the erosion less than the scenario at 2 km. To sum up, a wave farm can alter not just the wave conditions in its lee but also the morphology and the sediment transport of the beach.

7.3 Conclusions

The selection of the location for a wave farm is not trivial. This chapter proved that the degree of coastal protection afforded by a wave farm varies significantly as a function of its distance to the coastline. It was observed that the effects on the beach morphology of the wave farm closest to the coast were more pronounced than in the other scenarios, with average reductions of erosion on the beach face of 15% when the other scenarios did not exceed 10%. Nevertheless, the overall wave energy resource for

the closest farm was 10 % less than with the case of the furthest farm due to the attenuation of wave energy caused by the coastal processes that occur in shallow waters. On these grounds, the effects of the wave farm on the coast ought to be one of the main considerations, alongside the energy resource, in the selection of the wave farm location, not least in areas subject to erosion risks, where the wave farms can contribute considerably to its mitigation.

Chapter 8
Influence of the Wave Farm Layout

8. INFLUENCE OF THE WAVE FARM LAYOUT

The previous chapter showed that understanding the wave farm impacts on the wave conditions and the coastal morphology as a function of the key design parameters of wave farms is essential for the development of wave energy. In this context, this chapter evaluates the influence of the layout in the wave farm impacts. The role played by the wave farm layout of a co-located wave-wind farm has been examined by Astariz *et al.* (2015b) in order to study the reduction of the wave height within a wind park, however these results cannot be extrapolated to the coast given that co-located wave-wind farms are in general located in further distances from the coast, and consequently the effects on the coast were not addressed. Therefore, the aim of this chapter is to analyse the influence of varying the intra- and inter-row spacings between devices in the performance of the wave farm and in the coastal protection offered by the different layouts through a case study at Perranporth Beach.

8.1 MATERIALS AND METHODS

The wave farm was located at a distance of 3 km to the water depth contour of 10 m. This distance complements the results presented in the previous chapter, where distances of 2, 4 and 6 km were analysed. Four wave farm layouts were evaluated in this chapter plus the baseline scenario, combining the following intra- and inter-row distances: 2.2D (hereafter named 2D) – the most recommended in the bibliography (Beels *et al.*, 2010b; Carballo & Iglesias, 2013), 3D and 4D, with D the distance between the twin bows of an overtopping device, in this case D = 90 m for a WaveCat WEC (Iglesias *et al.*, 2008). Table 8.1 shows the configurations proposed, which were located around the water depth contour of 30 m.

Array configuration	Spacing (m)	
	Intra row	Inter row
2D-2D	198	198
2D-3D	198	270
3D-3D	270	270
4D-4D	360	360

Table 8.1 Array configurations, including intra- and inter-row spacing

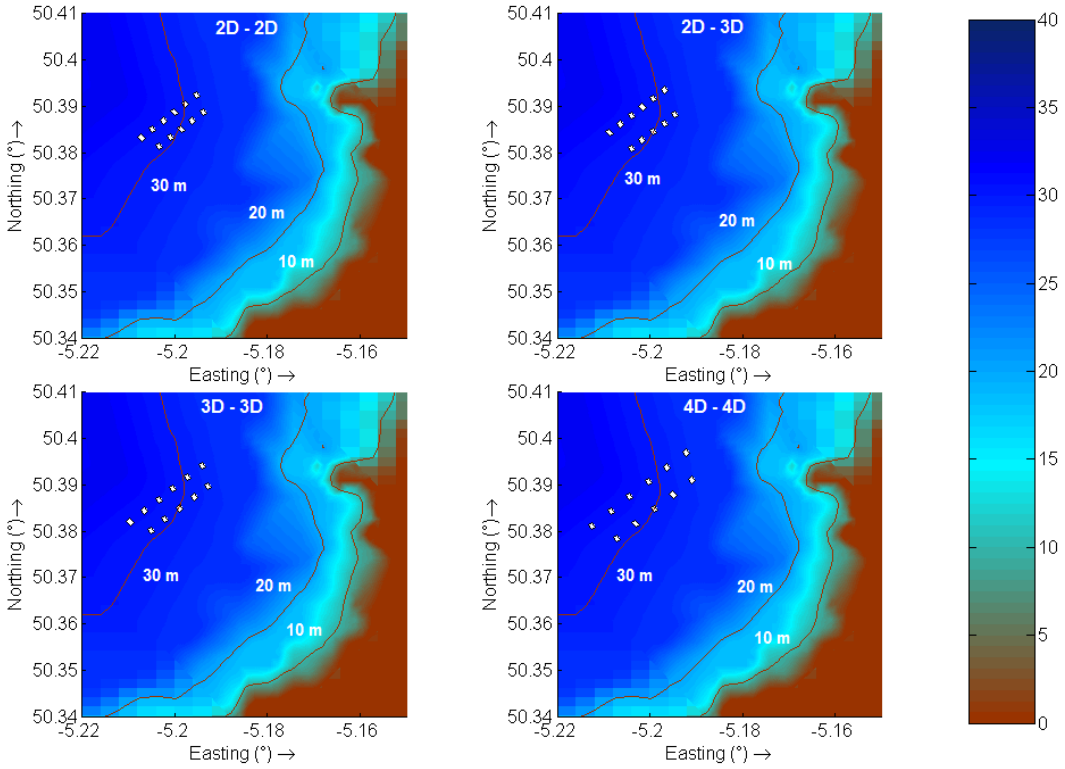

Figure 8.1 Wave farm layout. Water depth in relation to local chart datum [water depth in m]

A number of layouts are defined in order to analyse the sensitivity of the following two parameters in the design of wave farrms: the intra- and inter-row distance, i.e. the distance between WECs in the same row and the spacing between the rows of the wave farm, respectively. The 2D-2D configuration was used in the previous chapters and has been the most studied in the literature review (Carballo and Iglesias, 2013; Iglesias and Carballo, 2014). The configuration 2D-3D is selected to assess the effects of increasing the inter-row spacing. As the principle parameter for overtopping devices is the wave absorption, the incident wave power in the second row of devices is reduced by up to 25%. Then, whether this "destructive interaction" can be reduced by increasing the distance between rows will be analysed by comparing this configuration with the 2D-

2D layout. For their part, the layouts 3D-3D and 4D-4D allowed the influence of the intra- and inter-row spacings between WECs on wave conditions and beach morphology to be established (Figure 8.1).

The different wave farm layouts were implemented in the high-resolution grids of the wave propagation model at Perranporth. In order to compare the effects of varying the layout and the farm-to-coast distance on the coast, the wave conditions of the case study CS1 (defined in Table 7.1) were selected, with offshore values of significant wave height, peak period and direction equal to 3.5 m, 11 s, 315° (NW), respectively.

8.2 RESULTS

The impacts of the different array configurations on the nearshore wave conditions were presented based on the results of the wave propagation model. Figure 8.2 shows the modification of the significant wave height patterns varying the intra- and inter-row spacings, i.e. for the 2D-2D, 3D-3D and 4D-4D configurations. It was found that the increase of both intra- and inter-row spacings had a bearing on the shadow caused by the wave farm. The main difference in the impacts on the wave conditions between the array configurations lied in the area occupied by the farm, the larger the spacing between devices, the greater the area occupied by the farm and therefore the greater the shadow in its lee. However, the greatest shadows were not associated with the greatest reductions in wave height, which were more pronounced in the cases of lower spacing since this distance between WECs led to the merge of the individual wakes, increasing the reduction in wave height in the lee of the farm.

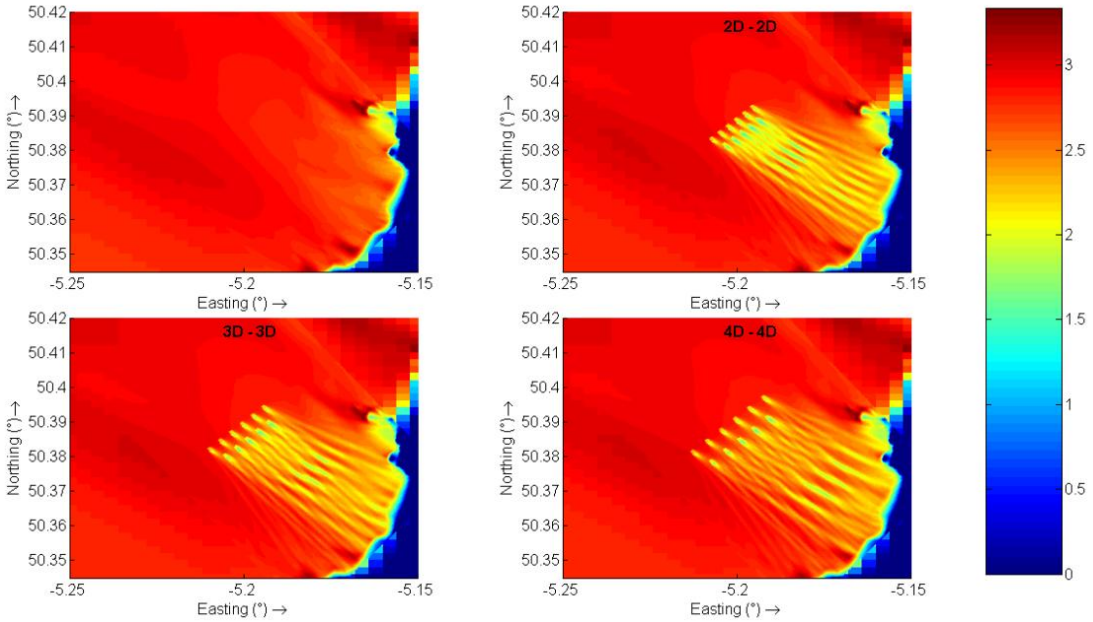

Figure 8.2 Significant wave height (m) in the baseline scenario and in the presence of the farm with the following configurations 2D-2D, 3D-3D and 4D-4D (clockwise from above left).

In the case of the 2D-2D configuration, the reduction of the significant wave height peaked at a distance of 1 km from the second row of WECs, while the peak values in the 3D-3D and 4D-4D configuration occurred at distances of 2 and 3 km, respectively, with less significant values. In the case of keeping constant the intra-row spacing (2D), but increasing the inter-row distance (3D instead of 2D), the differences of the effects on the wave patterns between both layouts were practically negligible (Figure 8.3).

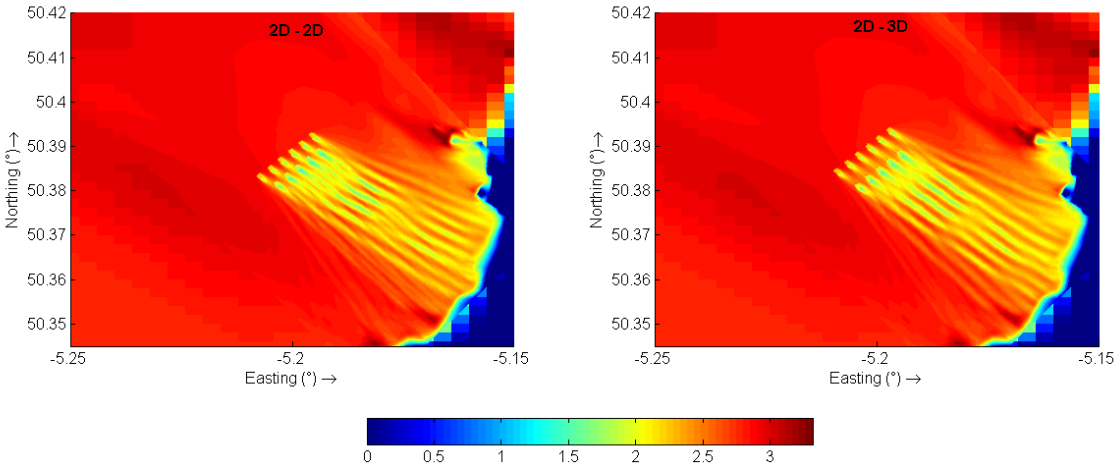

Figure 8.3 Significant wave height (m) in the presence of the farm with the following configurations 2D-2D (left) and 2D-3D (right).

To analyse the shadows caused by the different array configurations, the significant wave height along the 20 m water depth contour was studied (Figure 8.4). It was found that the wakes generated by the WECs that form the 4D-4D configuration achieved the greatest values of reduction of significant wave height at this water depth given that the wakes converged at greater distances than the other layouts. However, the impact was reduced to the isolated wakes caused by the WECs, with distances between peaks over 500 m, and with negligible reduction between them. Reducing the intra-row spacing between WECs, the distance between the wake peaks was reduced – approx. 400 m and 250 m in the case of 3D-3D and 2D-3D configurations, respectively. At this water depth, the influence of the inter-row spacing was more evident, while in the 2D-3D layout the wakes could be easily identified, in the 2D-2D the shadows merged into a large one.

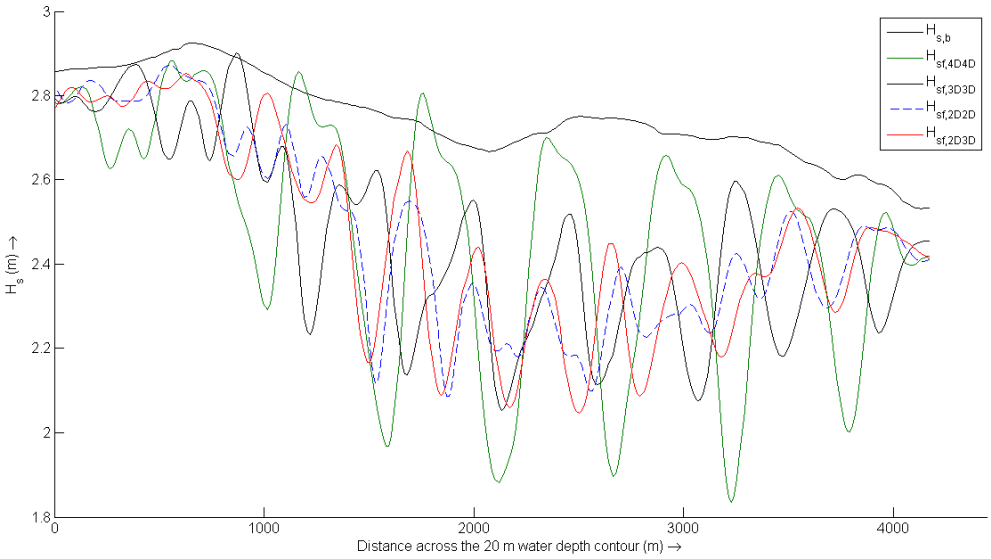

Figure 8.4 Significant wave height [in m] in the baseline scenario ($H_{s,b}$) and in the presence of the farm with the following array configurations: 2D-2D ($H_{sf,2D\text{-}2D}$), 2D-3D ($H_{sf,2D\text{-}3D}$), 3D-3D ($H_{sf,3D\text{-}3D}$) and 4D-4D ($H_{sf,4D\text{-}4D}$) along the 20 m water depth contour

Other relevant difference in the impact was the area affected by the wave farm in its lee, in the case of the 3D-3D and 4D-4D configurations the shadow was extended practically along the same area (approx. 4 km) despite the wave farms occupied

different spaces (the 4D-4D configuration area was 500 m larger). This shadow was extended along a smaller section in the case of the 2D-2D and 2D-3D layouts, with a wide of approx. 2.5 km.

In order to quantify the wave farm impacts on the wave conditions the indicator $RSH_{XD\text{-}XD}$ (Reduction in the Significant wave Height) was applied. The results (Figure 8.5) illustrated that the greatest values of reduction were found for the intra- and inter-row distances of 2D, exceeding 50% at a distance of 1 km from the second row of WECs. These peaks corresponded with the merge of the wakes mentioned above. Although, this reduction was less significant towards the coastline owing to the energy diffracted into the shadow, it cannot be overlooked, with values at the 10 m water depth contour over 15%. In the cases of larger intra-row spacings, the peaks of wave height reduction did not exceed 35% and took place close to the coast.

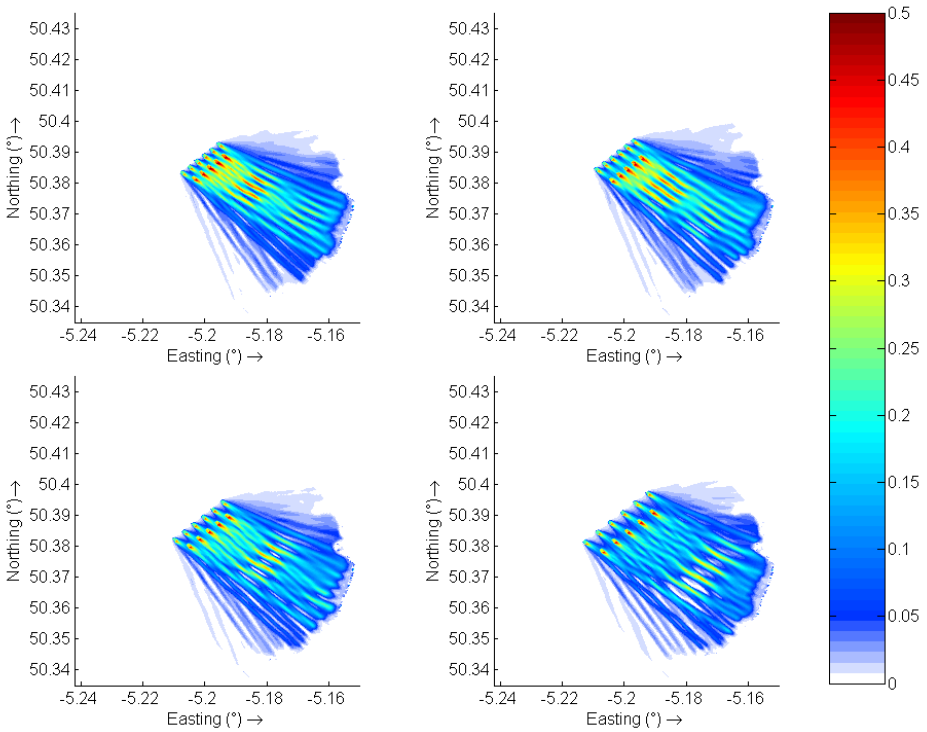

Figure 8.5 Reduction of the significant wave height (%) for the following wave farm layouts: 2D-2D ($RSH_{2D\text{-}2D}$), 2D-3D ($RSH_{2D\text{-}3D}$), 3D-3D ($RSH_{3D\text{-}3D}$) and 4D-4D ($RSH_{4D\text{-}4D}$) [clockwise from above left].

One of the advantages of increasing the inter- and intra-row spacings was the larger resource available. The larger distance between devices reduced the shadow effects caused by the wave energy extraction of the first row of devices on the second row. In view to having a more detailed wave energy resource within the wave farm, the available average resource in front of a generic WEC of the wave farm ($\overline{J}_{WEC}$) was analysed during a year (Nov 2007 – Oct 2008), which allowed the comparison with the results found in the previous section varying the farm-to-coast distance (Table 8.2). It was found that from the farm-to-coast distance of 3 km (relative to the 10 m water depth contour) the available resource did not increase significantly with the distance for the 2D-2D layout, with practically the same resource for the distances of 3 and 4 km.

Farm to coast distance	Farm layout		$\overline{J}_{WEC}$
	Intra-row spacing	Inter-row spacing	
2 km	2D	2D	14.46
3 km	2D	2D	16.47
	2D	3D	17.24
	3D	3D	17.11
	4D	4D	18.34
4 km	2D	2D	16.44
6 km	2D	2D	17.26

Table 8.2 Average resource available in a WEC of the wave farm ($\overline{J}_{WEC}$) for the different coast-to-farm distances and layout scenarios from Nov 2007 to Oct 2008 [kW/m].

However, the $\overline{J}_{WEC}$ values varied considerably as a function of the layout, obtaining the same resource at 3 km with a greater distance between rows (2D-3D) than at 6 km with the 2D-2D layout. As the absorption coefficient of the second row of devices is modelled with the same value as the first row, increasing the distance between rows reduces the "destructive" interaction induced by the WEC absorption. For instance, although the differences in the incident wave power at the first row of devices between the scenario with the farm at 3 km and at 6 km was 4%, Table 8.2 shows that the annual mean power is practically the same for both scenarios when considering the inter-row

spacing of 3D at a distance of 3 km. This means that 4% is the percentage brought about by placing the rows 90 m further away from the first row (3D instead of 2D).

In this context, the scenario at 3 km with intra- and inter-row spacings of 4D presented the greatest resource, which was 21% greater than the one with the farm at 2 km (2D-2D), 10% more than with the 2D-2D layout at 3 and 4 km, and 6% more than with the farm layouts of 2D-3D, 3D-3D at 3 km and the 2D-2D layout at a distance of 6 km. This finding showed that in certain areas where the area occupied by the wave farm is not an issue, it is not necessary to place wave farms at further distances to increase the resource available within it, but thus can also be achieved by increasing the spacing between devices, especially the inter-row one.

Having analysed the role played by the layout in the effects on the wave patterns, the response of the beach with a wave farm operating nearshore was analysed. The results from the wave propagation model along the 20 m water depth contour were the input on the coastal processes model. The storms were studied during a day that was the average duration of these frequent wave conditions based on the analysis of the data from the wave buoy off Perranporth.

Figure 8.6 shows the *BLI* results for the different layout configurations in the area of interest at Perranporth Beach. It was observed that the scenarios with an intra-row spacing of 2D did not present significant differences, with the greatest reductions of erosion found on the beach face. This reduction of the erosion led to less deposition of the eroded material in the lower sections of the beach in relation to the baseline scenario. Thus, negative values of *BLI* where found in deeper sections with values up to -1.2 m in these two scenarios. Both positive and negative *BLI* values were less remarkable in the scenario with an intra- and inter-row spacing of 3D, and nearly negligible with the 4D-4D layout.

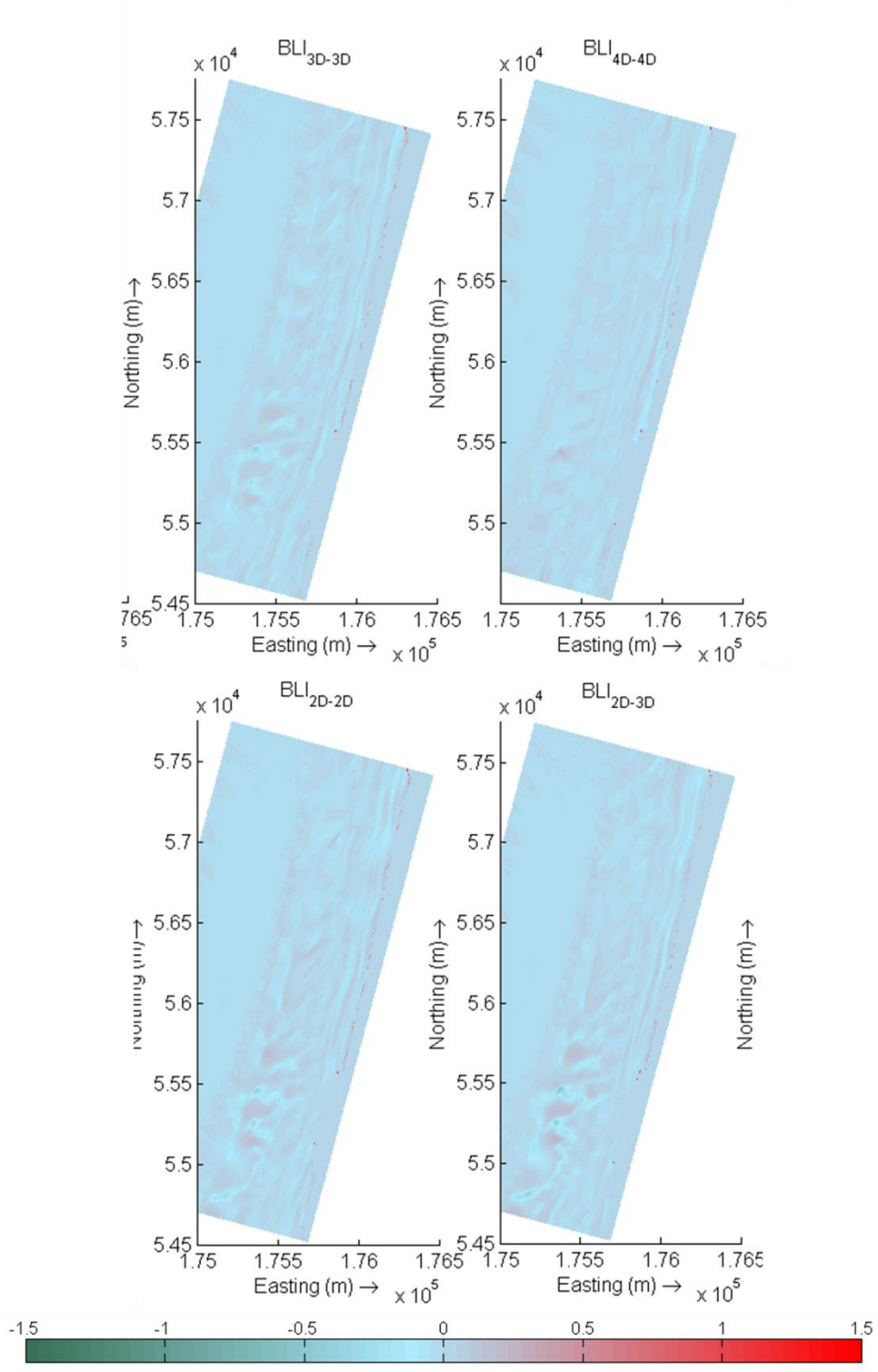

Figure 8.6 Bed Level Impact (*BLI*, in m) in the area of interest with the different wave farm configurations: 2D-2D (BLI_{2D-2D}), 2D-3D (BLI_{2D-3D}), 3D-3D (BLI_{3D-3D}) and 4D-4D (BLI_{4D-4D}).

These erosion patterns can be better identified analysing the evolution of the profiles P1, P2 and P3 (identified in Figure 6.3). The material eroded on the beach face area in the different scenarios was redistributed along the lower sections of the profile, with the greatest volumes of erosion on the beach face corresponding to the no farm

scenario and the 4D-4D layout (Figure 8.7). The profiles P2 and P3 showed similar patterns of erosion as the morphology of these profiles – smooth slope and back by a well-developed dune system – did not present significant differences. A different case was the profile P1, which despite being back by the dune system, was formed by a very flat intertidal area and a steepness dune that started at a bed level of 1 m. These features led to different erosion patterns: while in profiles P2 and P3, beach face erosion occurred mainly at bed levels of approx. 3 m; in the section with the advanced dune (P1) it mainly occurred from the toe of the dune to bed levels of approx. 5 m. In the comparison between scenarios, it was observed that the wave farm with an intra- and inter-row spacing of 2D presented the lowest values of erosion in the beach face. The results varied as a function of the profile but in some sections the reduction in the erosion for the 3D-3D and especially the 2D-3D layout was very close to the results obtained for the 2D-2D layout.

For a better understanding of the role played by the layout in the area eroded on the beach face, the impact indicators *FEA* and *NER* were applied. As found in previous chapters, the greatest *FEA* (Figure 8.8) values were found in the southernmost points section of the beach, which corresponded to the area not backed by the dune. The other area that also presented different patterns compared to the general response of the beach was the section of the steepness and advanced dune (500 m < y < 1100 m). In these two sections the influence of the wave farm was not as significant as in the rest of the beach, where in general the scenario without the wave farm presented the greatest values of erosion in the beach face, just exceeded in some areas by the wave farm with an intra- and inter-row spacing of 4D. The results between the wave farms with intra-row spacing of 2D (2D-2D and 2D-3D) and 3D (3D-3D) presented very similar patterns, although the *FEA* values of the scenario 2D-2D were slightly smaller than the other two scenarios.

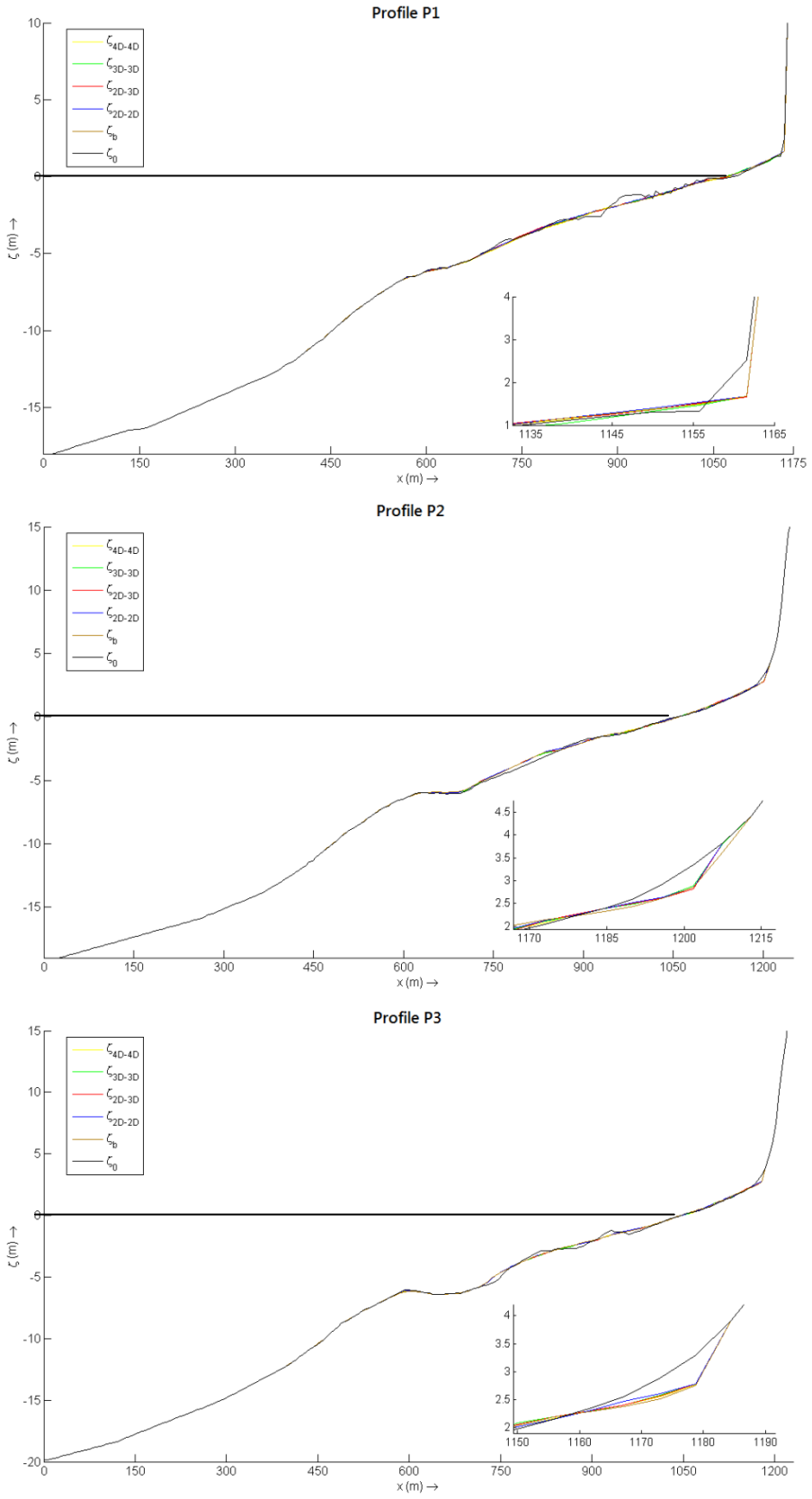

Figure 8.7 Bed level at Profiles P1, P2 and P3: initial (ζ_0) and at the end of the storm in the baseline scenario (ζ_b) and with the wave farm with the different wave farm configurations: 2D-2D ($\zeta_{2D\text{-}2D}$), 2D-3D ($\zeta_{2D\text{-}3D}$), 3D-3D ($\zeta_{3D\text{-}3D}$) and 4D-4D ($\zeta_{4D\text{-}4D}$). SWL included in the plots.

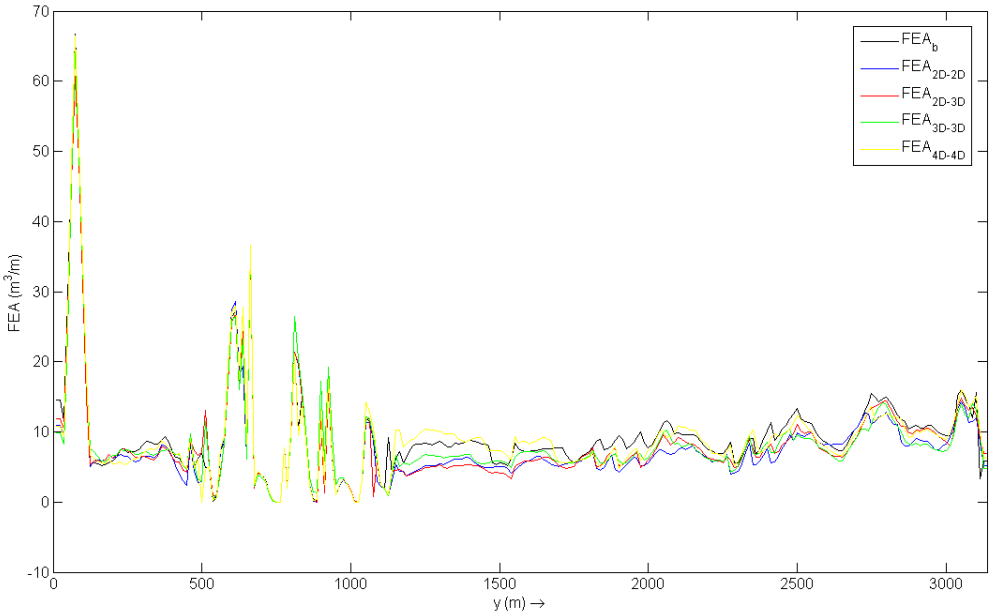

Figure 8.8 Beach face eroded area in the baseline scenario (FEA_b) and with the different wave farm configurations: 2D-2D ($FEA_{2D\text{-}2D}$), 2D-3D ($FEA_{2D\text{-}3D}$), 3D-3D ($FEA_{3D\text{-}3D}$) and 4D-4D ($FEA_{4D\text{-}4D}$).

The *NER* factor allowed the comparison between the wave farm and the baseline scenarios (Figure 8.9). This impact indicator corroborated the erosion patterns in the different sections of the beach identified through the application of the *FEA* indicator. The area with the steepness dune (500 m < y < 1100 m) presented high variability in the *FEA* values due to the isolated response of some profiles, for instance a few profiles presented no erosion in the baseline scenario and this conducted to negative *NER* values. However, to a greater or lesser extent, the wave farms contributed to reducing the erosion in the beach farm as can be concluded from the analysis of the average reduction of the erosion along the whole beach with values of approx. 16%, 10%, 5% and 1% for the scenarios 2D-2D, 2D-3D, 3D-3D and 4D-4D, respectively. These values showed that despite the similar trends between the three first scenarios, the 2D-2D scenario offered the highest degree of coastal protection in the coast. Analysing only the north section of the beach (y > 1200 m) the reduction of the erosion increased with *NER* values of approx. 18% for the 2D-2D scenario, 14% for the 2D-3D and 3D-3D and 3% for the 4D-4D. Thus, it was observed that without accounting for the section of the

steepness dune, the reduction of the erosion was larger for all the scenarios, particularly remarkable for the 3D-3D scenario, where the *NER* values were practically 10% greater.

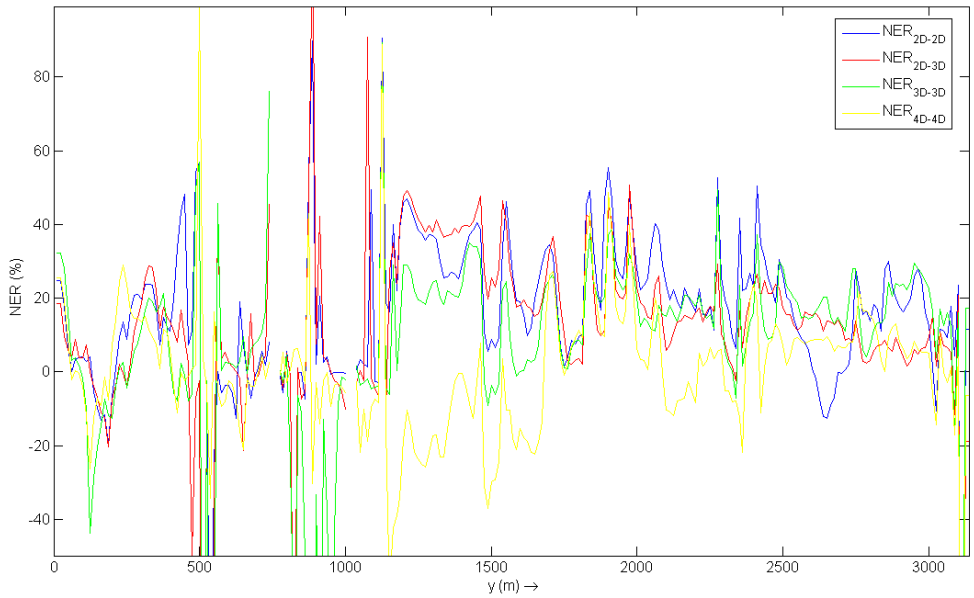

Figure 8.9 Non-dimensional erosion reduction at the beach face in the baseline scenario (NER_b) and with the different wave farm configurations: 2D-2D ($NER_{2D\text{-}2D}$), 2D-3D ($NER_{2D\text{-}3D}$), 3D-3D ($NER_{3D\text{-}3D}$) and 4D-4D ($NER_{4D\text{-}4D}$).

Finally, the comparison of the sediment transport patterns between the different scenarios was studied by means of the Cumulative Erosion Area (*CEA*) impact factor. The *CEA* factor represents the difference between the average cumulative volume of material along the profile at the initial and the final point in time for the different scenarios in the northern (CEA^N) and southern section (CEA^S) of the beach taking as reference one of the following profiles: P1, P2 and P3. The results of the *CEA* factor are shown in Figure 8.10 for the scenarios with an intra-row spacing of 2D (2D-2D and 2D-3D) and in Figure 8.11 for the scenarios with greater spacing between devices (3D-3D and 4D-4D). While the greatest average values of erosion ($CEA > 0$) were found northern to the profile P3 and southern to the profile P1, the central section of the beach, in particular the area of the steepness dune presented the greatest values of deposition ($CEA < 0$). In general, in the deepest sections of the beach deposition occurred as consequence of the material eroded from the beach face. This pattern peaked in the

sections that accounted for the steepness dune (northern to the Profile P1 and southern to the profiles P2 and P3) at the toe of the dune (x ~ 1250 m) and turned into erosion for the southern and northern areas of the beach from water depths of 5 m (x ~ 800 m). The erosion reached the greatest values in the area of the beach face (1200 m < x < 1400 m), which was followed in deeper sections by a drop of these values as a result of the deposition of the material eroded. In the case of the Profile P1 this peak took place at x ~ 1200 m given that most part of the south section is not back by the dune. On the other hand, for the profiles P2 and P3 the greatest values were found at x ~ 1500 m, which corresponded to the toe of the sandy dune.

In the comparison between scenarios, it was observed that the differences of material moved into the deepest sections of the profile (x < 600 m) between the farm and the baseline scenarios were larger with the intra-row spacing of 2D (less deposition due to less material eroded in the beach face area) than with 3D and 4D, where similar amounts of materials were moved in relation to the baseline scenario. Taking as reference the profile P2 and analysing the northern section, it was found that the wave farm scenarios with intra-row distance of 2D presented the greatest reductions of erosion (approx. 2 m^3/m), while in the scenario with the 3D-3D layout the erosion was less and with 4D-4D the results were very similar to the baseline scenario. These results are similar to the northern section of Profile P1, where the erosion at the toe of the dune in the baseline scenario was greater than the wave farms with intra-row spacing of 2D, in which the volume of material was practically the same than the initial one.

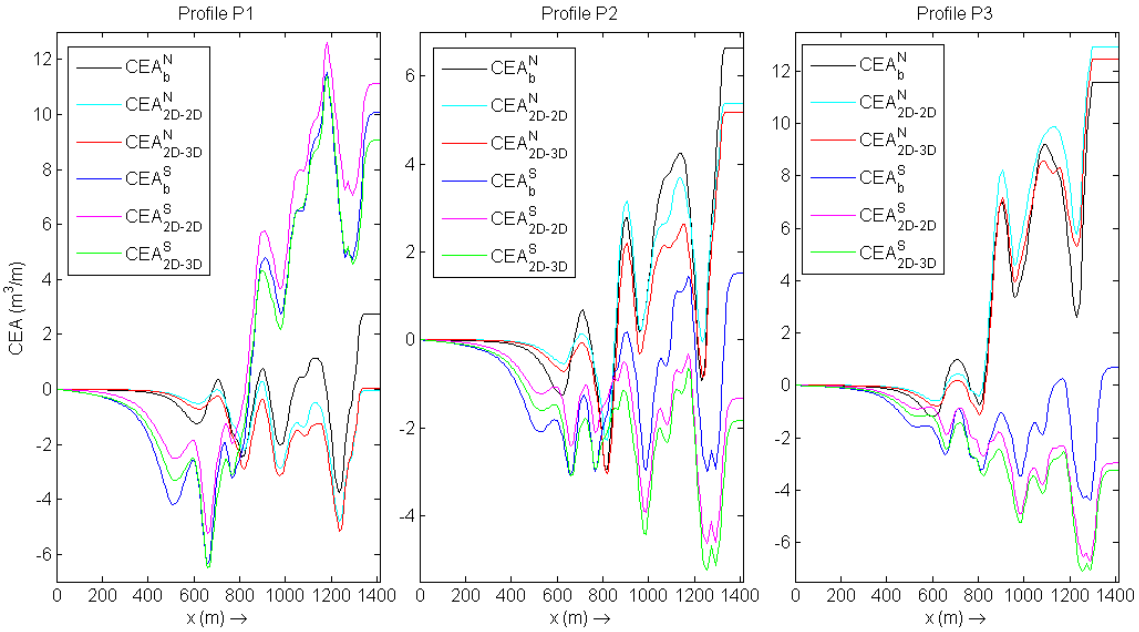

Figure 8.10 Mean cumulative eroded area in the baseline scenario (CEA_b) and in presence of the wave farm with 2D-2D (NER_{2D-2D}) and 2D-3D (NER_{2D-3D}) layout across each of the reference profiles P1, P2 and P3. The *x*-coordinate represents the distance along the profile, with $x = 0$ the most offshore point.

The scenario with an intra- and inter-row distance of 3D presented the greatest modifications of the sediment transport patterns with the greatest volumes of erosion in the southern section of the beach (Profile P1), but with values of the average erosion in the northern section similar to the 2D-2D and 2D-3D scenarios, and in some sections offering even a greater degree of coastal protection (see Profile P3). In these two latter scenarios, higher volumes of material of deposition were found at distances along the profile between 800 and 1000 m despite having less volumes of erosion in relation to the baseline scenario. However, the deposition in the baseline scenario in the deepest sections of the profile was higher than in any scenario with the wave farm, which would indicate that the reduction of wave height contributed to maintaining the sediment in the surf zone. This could be also complemented in some sections with longshore sediment transport, for instance the central section of the beach receiving part of the material eroded in the south, which is in line with the results presented for the *NER* indicator (e.g. an increase of 10% was observed in the reduction of the beach face erosion for the 3D-3D scenario when the indicator was applied just to the north section of the beach).

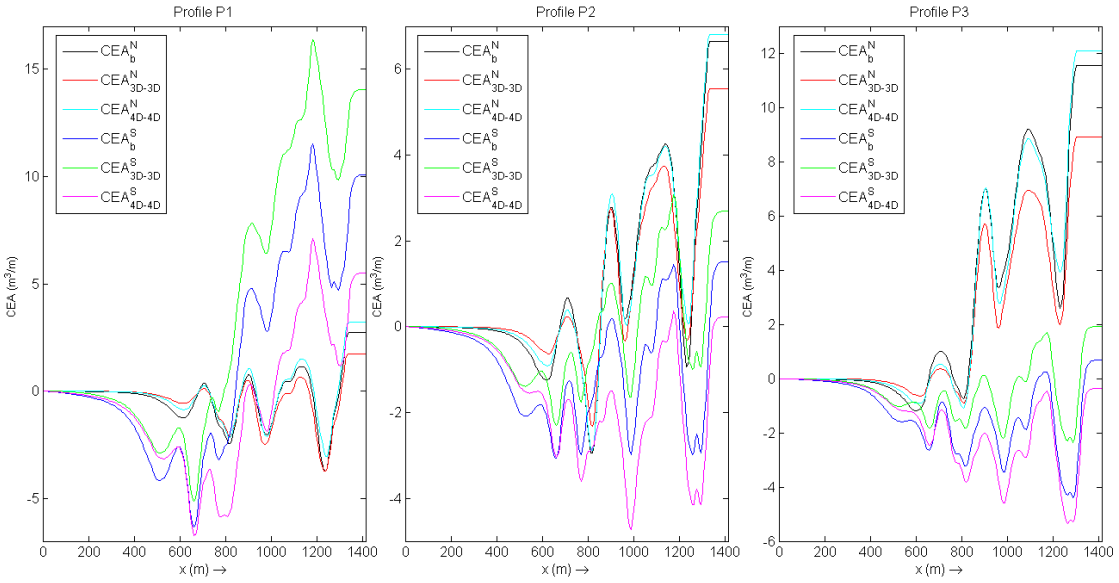

Figure 8.11 Mean cumulative eroded area in the baseline scenario (CEA_b) and in presence of the wave farm with 3D-3D (CEA_{3D-3D}) and 4D-4D (CEA_{4D-4D}) layout across each of the reference profiles P1, P2 and P3. The *x*-coordinate represents the distance along the profile, with $x = 0$ the most offshore point.

8.3 CONCLUSIONS

This chapter revealed that the degree of coastal protection offered by a wave farm and the wave energy resource varied considerably as a function of the layout. It was found that the greater the intra-row distance, the lesser the degree of coastal protection but also the greater the resource available. By comparing with the results obtained in the previous chapter, it was found that from certain distances it is most effective to increase the spacing between devices than locating the wave farm in further distances to the coast. However, although these wave farm layouts would maximise the available resource, they would also result in an increase of the wave farm infrastructure costs, such as the cable costs. Therefore, it is essential to determine whether the increase of the wave energy resource, and consequently the electricity generated, is enough to cover the rise of the wave farm costs. Other aspect that needs to be accounted in amortising this increase of the costs, it is the degree of coastal protection offered when the intra- and inter-row spacing is increased in relation to the most studied layout (2D-2D), which is of special interest in areas with erosion issues. In this context, it was found that the

effectiveness of the wave farm with a spacing of 4D was practically negligible in relation to the baseline scenario. On the other hand, the scenarios 3D-3D and especially 2D-3D reduced considerably the erosion, although in some sections the results were far from the degree of coastal protection offered by the 2D-2D layout.

Chapter 9
Impacts on the Modal State of the Beach

9. IMPACTS ON THE MODAL STATE OF THE BEACH

Finally, having established the impacts of wave farms on the sediment transport patterns at different time scales, this chapter aims to determine whether the beach morphology can be altered by the operation of the wave farm, and if so, to quantify this alteration. This alteration of the beach morphology is conducted by means of the modal state of the beach, which is defined based on an empirical classification that accounts for wave conditions, tidal regime and sediment size. As a beach typically goes through different modal states, the percentages of time in an average year corresponding to each state in the baseline scenario and with the wave farm are determined. The contents presented in this chapter, which focusses on a case study at Perranporth Beach, are published in the paper of Marine Geology (5-year impact factor: 3.375): "**Wave farm impact on beach modal state**", which was accepted for publication on the 28 January 2015.

9.1 MATERIAL AND METHODS

To analyse the spatial variability of the beach three beach profiles were selected to determine the beach modal state. Their relevant features can be readily observed (Figure 9.1): a submarine bar at a water depth between 5 and 10 m and a well-developed dune system that backs the landward end of the beach. The latter aspect does not play a role in the modal state, which only considers the intertidal area, but the bar system does – and is indicative of a dissipative or intermediate state. In the case of profile P3, two submarine bars are distinct – typical of a barred dissipative state.

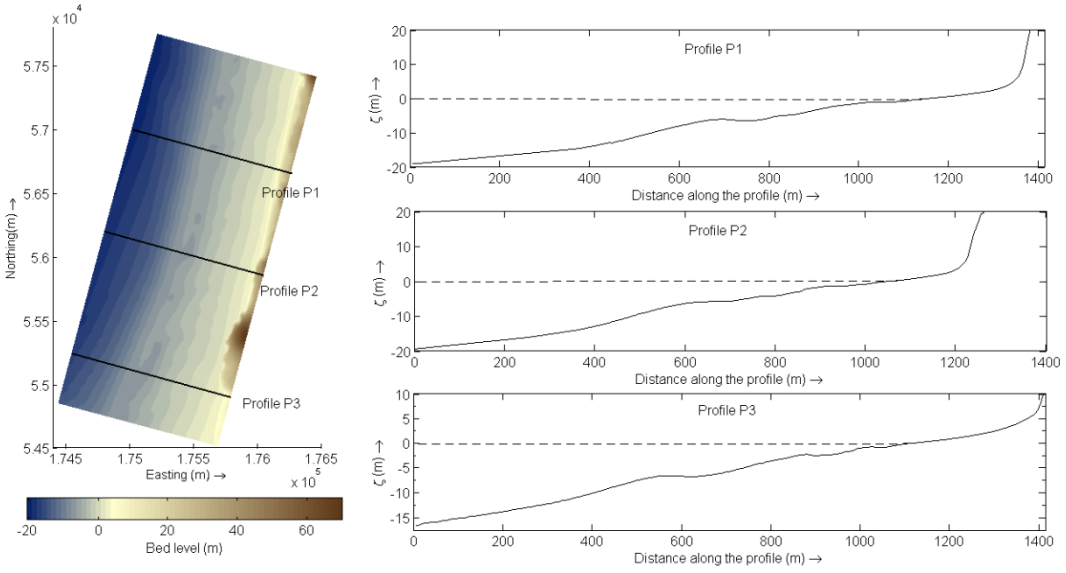

Figure 9.1 Three different profiles at Perranporth Beach and their respective localisation. Water depth in relation to local chart datum [in m].

In this context, the characterisation obtained in the present chapter contributes to understanding the behaviour of Perranporth by providing quantitative estimates of its morphodynamical variability throughout a year, as Perranporth has been described as dissipative (Butt, Russell & Turner, 2001; Masselink *et al.*, 2005) and as a low-tide bar rip system (Scott, Masselink & Russell, 2011; Scott *et al.*, 2007), with Austin *et al.* (2010) indicating that it is at the transition between the low tide bar/rip and dissipative beach.

To analyse the seasonal variability, the modal state of the beach was quantified during a year (from 1st of November 2007 to 31st of October 2008) and during its "winter" (Nov 2007 – Apr 2008) and "summer" (May 2008 – Oct 2008) periods. The average values of the significant wave height, peak period and direction during the year were 1.60 m, 10.37 s and 282.59 °, respectively. The values in "winter" of the significant wave height, peak period and direction were 1.98 m, 11.30 s and 285.23 °, respectively, and in "summer" 1.32 m, 9.62 s and 279.95°.

Regarding the wave farm scenarios, the three farm-to-coast distances analysed in Section 7 (2, 4 and 6 km from the 10 m contour) were considered in this chapter (Figure 7.1).

In this case a different methodology was used and to characterise the modal state of the beach, process-based modelling (SWAN), analytical solutions (breaking wave formulation) and empirical classifications (conceptual beach model) were applied, which will be described in the following headings.

9.1.1 CONCEPTUAL BEACH MODEL

The conceptual beach classifications are empirical models based on the relationships between the characteristics of different types of beaches (wave climate, sediment size and tidal regime) and field observations. Therefore, these models allow the evolution of beach dynamics as a function of the beach features to be predicted, and also, the quantification of the potential changes induced by a modification of these, such as the reduction of wave energy brought about by a wave farm.

The classification presented by Wright and Short (1984), also called the Australian beach model, is based on the field observations collected in Australia for microtidal beaches. This classification indicates the prevailing conditions in the surf zone: dissipative, intermediate or reflective, as a function of the dimensionless fall velocity parameter (Ω), also known as Dean's number (Dean, 1973),

$$\Omega = \frac{H_b}{w_s T} \tag{9.1}$$

where H_b is the breaking wave height, T is the wave peak period corresponding to the breaking conditions and w_s is the sediment fall velocity, which is defined for the

present paper according the Shore Protection Manual (US Army Corps Of Engineers, 1984),

$$B = (\frac{\gamma_s}{\gamma_w} - 1)\frac{gD_{50}^3}{\nu^2} \tag{9.2}$$

$$w_s = \begin{cases} (\frac{\gamma_s}{\gamma_w} - 1)\frac{gD_{50}^2}{18\nu}; & B < 39, \\ (\frac{\gamma_s}{\gamma_w} - 1)^{0.7}\frac{g^{0.7}D_{50}^{1.1}}{6\nu^{0.4}}; & 39 < \mathrm{B} < 10^4 \\ \left[(\frac{\gamma_s}{\gamma_w} - 1)\frac{gD_{50}}{0.91}\right]^{0.5}; & \mathrm{B} > 10^4 \end{cases} \tag{9.3}$$

where γ_s and γ_w is the density of the sediment and water, respectively, g the gravitational acceleration, D_{50} the sediment grain size and ν the fluid kinematic viscosity.

This model represents the evolution of microtidal beaches well; however, it does not account for the influence of the tide on the swash, surf zone and shoaling wave processes (Davis & Hayes, 1984). This was corrected with the introduction of another parameter: the Relative Tide Range (RTR), which allows the characterisation of all wave-dominated beaches in all tidal ranges (Masselink & Short, 1993):

$$RTR = \frac{MSR}{H_b}\ , \tag{9.4}$$

where *MSR* is the Mean Spring tidal Range.

Figure 9.2 shows the relationships between the dimensionless fall velocity and the relative tide range parameters that are used to establish the modal beach state. As the RTR parameter increases the beach evolves from a classic reflective state through the

formation of a low tide terrace at the toe of the beach face and low tide rips to a steep beach face fronted by a dissipative low tide terrace. In the case of an intermediate barred beach, the increase in the tidal range moves the bar down to the low tide level generating a low tide bar and rips. Finally, for barred dissipative beaches characterised by multiple subdued bars at different water depths, the increase of RTR results in the disappearance of these bars. The latter two groups shift to ultra-dissipative beaches with values of RTR between 7-15. For values of RTR greater than 15 the resulting beach is fully tide-dominated.

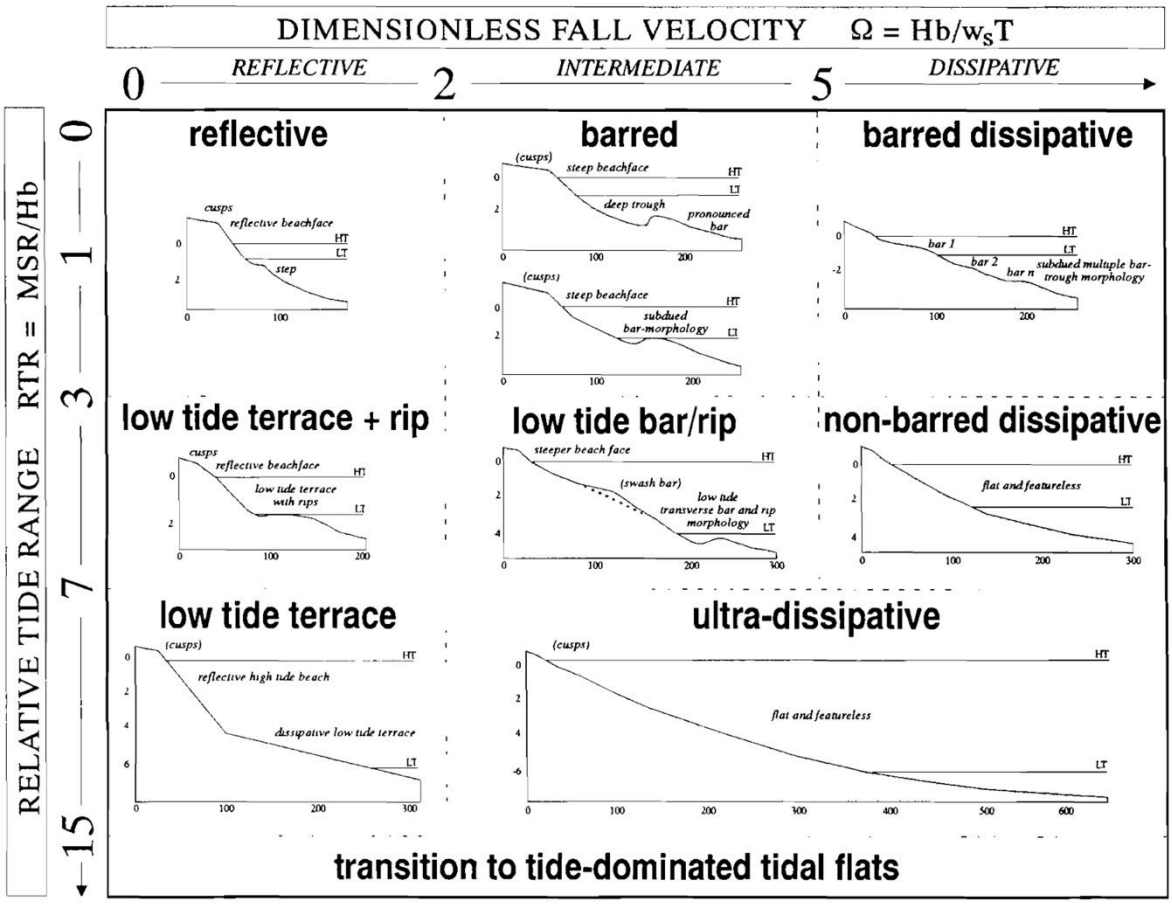

Figure 9.2 Conceptual beach model (Masselink & Short, 1993).

9.1.2 WAVE PROPAGATION MODEL

The wave conditions necessary to establish the morphological beach state – breaking wave height (H_b) and peak period (T_p) – were determined by coupling the

previously described wave propagation model to the Kamphuis' formulae (Kamphuis, 1991a), a breaking criterion for irregular waves based on the following expressions:

$$H_{sb} = 0.095 e^{4m} L_{bp} \tanh\left(\frac{2\Pi d_b}{L_{bp}}\right) \text{ , and} \tag{9.5}$$

$$\frac{H_{sb}}{d_b} = 0.56 e^{3.5m} \text{ ,} \tag{9.6}$$

where H_{sb} represents the breaking significant wave height, m the beach slope, L_{bp} the breaking wave length and d_b the breaking water depth. Once the breaking wave height was determined, the corresponding period was selected.

9.2 RESULTS

Based on the results of the wave propagation model the modal state of the beach is determined. In order to investigate the spatial variability of the impact along with its seasonal variability, three profiles (Figure 9.1) are selected: profiles P1, P2 and P3 corresponded with the south, middle and north section of the beach.

First, the results for the south section of the beach are shown in Table 9.1. This section of the beach is predominantly dissipative (third column in the table), although the percentage that the beach is found to be intermediate (second column) is far from negligible. Indeed, in the case with the farm at a distance of 2 km, the low tide bar/rip becomes the most frequent state. The comparison between the baseline and farm scenarios reflects a slight modification of the modal state of the beach owing to the low impact of the wave farm on the wave conditions in this area. The maximum difference between the baseline and the farm scenarios is the case of the non-barred dissipative state, in which the reduction does not exceed 1%. In any case, the trends due to the reduction of the significant wave height are shown in the results; for instance, the

percentage of low tide bar/rip state increases as the wave farm become closer, because the Relative Range Tidal parameter (*RTR*) is inversely proportional to the breaking wave height. On the other hand, the dimensionless fall velocity parameter (Ω) is directly proportional to the breaking wave height, and, therefore the barred dissipative state occurred more frequently in the baseline scenario than in the cases with the farm.

Profile P1: South section					
Reflective		Barred		Barred dissipative	
Baseline	0.00	Baseline	0.07	Baseline	16.04
6 km	0.00	6 km	0.07	6 km	15.96
4 km	0.00	4 km	0.07	4 km	15.90
2 km	0.00	2 km	0.07	2 km	15.70
Low tide Terrace + rip		Low tide bar/rip		Non-barred dissipative	
Baseline	0.00	Baseline	25.50	Baseline	26.59
6 km	0.00	6 km	25.70	6 km	26.39
4 km	0.00	4 km	25.98	4 km	26.18
2 km	0.00	2 km	26.18	2 km	25.77
Low tide terrace		Ultra-dissipative			
Baseline	3.36	Baseline	22.89		
6 km	3.36	6 km	22.89		
4 km	3.43	4 km	22.82		
2 km	3.36	2 km	23.24		
Transition to tide-dominated tidal flat					
Baseline			5.55		
6 km			5.63		
4 km			5.62		
2 km			5.69		

Table 9.1 Percentages of the beach modal state for the south section of the beach (Profile P1) from 1st November 2007 to 31st October 2008. In green shaded the most frequent modal state for each scenario.

Second, in the case of the middle of the beach (Table 9.2), the results were slightly different compared with the south section, due to the morphological differences between them (see Figure 9.1). In this area, the wave farm impacts are greater compared to the south section. Whereas the wave farm at 4 km and 6 km do not present significant differences compared with the baseline scenario, the wave farm at 2 km changes the behaviour of the beach significantly, reducing the barred dissipative state by more than 5% or 20 days per year, and increasing the ultradissipative state by more than 15 days.

Overall, with the wave farm at 2 km the most frequent state shifted from non-barred dissipative (baseline) to ultra-dissipative due to the reduction of breaking wave height.

Profile P2: Middle section					
Reflective		Barred		Barred dissipative	
Baseline	0.00	Baseline	0.07	Baseline	21.73
6 km	0.00	6 km	0.07	6 km	20.90
4 km	0.00	4 km	0.07	4 km	20.29
2 km	0.00	2 km	0.00	2 km	16.04
Low tide Terrace + rip		Low tide bar/rip		Non-barred dissipative	
Baseline	0.00	Baseline	22.76	Baseline	26.11
6 km	0.00	6 km	22.69	6 km	25.63
4 km	0.00	4 km	22.62	4 km	25.29
2 km	0.07	2 km	23.85	2 km	25.29
Low tide terrace		Ultra-dissipative			
Baseline	2.06	Baseline	22.69		
6 km	2.19	6 km	23.85		
4 km	2.19	4 km	24.81		
2 km	3.29	2 km	26.32		
Transition to tide-dominated tidal flat					
Baseline			4.59		
6 km			4.66		
4 km			4.73		
2 km			5.14		

Table 9.2 Percentages of the beach modal state for the middle section of the beach (Profile P2) from 1st November 2007 to 31st October 2008. In green shaded the most frequent modal state for each scenario.

Third, the north section of the beach is the area that presented the greatest differences between the baseline and the farm scenarios (Table 9.3). The trends mentioned in previous paragraphs are accentuated in this area, the reduction in the barred and non-barred dissipative states results in a greater occurrence of the ultra-dissipative beach, from 5 days to 36 days per year in the case of the farm at 6 and 2 km, respectively – a very substantial change in the morphological behaviour of the beach. As regards the Ω parameter, it is observed that the closest wave farm make the low tide terrace and the low tide bar and rip states more frequent by 10 and 12 days per year, respectively, compared with the baseline scenario.

Profile P3: North section					
Reflective		Barred		Barred dissipative	
Baseline	0.00	Baseline	0.14	Baseline	16.59
6 km	0.00	6 km	0.07	6 km	15.49
4 km	0.00	4 km	0.07	4 km	14.39
2 km	0.00	2 km	0.07	2 km	6.18
Low tide Terrace + rip		Low tide bar/rip		Non-barred dissipative	
Baseline	0.00	Baseline	28.10	Baseline	28.71
6 km	0.00	6 km	27.55	6 km	28.92
4 km	0.00	4 km	28.24	4 km	28.71
2 km	0.00	2 km	31.11	2 km	22.62
Low tide terrace		Ultra-dissipative			
Baseline	0.89	Baseline	22.68		
6 km	0.96	6 km	23.99		
4 km	1.03	4 km	24.40		
2 km	3.49	2 km	32.28		
Transition to tide-dominated tidal flat					
Baseline			2.89		
6 km			3.02		
4 km			3.16		
2 km			4.25		

Table 9.3 Percentages of the beach modal state for the north section of the beach (Profile P3) from 1st November 2007 to 31st October 2008. In green shaded the most frequent modal state for each scenario.

Finally, regarding the seasonal variability, significant differences between "summer" and "winter" are found. These differences are analysed with reference to the north section (Table 9.4) for the sake of space – similar trends were found in the other sections. The main feature that distinguishes the winter from the summer is the presence of the bar in the baseline scenario. In winter, the beach is predominantly barred dissipative, what is usually called a "winter" or "storm" profile. The more energetic conditions increase the erosion, and lower the beach face as sand is moved offshore and deposited on submarine bars, which help to protect the beach by causing the waves to break further offshore. In summer, the state of the beach shifts from barred to non-barred – non-barred dissipative or ultra-dissipative – due to the milder wave conditions, and, therefore, the reduction of offshore sediment transport.

Profile P3: North section								
Reflective			**Barred**			**Barred dissipative**		
Scenario	Summer	Winter	Scenario	Summer	Winter	Scenario	Summer	Winter
Baseline	0.00	0.00	Baseline	0.00	0.27	Baseline	4.66	28.53
6 km	0.00	0.00	6 km	0.00	0.14	6 km	4.11	26.89
4 km	0.00	0.00	4 km	0.00	0.14	4 km	3.42	25.38
2 km	0.00	0.00	2 km	0.00	0.14	2 km	0.68	11.66
Low tide Terrace + rip			**Low tide bar/rip**			**Non-barred dissipative**		
Scenario	Summer	Winter	Scenario	Summer	Winter	Scenario	Summer	Winter
Baseline	0.00	0.00	Baseline	29.86	26.34	Baseline	29.59	27.85
6 km	0.00	0.00	6 km	29.59	25.51	6 km	29.18	28.67
4 km	0.00	0.00	4 km	30.00	26.48	4 km	28.63	28.81
2 km	0.00	0.00	2 km	27.67	34.57	2 km	18.77	26.47
Low tide terrace			**Ultra-dissipative**					
Scenario	Summer	Winter	Scenario	Summer		Winter		
Baseline	0.27	1.51	Baseline	33.15		12.21		
6 km	0.27	1.65	6 km	34.25		13.72		
4 km	0.41	1.65	4 km	34.79		13.99		
2 km	4.66	2.33	2 km	44.66		19.89		
Transition to tide-dominated tidal flat								
Scenario			Summer			Winter		
Baseline			3.29			2.47		
6 km			3.43			2.60		
4 km			3.57			2.74		
2 km			4.94			3.56		

Table 9.4 Percentages of the beach modal state for the north section of the beach (Profile P3) in "summer" (1st November 2007 - 31st April 2008) and "winter" (1st May 2008 - 31st October 2008). In green and brown shaded the most frequent modal state during the winter and summer period, respectively.

In the scenarios with the farm this seasonal behaviour changes specially with the farm at 2 km. In winter, the barred dissipative state becomes less frequent in favour of ultra-dissipative and low tide bar/rip states. In the latter, the beach keeps the bar system but enlarges the intertidal flat, with the result that the system behaves as an intermediate beach at mid tide, reflective at high tide and dissipative at low tide. By contrast, in summer, the increase of the occurrence of ultra-dissipative state is very significant given that the beach behaves according this state during almost half of the summer.

In summary, Perranporth beach is found to be at the transition between the low tide bar/rip and dissipative beach states in the scenario without the farm. Despite the spatial

variations between the different profiles, the greatest differences are observed in the seasonal study. The absence of the bar distinguished the behaviour of the beach during summer from winter. However, the presence of the wave farm affects the modal state of the beach drastically, decreasing the occurrence of wave-dominated states (barred and non-barred dissipative states) in the favour of tide-dominated (low tide bar and rip in winter and ultra-dissipative in summer). The reduction of the breaking wave height brought about by the wave farm (~18%, comparing the baseline scenario with the nearest farm) results in a significant modification of the morphological response of the beach. The reduction of the wave-dominated states would seem to lead to an increase in the onshore sediment transport and the removal of the offshore bar, the materials of which would cause accretion on the beach – in line with the findings showed in the previous chapters.

9.3 CONCLUSIONS

The modal state at Perranporth varies along the beach, although large spatial differences are not observed concurrently. However, the seasonal variability is far more pronounced. In winter the beach is wave-dominated, the energetic wave conditions increasing offshore sediment transport and forming a submarine bar. In summer, under milder wave conditions, the beach is tide-dominated.

The milder wave conditions in the lee of the wave farm, especially apparent in the north and middle section, can lead to an alteration of the predominantly wave-dominated character of the beach during winter to tide-dominated. This would imply a significant modification of the morphological behaviour of the beach. For instance, in the north section the predominant state is a low tide bar/rip in the baseline scenario, which turns into an ultra-dissipative system in the case of the nearest (2 km) wave farm to the coast. In this case, the wave-dominated states are reduced by over 10%, or over

36 days per year. This modification also is predicted in the cases with farm-to-coast distances of 4 km and 6 km, albeit to a lesser extent: the barred dissipative states become less frequent (by up to 10 days per year) and accordingly, the tide-dominated states, e.g., ultra-dissipative or transition to tide-dominated tidal flat, occur more often. The reduction in the occurrence of the barred states corresponds to an increase in the onshore sediment transport and the removal of the offshore bar, which in turn would lead to accretion of the beach.

In sum, this work showed that a wave farm can alter the behaviour of a beach in its lee considerably. This in itself need not be regarded as a negative impact; on the contrary, the wave farm can lead to beach accretion and thus serve to counter erosional trends. Moreover, the effects of the wave farm on the beach can be controlled by locating the farm closer to, or further from, the shoreline.

Chapter 10
Synthesis and Conclusions

10. SYNTHESIS AND CONCLUSIONS

10.1 DISCUSSION

Wave energy is generally considered as an expensive form of renewable energy. This is due, in part, to the early stage of development of the technology, and in part, to the difficulties posed by the harsh marine environment. In any case, for wave energy to truly take off, its costs must decrease substantially. In addition to the cost reductions which can be obtained by optimising the installation and construction processes (Astariz & Iglesias, 2015a) and the WEC design, there is a "strategic" approach for reducing the costs: the synergetic application of wave farms to generate carbon-free energy and coastal protection. This synergy would enhance the economic viability of wave farms through savings in conventional defence schemes. In this sense, this PhD Thesis has proven that wave farms can effectively protect the coast at different locations, and that the degree of coastal protection can be controlled by the key design parameters of the wave farms, such as the farm-to-coast distance and the layout.

Importantly, the case studies showed that wave farms would be particularly effective in mitigating beach erosion, which is one of the major threats affecting beaches worldwide in the current transition scenario. Figure 10.1 shows the magnitude of beach erosion after storm events during the winter 2013/2014 at Perranporth (UK) and Soulac-sur-Mer (France), with dramatic environmental and socioeconomic consequences in the latter case, in which where the erosion in the dune affected the foundation of the property illustrated in the picture, and consequently, led to the demolition of the building.

Wave farms were found to not only reduce beach erosion, but also to alter the sediment transport patterns, displacing the landward extreme of the eroded area by up to 30 m towards the sea. This displacement can be of particular relevance in cases such as

Soulac-sur-Mer, where some buildings were at risk due to storm-induced erosion at the toe of the foundations. Had a wave farm been deployed off that section of the coast, the demolition of many a building might well have been avoided.

Figure 10.1 Consequences of 13/14 winter storms at Perranporth Beach (UK) and Soulac-sur-Mer (France) on the left and right hand, respectively

However, the effects of wave farms on the coast do not lend themselves to general statements, for they will depend on the characteristics of the area in question (wave energy resource, wave climate and grain size distribution, among others), of the WECs and their layout. The results obtained for the different locations and layouts are discussed below, in addition to the importance of the wave farm performance and the type of WEC.

10.1.1 INTER-SITE COMPARISONS

Two locations along the Atlantic façade of Europe were selected to analyse and compare wave farm impacts on the coast: Perranporth Beach in SW England and Xago Beach in N Spain. The selection was based on the resource characterisation (Iglesias & Carballo, 2010b; Martinho & Soares, 2011) in conjunction with the distance to populated areas, the availability of data (both wave and bathymetric), and importantly, the need for enhancing coastal protection.

The site for the wave farm off Xago beach was selected by the Asturian Institution for Energy Development (Federacion Asturiana de ENergia, FAEN) for the deployment

of the first offshore wave farm in Spain. For its part, in the case of Perranporth there is no defined location for the wave farm, which prompted the investigation of relevant parameters, e.g. the role played by the farm-to-coast distance.

Regarding the wave energy resource, the offshore average power in both areas was found to be well above 20 kWm^{-1}; which represents the threshold for commercial scale resource according to the literature (The Crown State, 2013). The analysis, which covered a 12-month period, yielded the following values: significant wave height and mean period of 2.28 m and 9.83 s, respectively, at Perranporth; and 2.11 m and 10.07 s at Xago. In terms of average offshore wave power the values were approx. 29 kW/m and 26 kW/m at Perranporth and Xago, respectively.

As regards the wave resource at the farm sites, the average wave power available to a generic WEC ($\bar{J}_{WEC}$) was 20.21 kW/m in the case of Xago (with a farm-to-coast distance of 1.7 km, at a water depth of 30 m) and 14.46 kW/m at Perranporth (with the farm at a similar distance from the coast and water depth). The resource at Xago was found to be even higher than at Perranporth with a farm-to-coast distance of 6 km (17.26 kW/m).

The significantly higher resource at Xago is explained by the irregular bathymetry in the area, which effectively creates a *nearshore hotspot* at the site (Hadadpour et al., 2014; Iglesias & Carballo, 2010a). It can be observed that the average offshore resource (26 kW/m) was similar to the resource found in the WECs located in the first row of the wave farm (25 kW/m), so the energy dissipation associated to the wave propagation from offshore to nearshore is compensated by the irregular bathymetry of the area selected for the wave farm at Xago. These *nearshore hotspots* are strongly recommended for the deployment of wave farms given that high wave energy resources can be found in locations relatively close to the coast.

The overall mean incident power of the wave farm consists of multiplying the annual mean values by the capture width (90 m, the distance between the twin bows) and the number of WECs (11). In order to obtain the total production of the farm, the efficiency of the device needs to be considered. This value is generally extracted from physical campaigns at prototype scale to prove the viability of the technology, as will be shown in the following subsection; however, the nascent state of this renewable technology limits the number of WECs deployed on the sea. On this basis, the values presented in Fernandez *et al.* (2012) during laboratory tests at a scale of 1:50 are used. Considering this, the total production of the wave farm would be 4.7 and 3.4 MW for the cases of Xago and Perranporth (with the farm at 2 km from the coast), respectively. The contribution of each WEC would be 0.4 and 0.3 MW for both locations. Translating this to the monthly mean production of the wave farm, at Xago the production would be 3.4 GWh and at Perranporth it would vary from 2.9 GWh for the farm at 6 km from the coast to 2.4 GWh for the closest farm to the shore. The economic viability of wave farms compared to other sources of energy will be also discussed in the following section.

Regarding the impact on the sediment transport, although in both locations the wave farm contributed to reducing storm-induced erosion; significant differences in the response of the beach to the wave farm were found between places. While in the case of Perranporth, the reduction in erosion occurred mainly on the beach face and to a lesser extent on the submarine bar, in the case of Xago it was particularly evident on the dune.

It is important to consider that the comparison is carried out with different wave conditions and time duration. In the case of Perranporth, the response of the beach was studied during a week with average values of significant wave height and peak period of

4.2 m and 12.1 s, respectively. For its part, Xago was forced with a storm of 9 days with the following average conditions: H_s = 3.72 m and T_p = 10.5 s.

The results obtained applying the Bed Level Indicator (*BLI*), which refers to the bed level difference at the end of the storm period between the baseline and the wave farm scenario, presented significant differences. Although the maximum *BLI* values at Perranporth (*BLI* > 4 m) were greater than at Xago (*BLI* > 2 m); analysing the 3D response of the beach it is found that these peak values at Perranporth are the consequence of the isolated response of some profiles since the average value along the beach was around 1 m. On the other hand, the erosion reduction at Xago was practically constant along the entire beach, with values around 2 m, with the exception of the central section of the beach. There are two main reasons for this: first, the smaller farm-to-coast distance at Xago (1.7 km) in relation to Perranporth (6 km), in the case of the short-term 3D analysis (Chapter 5); and second, the presence of the submarine bar at Perranporth, which forms part of the response mechanism of the natural system to protect the beach and thus led to lesser values of erosion in the baseline scenario.

It is also remarkable that the greatest reductions in erosion were found at Perranporth in the beach face. Indeed, the Non-dimensional Erosion Reduction (*NER*) indicator at the beach face presented values over 40% along a stretch of 1500 m (practically half of the beach). For its part, at Xago although the maximum *NER* values were even higher than at Perranporth (with reductions over 60%), they were found in a smaller section of the beach. In the rest, the protection afforded by the farm was practically constant with values around 20%.

In any case, the impacts identified at both places are beneficial for the beach, as the main threats found at Perranporth and Xago Beach are the erosion of the beach face and

the dune, respectively; and the location of a wave farm nearshore was found to be effective in protecting the beach in both cases.

10.1.2 INTRA-SITE COMPARISON

The previous heading showed that the effects of wave farms varied according to the area in question; however, these effects can also vary at the same location. In this sense, the objective of this section is to discuss the results obtained in the short- and medium-term analysis at Perranporth Beach, and the role played by the farm-to-coast distance and layout.

10.1.2.1 Short term vs long term

The results of the short- and medium-term analysis show that the wave farm is more effective in protecting the coast under storm conditions. This can be regarded as a controversial aspect, as generally many of the WECs adopt survival strategies under storm conditions so as to reduce the probability of damage through mechanical or mooring failure. However, during the laboratory tests of the WaveCat WEC conducted at the COAST Lab of Plymouth in the framework of the EU WAVEIMPACT project, it was found that in the case of the WaveCat, the device can cope effectively with large wave heights by means of varying the angle between the twin hulls of the model (the greater the wave height, the smaller angle and consequently the wave loading on the device). This aspect will be discussed in Section 10.2.

In the medium-term analysis, the greatest reductions in eroded area in the beach face (*NER*) coincided with stormy periods. For instance, after 1 month (December) and 3 months (February) of simulation the *NER* values exceed 30% and 35% respectively in the case of the beach profile in the north section of the beach. However, at the end of the simulation (April), with milder wave conditions, the *NER* values dropped to 20%. In any case, this is still a significant erosion reduction, which cannot be overlooked.

Although the medium-term analysis was conducted in a 2D (*x*,*z*) mode, two profiles were considered to evaluate the alongshore variability. This was found of relevance, with greater reductions of erosion in the north section of the beach (approx. 10% more than the central section of the beach) - the area most sheltered by the wave farm. This fact was corroborated by the 3D (*x*,*y*,*z*) study, in which the greater reduction in erosion (*NER* ~ 40%) was found in the north area of the beach. It can be observed that the values of reduction of erosion (*NER*) at the end of storm periods in the short- and long-term analysis are very similar.

Therefore, considering that the section with reductions over 40% exceeded 1500 m (~40% of the total length of the beach) and the similarities between the results in the short- and long-term analysis, it may be estimated that the wave farm would protect most of the beach effectively, and would have a less significant but still considerable effect on the rest of the beach. However, before the actual deployment of wave farms, their long-term effects on the coast and the multi-decadal response of the beach with a wave farm operating nearshore must be quantified, and this will form part of the future investigations that will be explained further in the future research lines.

10.1.2.2 Influence of the key design parameters of wave farms

The definition of an optimum location for a wave farm is crucial in the performance of the wave farm and the degree of coastal protection associated. The role played by the wave farm layout and the farm-to-coast distance in the beach evolution (sediment transport and modal state of the beach) is discussed in this section.

Regarding the farm-to-coast distance, the wave farm located 2 km off the beach afforded the greatest degree of coastal protection based on both the sediment transport and the modal state of the beach. There is a clear connection between these two aspects given that, in order to interpret the evolution of the modal state of the beach, it is

essential to understand in which manner wave energy extraction affects the sediment transport patterns.

In this sense, the previous finding that wave farms were particularly effective in reducing the erosion at the beach face in the case studies is amplified in the case of a wave farm at a distance of 2 km (as seen at Xago as well). Thus, the lower volume of storm-induced erosion in the beach results in a less steep beach face and in a flatter beach profile. This modification of the sediment transport would change the morphology of the beach, which was corroborated in the analysis of the beach modal state during an average year. Perranporth, which in the baseline scenario is in the transition between the low tide bar and rip state and the barred and non-barred dissipative states, would change its predominant state to ultra-dissipative, which is characterised by the absence of features and a flat beach profile (Figure 10.2).

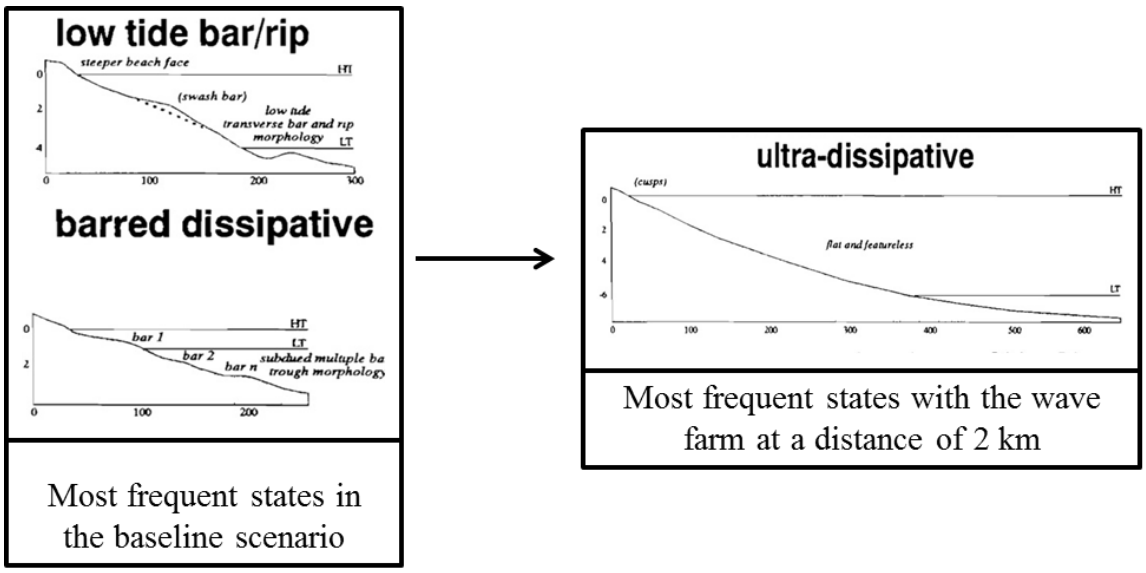

Figure 10.2 Evolution of the modal state of the beach with a wave farm operating nearshore

This change would be associated to the reduction in erosion in the beach face, and may have positive effects on the beach dynamics such as beach accretion. The milder wave climate nearshore would bring about the deposition of the material from the

submarine bar (typical of barred dissipative and low tide bar and rip states) onto the beach face, resulting in a smoother and featureless beach profile.

Regarding the other two farm-to-coast distances, similar beach responses were found. Although, the reduction of the erosion was less significant than with the farm at 2 km, the average reduction of erosion at the beach face along the whole beach for both distances was around 10%, value that cannot be overstated considering that the model was run under frequent storm conditions. This lower degree of coastal protection afforded by the farm at these distances was reflected in the modal state of the beach. While with the closest wave farm certain modal states of the beach varied by up to 40 days per year, with the farm at distances of 4 and 6 km this modification did not exceed 10 days per year.

Regarding the wave farm layout, it was found to be particularly relevant in the wave energy resource, for instance increasing the inter-row distance between devices (farm configuration 2D-3D) the same resource in a generic WEC of the wave farm can be found locating it at a distance of 3 km to the coast than at 6 km with a farm configuration of 2D-2D. However, although these wave farm layouts would maximise the available resource, they would also result in an increase of the wave farm infrastructure costs, such as the cable costs, which would be increased by approx. 0.7 M € in the 2D-3D scenario in relation to the 2D-2D configuration, following the data provided by Astariz *et al.* (2015a).

Furthermore, the degree of coastal protection offered by the wave farms with greater spacing between WECs is lower. For instance, placing the wave farm at a distance of 3 km to the coast, the average reduction of the erosion on the beach face with a layout configuration of 2D-2D was 20%, while with a 2D-3D configuration it was 10%.

10.1.3 PERFORMANCE OF WAVE FARMS AND THEIR ECONOMIC VIABILITY

Although the focus of this thesis is to establish the impacts of wave farms on the coast, and consequently determine their performance to protect the coast, needless to say that the main purpose of wave energy is to generate carbon-free energy, and its probability to truly take off will fully depend on accomplishing this primary objective. Thus, this section will discuss about the performance of wave farms according the type of WEC, and their economic viability, including its potential enhancement due to their synergetic applications: wave farm to protect the coast and co-located wave-wind farms.

As mentioned in the previous section, the premature stage of wave energy leads the author to consider that it is a more expensive form of renewable energy than others, such as wind, tidal and solar energy with a more mature status of the technology. Generally, this is supported by economic studies that are usually oversimplified and whose results might generate erroneous conclusions about the wave energy competitiveness. However, including key issues in an economic analysis, namely externalities, the gap between the LCOE of wave energy and other sources is practically negligible, as shown in Astariz *et al.* (2015a). Externalities refer to the damage provoked to third parties when a product or service is consumed. In other words, the approach to achieve an accurate comparison between the LCOE of different energy sources lies in internalizing these external costs in the energy price, which will be assumed by the consumer. This study places the levelised cost of wave energy very close to traditional and very well developed forms of producing energy, such as coal-fired plants (Figure 10.3).

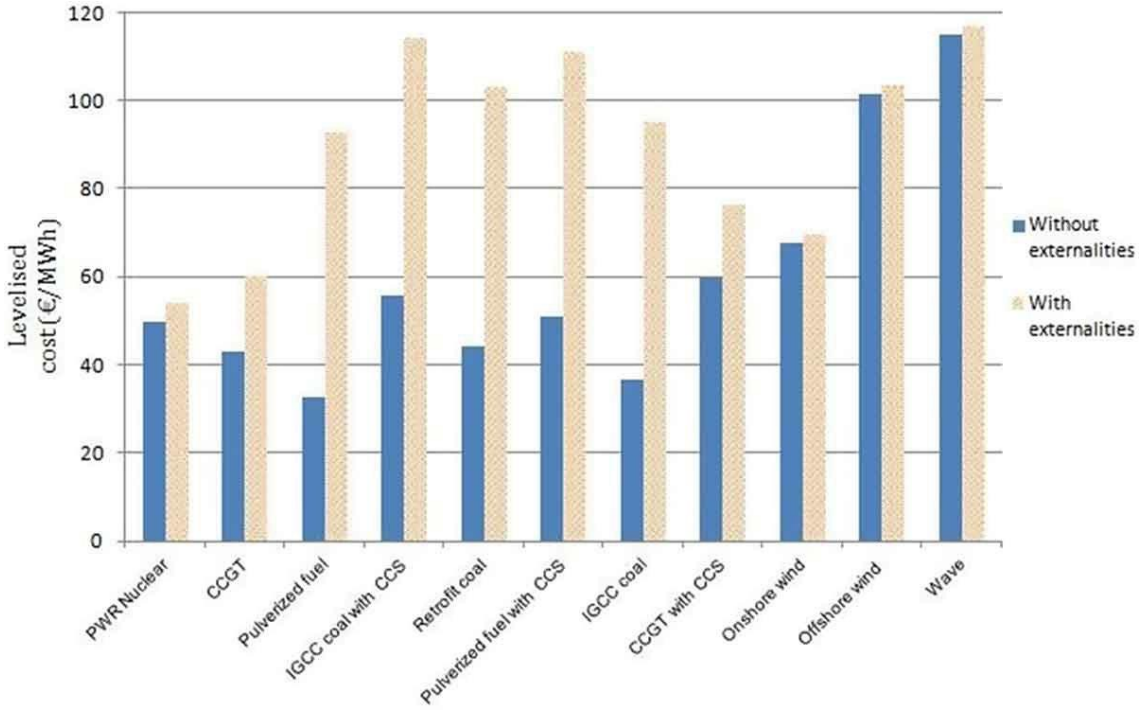

Figure 10.3 Levelised cost (€/MWh) of different technologies including external costs (Astariz *et al.*, 2015a)

An important aspect that was also taken into account in the study was the learning curve, a parameter that identifies cost reductions arising through economies of scale and technological effects, such as technological advances and improvements by practice. The LCOE for wave energy depicted in the graph (114.81 €/MWh) considered an optimistic scenario of this learning curve. However, if we consider the current status of wave energy the levelised cost value presents a broad range from 185.45 €/MWh to 1,595.66 €/MWh. In this sense, the cost of 1 MWh produced by a wave farm would be more expensive than with any non-renewable energy technology, and even more expensive than with most other renewables. Thus, these figures show the necessity of enhancing the viability of wave farms through their synergetic application either: (i) to protect the coast and/or (ii) to share costs and infrastructure with wind energy (co-located offshore wind and wave farms).

An aspect that warrants discussion is the large variability in the LCOE of wave energy at the current status. This is related to several aspects: (i) the type of WEC, (ii)

the wave farm layout and (iii) the site characterisation, which includes water depth, wave conditions and farm-to-coast distance. While the second and the third aspects were already studied under the two previous headings, the performance of the wave farm according to the type of WEC will be discussed below.

The performance of wave energy depends on two main aspects: the efficiency of the device and the capacity factor of the wave farm. The former refers to the ratio between the installed power and the absorbed energy and the latter is the ratio between the average annual energy and the theoretical maximum energy (Astariz & Iglesias, 2015b).

The efficiency of the device depends on its rated power, which varies significantly according to the type of WEC. Table 10.1 shows the rated power for four types of WEC: two oscillating bodies, Aquabuoy and Pelamis; and two overtopping devices, Wave Dragon and WaveCat. It is readily observed that the oscillating bodies present a lower rated power than the overtopping devices; although there is no clear relationship between the rated power and the estimated cost per MW, as this analysis places WaveCat and Aquaboy as the most efficient devices.

Technology	Wave Dragon	WaveCat	Aquabuoy	Pelamis
Rated power (kW)	7,000	1,200	250	750
Estimated cost (€/MW)	2,100	687	720	3,000

Table 10.1 Rated power and estimated cost of WaveDragon, Pelamis and Aquabuoy (Astariz & Iglesias, 2015b; Astariz *et al.*, 2015a; Barrero, 2011)

The efficiency of the devices depends on the mechanical performance of converting the hydrodynamic power into electrical energy and the efficiency of the electrical energy transmission. To obtain this ratio more accurately it is necessary to deploy prototypes in the water, and unfortunately due to the nascent stage of the technology, the number of them is not abundant. In any case, the information presented in Table

10.2 summarises the data from the most relevant WECs installed, revealing that their efficiency is rather high.

Device	Efficiency (%)	Capacity factor (%)
SWAN DK3	54	11
Point absorber	72	8
Bolgehovlen	81	2
Bolgemollen	85	20
Wave Dragon	81	11
Bolgeturbinen	85	1
Wave Plunge	72	9
Bolgemollen	72	1
DWP	72	14
Planta de Pico	54	18
Pelamis	72	5
Mighty Whale	54	3

Table 10.2 Efficiency and capacity factor of different WECs using data extracted from prototypes (Fernandez Diez, 2004)

However, the results from the capacity factor of the wave farms reveal that at this time of development, standalone wave energy is not viable. With the aim of bridging this gap appears the idea of co-located wave and wind farms, which would share the costs of the infrastructure and the transmission of the electricity. Astariz *et al.* (2015a) found that in a co-located wave and wind farm the cost of the energy was around 300 €/MWh, which would involve reductions about 55% with regard to the cost of the isolated wave farm for the case of the WaveCat. Furthermore, if the expected learning curve within ten years was considered, the cost would be reduced to approx. 150 €/MWh, a similar cost of other novel renewables like offshore wind energy.

Another possibility exists whereby the economic viability of wave energy extraction may be enhanced, which was the main focus of this document: protecting the coast in

conjunction with generating carbon-free energy. Moreover this synergetic application is compatible with the co-located wave-wind farm, which would even make wave energy a more competitive renewable.

If a wave farm was deployed with the aim of protecting the coast, its cost would be reduced thanks to the savings in coastal protection. Table 10.3 shows the costs in thousands of pounds of the most common coastal protection means per linear meter of coastal structure or per linear meter of beach. It is important to highlight that the service life of some of these means are equivalent to the one of the wave farm (25-50 years), but others, such as the beach nourishment needs to be conducted periodically (e.g. each 5 years), which increases the budget devoted for protecting the coast.

Taking into account these figures and considering as a case study Perranporth with a beach length of approximately 4 km, the cost of a coastal protection project would range from £30M (hard structure) to £80M (periodic beach nourishment). While the latter is a soft engineering measure, i.e. its environmental impacts are very low; the former, whose price is lower, will have a very significant impact on the location, not only the species that habit there, but also on the coastal morphology due to the drastic change of the morphodynamics. Indeed, the current trends followed by coastal practitioners for coastal management prefer the application of soft engineering means due to the reduction of the aforementioned externalities (Borsje et al., 2011; French, 2004; Grooatert et al., 2006; Hanson et al., 2002).

Coastal protection mean	Significance			Indicative cost (£k/m)
	Enabling costs	Capital costs	Maintenance costs	
Beach recharge and breakwater	Medium	High	Medium	2.7-7.3
Beach recharge and groynes	Medium	High	Medium	1.6-4.7
Rock armour	Medium	High	Low	1.3-6
Seawalls	Medium	High	Low	0.7-5.4
Rock revetments	Medium	High	Low	0.6-2.8
Nearshore breakwaters	Medium	Medium	Low	1.7-4.3
Beach nourishment	Medium	Medium	Medium	0.4-6.4

Table 10.3 Indicative costs associated with the cost of coastal protection (DEFRA, 2015a)

Thus, to obtain the reduction of the cost in the MW per hour due to the savings in coastal protection, it is necessary to discount the cost of these means to the total cost of the wave farm project. Considering the above and using the WaveCat as a reference WEC (with a cost per MWh of 687 €), the savings in coastal protection would suppose a reduction of 25% in the case of the beach nourishment and a reduction of 10% in the case of a detached offshore breakwater. In sum, considering these reductions and an optimistic scenario of the learning curve, the cost of the standalone wave energy could be around 300 MWh, a considerably lower figure.

Furthermore, the environmental impacts of deploying WECs to protect the coast are lower than the aforementioned solutions. Although the greatest advantage of wave farms comprised of floating WECs against the traditional means of coastal protection is their adaptability to climate change, particularly to sea level rise. While coastal structures can become obsolete due to the higher water levels and beach nourishment

can increase the number of periodical campaigns, WECs would adapt to this water level rise without any external cost, either economical or environmental.

On the other hand, it is important to mention that these results have been extracted from a scenario where the wave farm itself would be capable of protecting the whole beach, case that was not observed in the previous chapters. In any case, if a wave farm was deployed to protect the coast in conjunction with soft engineering means, for instance beach nourishment, but with larger periods of beach regeneration, e.g. 10 years instead of 5, the reduction would be still considerable, at least greater than 10%.

These reductions in the LCOE of wave energy have been obtained considering a wave farm comprised of WaveCat WECs. Although the results of this specific WEC cannot lead to general conclusions, it is observed in the literature review that, at least for overtopping WECs, the results of energy absorbed are very similar (Verbrugghe et al., 2016). An example of this is the Wave Dragon WEC, an overtopping type, whose transmission coefficients were studied either physically or numerically by Nørgaard and Andersen (2012). Both sources indicated that the transmission coefficient of these devices presented low variability; despite they were tested for a wide range of wave conditions, ranged from H_s = 1 m and T_p = 5.2 s to H_s = 5 m and T_p = 11 s. Values of transmission coefficients very similar to the WaveCat (Kt ~ 0.75) were found, from 0.6 to 0.8.

Then, the impacts on the nearshore wave conditions of wave farms comprised by Wave Dragons WEC were very similar results to the result presented in this document. For instance, Figure 2.19 show that the disturbance of the wave conditions, i.e. the wave height difference between the baseline and the wave farm scenario, at a distance of 1 km from the wave farm peaked in 0.45, trend that was observed for the WaveCat at both locations considered in this thesis: Perranporth in Figure 6.4 and Xago in Figure 6.19.

However, when it comes to the impacts on the beach morphology results, it is impossible to compare and generalise the impacts caused by the wave farms, as the novelty of this thesis lies in the evaluation for the first time of the reduction in storm-induced erosion brought about by wave farms due to the absorption of wave energy. Although, it could be stated that whether the impacts on the wave patterns between overtopping devices are analogous despite the different site characteristics, the results expected on the beach morphology should follow this trend.

Extrapolation to other type of devices, namely Oscillating Water Columns and Oscillating bodies, is not that straightforward. While the working principle of overtopping devices is mainly wave energy absorption, the other two types of WECs are mainly governed by processes such as radiation and diffraction, which make more complex the resolution of the wave patterns in the lee of the farm. As seen in Figure 2.16Figure 2.16 Perturbed wave field normalized by recorded undisturbed wave field for the 5 x 5 WEC array configuration (Stratigaki *et al.*, 2014). The basin width (X, columns) and length (Y, rows) are expressed in number of WEC unit diameters, D = 0.315 m., the evolution of the disturbed wave field varied significantly compared to the cases with overtopping WECs; with an increase of the wave height in the points near the WECs due to the effects of the radiated waves. Nevertheless, mowing towards the coast, a reduction of the wave height is found to not exceed 20%, very different to the aforementioned 45%.

As for the coastal impacts, the comparison of the effects on the longshore sediment transport between different types of devices show that overtopping devices are the most efficient type of WECs to protect the coast, though the other type of WECs can reach the same level of protection increasing the number of WECs deployed in the farm. For instance, in the study carried out by Mendoza *et al.* (2014), a wave farm form by 3

Wave Dragon WECs was capable to protect the beach as much as a farm comprised of 45 DEXA devices (oscillating body).

Last but not least, the survivability of the WECs under extreme events is one of the most important topics in wave energy. Brown et al. (2010) defined WEC survivability as "the ability of a marine energy system to avoid damage, during sea states that are outside of intended operating conditions, that results in unplanned down time and the need for service". The complexity of the problem lies in the large number of mode of failures that can occur. For any moored device, loads within the mooring system, including anchors, mooring lines and connection points must be considered. As a result, the vulnerability of WECs in most of the cases depends more on the survivability of the anchor system rather than the WEC itself (Coe & Neary, 2014; Ransley et al., 2013).

The primary goal of a WEC when waves get larger is to transition from efficient energy production to survival. The nature of this transition and under what wave conditions this must occur is completely dependent on the type of device. Then, the question that emerges is whether this reduction of effectiveness in the energy production can affect the wave energy absorption, and, therefore, the degree of coastal protection provided by the wave farm.

During these extreme events, generally WECs adopt survival strategies in order to reduce the chance of damage, mechanical failure or devices breaking free from moorings. These mechanisms might include disengaging the power take-off, changing the mooring orientation, or pulling the device underwater. In the case of the WaveCat, the model adapts the angle between the hulls of the device to reduce the wave loading, i.e. the greater the wave height, the smaller the angle. As a result, the farm effectiveness as wave energy absorber might be reduced, although never completely, as the device will stand there and will have an impact on the wave patterns. However, it is hard to

estimate in the degree to which coastal protection could be diminished compared to the operational conditions. For this purpose, it is necessary to conduct physical tests that allow this determination, which is the objective of the EU WaveImpact project that will be described in the following section.

10.2 FUTURE RESEARCH LINES

From the promising results presented above, a question emerges: can wave farms complement, or even substitute in certain locations, typical coastal protection measures such as groynes and detached breakwaters? The reduction of storm-induced erosion found in this document can lead to a positive answer; however prior to actually developing wave farms with a view to generating carbon-free renewable energy and protecting the coast, the following aspects must be addressed in the future: (i) the assessment of the effectiveness of wave farms under extreme events to absorb energy, and consequently to protect the coast; (ii) the quantification of the wave farm impacts on the coast in the long term (multi decadal scale); and (iii) the evaluation of the effectiveness of wave farms to reduce the flooding and its effects on coastal structures.

The wave field-wave farm interaction must be characterised under a larger number of case studies. In the present document the WEC-wave interaction was modelled using the transmission coefficients obtained during the laboratory tests reported by Fernandez *et al.* (2012). This study showed the low variability of the coefficient transmission under operational conditions ($\kappa_t \sim 0.76$); however extreme wave conditions were not tested. On these grounds, the ongoing EU WaveImpact project aims to characterise the interaction of the WaveCat WEC with the wave field in both the operational and the survival mode by means of laboratory tests.

As mentioned above, a number of distinct survival modes and strategies have been developed for WECs. A robust WEC survival design process requires a set of modeling tools, particularly with regard to the physical modeling that allows a well-targeted validation, consequently, identifying in which manner survival modes can vary the effectiveness of WECs to extract energy is one of the major objectives of the WaveImpact project. Moreover, this upgraded WEC-wave interaction can be incorporated into wave propagation models accounting for frequency-dependent wave transmission coefficients (Ruehl et al., 2013; Smith, Pearce & Millar, 2012) and thus lead to more accurate representations of the impacts, especially in the long-term.

A case that reflects the importance of the long-term evolution is how reduction in wave energy in certain sections of the beach (e.g. north part in Perranporth) which will affect beach dynamics in the long term, as the beach could begin an anticlockwise rotation similar to those seen in pocket beaches affected by ENSO oscillations (Ranasinghe et al., 2004; Storlazzi & Griggs, 2000). This rotation may well cause permanent erosion at the south end of the beach and permanent accretion at the north end.

For this purpose, new modelling techniques are necessary, as in this document, process-based models have been used to determine the impacts on the coast in the short- and medium-term scale; and the long-term analysis cannot rely on the extrapolation of the current results owing to the highly nonlinear processes involved, the lack of an up-scaling closure theory and the relevance of wave-induced beach recovery between storm events (Houser, 2009). Although process-based models, which iteratively resolve the hydrodynamics, sediment transport and bathymetric evolution, are successfully used to assess the beach response under storm conditions, they struggle to simulate post-storm beach recovery (Kobayashi, Payo & Schmied, 2008; Plant et al., 2004) – a fundamental

shortcoming when it comes to simulating long-term coastal behaviour. For these reasons, this aspect needs to be addressed through behavioural models, which simulate known behaviours, such as the tendency for a beach to develop towards an equilibrium form. The results of this future research line will be essential to determining whether wave farms can be used for protecting the coast in synergy with their main purpose of generating carbon-free energy.

Finally, the last research line considered key in the assessment of the wave farm impacts impact is their effects on water levels, and subsequently the determination of their effectiveness to reduce coastal flooding. This topic is of particular relevance in the current transition scenario, where sea-level rise and, potentially, increased storminess (Pye & Blott, 2008) will exponentially increase coastal flood risks (Lewis et al., 2011). Furthermore, many of the existing coastal defence structures will quickly become obsolete, and this will lead to the necessity of enhancing coastal protection.

10.3 CONCLUSIONS

The thesis provides a comprehensive assessment of the wave farm impacts on the beach morphology at two different locations (Perranporth and Xago), constituting the first document that quantifies the impacts on the coast. The degree of coastal protection afforded by a wave farm was investigated in the short and medium term. Although the study was focussed on a type of WEC, WaveCat, the results could be arguably extrapolated at least for overtopping-type devices. Thus, from the different areas and wave conditions analysed the following points are distilled to address the central aim of the document, in which manner the wave energy extraction caused by the WaveCat WECs that form a wave farm affects the coast:

- The reduction of wave height peaks in the lee of the wave farm, and although it decreases towards the coastline due to the wave energy diffracted from the edges of the shadow, the values found on the coast are still significant and capable to alter the morphology of the beach located in the lee of the farm.
- Wave farms are particularly effective in reducing storm-induced erosion in the areas most at risk from this phenomenon. For instance, while in Perranporth the main reduction of erosion is found at the beach face, in Xago Beach the sandy dune that backs the beach experienced the greatest attenuations.
- The greatest degree of coastal protection afforded by the wave farms occurs under storm conditions, however the protection provided in the medium term, with reductions of erosion greater than 20%, cannot be overlooked.
- Wave farms not only reduce the volume of storm-induced erosion, but also modify the sediment transport patterns. The landward extreme of the eroded area is displaced significantly towards the sea side at the end of storm conditions, which is of particular relevance to avoid damages in the foundations of buildings in the waterfront.
- The modal state of the beach is also altered by the presence of a wave farm, transforming the predominant wave-dominated character of the beach to tide-dominated. The reduction of the wave-dominated states in addition to the potential removal of the offshore bar would lead to an increase of the onshore sediment transport: beach accretion.
- The wave energy resource and subsequently the performance of the wave farm highly depend on the distance of the farm to the coast and the wave farm layout. Although, the statement: “the greater farm-to-coast distance,

the greater the available resource" is generally valid, the relationship between these two parameters is not proportional. Indeed, in some cases placing the wave farm the furthest possible is not the best solution considering the increase of costs in submarine cable and mooring lines, among others. Furthermore, it is observed that increasing the distance between devices, similar wave energy resource to the one obtained placing the wave farm at further distances can be achieved.

- The farm-to-coast distance is also a key element in the degree of coastal protection afforded by the farm: The closer the wave farm to the coast, the greater the reduction of erosion. Therefore, the effects of the wave farm on the beach can be controlled by locating the farm closer to, or further from, the shoreline.

In sum, this document presents how a wave farm can alter the behaviour and response of a beach in its lee based on the results of two case studies. This knowledge of the wave energy impacts is essential for the consolidation of one of the most promising marine renewable energies, particularly when its impacts need not be regarded as negative; on the contrary, it can contribute to reducing the erosion on the beach, and thus serve to counter erosion. Moreover, wave energy is essential to meeting the objectives of greenhouse gas reduction established by the Kyoto protocol and other treaties. Therefore, this thesis illustrated that wave energy is emerging as a renewable resource capable of tackling climate change on the double front of its causes (through reduced carbon emissions) and effects, particularly on the coast (erosion).

REFERENCES

REFERENCES

Abanades, J., Greaves, D. & Iglesias, G. (2014a) 'Coastal defence through wave farms'. *Coastal Engineering*, 91 (0). pp 299-307.

Abanades, J., Greaves, D. & Iglesias, G. (2014b) 'Wave farm impact on the beach profile: A case study'. *Coastal Engineering*, 86 (0). pp 36-44.

Abanades, J., Greaves, D. & Iglesias, G. (2015a) 'Wave farm impact on beach modal state'. *Marine Geology*, 361 pp 126-135.

Abanades, J., Greaves, D. & Iglesias, G. (2015b) 'Coastal defence using wave farms: The role of farm-to-coast distance'. *Renewable Energy*, 75 (0). pp 572-582.

ABPmer (2008) 'Atlas of UK Marine Renewable Energy Resources'. [Online]. Available at: http://www.renewables-atlas.info.

Armaroli, C., Grottoli, E., Harley, M. D. & Ciavola, P. (2013) 'Beach morphodynamics and types of foredune erosion generated by storms along the Emilia-Romagna coastline, Italy'. *Geomorphology*, 199 (0). pp 22-35.

Astariz, S. & Iglesias, G. (2015a) 'The economics of wave energy: A review'. *Renewable and Sustainable Energy Reviews*, 45 (0). pp 397-408.

Astariz, S. & Iglesias, G. (2015b) 'The economics of wave energy: A review'. *Renewable and Sustainable Energy Reviews*, 45 pp 397-408.

Astariz, S., Perez-Collazo, C., Abanades, J. & Iglesias, G. (2015a) 'Co-located wave-wind farms: economic assessment as a function of layout '. *Renewable Energy*, In press

Astariz, S., Perez-Collazo, C., Abanades, J. & Iglesias, G. (2015b) 'Co-located wind-wave farm synergies (Operation & Maintenance): A case study'. *Energy Conversion and Management*, 91 pp 63-75.

Astariz, S., Perez-Collazo, C., Abanades, J. & Iglesias, G. (2015c) 'Towards the optimal design of a co-located wind-wave farm'. *Energy*, 84 pp 15-24.

Austin, M., Scott, T., Brown, J., Brown, J., MacMahan, J., Masselink, G. & Russell, P. (2010) 'Temporal observations of rip current circulation on a macro-tidal beach'. *Continental Shelf Research*, 30 (9). pp 1149-1165.

AWS Ocean Energy (2015) 'AWS Ocean Energy web page'.

Babarit, A. (2010) 'Impact of long separating distances on the energy production of two interacting wave energy converters'. *Ocean Engineering*, 37 (8–9). pp 718-729.

Bahaj, A. S. (2011) 'Generating electricity from the oceans'. *Renewable and Sustainable Energy Reviews*, 15 (7). pp 3399-3416.

Baldock, T. E., Alsina, J. A., Caceres, I., Vicinanza, D., Contestabile, P., Power, H. & Sanchez-Arcilla, A. (2011) 'Large-scale experiments on beach profile evolution and surf and swash zone sediment transport induced by long waves, wave groups and random waves'. *Coastal Engineering*, 58 (2). pp 214-227.

Baldock, T. E., Manoonvoravong, P. & Pham, K. S. (2010) 'Sediment transport and beach morphodynamics induced by free long waves, bound long waves and wave groups'. *Coastal Engineering*, 57 (10). pp 898-916.

Barrero, A. (2011) 'España apuesta por las olas'. *Energías Renovables, especial Energías del Mar*, 106 pp 10.

Beels, C., Troch, P., De Backer, G., Vantorre, M. & De Rouck, J. (2010a) 'Numerical implementation and sensitivity analysis of a wave energy converter in a time-dependent mild-slope equation model'. *Coastal Engineering*, 57 (5). pp 471-492.

Beels, C., Troch, P., De Visch, K., Kofoed, J. P. & De Backer, G. (2010b) 'Application of the time-dependent mild-slope equations for the simulation of wake effects in the lee of a farm of Wave Dragon wave energy converters'. *Renewable Energy*, 35 (8). pp 1644-1661.

Berkhoff, J. (1974) *Computation of combined refraction-diffraction.* Delft Hydraulics Laboratory.

Bernhoff, H., Sjöstedt, E. & Leijon, M. (2006) 'Wave energy resources in sheltered sea areas: A case study of the Baltic Sea'. *Renewable Energy*, 31 (13). pp 2164-2170.

Blott, S. J. & Pye, K. (2001) 'GRADISTAT: a grain size distribution and statistics package for the analysis of unconsolidated sediments'. *Earth surface processes and Landforms*, 26 (11). pp 1237-1248.

Booij, N., Holthuijsen, L. & Ris, R. (1996) 'The" SWAN" wave model for shallow water', *Coastal engineering conference*. ASCE AMERICAN SOCIETY OF CIVIL ENGINEERS, pp. 668-676.

Booij, N., Ris, R. C. & Holthuijsen, L. H. (1999) 'A third-generation wave model for coastal regions: 1. Model description and validation'. *Journal of Geophysical Research: Oceans*, 104 (C4). pp 7649-7666.

Borgarino, B., Babarit, A. & Ferrant, P. (2012) 'Impact of wave interactions effects on energy absorption in large arrays of wave energy converters'. *Ocean Engineering*, 41 (0). pp 79-88.

Borsje, B. W., van Wesenbeeck, B. K., Dekker, F., Paalvast, P., Bouma, T. J., van Katwijk, M. M. & de Vries, M. B. (2011) 'How ecological engineering can serve in coastal protection'. *Ecological Engineering*, 37 (2). pp 113-122.

Brown, A., Paasch, R., Tumer, I. Y., Lenee-Bluhm, P., Hovland, J., von Jouanne, A. & Brekken, T. (2010) 'Towards a definition and metric for the survivability of ocean wave energy converters', *ASME 2010 4th International Conference on Energy Sustainability*. American Society of Mechanical Engineers, pp. 917-927.

Butt, T., Russell, P. & Turner, I. (2001) 'The influence of swash infiltration–exfiltration on beach face sediment transport: onshore or offshore?'. *Coastal Engineering*, 42 (1). pp 35-52.

Callaghan, D. P., Ranasinghe, R. & Roelvink, D. (2013) 'Probabilistic estimation of storm erosion using analytical, semi-empirical, and process based storm erosion models'. *Coastal Engineering*, 82 (0). pp 64-75.

Carballo, R. & Iglesias, G. (2012) 'A methodology to determine the power performance of wave energy converters at a particular coastal location'. *Energy Conversion and Management*, 61 pp 8-18.

Carballo, R. & Iglesias, G. (2013) 'Wave farm impact based on realistic wave-WEC interaction'. *Energy*, 51 pp 216-229.

Carballo, R., Sánchez, M., Ramos, V., Fraguela, J. & Iglesias, G. (2015) 'The intra-annual variability in the performance of wave energy converters: A comparative study in N Galicia (Spain)'. *Energy*,

Castelle, B., Marieu, V., Bujan, S., Splinter, K. D., Robinet, A., Sénéchal, N. & Ferreira, S. (2015) 'Impact of the winter 2013–2014 series of severe Western Europe storms on a double-barred sandy coast: Beach and dune erosion and megacusp embayments'. *Geomorphology*, 238 (0). pp 135-148.

Child, B. & Venugopal, V. (2007) 'Interaction of waves with an array of floating wave energy devices', *Proceedings of the 7th European Wave and Tidal Energy Conference, Porto, Portugal*.

Child, B. F. M. & Venugopal, V. (2010) 'Optimal configurations of wave energy device arrays'. *Ocean Engineering*, 37 (16). pp 1402-1417.

Chini, N., Stansby, P., Leake, J., Wolf, J., Roberts-Jones, J. & Lowe, J. (2010) 'The impact of sea level rise and climate change on inshore wave climate: A case study for East Anglia (UK)'. *Coastal Engineering*, 57 (11). pp 973-984.

CISCAG (2011) *Shoreline Management Plan* Cornwall and Isles of Scilly Coastal Advisory Group. Available.

Clément, A., McCullen, P., Falcão, A., Fiorentino, A., Gardner, F., Hammarlund, K., Lemonis, G., Lewis, T., Nielsen, K., Petroncini, S., Pontes, M. T., Schild, P., Sjöström, B.-O., Sørensen, H. C. & Thorpe, T. (2002a) 'Wave energy in Europe: current status and perspectives'. *Renewable and Sustainable Energy Reviews*, 6 (5). pp 405-431.

Clément, A., McCullen, P., Falcão, A. F. d. O., Fiorentino, A., Gardner, F., Hammarlund, K., Lemonis, G., Lewis, T., Nielsen, K., Petroncini, S., Pontes, M. T., Schild, P., Sjöström, B., Sørensen, H. C. & Thorpe, T. W. (2002b) 'Wave energy in Europe: current status and perspectives'. *Renewable and Sustainable Energy Reviews*, 6 (5). pp 405-431.

Coe, R. G. & Neary, V. S. (2014) 'Review of methods for modeling wave energy converter survival in extreme sea states'.

Cornett, A. M. (2008) 'A global wave energy resource assessment'. *ISOPE--579*,

Cowell, P. & Thom, B. (1994) *Morphodynamics of coastal evolution.* Cambridge University Press, Cambridge, United Kingdom and New York, NY, USA.

Dalrymple, R. A. & Dean, R. G. (1991) *Water wave mechanics for engineers and scientists.* Prentice-Hall.

Davis, R. A. & Hayes, M. O. (1984) 'What is a wave-dominated coast?'. *Marine Geology*, 60 (1). pp 313-329.

Dean, R. G. (1973) 'Heuristic models of sand transport in the surf zone', *First Australian Conference on Coastal Engineering, 1973: Engineering Dynamics of the Coastal Zone*. Institution of Engineers, Australia, pp. 215.

Defne, Z., Haas, K. A. & Fritz, H. M. (2009) 'Wave power potential along the Atlantic coast of the southeastern USA'. *Renewable Energy*, 34 (10). pp 2197-2205.

DEFRA (2015a) *Cost estimation for coastal protection – summary of evidence.* Available.

DEFRA (2015b) *Central Government Funding for Flood and Coastal Erosion Risk Management in England.* Available.

Drew, B., Plummer, A. & Sahinkaya, M. N. (2009a) 'A review of wave energy converter technology'. *Proceedings of the Institution of Mechanical Engineers, Part A: Journal of Power and Energy*, 223 (8). pp 887-902.

Drew, B., Plummer, A. R. & Sahinkaya, m. N. (2009b) 'A review of wave energy converter technology'. *Journal of Power and Energy*, 223 (8). pp 887-902.

Egbert, G. D., Bennett, A. F. & Foreman, M. G. (1994) 'TOPEX/POSEIDON tides estimated using a global inverse model'. *Journal of Geophysical Research: Oceans (1978–2012)*, 99 (C12). pp 24821-24852.

EU-OEA (2010) *Oceans of Energy. European Ocean Energy Roadmap 2010-2050.* Bietlot, Belgium: European Ocean Energy Association,. 36 pp. Available at: http://www.eu-oea.com/wp-content/uploads/2012/02/EUOEA-Roadmap.pdf.

European Commission (2007) *A European Strategic Energy Technology Plan (SET-Plan)–Towards a low-carbon future.* 723

European Commission, U. N., UNEP, Energy, National Renewable Energy Laboratory, American Wind Energy Association (2009) 'Clean future'. [Online]. Available at: Clean-future.com.

EVE (2014) 'Ente Vasco de la Energia'.

EWEA, ECN, 3E & SOW (2012) *Delivering offshore electricty to the EU. Spatial planning of offshore renewable energies and electricity grid infrastrutures in an integrated EU maritime policy.* 80 pp. Available at: www.seanergy2020.eu.

Falcão, A. F. d. O. (2010a) 'Wave energy utilization: A review of the technologies'. *Renewable and Sustainable Energy Reviews*, 14 (3). pp 899-918.

Falcão, A. F. O. (2010b) 'Wave energy utilization: A review of the technologies'. *Renewable and Sustainable Energy Reviews*, 14 (3). pp 899-918.

Falnes, J. (2007) 'A review of wave-energy extraction'. *Marine Structures*, 20 (4). pp 185-201.

Fernandez Diez, P. (2004) 'II Modificación de la Energía de las olas'.[in Departamento. (Accessed:Fernandez Diez, P.

Fernandez, H., Iglesias, G., Carballo, R., Castro, A., Fraguela, J. A., Taveira-Pinto, F. & Sanchez, M. (2012) 'The new wave energy converter WaveCat: Concept and laboratory tests'. *Marine Structures*, 29 (1). pp 58-70.

Flor-Blanco, G., Flor, G. & Pando, L. (2013) 'Evolution of the Salinas-El Espartal and Xagó beach/dune systems in north-western Spain over recent decades: evidence for responses to natural processes and anthropogenic interventions'. *Geo-Marine Letters*, 33 (2-3). pp 143-157.

Flor-Blanco, G., Pando, L., García-Quintana, Y., Barranco, A., Suárez, J., Rey, J. & Flor, G. (2011) 'Prospección geológico-geotécnica para la instalación de una estación experimental de energías renovables en la plataforma Off Shore de Asturias'.

Flor, G., Flor-Blanco, G. & Flores-Soriano, C. (2015) 'Cambios ambientales por los temporales de invierno de 2014 en la costa asturiana (NO de España)'. *Trabajos de Geología*, 34 (34).

French, P. W. (2004) 'The changing nature of, and approaches to, UK coastal management at the start of the twenty-first century'. *The Geographical Journal*, 170 (2). pp 116-125.

Galappatti, G. & Vreugdenhil, C. (1985) 'A depth-integrated model for suspended sediment transport'. *Journal of Hydraulic Research*, 23 (4). pp 359-377.

Gonçalves, M., Martinho, P. & Guedes Soares, C. (2014a) 'Assessment of wave energy in the Canary Islands'. *Renewable Energy*, 68 (0). pp 774-784.

Gonçalves, M., Martinho, P. & Guedes Soares, C. (2014b) 'Wave energy conditions in the western French coast'. *Renewable Energy*, 62 (0). pp 155-163.

Gonzalez-Santamaria, R., Zou, Q.-P. & Pan, S. (2013) 'Impacts of a Wave Farm on Waves, Currents and Coastal Morphology in South West England'. *Estuaries and Coasts*, pp 1-14.

Gonzalez, R., Zou, Q. & Pan, S. (2012) 'Modelling of the impact of a wave farm on nearshore sediment transport'. *Proceedings of the international conference of Coastal Engineering 2012*,

Grooatert, P., Maelfait, J.-P., Mathys, M., Provoost, S., Sabbe, K., Stienen, E. W. & Van Lancker, V. (2006) 'Beach nourishment: an ecologically sound coastal defence alternative? A review'.

Günther, H., Hasselmann, S. & Janssen, P. A. (1992) *The WAM model, Cycle 4.* DKRZ.

Hadadpour, S., Etemad-Shahidi, A., Jabbari, E. & Kamranzad, B. (2014) 'Wave energy and hot spots in Anzali port'. *Energy*, 74 (0). pp 529-536.

Halcrow (2006) *Wave Hub Environmental Statement.* South West of England Regional Development Agency. Available.

Hanson, H., Brampton, A., Capobianco, M., Dette, H. H., Hamm, L., Laustrup, C., Lechuga, A. & Spanhoff, R. (2002) 'Beach nourishment projects, practices, and objectives—a European overview'. *Coastal Engineering*, 47 (2). pp 81-111.

Hasselmann, K. (1971) 'On the mass and momentum transfer between short gravity waves and larger-scale motions'. *Journal of Fluid Mechanics*, 50 (01). pp 189-205.

Holthuijsen, L. H. (2007) *Waves in oceanic and coastal waters.* Cambridge University Press.

Houser, C. (2009) 'Synchronization of transport and supply in beach-dune interaction'. *Progress in Physical Geography*,

Iglesias, G. & Abanades, J. (2014) 'Characterisation of the wave resource: The crucial points'. *RENEW 1st International Conference on Renewable Energies Offshore*. Lisbon.

Iglesias, G., Alvarez, M. & García, P. (2010) 'WAVE ENERGY CONVERTERS', in *Encyclopedia of Life Support Systems (EOLSS)*. UNESCO.

Iglesias, G. & Carballo, R. (2009) 'Wave energy potential along the Death Coast (Spain)'. *Energy*, 34 (11). pp 1963-1975.

Iglesias, G. & Carballo, R. (2010a) 'Wave energy and nearshore hot spots: The case of the SE Bay of Biscay'. *Renewable Energy*, 35 (11). pp 2490-2500.

Iglesias, G. & Carballo, R. (2010b) 'Offshore and inshore wave energy assessment: Asturias (N Spain)'. *Energy*, 35 (5). pp 1964-1972.

Iglesias, G. & Carballo, R. (2010c) 'Wave power for la isla bonita'. *Energy*, 35 (12). pp 5013-5021.

Iglesias, G. & Carballo, R. (2011) 'Wave resource in El Hierro—an island towards energy self-sufficiency'. *Renewable Energy*, 36 (2). pp 689-698.

Iglesias, G. & Carballo, R. (2014) 'Wave farm impact: The role of farm-to-coast distance'. *Renewable Energy*, 69 (0). pp 375-385.

Iglesias, G., Carballo, R., Castro, A. & Fraga, B. (2008) 'DEVELOPMENT AND DESIGN OF THE WAVECAT™ ENERGY CONVERTER'. *Coastal Engineering*, pp 3970-3982.

Iglesias, G., López, M., Carballo, R., Castro, A., Fraguela, J. A. & Frigaard, P. (2009) 'Wave energy potential in Galicia (NW Spain)'. *Renewable Energy*, 34 (11). pp 2323-2333.

Jeffrey, H. & Sedgwick, J. (2011) *ORECCA. European Offshore Renewable Energy roadmap.* 201 pp. Available at: http://www.orecca.eu/.

Kamphuis, J. (1991a) 'Wave transformation'. *Coastal Engineering*, 15 (3). pp 173-184.

Kamphuis, J. W. (1991b) 'Alongshore sediment transport rate'. *Journal of Waterway, Port, Coastal, and Ocean Engineering*, 117 (6). pp 624-640.

Kendon, M. & McCarthy, M. (2015) 'The UK's wet and stormy winter of 2013/2014'. *Weather*, 70 (2). pp 40-47.

Kenney, J. (2009) 'SW Wave Hub metocean design basis'. *SWRDA.[Online] Available at*,

Kerr, D. (2007) 'Marine energy'. *Philos Transact A Math Phys Eng Sci*, 365 (1853). pp 971-992.

Kobayashi, N., Payo, A. & Schmied, L. (2008) 'Cross-shore suspended sand and bed load transport on beaches'. *Journal of Geophysical Research: Oceans (1978–2012)*, 113 (C7).

Kofoed, J. P., Frigaard, P., Friis-Madsen, E. & Sørensen, H. C. (2006) 'Prototype testing of the wave energy converter wave dragon'. *Renewable Energy*, 31 (2). pp 181-189.

Larson, M. & Kraus, N. C. (1989) *SBEACH: numerical model for simulating storm-induced beach change. Report 1. Empirical foundation and model development.* DTIC Document. Available.

LCICG (2012) *Technology Innovation Needs Assessment (TINA): Marine Energy.* Available.

Lenee-Bluhm, P., Paasch, R. & Özkan-Haller, H. T. (2011) 'Characterizing the wave energy resource of the US Pacific Northwest'. *Renewable Energy*, 36 (8). pp 2106-2119.

Lewis, M., Horsburgh, K., Bates, P. & Smith, R. (2011) 'Quantifying the uncertainty in future coastal flood risk estimates for the UK'. *Journal of Coastal Research*, 27 (5). pp 870-881.

Liberti, L., Carillo, A. & Sannino, G. (2013) 'Wave energy resource assessment in the Mediterranean, the Italian perspective'. *Renewable Energy*, 50 pp 938-949.

Longuet-Higgins, M. S. & Stewart, R. (1961) 'The changes in amplitude of short gravity waves on steady non-uniform currents'. *Journal of Fluid Mechanics*, 10 (04). pp 529-549.

López, I., Pereiras, B., Castro, F. & Iglesias, G. (2014) 'Optimisation of turbine-induced damping for an OWC wave energy converter using a RANS–VOF numerical model'. *Applied Energy*, 127 (0). pp 105-114.

Martinho, P. & Soares, C. G. (2011) 'Modelling wave energy resources for UK's southwest coast', *OCEANS, 2011 IEEE-Spain*. IEEE, pp. 1-8.

Masselink, G., Evans, D., Hughes, M. G. & Russell, P. (2005) 'Suspended sediment transport in the swash zone of a dissipative beach'. *Marine Geology*, 216 (3). pp 169-189.

Masselink, G. & Short, A. D. (1993) 'The effect of tide range on beach morphodynamics and morphology: a conceptual beach model'. *Journal of Coastal Research*, pp 785-800.

McCall, R. T., Van Thiel de Vries, J. S. M., Plant, N. G., Van Dongeren, A. R., Roelvink, J. A., Thompson, D. M. & Reniers, A. J. H. M. (2010) 'Two-dimensional time dependent hurricane overwash and erosion modeling at Santa Rosa Island'. *Coastal Engineering*, 57 (7). pp 668-683.

McCormick, M. E. (1981) *Ocean Wave Energy Conversion.* New York: Wiley-Interscience.

Mendoza, E., Silva, R., Zanuttigh, B., Angelelli, E., Lykke Andersen, T., Martinelli, L., Nørgaard, J. Q. H. & Ruol, P. (2014) 'Beach response to wave energy converter farms acting as coastal defence'. *Coastal Engineering*, 87 (0). pp 97-111.

Millar, D. L., Smith, H. C. M. & Reeve, D. E. (2007) 'Modelling analysis of the sensitivity of shoreline change to a wave farm'. *Ocean Engineering*, 34 (5-6). pp 884-901.

Moccia, J., Arapogianni, A., Wilkes, J., Kjaer, C. & Gruet, R. (2011) *Pure Power. Wind energy targets for 2020 and 2030.* Brussels, belgium: European Wind Energy Association. 97 pp. Available at: http://www.ewea.org.

Monbaliu, J., Padilla-Hernandez, R., Hargreaves, J. C., Albiach, J. C. C., Luo, W., Sclavo, M. & Guenther, H. (2000) 'The spectral wave model, WAM, adapted for applications with high spatial resolution'. *Coastal Engineering*, 41 (1). pp 41-62.

Neill, S. & Iglesias, G. (2012) 'Impact of wave energy converter (WEC) array operation on nearshore processes'.

Neill, S., Scourse, J., Bigg, G. & Uehara, K. (2009) 'Changes in wave climate over the northwest European shelf seas during the last 12,000 years'. *Journal of Geophysical Research: Oceans*, 114 (C6).

Neill, S. P., Lewis, M. J., Hashemi, M. R., Slater, E., Lawrence, J. & Spall, S. A. (2014) 'Inter-annual and inter-seasonal variability of the Orkney wave power resource'. *Applied Energy*, 132 pp 339-348.

Nørgaard, J. H. & Andersen, T. L. (2012) 'Investigation of wave transmission from a floating wave dragon wave energy converter', *The Twenty-second International Offshore and Polar Engineering Conference*. International Society of Offshore and Polar Engineers.

Nørgaard, J. H., Andersen, T. L. & Kofoed, J. P. (2011) 'Wave Dragon Wave Energy Converters Used as Coastal Protection'. *Proceedings of the international conference of Coastal Structures 2011*. Yokohama: Imperial College Press.

Ocean Power Technologies Inc (2014) 'OPT web page'.

Palha, A., Mendes, L., Fortes, C. J., Brito-Melo, A. & Sarmento, A. (2010) 'The impact of wave energy farms in the shoreline wave climate: Portuguese pilot zone case study using Pelamis energy wave devices'. *Renewable Energy*, 35 (1). pp 62-77.

Pelamis Wave Power Ltd 'Pelamis Wave'. [Online]. Available at: http://www.pelamiswave.com/ (Accessed: March 2013).

Pelc, R. & Fujita, R. M. (2002) 'Renewable energy from the ocean'. *Marine Policy*, 26 (6). pp 471-479.

Pender, D. & Karunarathna, H. (2013) 'A statistical-process based approach for modelling beach profile variability'. *Coastal Engineering*, 81 (0). pp 19-29.

Peregrine, D. H. (1967) 'Long waves on a beach'. *Journal of Fluid Mechanics*, 27 (04). pp 815-827.

Pérez-Collazo, C., Greaves, D. & Iglesias, G. (2015) 'A review of combined wave and offshore wind energy'. *Renewable and Sustainable Energy Reviews*, 42 (0). pp 141-153.

Perez Collazo, C., Astariz, S., Abanades, J., Greaves, D. & Iglesias, G. (2014) 'CO-LOCATED WAVE AND OFFSHORE WIND FARMS: A PRELIMINARY CASE STUDY OF AN HYBRID ARRAY', *International Conference in Coastal Engineering (ICCE)*.

Plant, N. G., Holland, K. T., Puleo, J. A. & Gallagher, E. L. (2004) 'Prediction skill of nearshore profile evolution models'. *Journal of Geophysical Research: Oceans (1978–2012)*, 109 (C1).

Pontes, M., Athanassoulis, G., Barstow, S., Cavaleri, L., Holmes, B., Mollison, D. & Pires, H. O. (1996) 'WERATLAS–Atlas of Wave Energy Resource in Europe'. *Report to the European Commission, JOULE II Programme, 96p*,

Pontes, M. T., Aguiar, R. & Pires, H. O. (2005) 'A nearshore wave energy atlas for Portugal'. *Journal of Offshore Mechanics and Arctic Engineering*, 127 pp 249.

Pugh, D. (2004) *Changing sea levels: effects of tides, weather and climate.* Cambridge University Press.

Pye, K. & Blott, S. (2008) 'Decadal-scale variation in dune erosion and accretion rates: an investigation of the significance of changing storm tide frequency and magnitude on the Sefton coast, UK'. *Geomorphology*, 102 (3). pp 652-666.

Ranasinghe, R., McLoughlin, R., Short, A. & Symonds, G. (2004) 'The Southern Oscillation Index, wave climate, and beach rotation'. *Marine Geology*, 204 (3). pp 273-287.

Ransley, E., Hann, M., Greaves, D., Raby, A. & Simmonds, D. (2013) 'Numerical and physical modeling of extreme waves at Wave Hub'. *Journal of Coastal Research*, 65 (sp2). pp 1645-1650.

Reeve, D., Chen, Y., Pan, S., Magar, V., Simmonds, D. & Zacharioudaki, A. (2011a) 'An investigation of the impacts of climate change on wave energy generation: The Wave Hub, Cornwall, UK'. *Renewable Energy*, 36 (9). pp 2404-2413.

Reeve, D. E., Chen, Y., Pan, S., Magar, V., Simmonds, D. J. & Zacharioudaki, A. (2011b) 'An investigation of the impacts of climate change on wave energy generation: The Wave Hub, Cornwall, UK'. *Renewable Energy*, 36 (9). pp 2404-2413.

Roelvink, D., Reniers, A., van Dongeren, A., van Thiel de Vries, J., McCall, R. & Lescinski, J. (2009) 'Modelling storm impacts on beaches, dunes and barrier islands'. *Coastal Engineering*, 56 (11–12). pp 1133-1152.

Roelvink, J., Reniers, A., Van Dongeren, A., Van Thiel de Vries, J., Lescinski, J. & McCall, R. (2006) 'XBeach model description and manual'.[in UNESCO-IHE Institute for Water Education. (Accessed:Roelvink, J., Reniers, A., Van Dongeren, A., Van Thiel de Vries, J., Lescinski, J. & McCall, R.

Ruehl, K., Porter, A., Posner, A. & Roberts, J. (2013) 'Development of SNL-SWAN, a Validated Wave Energy Converter Array Modeling Tool'.[in EWTEC. (Accessed:Ruehl, K., Porter, A., Posner, A. & Roberts, J.

Ruol, P., Zanuttigh, B., Martinelli, L., Kofoed, P. & Frigaard, P. (2011) 'Near-shore floating wave energy converters: applications for coastal protection'. *Proceedings of the international conference of Coastal Engineering 2010*. Shanghai. Available at: http://journals.tdl.org/icce/index.php/icce/article/view/1419.

Rusu, E. & Guedes Soares, C. (2013) 'Coastal impact induced by a Pelamis wave farm operating in the Portuguese nearshore'. *Renewable Energy*, 58 (0). pp 34-49.

Rusu, L. & Guedes Soares, C. (2012) 'Wave energy assessments in the Azores islands'. *Renewable Energy*, 45 (0). pp 183-196.

Scott, T., Masselink, G. & Russell, P. (2011) 'Morphodynamic characteristics and classification of beaches in England and Wales'. *Marine Geology*, 286 (1–4). pp 1-20.

Scott, T., Russell, P., Masselink, G., Wooler, A. & Short, A. (2007) 'Beach rescue statistics and their relation to nearshore morphology and hazards: a case study for southwest England'. *Journal of Coastal Research*, 50 pp 1-6.

Scott, T., Russell, P., Masselink, G., Wooler, A. & Short, A. (2008) 'High volume sediment transport and its implications for recreational beach risk', *Proceedings 31st International Conference on Coastal Engineering. ASCE, Hamburg, Germany*. World Scientific, pp. 4250-4262.

Senechal, N., Coco, G., Castelle, B. & Marieu, V. (2015) 'Storm impact on the seasonal shoreline dynamics of a meso- to macrotidal open sandy beach (Biscarrosse, France)'. *Geomorphology*, 228 (0). pp 448-461.

Sibley, A., Cox, D. & Titley, H. (2015) 'Coastal flooding in England and Wales from Atlantic and North Sea storms during the 2013/2014 winter'. *Weather*, 70 (2). pp 62-70.

Slingo, J., Belcher, S., Scaife, A., McCarthy, M., Saulter, A., McBeath, K., Jenkins, A., Huntingford, C., Marsh, T. & Hannaford, J. (2014) 'The recent storms and floods in the UK'.

Smith, H., Millar, D. & Reeve, D. (2007) 'Generalisation of wave farm impact assessment on inshore wave climate', *Proceedings of the 7th European Wave and Tidal Energy Conference*.

Smith, H. C. M., Pearce, C. & Millar, D. L. (2010) 'Further analysis of change in nearshore wave climate due to an offshore wave farm: An enhanced case study for the Wave Hub site'. *Renewable Energy*, 40 (1). pp 51-64.

Smith, H. C. M., Pearce, C. & Millar, D. L. (2012) 'Further analysis of change in nearshore wave climate due to an offshore wave farm: An enhanced case study for the Wave Hub site'. *Renewable Energy*, 40 (1). pp 51-64.

Spencer, T., Brooks, S. M., Evans, B. R., Tempest, J. A. & Möller, I. (2015) 'Southern North Sea storm surge event of 5 December 2013: Water levels, waves and coastal impacts'. *Earth-Science Reviews*, 146 (0). pp 120-145.

Splinter, K. D., Carley, J. T., Golshani, A. & Tomlinson, R. (2014) 'A relationship to describe the cumulative impact of storm clusters on beach erosion'. *Coastal Engineering*, 83 (0). pp 49-55.

Stocker, T., Qin, D., Plattner, G.-K., Tignor, M., Allen, S. K., Boschung, J., Nauels, A., Xia, Y., Bex, V. & Midgley, P. M. (2014) *Climate change 2013: The physical science basis.* Cambridge University Press Cambridge, UK, and New York.

Stopa, J. E., Cheung, K. F. & Chen, Y.-L. (2011) 'Assessment of wave energy resources in Hawaii'. *Renewable Energy*, 36 (2). pp 554-567.

Storlazzi, C. D. & Griggs, G. B. (2000) 'Influence of El Niño–Southern Oscillation (ENSO) events on the evolution of central California's shoreline'. *Geological Society of America Bulletin*, 112 (2). pp 236-249.

Stoutenburg, E. D., Jenkins, N. & Jacobson, M. Z. (2010) 'Power output variations of co-located offshore wind turbines and wave energy converters in California'. *Renewable Energy*, 35 (12). pp 2781-2791.

Stratigaki, V., Troch, P., Stallard, T., Forehand, D., Kofoed, J. P., Folley, M., Benoit, M., Babarit, A. & Kirkegaard, J. (2014) 'Wave Basin Experiments with Large Wave Energy Converter Arrays to Study Interactions between the Converters and Effects on Other Users in the Sea and the Coastal Area'. *Energies*, 7 (2). pp 701-734.

SWAN (2007) 'SWAN technical documentation'. *Delft University of Technology. The Netherlands*,

Tedd, J. & Kofoed, J. P. (2009) 'Measurements of overtopping flow time series on the Wave Dragon, wave energy converter'. *Renewable Energy*, 34 (3). pp 711-717.

The Crown State (2013) *UK Wave and Tidal: Key Resource Areas Project.* Available.

Thorpe, T. W. (1999) *A brief review of wave energy.* Harwell Laboratory, Energy Technology Support Unit.

Tolman, H. (2002a) 'Validation of WAVEWATCH III version 1.15 for a global domain'. *Technical Note*, (213). pp 33.

Tolman, H. L. (2002b) 'User manual and system documentation of WAVEWATCH-III version 2.22'.

Twidell, J. (2005) *Renewable energy resources.* Taylor & Francis.

US Army Corps Of Engineers (1984) 'Shore protection manual'. *Army Engineer Waterways Experiment Station, Vicksburg, MS. 2v*, pp 37-53.

Van Dongeren, A. R., Battjes, J. & Svendsen, I. (2003) 'Numerical modeling of infragravity wave response during DELILAH'. *Journal of Geophysical Research*, 108 (C9). pp 3288.

van Nieuwkoop, J. C., Smith, H. C., Smith, G. H. & Johanning, L. (2013) 'Wave resource assessment along the Cornish coast (UK) from a 23-year hindcast dataset validated against buoy measurements'. *Renewable Energy*, 58 pp 1-14.

Van Thiel de Vries, J. (2009) *Dune erosion during storm surges*. PhD Thesis. Delft University of Technology.

Veigas, M. & Iglesias, G. (2013) 'Wave and offshore wind potential for the island of Tenerife'. *Energy Conversion and Management*, 76 (0). pp 738-745.

Veigas, M., López, M. & Iglesias, G. (2014) 'Assessing the optimal location for a shoreline wave energy converter'. *Applied Energy*, 132 (0). pp 404-411.

Venugopal, V. & Smith, G. (2007) 'Wave climate investigation for an array of wave power devices'. *Proceedings of the 7th European Wave and Tidal Energy Conference, Porto, Portugal*, pp 11-14.

Verbrugghe, T., Devolder, B., Troch, P. & Kortenhaus, A. (2016) 'Numerical modelling of wave energy converters', *VLIZ Marine Scientist Day*. pp. 130-130.

Vicinanza, D., Contestabile, P. & Ferrante, V. (2013) 'Wave energy potential in the north-west of Sardinia (Italy)'. *Renewable Energy*, 50 pp 506-521.

Vidal, C., Méndez Fernando, J., Díaz, G. & Legaz, R. (2007) 'Impact of Santoña WEC installation on the littoral processes'. *Proceedings of the 7th European wave and tidal energy conference, Porto, Portugal*,

Watknis, D. (2014) 'The winter storms of 2014: How Cornwall fared'. *Cornwall Community Flood Forum*.

Wave Dragon AS (2005) 'Wave Dragon web page'.

Wright, L. & Short, A. D. (1984) 'Morphodynamic variability of surf zones and beaches: a synthesis'. *Marine Geology*, 56 (1). pp 93-118.

Zanuttigh, B. & Angelelli, E. (2013) 'Experimental investigation of floating wave energy converters for coastal protection purpose'. *Coastal Engineering*, 80 pp 148-159.

Zijlema, M. (2010) 'Computation of wind-wave spectra in coastal waters with SWAN on unstructured grids'. *Coastal Engineering*, 57 (3). pp 267-277.

Appendix I

First author journal papers

Coastal Engineering 86 (2014) 36–44

Contents lists available at ScienceDirect

Coastal Engineering

journal homepage: www.elsevier.com/locate/coastaleng

Wave farm impact on the beach profile: A case study

J. Abanades *, D. Greaves, G. Iglesias

Plymouth University, School of Marine Science and Engineering, Marine Building, Drake Circus, Plymouth PL4 8AA, UK

ARTICLE INFO

Article history:
Received 13 June 2013
Received in revised form 10 January 2014
Accepted 13 January 2014
Available online 14 February 2014

Keywords:
Wave energy
Wave farm
Wave Energy Converter
Nearshore impact
Beach profile
Erosion

ABSTRACT

If wave energy is to become a fully-fledged renewable, its environmental impacts must be fully understood. The objective of the present work is to examine the impact of a wave farm on the beach profile through a case study. The methodology is based on two coupled numerical models: a nearshore wave propagation model and a morphodynamic model, which are run in two scenarios, both with and without the wave farm. Wave data from a nearby coastal buoy are used to prescribe the boundary conditions. A positive effect on the wave climate, the cross-shore sediment transport and, consequently, the evolution of the beach profile itself due to the presence of the wave farm was found. The wave farm leads to a reduction in the erosion of the beach face. This work constitutes the first stage of the investigation of the effectiveness of a wave farm as a coastal defence measure, and the accuracy of the quantification of the erosion reduction will be enhanced in future research. In any case, the overarching picture that emerges is that wave farms, in addition to providing carbon-free energy, can be used as elements of a coastal defence scheme.

1. Introduction

Marine renewable energy and, in particular, wave energy is called to play a major role in achieving the renewable energy targets of the European Union for 2020 — the so-called 20-20-20 targets (European Commission, 2007). Among other advantages, wave energy boasts one of the highest energy densities of the renewable energy sector (Clément et al., 2002). At present, the main research areas in wave energy are: (i) the characterisation of the resource (Cornett, 2008; Iglesias and Carballo, 2009, 2010, 2011; Pontes et al., 1996; Vicinanza et al., 2013); (ii) the development of the technology (Falcão, 2007; Falcão and Justino, 1999; Kofoed et al., 2006); and, finally (iii) the environmental impact of wave farms, including the impact on the physical environment with which this work is concerned.

Knowledge of the impacts, positive or negative, is important for the development of the different types of marine energy because an Environmental Impact Assessment (EIA) is required for any such project. In the case of wave energy, the studies so far have dealt with the impact of a wave farm on the wave conditions in its lee. As waves propagate through the wave farm, their height is reduced according to an energy transmission coefficient. This coefficient depends on the performance of the Wave Energy Converters (WECs) selected. Millar et al. (2007) used SWAN (Booij et al., 1999), a phase-averaged spectral model, to quantify the impact on the wave climate and the shoreline changes for the Wave Hub project (UK). Notional values of the transmission coefficient (0, 40, 70 and 90%) were used due to the lack of information about the performance of the WECs at the time. In the same vein, Palha et al. (2010) used the parabolic mid slope wave model REFDIF to perform a sensitivity analysis to study the impact on the shoreline using different layouts for the wave farm; and Vidal et al. (2007) studied the impact of a small wave farm on the wave climate and the nearshore sediment transport.

Another line of work used physical modelling to investigate the wave–WEC interaction. Carballo and Iglesias (2013) studied the modification of the nearshore wave climate using values of the energy transmission coefficient obtained from ad hoc physical model tests of a WaveCat WEC (Iglesias et al., 2008). Taking into account of these values, a sensitivity analysis was performed with different layouts of the wave farm to assess its impact on the nearshore wave conditions. Mendoza et al. (in press) compared the impact of two wave farms with different WECs on the coastline. The results showed that a wave farm nearshore could produce accretion to some extent in some sections of the beach. In this context, Ruol et al. (2011), Nørgaard et al. (2011) and Zanuttigh and Angelelli (2013) put forward the idea of using a wave farm for shore protection based on the reduction of the nearshore wave height caused by the wave farm.

If a wave farm is to be used for the purpose of coastal protection, it is essential to understand its impact on the beach profile — an aspect of great practical relevance that has not been investigated so far. This is the main objective of the present work, which is conducted through a case study: Perranporth Beach.

Perranporth Beach is a 3 km sandy beach located in Cornwall, SW England (Fig. 1). Composed of medium quartz sand (Austin et al., 2010), it has a semi-diurnal tidal regime and a tidal range of 6.3 m (macrotidal). The area has a great potential for wave energy (Thorpe, 2001); indeed, it was selected as the site for the Wave Hub Project, a grid-connected offshore facility for sea trials of WECs (Gonzalez et al.,

* Corresponding author.
E-mail address: Javier.abanadestercero@plymouth.ac.uk (J. Abanades).

0378-3839/$ – see front matter © 2014 Elsevier B.V. All rights reserved.
http://dx.doi.org/10.1016/j.coastaleng.2014.01.008

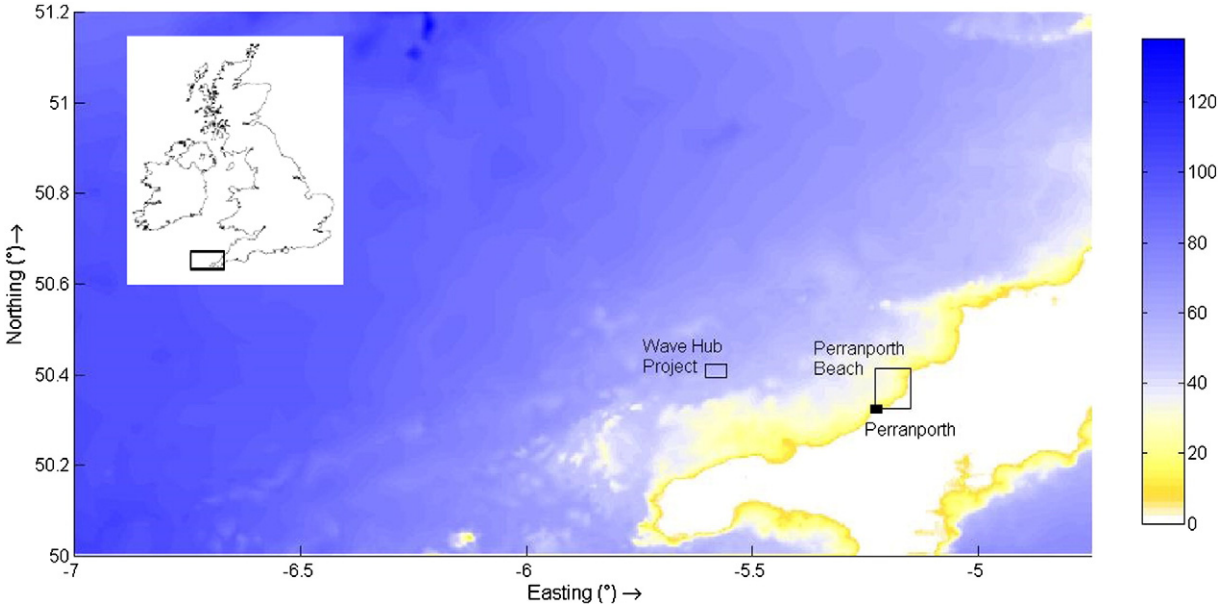

Fig. 1. Bathymetry of SW England including the location of Perranporth Beach and the WaveHub Project [water depths in m].

2012; Reeve et al., 2011). The study covered the period from November 2007 to May 2008, corresponding to the part of the annual cycle with the highest frequency of storms based on the onsite wave buoy data (Section 2.1). This time scale allows the assessment of the morphological changes in beaches, such as scarp formation, profile erosion and accretion, and bar evolution (Cowell and Thom, 1994).

Wave propagation was simulated using SWAN and the beach profile evolution with XBeach, a numerical model of nearshore processes (Roelvink et al., 2006). XBeach was successfully applied in a number of studies to describe the behaviour of beach profiles. Roelvink et al. (2009) assessed the beach erosion due to storms and McCall et al. (2010) focussed on the impact caused by hurricanes. Other authors, such as Jamal et al. (2011) and Williams et al. (2012), used XBeach to investigate gravel beaches. More recently, Pender and Karunarathna (2012, 2013) demonstrated that XBeach is capable of modelling the medium-term evolution of the beach profile of a sandy beach. Their results showed a good fit to the measured profiles after each storm period. On these grounds, XBeach is used in the present work to compare the evolution of the beach profile with and without the presence of a wave farm situated close to Perranporth Beach.

This article is structured as follows. In Section 2, the main characteristics of the data sets – which include wave, wind, tide and beach profile data – are presented, and the models are briefly described. This is followed by Section 3, in which the results describing the impact of the wave farm on the wave conditions and the evolution of the beach profiles are presented and discussed. Finally, in Section 4, conclusions are drawn concerning the effects of a wave farm on the beach profile and, on these grounds, its applicability for coastal protection purposes.

2. Materials and methods

2.1. Data

The wave data used for this study were hindcast and onsite wave buoy data. The directional wave buoy of the Coastal Channel Observatory located in front of Perranporth beach (Fig. 2), in approximately 10 m of water depth with reference to the local chart datum (LCD), provided half-hourly data. The wave buoy data were used in conjunction with hindcast data from WaveWatch III, a third-generation offshore wave model consisting of global and regional nested grids with a resolution

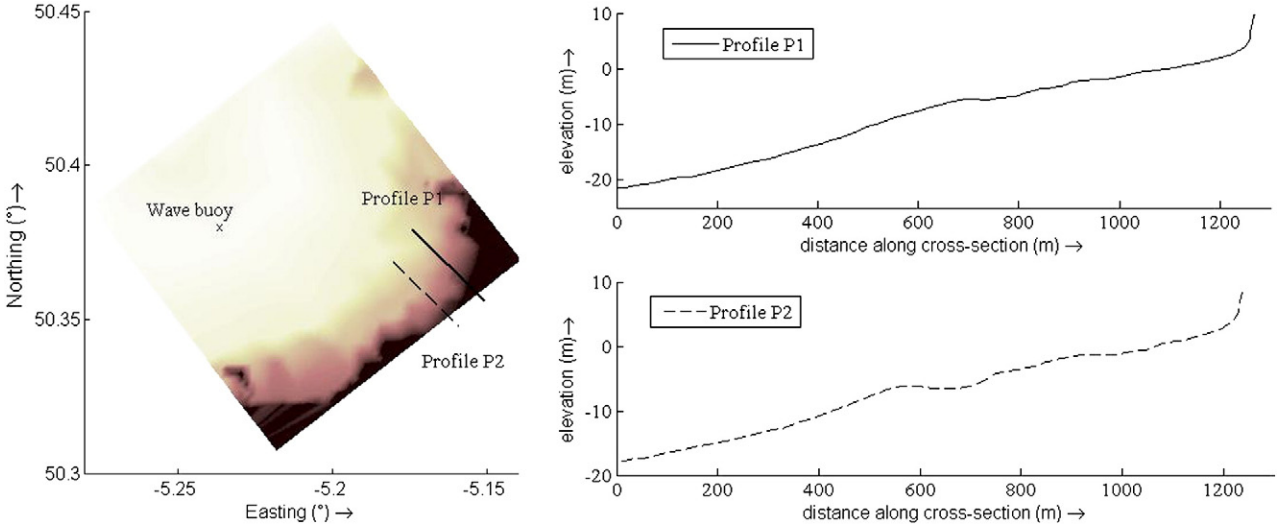

Fig. 2. Initial beach profiles (P1 and P2) including their location and the position of the wave buoy. Water depth in relation to local chart datum.

of 100 km (Tolman, 2002), to validate the high-resolution nearshore wave propagation model. In the period selected for the study, from November 2007 to April 2008, a number of storms with significant wave heights over 6 m occurred (Fig. 5). The mean values of significant wave height, H_s, and peak wave period, T_p, were 2.4 m and 13 s, respectively. Given the orientation of the coastline and its exposure to the long Atlantic fetch, the relevant wave direction is from the IV quarter (from W to N), prevailing NW.

Wind data with a three-hourly frequency obtained from the Global Forecast System (GFS) weather model were used as input of the wave model. In the period covered in the study the mean wind velocity magnitude at a height of 10 m above the sea surface was $u_{10} = 9.5\ \mathrm{ms}^{-1}$. The strongest winds came from the NW, with u_{10} values exceeding $20\ \mathrm{ms}^{-1}$.

The SW coast of England is characterised by a large tidal range, which may affect the beach morphodynamics. For this reason, the tide was included into the morphodynamic model with constituents obtained from the TPXO 7.2 global database, a global model of ocean tides that solves the Laplace equations using data from tide gauges and the TOPEX/Poseidon Satellite (Egbert et al., 1994).

The beach profiles were obtained through field survey by the Coastal Channel Observatory. The initial profiles (Fig. 2), typical of the end of summer at Perranporth Beach, are associated with less energetic wave conditions. The beach profile evolution is characterised during the summer by an increase of the sediment transport onshore. In contrast, offshore movement of sediment is the predominant phenomenon during the winter owing to the more energetic wave conditions, which results in a lowering of the intertidal beach face. Indeed, most of the profile change at Perranporth Beach occurs in the lower intertidal to sub-tidal active regions (Scott et al., 2011).

2.2. Wave propagation model

The assessment of the wave height reduction on the shore due to the wave farm was carried out using SWAN (Simulating WAves Nearshore), a third-generation numerical wave model developed to model nearshore wave climate transformations. SWAN computes the evolution of the wave spectrum based on the spectral wave action balance equation,

$$\frac{\partial N}{\partial t} + \nabla \cdot \left(\vec{C} N\right) + \frac{\partial (C_\theta N)}{\partial \theta} + \frac{\partial (C_\sigma N)}{\partial \sigma} = \frac{S}{\sigma} \tag{1}$$

where N is the wave action density, t the time, $\vec{C}$ the propagation velocity in the geographical space, θ the wave direction, σ the relative frequency, and C_θ and C_σ the propagation velocity in the θ- and σ-space, respectively. Therefore, on the left-hand side of Eq. (1), the first term represents the rate of change of wave action in time, the second term describes the spatial propagation of wave action, and the third and fourth terms stand for the refraction and changes in the relative frequencies respectively induced by depth and currents. Finally, on the right-hand side, S is the source term representing the generation and dissipation of energy density by the different processes involved.

In the present study two computational grids were used (Fig 3): (i) a coarse grid from offshore to the coast encompassing an area of approx. 100 km × 50 km with a resolution of 400 m × 200 m; and (ii) a fine, nested grid focussed on Perranporth Beach, covering an area of approx. 15 km × 15 km with a resolution of 20 m × 20 m. The high resolution of the nested grid is allowed in defining the position of the WECs in the array and simulates their individual wakes with accuracy. This is a prerequisite to a detailed assessment of the wave farm effects on the beach profile (Carballo and Iglesias, 2013). The bathymetric data, from the UK data centre Digimap, were interpolated onto this grid.

To study the effects of wave energy exploitation on the beach profile an array of 11 WaveCat WECs arranged in two rows was considered. With the same layout as in Carballo and Iglesias (2013), the array was located in a water depth of 35–40 m (Fig. 4). The distance between devices was $2.2D$, where $D = 90$ m is the distance between the twin bows of a single WaveCat WEC. Finally, the wave transmission coefficient of the WECs, obtained from the laboratory tests carried out by Fernandez et al. (2012), was input into the coastal propagation model. Based on the results of these tests, which showed a very small variability in the wave transmission coefficient (with the exception of an outlier), the value $K_t = 0.76$ was adopted. This constitutes an approximation in that the tests carried out by Fernandez et al. (2012) did not cover all the wave conditions simulated in the present work; in future work, as more experimental data on WEC behaviour become available, this approximation will be refined.

2.3. Morphodynamic model

The input conditions to XBeach were obtained from the output of the SWAN wave propagation model. XBeach is a two-dimensional model for wave propagation, long waves and mean flow, sediment transport and morphological changes of the nearshore area, beaches, dunes and back barrier during storms. XBeach concurrently solves the time-dependent short wave action balance, the roller energy equations, the nonlinear shallow water equations of mass and momentum, sediment transport formulations and bed update on the scale of wave groups (Roelvink et al., 2006).

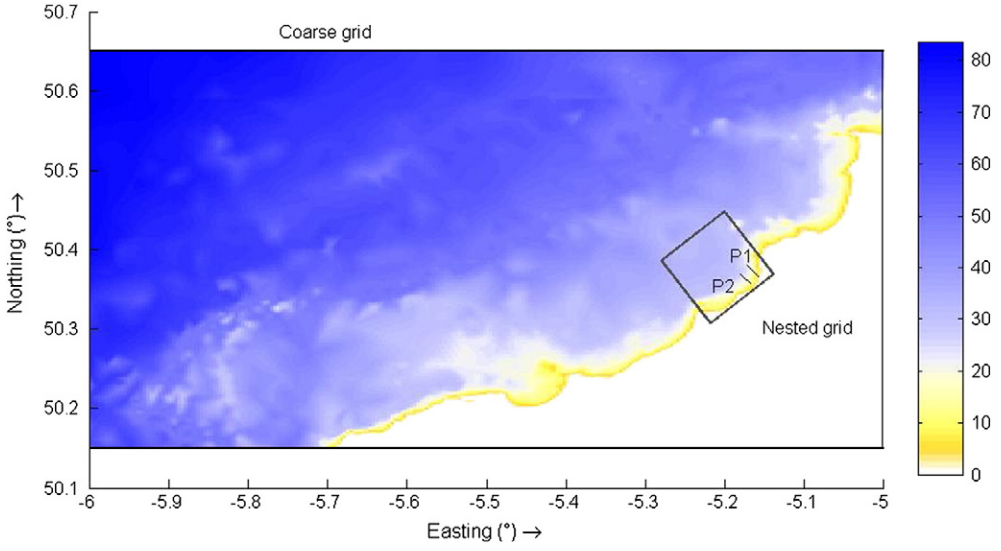

Fig. 3. Computational grids of the wave propagation model [water depths in m]. Profiles P1 and P2 are shown.

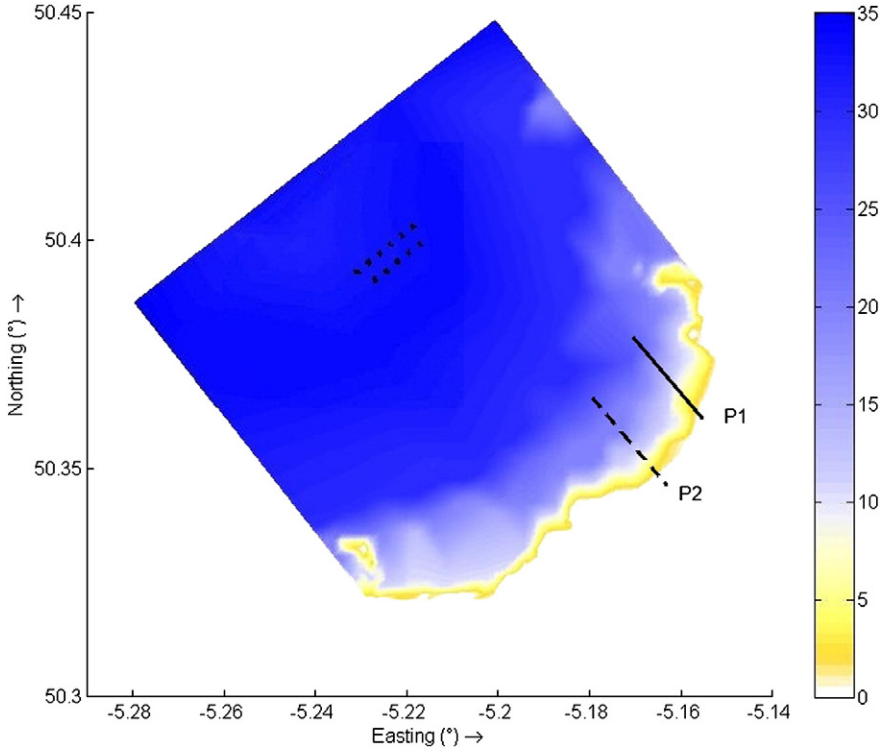

Fig. 4. Schematic of wave farm considered off Perranporth Beach, at a distance of approx. 7 km from the shoreline [water depths in m]. Profiles P1 and P2 are shown.

The sediment transport is modelled with a depth-averaged advection diffusion equation (Galappatti and Vreugdenhil, 1985). The equation is:

$$\frac{\partial(hC)}{\partial t}+\frac{\partial\left(hCu^E\right)}{\partial x}+\frac{\partial}{\partial x}\left(D_s h\frac{\partial C}{\partial x}\right)+\frac{\partial\left(hCv^E\right)}{\partial y}+\frac{\partial}{\partial y}\left(D_s h\frac{\partial C}{\partial y}\right)=\frac{hC_{eq}-hC}{T_S} \quad (2)$$

where C represents the depth-averaged sediment concentration, which varies on the wave-group time scale, D_s is the sediment diffusion coefficient, the terms u^E and v^E represent the Eulerian flow velocities, T_s is the sediment concentration adaptation time scale that depends on the local water depth and the sediment fall velocity, and C_{eq} is the equilibrium concentration, thus representing the source term in the sediment transport equation. The sediment transport formula defined by Van Thiel de Vries (2009) was used to determine the sediment equilibrium concentration.

In the present study, the model was applied in 1DH mode (x, z) to simulate the beach profile evolution. From the results of the nearshore wave propagation model, spectra with a frequency of 6 h were obtained with and without the wave farm to compare the impact on the coast. These spectra were the input of the morphodynamic model, which provided beach profile results every 6 min to compare the evolution of the profile in both cases.

A varying grid size was employed in the morphodynamic model: the resolution was defined as a function of the water depth and the offshore wave conditions, and subjected to the grid size smoothness constraints. On these grounds, the Courant condition was applied to find the optimal grid size. The optimised grid was coarser in high water depths and finer in the intertidal zone, where a size of 1 m was adopted so as to accurately characterise the evolution of the profile.

Finally, to describe properly the behaviour of the beach, the time series of wave data was broken down into a number of segments. These segments were grouped into two types, Type A (Accretion) and Type E (Erosion), depending on the values of the wave parameters and the consequent nature of the beach profile changes, either accretionary or erosionary. Type A, associated with calm conditions, was set with a stationary constant wave energy distribution, based on given values of root mean square wave height (H_{rms}), mean absolute wave period (T_{m01}), mean wave direction (θ_m) and directional spreading coefficient (s), obtained from the nearshore wave propagation model. Type E, associated with storm periods, used the parametric spectra as input to create time-varying wave amplitudes, i.e., the envelopes of wave groups (Van Dongeren et al., 2003). The difference in approach between the two categories is the way that wave groups were treated. Type A segments included wave groups, as they are important to describe the behaviour of the beach during erosion conditions. In contrast, wave groups were not taken into account in Type E segments because this would result in an overestimation of erosion (Baldock et al., 2010).

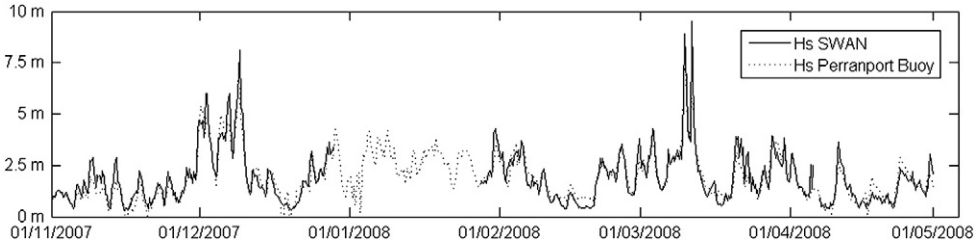

Fig. 5. Time series of simulated (*Hs, SWAN*) and measured (*Hs, buoy*) significant wave height.

2.4. Assessment of the impact of the wave farm on the beach profile

To quantify the impact of the wave farm on the beach profile the following parameters were defined: the Bed Level Impact (*BLI*), the eroded area in the baseline scenario (*A*), the eroded area in the presence of the farm (A_f), and the Erosion Impact (*EI*) index.

The Bed Level Impact (*BLI*, in m) was defined as

$$BLI(x) = \zeta_f(x) - \zeta(x), \tag{3}$$

where x is the horizontal coordinate along the profile, $\zeta_f(x)$ is the bed level in the presence of the farm, and $\zeta(x)$ is the bed level in the baseline scenario. The *BLI* index represents the change in the bed level drop due to the shelter afforded by the wave farm.

For their part, the eroded area in the baseline scenario (A, in m^3 per linear metre of beach) and the eroded area in presence of the farm (A_f, in m^3 per linear metre of beach) were defined as

$$A = \int_{x_0}^{x_{max}} [\zeta_0(x) - \zeta(x)]dx, \tag{4}$$

$$A_f = \int_{x_0}^{x_{max}} \left[\zeta_0(x) - \zeta_f(x)\right]dx, \tag{5}$$

where $\zeta_0(x)$ is the initial bed level and x_{max} and x_0 are the limits of integration, with x_{max} the maximum value of the x coordinate (which corresponds to the landward end of the profile) and x_0 the value corresponding to a bed level of 0, i.e., $\zeta(x_0) = 0$.

Finally, the Erosion Impact (*EI*, *in %*) index was defined as

$$EI = \frac{1}{(x_{max} - x_0)} \int_{x_0}^{x_{max}} \left[\zeta_f(x) - \zeta(x)\right][\zeta_0(x) - \zeta(x)]^{-1}dx. \tag{6}$$

EI index is a dimensionless parameter that represents the reduction of the eroded area brought about by the wave farm as a fraction of the total eroded area.

3. Results and discussion

3.1. Wave propagation model

The results obtained from the nearshore wave propagation model were validated with the wave buoy data during the period from November to December 2007 and February to April 2008 owing to the lack of data during January. A very good fit was achieved between the simulated and measured time series (Figs. 5 and 6). This is further confirmed by the error statistics: $RMSE = 0.46$ *m* and $R^2 = 0.84$ (with *RMSE* the Root Mean Square Error and R^2 the coefficient of determination).

Having validated the numerical model, it was used to compare the wave patterns with and without the wave farm and to determine the wave conditions that were used as input to the morphodynamic model. As an example of the effects of the wave farm on the wave patterns, the wave propagation corresponding to the peak of a storm on 10 March 2008 is shown in Fig. 7. The deep water wave conditions were: significant wave height, $H_{s0} = 10.01$ m; peak wave period, $T_p = 15.12$ s; and peak wave direction, $\theta_p = 296.38°$. A substantial decrease of the significant wave height, exceeding 30% along the wakes of the WECs, is apparent in the more detailed graph of the wave farm area (Fig. 8). This decrease is less marked on the beach itself. In the northern section of the beach the reduction of wave height is more pronounced than elsewhere owing to the deep water wave direction (approx. WNW).

The average reduction of the wave energy flux, *J*, during the period studied at different points along the 10 m contour is shown in Table 1. The areas most sheltered by the wave farm are the middle and, especially, the northern sections of the beach. On these grounds two profiles in the northern and middle sections of Perranporth Beach were selected for the analysis of the impacts of the wave farm (Fig. 2).

3.2. Morphodynamic model

The impact of the wave power reduction on the beach was studied through the evolution of the two profiles of Perranporth Beach. This was carried out using the spectra generated by the wave propagation model with and without the wave farm in the morphodynamic model. The series were split, as explained in Section 2.3, to describe suitably

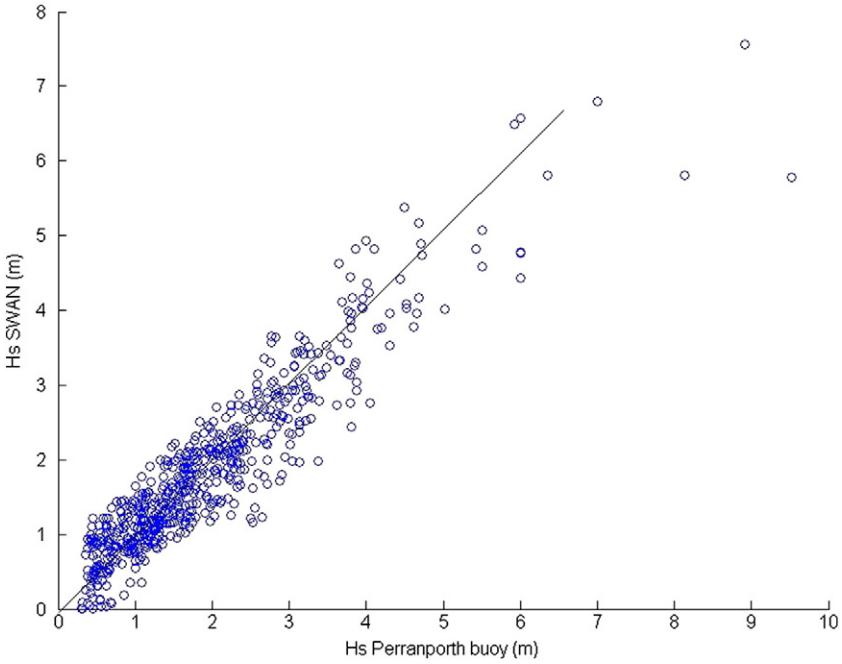

Fig. 6. Scatter diagram: simulated (*Hs, SWAN*) vs. measured (*Hs, buoy*) significant wave height.

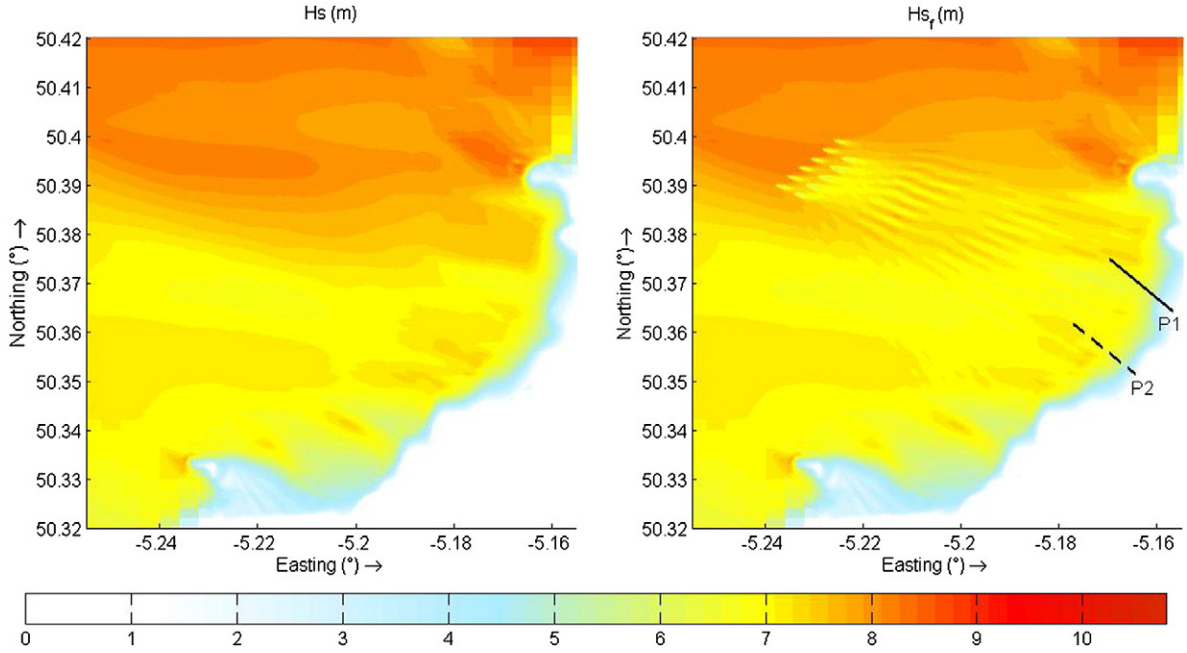

Fig. 7. Significant wave height in the baseline scenario (*Hs*) and in the presence of the farm (*Hsf*) at the peak of a storm (10 Mar 2008, 18:00 UTC) [deep water wave conditions: $H_{s0} =$ 10.01 m, $T_p =$ 15.12 s, $\theta_p =$ 296.38°]. Profiles P1 and P2 are shown.

the behaviour of the beach in different periods. The results showed that type E segments are mainly responsible for the erosion of the profiles.

Fig. 9 shows the evolution of the initial Profiles 1 (P1) and 2 (P2) after a storm. The graph compares the initial beach profiles with those after three months of operation of the wave farm. Both graphs illustrate that the erosion of the profiles is concentrated mainly in the beach face, which is the section of the profile exposed to wave uprush. The eroded material is moved to a lower section of the profile.

To better visualise the effect of wave energy extraction, the situation of profile P2 with and without the farm is shown in Fig. 10. The reduction of the wave energy flux at the beach leads to a substantial reduction (of the order of 3 m) in the erosion of the dune delineating the landward limit of the beach.

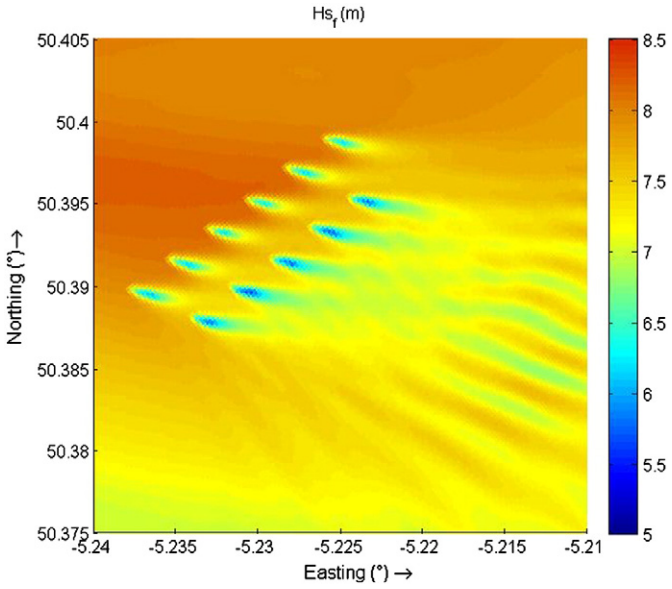

Fig. 8. Significant wave height (*Hsf*) within the wave farm at the peak of a storm (10 Mar 2008, 18:00 UTC) [deep water wave conditions: $H_{s0} =$ 10.01 m, $T_p =$ 15.12 s, $\theta_p =$ 296.38°].

The impact of the wave farm on the beach profile was analysed through the parameters defined in Section 2.4. The *BLI* parameter along Profiles P1 and P2 is illustrated in Fig. 11 for three different points in time: 1 month (*M1*), 3 months (*M3*) and 6 months (*M6*) after the beginning of the study period. The results for both profiles show a significant reduction of the erosion in the beach face and in the bar (around $x =$ 600 m). The bar forms part of the response mechanism of the natural system to protect the beach face from increased wave attack. Fig. 11 proves that the effect of the wave farm is a reinforcement of the bar, and therefore enhanced protection for the beach face in storms. Advancing in time, the *BLI* values increase in the bar area, i.e., the aforementioned effect is intensified.

As regards the beach face, the *BLI* values for both profiles are also significant and show that the wave farm reduces the erosion. This is nowhere more apparent than on the dune at the landward end of the profile, where *BLI* values exceed 1 m. Table 2 shows the values of the eroded areas at the beach face at the same points in time as in Fig. 11. It is observed for both profiles and especially in Profile P1 that the erosion is higher at the first two points in time (*M1* and *M3*) than at the last one, which is associated with less energetic conditions (Fig. 5). Further, the *EI* values confirm the significant reduction in the erosion owing to the presence of the wave farm. It is also noted that the effect of the wave farm is more significant in the north of the beach (Profile P1) than in the middle of the beach (Profile P2), as may be seen in Table 1.

The results showed a significant reduction of the erosion along Profiles P1 and P2, which may indicate some degree of coastal protection owing to the presence of the wave farm nearshore. The present work was framed as the first step in the assessment of the impact of wave farms on the beach profile – a relevant aspect for the development of

Table 1
Significant wave height reduction (ΔH_s) and wave power reduction (ΔJ) caused by the wave farm at different points along the 10 m contour.

Beach Point	Coordinates		ΔH_s (%)	ΔJ (%)
	Easting (°)	Northing (°)		
North	−5.17	50.36	3.26	13.25
Middle	−5.18	50.35	1.75	7.90
South	−5.21	50.34	0.70	0.93

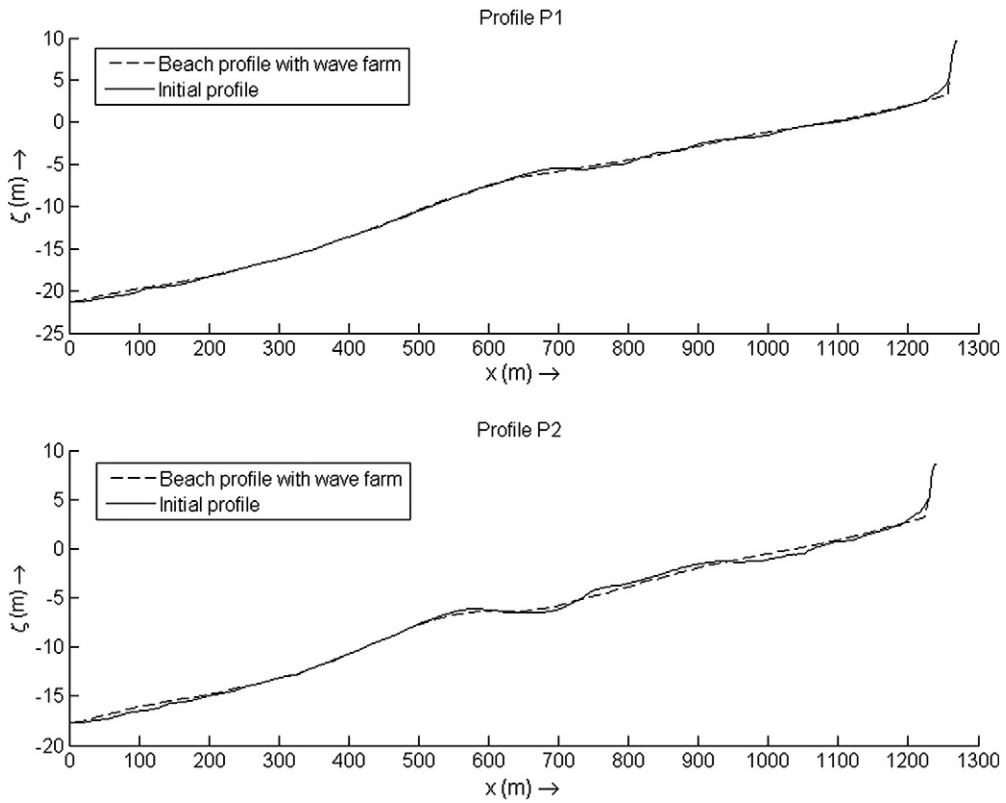

Fig. 9. Bed level at Profile P1 and P2: initial [1 Nov 2007, 0000 UTC] and after three months with and the wave farm [22 Jan 2008, 15:47 UTC].

wave energy, and one which was not investigated to date – and the accuracy of its results will likely be enhanced in future research.

4. Conclusions

In this paper, the impact of a wave farm consisting of 11 WaveCat WECs on the beach profile was investigated through a case study. This is the first study focussed on the effect of wave energy on the beach profile evolution. A high-resolution nearshore wave propagation model was coupled to a morphodynamic model to assess the wave farm impacts over a medium-term period.

First, to study the effect of the wave farm a high-resolution grid was employed on Perranporth beach to describe properly the interaction of the wave farm and the sea. The transmission coefficient of the WEC employed was obtained through laboratory tests.

It was found that the wave farm effect varies in the different areas of the beach, affecting, in particular, the northern section of the beach and reducing its wave energy flux up to 12%. This extraction of energy modifies the coastal processes in the nearshore.

Second, a morphodynamic model was employed to investigate the impact of the wave energy extraction. Two profiles were studied, the first in the north of the beach and the second in the middle. The impact of the wave energy exploitation on the profiles was analysed through several parameters. These allowed the assessment of the impact of the wave farm on the bed level and the eroded area compared to the baseline scenario. The Bed Level Impact (*BLI*) parameter showed a substantial effect on the bar and on the beach face. *BLI* values exceeded 1 m at some points in time. Concerning the Erosion Impact (*EI*) parameter, the reduction of the eroded area reached values of up to 35% at the first points in time (*M1* and *M3*) and 21% at the last (*M6*) in the north

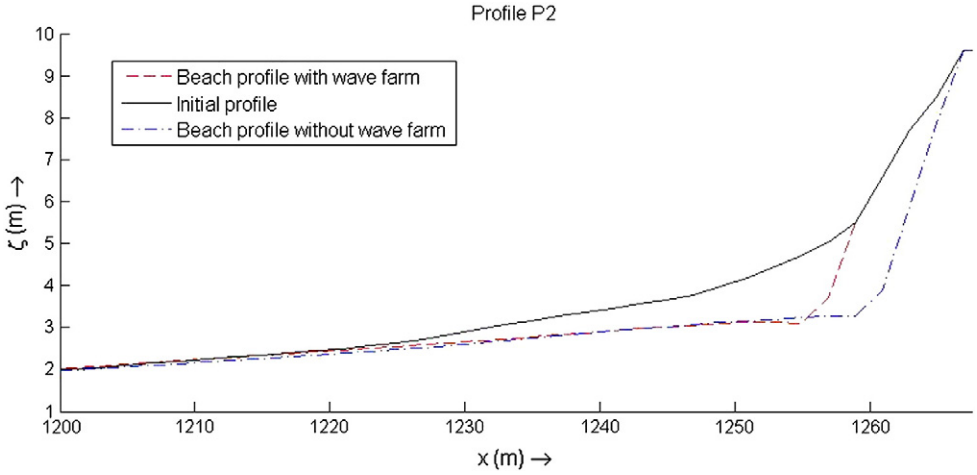

Fig. 10. Beach face level at Profile P2: initial [1 Nov 2007, 0000 UTC] and after three months with and without the wave farm [22 Jan 2008, 15:47 UTC].

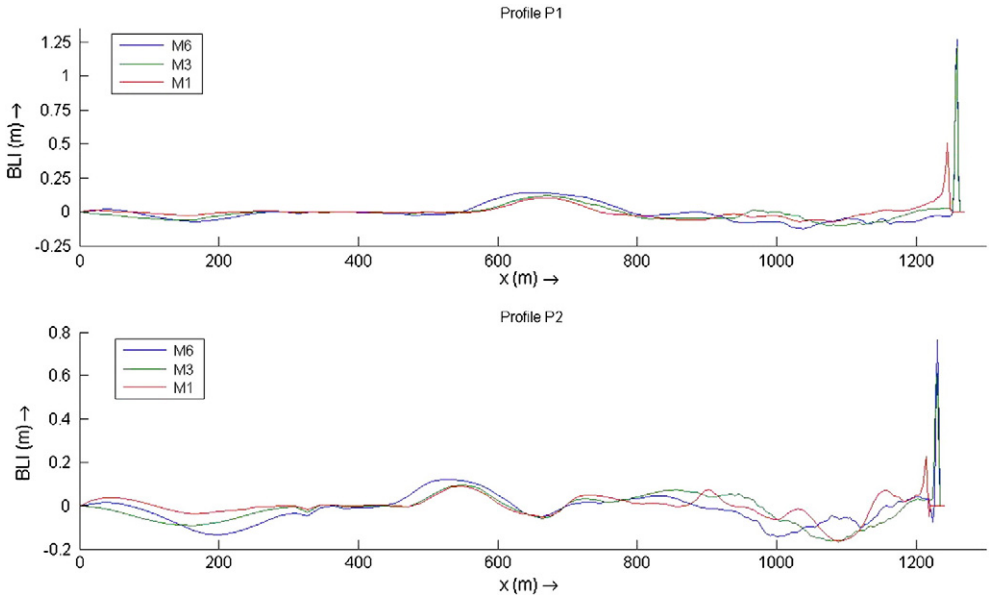

Fig. 11. Evolution of *BLI* along Profiles P1 and P2 at different points in time: 1 month (*M1*), 3 months (*M3*) and 6 months (*M6*) after the beginning of the study period.

Table 2
Eroded area in the baseline scenario (A), in the presence of the farm (A_f), and Erosion Impact (EI) index for Profiles P1 and P2 at different points in time: 1 month (*M1*), 3 months (*M3*) and 6 months (*M6*) after the beginning of the study period.

Profiles	*M1*			*M3*			*M6*		
	A	A_f	EI	A	A_f	EI	A	A_f	EI
Profile P1	20.53	14.11	31.27	16.3	10.42	36.07	23.85	18.66	21.76
Profile P2	15.69	12.91	17.72	21.31	16.85	20.93	25.53	21.42	16.10

of the beach. In the middle of the beach the reduction was lower, reaching values up to 20% at the first points in time (*M1* and *M3*) and 16% at the end of the period studied (*M6*).

This substantial reduction in the erosion of the profiles constitutes an added benefit of the wave farm. This is corroborated by the results of the present work, which dealt with the impacts of a relatively small, hypothetical wave farm (with 11 WECs distributed in an area of 1.5 km^2); despite its size, the wave farm was shown to have a significant effect in reducing the erosion of the beach face. This effect would likely be even more significant in the case of a larger wave farm.

In conclusion, a wave farm can be considered a *green* alternative to conventional forms of coastal protection, in the sense that it provides not only some degree of coastal protection but also *green* (carbon-free) energy. This synergy enhances the viability of wave farms.

Acknowledgments

This research was carried out in the framework of the Atlantic Power Cluster Project, funded by the Atlantic Arc Programme of the European Commission. The authors are grateful to the Coastal Channel Observatory and DIGIMAP for providing the data.

References

Austin, M., et al., 2010. Temporal observations of rip current circulation on a macro-tidal beach. Cont. Shelf Res. 30 (9), 1149–1165.
Baldock, T.E., Manoonvoravong, P., Pham, K.S., 2010. Sediment transport and beach morphodynamics induced by free long waves, bound long waves and wave groups. Coast. Eng. 57 (10), 898–916.
Booij, N., Ris, R.C., Holthuijsen, L.H., 1999. A third-generation wave model for coastal regions: 1. Model description and validation. J. Geophys. Res. Oceans 104 (C4), 7649–7666.
Carballo, R., Iglesias, G., 2013. Wave farm impact based on realistic wave–WEC interaction. Energy 51, 216–229.
Clément, A., et al., 2002. Wave energy in Europe: current status and perspectives. Renew. Sust. Energ. Rev. 6 (5), 405–431.
Cornett, A.M., 2008. A Global Wave Energy Resource, Assessment. ISOPE–579.
Cowell, P., Thom, B., 1994. Morphodynamics of Coastal Evolution. Cambridge University Press, Cambridge, United Kingdom and New York, NY, USA.
Egbert, G.D., Bennett, A.F., Foreman, M.G., 1994. Topex/poseidon tides estimated using a global inverse model. J. Geophys. Res. Oceans (1978–2012) 99 (C12), 24821–24852.
European Commission, 2007. A European Strategic Energy Technology Plan (Set-Plan) — Towards a Low-Carbon Future. Communication from the Commission to the Council, the European Parliament, the European Economic and Social Committee and the Committee of the Regions, COM.
Falcão, A.F.O., 2007. Modelling and control of oscillating-body wave energy converters with hydraulic power take-off and gas accumulator. Ocean Eng. 34 (14–15), 2021–2032.
Falcão, A.F.O., Justino, P.A.P., 1999. Owc wave energy devices with air flow control. Ocean Eng. 26 (12), 1275–1295.
Fernandez, H., et al., 2012. The new wave energy converter wavecat: concept and laboratory tests. Mar. Struct. 29 (1), 58–70.
Galappatti, G., Vreugdenhil, C., 1985. A depth-integrated model for suspended sediment transport. J. Hydraul. Res. 23 (4), 359–377.
Gonzalez, R., Zou, Q., Pan, S., 2012. Modelling of the Impact of a Wave Farm on Nearshore Sediment Transport. Proceedings of the international conference of Coastal Engineering 2012.
Iglesias, G., Carballo, R., 2009. Wave energy potential along the death coast (Spain). Energy 34 (11), 1963–1975.
Iglesias, G., Carballo, R., 2010. Offshore and inshore wave energy assessment: Asturias (n Spain). Energy 35 (5), 1964–1972.
Iglesias, G., Carballo, R., 2011. Choosing the site for the first wave farm in a region: a case study in the Galician southwest (Spain). Energy 36 (9), 5525–5531.
Iglesias, G., Carballo, R., Castro, A., Fraga, B., 2008. Development and design of the wavecat ™ energy converter. Coast. Eng. 3970–3982.
Jamal, M.H., Simmonds, D.J., Magar, V., Pan, S., 2011. Modelling infiltration on gravel beaches with an xbeach variant. Proc. Int. Conf. Coastal Eng. 1 (32), 41 (sediment).
Kofoed, J.P., Frigaard, P., Friis-Madsen, E., Sørensen, H.C., 2006. Prototype testing of the wave energy converter wave dragon. Renew. Energy 31 (2), 181–189.
McCall, R.T., et al., 2010. Two-dimensional time dependent hurricane overwash and erosion modeling at Santa Rosa Island. Coast. Eng. 57 (7), 668–683.
Mendoza, E., et al., 2013. Beach response to wave energy converter farms acting as coastal defence. Coast. Eng. http://dx.doi.org/10.1016/j.coastaleng.2013.10.018 (in press).
Millar, D.L., Smith, H.C.M., Reeve, D.E., 2007. Modelling analysis of the sensitivity of shoreline change to a wave farm. Ocean Eng. 34 (5–6), 884–901.
Nørgaard, J.H., Andersen, T.L., Kofoed, J.P., 2011. Wave Dragon Wave Energy Converters Used as Coastal Protection, Proceedings of the International Conference of Coastal Structures 2011. Imperial College Press, Yokohama.
Palha, A., Mendes, L., Fortes, C.J., Brito-Melo, A., Sarmento, A., 2010. The impact of wave energy farms in the shoreline wave climate: Portuguese pilot zone case study using pelamis energy wave devices. Renew. Energy 35 (1), 62–77.
Pender, D., Karunarathna, H., 2012. Modeling Beach Profile Evolution — A Statistical-Process Based Approach.
Pender, D., Karunarathna, H., 2013. A statistical-process based approach for modelling beach profile variability. Coast. Eng. 81, 19–29.
Pontes, M., et al., 1996. Weratlas-Atlas of Wave Energy Resource in Europe. Report to the European Commission. JOULE II Programme (96 pp.).

Reeve, D.E., et al., 2011. An investigation of the impacts of climate change on wave energy generation: the wave hub, cornwall, UK. Renew. Energy 36 (9), 2404–2413.
Roelvink, J., et al., 2006. Xbeach Model Description and Manual. UNESCO-IHE Institute for Water Education.
Roelvink, D., et al., 2009. Modelling storm impacts on beaches, dunes and barrier islands. Coast. Eng. 56 (11–12), 1133–1152.
Ruol, P., Zanuttigh, B., Martinelli, L., Kofoed, P., Frigaard, P., 2011. Near-Shore Floating Wave Energy Converters: Applications for Coastal Protection. Proceedings of the international conference of Coastal Engineering 2010, Shanghai.
Scott, T., Masselink, G., Russell, P., 2011. Morphodynamic characteristics and classification of beaches in England and Wales. Mar. Geol. 286 (1–4), 1–20.
Thorpe, T., 2001. The Wave Energy Programme in the UK and the European Wave Energy Network.
Tolman, H.L., 2002. User Manual and System Documentation of Wavewatch-III Version 2.22.
Van Dongeren, A.R., Battjes, J., Svendsen, I., 2003. Numerical modeling of infragravity wave response during delilah. J. Geophys. Res. 108 (C9), 3288.
Van Thiel de Vries, J., 2009. Dune Erosion during Storm Surges. (PhD Thesis) Delft University of Technology.
Vicinanza, D., Contestabile, P., Ferrante, V., 2013. Wave energy potential in the north-west of Sardinia (Italy). Renew. Energy 50, 506–521.
Vidal, C., Méndez Fernando, J., Díaz, G., Legaz, R., 2007. Impact of Santoña WEC Installation on the Littoral Processes. Proceedings of the 7th European wave and tidal energy conference, Porto, Portugal.
Williams, J.J., de Alegría-Arzaburu, A.R., McCall, R.T., Van Dongeren, A., 2012. Modelling gravel barrier profile response to combined waves and tides using xbeach: laboratory and field results. Coast. Eng. 63, 62–80.
Zanuttigh, B., Angelelli, E., 2013. Experimental investigation of floating wave energy converters for coastal protection purpose. Coast. Eng. 80, 148–159.

Coastal Engineering 91 (2014) 299–307

Contents lists available at ScienceDirect

Coastal Engineering

journal homepage: www.elsevier.com/locate/coastaleng

Coastal defence through wave farms

J. Abanades *, D. Greaves, G. Iglesias

Plymouth University, School of Marine Science and Engineering, Marine Building, Drake Circus, Plymouth PL4 8AA, UK

ARTICLE INFO

Article history:
Received 4 April 2014
Received in revised form 25 June 2014
Accepted 26 June 2014
Available online xxxx

Keywords:
Wave energy
Wave farm
Erosion
Nearshore impact
SWAN
XBeach

ABSTRACT

The possibility of using wave farms for coastal defence warrants investigation because wave energy is poised to become a major renewable in many countries over the next decades. The fundamental question in this regard is whether a wave farm can be used to reduce beach erosion under storm conditions. If the answer to this question is positive, then a wave farm can have coastal defence as a subsidiary function, in addition to its primary role of producing carbon-free energy. The objective of this work is to address this question by comparing the response of a beach in the face of a storm in two scenarios: with and without the wave farm. For this comparison a set of ad hoc impact indicators is developed: the bed level impact (*BLI*), beach face eroded area (*FEA*), non-dimensional erosion reduction (*NER*), and mean cumulative eroded area (*CEA*); and their values are determined by means of two coupled models: a high-resolution wave propagation model (SWAN) and a coastal processes model (XBeach). The study is conducted through a case study: Perranporth Beach (UK). Backed by a well-developed dune system, Perranporth has a bar between −5 m and −10 m. The results show that the wave farm reduces the eroded volume by as much as 50% and thus contributes effectively to coastal protection. This synergy between marine renewable energy and coastal defence may well contribute to improving the viability of wave farms through savings in conventional coastal protection.

1. Introduction

A wave farm extracts energy from the waves through Wave Energy Converters (WECs). The previous studies on the impact of wave farms on wave conditions (Beels et al., 2010; Iglesias and Carballo, 2014; Mendoza et al., 2013; Millar et al., 2007; Monk et al., 2013; Palha et al., 2010; Ruol et al., 2011; Rusu and Guedes Soares, 2013; Zanuttigh and Angelelli, 2013) demonstrated a significant reduction in the wave height in the lee of the wave farm. A sensitivity analysis of this reduction with different wave farm layouts was conducted by Carballo and Iglesias (2013). Abanades et al. (2014) studied the effects of the energy extraction by the wave farm on the beach profile (2D), analysing the evolution of several profiles during 6 months. This paper goes a step further by transcending the cross-shore (2D) analysis and examining the impact of wave energy exploitation on beach morphology (3D) — an aspect that has not been addressed so far, and whose importance can hardly be overstated in view of the intensive development of this novel renewable.

In this context, this work has a threefold objective: (i) to compare the response of a beach under storm conditions with and without a wave farm through a case study; (ii) to assess whether the nearshore attenuation of wave energy caused by the wave farm results in a reduction in the erosion on the beach; and, on these grounds, (iii) to establish whether a wave farm can contribute to coastal protection.

For the case study, a high-resolution wave propagation model coupled to a 2DH coastal processes model was applied in an area earmarked for wave energy development (Perranporth Beach, UK). First, the nearshore wave propagation model SWAN (Booij et al., 1996) was implemented on a high-resolution grid to resolve wave propagation past an array of WECs. The values of the wave transmission coefficients were obtained from laboratory tests (Fernandez et al., 2012). Second, the coastal processes model XBeach (Roelvink et al., 2006) was used to study the effect of the nearshore wave energy reduction on beach morphology. The suitability of XBeach to model storm impact on beaches has been proven in the recent work (Callaghan et al., 2013; McCall et al., 2010; Pender and Karunarathna, 2013; Roelvink et al., 2009; Splinter et al., 2014). In this paper the response of the beach under storm conditions was examined in two scenarios: without (baseline) and with the wave farm. Finally, to analyse the results, a new suite of core impact indicators was developed and applied.

This article is structured as follows: in Section 2, the case study and data set are presented. In Section 3, the models and impact factors are described. In Section 4, the results are analysed and discussed. Finally, conclusions are drawn in Section 5.

2. Case study: Perranporth Beach

The impact of wave energy exploitation on the beach was carried out through a case study. The wave resource played a major role in

* Corresponding author. Tel.: +44 7583544041.
E-mail address: Javier.abanadestercero@plymouth.ac.uk (J. Abanades).

http://dx.doi.org/10.1016/j.coastaleng.2014.06.009
0378-3839/

the selection of the study site. A number of wave resource assessments, conducted at different scales and areas (Bernhoff et al., 2006; Defne et al., 2009; Gonçalves et al., 2014; Iglesias and Carballo, 2009; 2010a; 2010b; 2011; Pontes et al., 1998; Rusu and Guedes Soares, 2012; Stopa et al., 2011; Thorpe, 2001; Vicinanza et al., 2013), highlighted the resource in the Atlantic façade of Europe. For the present study, Perranporth Beach (Fig. 1) was selected; the nearby Wave Hub – a grid-connected offshore facility for sea tests of WECs – is testimony to the potential of this area for wave energy exploitation (Gonzalez-Santamaria et al., 2013; Reeve et al., 2011). Perranporth (Austin et al., 2010; Masselink et al., 2005) is a 4 km beach with a relatively flat intertidal area, tan $\beta = 0.015–0.025$, and a medium sand size, $D_{50} = 0.27–0.29$ mm. The tidal range is 6.3 m (macro-tidal beach) and the tidal regime is semidiurnal.

As regards the wave climate, Perranporth is exposed to the Atlantic swell, and also receives locally generated wind waves. The average significant wave height (H_s), peak period (T_p) and peak direction (θ_p) from 2006 to 2012 (the available data) were: 1.79 m, 10.36 s and 280°, respectively. During the storm studied, from 5 December 2007 UTC 00:00 to 10 December 2007 UTC 06:00, the average wave conditions were: $H_s = 4.2$ m, $T_p = 12.1$ s and $\theta_p = 295°$.

The bathymetry of the beach was based on the data provided by the Coastal Channel Observatory. The elevation values ranged between −20 m and 25 m (Fig. 2) with reference to the local chart datum (LCD). A conspicuous feature of the profile is the submarine bar between −5 m and −10 m, which will be shown to be of relevance to the dynamics of the system. The bar is generally associated with the more energetic (winter) wave conditions and the consequent increase of offshore sediment transport, which results in a lowering of the intertidal beach face. Another feature of Perranporth Beach is the well-developed dune system (Fig. 10).

3. Materials and methods

3.1. Wave propagation model

The wave propagation was computed using the SWAN v40.41 (Simulating WAves Nearshore), a third-generation spectral wave model that

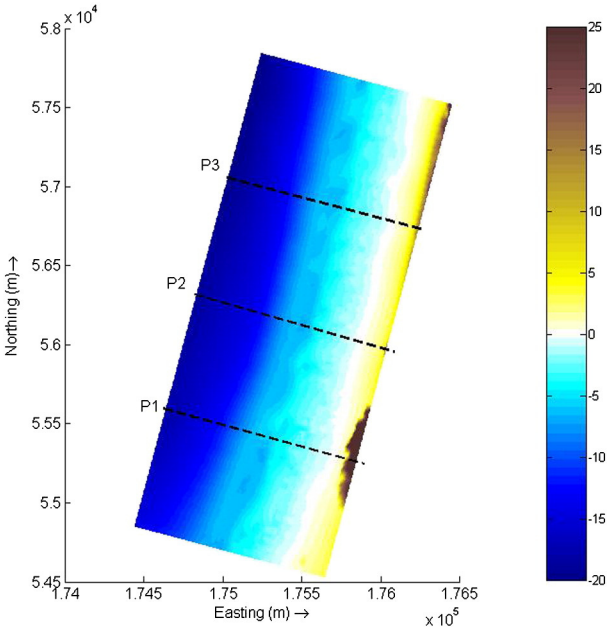

Fig. 2. Bathymetry of Perranporth Beach for the coastal processes model. Profiles P1, P2 and P3 included. Water depth in relation to local chart datum [in m].

solves the conservation of wave action equation considering the relevant wave generation and dissipation processes,

$$\frac{\partial N}{\partial t} + \nabla \cdot \left(\vec{C} N\right) + \frac{\partial (C_\theta N)}{\partial \theta} + \frac{\partial (C_\sigma N)}{\partial \sigma} = \frac{S}{\sigma} \quad , \tag{1}$$

where t is the time, N is the wave action density, $\vec{C}$ is the propagation velocity in the geographical space, θ is the wave direction, σ is the relative frequency, and C_θ and C_σ are the propagation velocity in the spectral space, θ- and σ-space, respectively. Therefore, the first term on the left-hand side of Eq. (1) represents the rate of change of wave action in time, the second term describes the propagation in the geographical space, and the third and fourth terms stand for the refraction and changes in

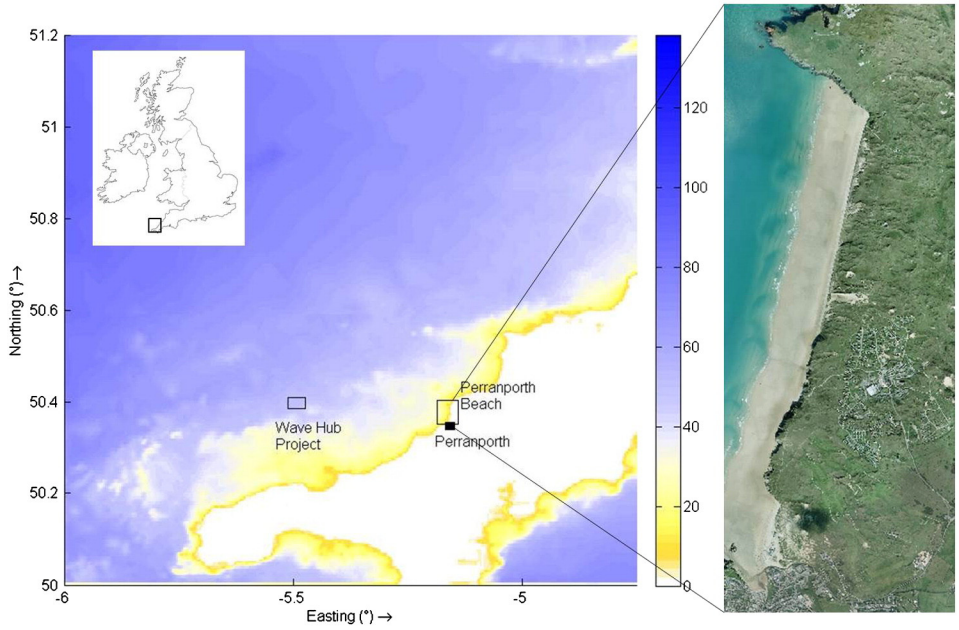

Fig. 1. Bathymetry of SW England [water depths in m] including the location of Perranporth Beach, the WaveHub Project and an aerial photo of Perranporth Beach. Source: Coastal Channel Observatory.

the relative frequencies respectively induced by depth and currents. On the right-hand side, S is the source term representing the effects of generation, dissipation, and nonlinear wave–wave interactions.

The model was validated using data from a wave buoy at Perranporth Beach covering the period November 2007 to April 2008. The input conditions implemented in the SWAN model were: (i) the hindcast wave data from WaveWatchIII (Tolman, 2002), a third-generation offshore wave model consisting of global and regional nested grids with a resolution of approx. 100 km; and (ii) the hindcast wind data from Global Forecast System (GFS), a global numerical weather prediction system.

The computational grid consisted of two grids with different spacings (Fig. 3): (i) the coarser grid extended approx. 100 km offshore and 50 km from north to south with a grid size of 400 × 200 m, respectively; and (ii) the finer (nested) grid covered the area of interest of approx. 15 × 15 km, with a resolution of 20 × 20 m, which allowed the exact position of the WECs to be defined within the array and the individual wake of each device to be resolved accurately. The energy transmission coefficient of the devices was input into the coastal propagation based on ad hoc laboratory tests (Fernandez et al., 2012). The wave farm layout was consisted of 11 WaveCat WECs arranged in two rows (Fig. 4), with a distance between devices of 2.2D, where $D = 90$ m is the distance between the twin bows of a single WaveCat WEC (Carballo and Iglesias, 2013).

3.2. Coastal processes model

Second, the coastal processes model, XBeach v1.20.3606, was coupled to the wave propagation model. XBeach is a two-dimensional model to study wave propagation, sediment transport and morphological changes of the coast. Wave processes are solved with the time-dependent wave action balance equation coupled to the roller energy equations and the nonlinear shallow water equations of mass and momentum and sediment transport are modelled with a depth-averaged advection diffusion equation (Galappatti and Vreugdenhil, 1985) on the scale of wave groups (Eq. (2)). The complete description of XBeach is given by Roelvink et al. (2006) or Roelvink et al. (2009).

$$\frac{\partial(hC)}{\partial t}+\frac{\partial\left(hCu^{E}\right)}{\partial x}+\frac{\partial}{\partial x}\left(D_s h\frac{\partial C}{\partial x}\right)+\frac{\partial\left(hCv^{E}\right)}{\partial y}+\frac{\partial}{\partial y}\left(D_s h\frac{\partial C}{\partial y}\right)=\frac{hC_{eq}-hC}{T_s} \tag{2}$$

where the x- and y-coordinate represent the cross-shore and longshore direction, respectively, C is the depth-averaged sediment concentration,

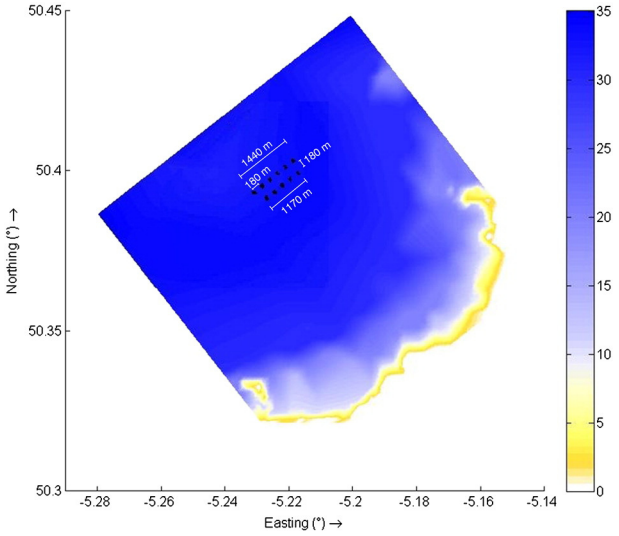

Fig. 4. Schematic of wave farm considered off Perranporth Beach, at a distance of approx. 7 km from the shoreline [water depths in m].

D_s is the sediment diffusion coefficient, the terms u^E and v^E represent the Eulerian flow velocities, T_s is the sediment concentration adaptation time scale that depends on the local water depth and the sediment fall velocity, and C_{eq} is the equilibrium concentration according to the Van Rijn–Van Thiel formulation (Van Thiel de Vries, 2009), thus representing the source term in the sediment transport equation.

In the present study, the model was applied in a 2DH mode (x, y, z) to study the impact of the wave farm on Perranporth Beach using the results of the wave propagation model. The response of the beach during the storm period studied was investigated in both scenarios: (i) in the baseline scenario (without the wave farm), and (ii) with the wave farm, to compare the evolution of the beach and establish the contribution of a wave farm to protect the coast.

The grid covered Perranporth Beach, extending 1250 m across shore and 3600 m alongshore with a resolution of 6.25 m and 18 m, respectively. The model used a number of spectral parameters obtained from the nearshore wave propagation model (the root-mean-square wave height, H_{rms}, mean absolute wave period, T_{m01}, mean wave direction, θ_m, and directional spreading coefficient, s) as input to create time-varying wave amplitudes, i.e., the envelopes of wave groups, which have crucial importance in describing the behaviour of a beach during erosion conditions (Baldock et al., 2011).

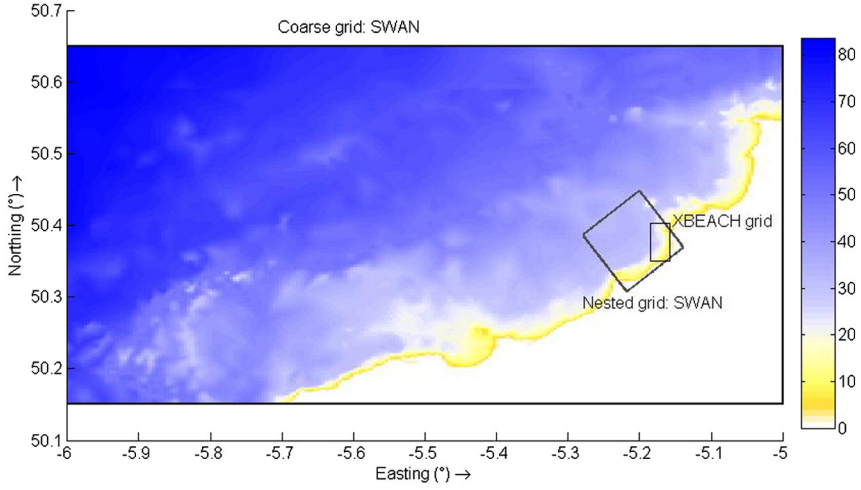

Fig. 3. Computational grids of the wave propagation and the coastal processes model [water depths in m].

3.3. Impact indicators

The importance of monitoring and controlling coastal erosion is reflected in the number of projects delving on these matters, such as CONSCIENCE and EUROSION. In these projects, different groups of impact indicators were proposed to assess the erosion during the medium- and long-term in pilot sites. On these grounds, and taking into account the specific needs of this work, a suite of impact indicators was developed ad hoc to analyse the effects of the wave farm on the beach and establish the corresponding degree of coastal protection: (i) bed level impact (*BLI*), (ii) each face eroded area (*FEA*), (iii) non-dimensional erosion reduction (*NER*), and (iv) mean cumulative eroded area (*CEA*).

The bed level impact (*BLI*), with units of m in the S.I., was defined as

$$BLI(x,y) = \zeta_f(x,y) - \zeta_b(x,y), \tag{3}$$

where $\zeta_f(x,y)$ and $\zeta_b(x,y)$ are the seabed levels with the farm and without it (baseline), respectively, at a generic point of the beach designated by its coordinates (x,y) in the horizontal reference plane. With this definition the datum for the seabed level (the elevation of the reference plane) is arbitrary, for it is the difference between the values of seabed level with and without the farm rather than their absolute values that determine the *BLI* indicator, Eq. (3). Within the reference horizontal plane the y-coordinate axis follows the general coastline orientation, with the y-coordinate increasing towards the northern end of the beach. A beach profile is defined as a section of the beach with $y =$ constant, and a particular point of the profile is defined by its x-coordinate; the orientation of the x-axis is taken such that x-values increase towards the landward end of the profile. The *BLI* indicator thus defined represents the change in bed level caused by the wave farm. A positive value signifies that the seabed level is higher with the farm than without it.

The beach face eroded area (*FEA*), with units of m^2 in the S.I., was defined in both scenarios, baseline (FEA_b) and with the wave farm (FEA_f):

$$FEA_b(y) = \int_{x_1}^{x_{\max}} [\zeta_0(x,y) - \zeta_b(x,y)]\,dx, \tag{4}$$

$$FEA_f(y) = \int_{x_1}^{x_{\max}} \left[\zeta_0(x,y) - \zeta_f(x,y)\right] dx, \tag{5}$$

where $\zeta_0(x,y)$ is the initial bed level at the point of coordinates (x,y), and x_1 and x_{max} are the values of the x-coordinate at the seaward end of the beach face and landward end of the profile, respectively. It should be noted that, unlike the bed level impact, which is a point function and therefore depends on two coordinates, $BLI = BLI(x,y)$, the beach face eroded area is a profile function, and hence depends on only one coordinate, $FEA = FEA(y)$. The *FEA* indicator can be seen as a (dimensional) parameter measuring the impact of the farm on the beach face.

The non-dimensional erosion reduction (*NER*) is also a profile function, in this case non-dimensional, defined as

$$NER(y) = 1 - (x_{\max} - x_1)^{-1} \int_{x_1}^{x_{\max}} \left[\zeta_0(x,y) - \zeta_f(x,y)\right] [\zeta_0(x,y) - \zeta_b(x,y)]^{-1} dx. \tag{6}$$

It expresses the variation in the eroded area of a generic profile (y) brought about by the wave farm as a fraction of the total eroded area of the same profile. A positive or negative value implies a reduction or increase in the eroded area as a result of the wave farm.

Finally, the mean cumulative eroded area (*CEA*), with units of m^2 (or m^3 per linear metre of beach), was determined both in the baseline scenario (CEA_b) and with the wave farm (CEA_f). For its definition three reference profiles were considered: P1, P2 and P3 (Fig. 2). For each of these the beach was divided into two parts, to the north (CEA_b^N and CEA_f^N) and south (CEA_b^S and CEA_f^S) of the reference profile, and the corresponding indicators were computed from

$$CEA_b^S(x) = (y_P - y_0)^{-1} \int_{y_0}^{y_P} \int_{x_0}^{x} [\zeta_0(\chi,y) - \zeta_b(\chi,y)]\,d\chi\,dy, \tag{7}$$

$$CEA_f^S(x) = (y_P - y_0)^{-1} \int_{y_0}^{y_P} \int_{x_0}^{x} \left[\zeta_0(\chi,y) - \zeta_f(\chi,y)\right] d\chi\,dy \tag{8}$$

$$CEA_b^N(x) = (y_{\max} - y_P)^{-1} \int_{y_P}^{y_{\max}} \int_{x_0}^{x} [\zeta_0(\chi,y) - \zeta_b(\chi,y)]\,d\chi\,dy, \tag{9}$$

$$CEA_f^N(x) = (y_{\max} - y_P)^{-1} \int_{y_P}^{y_{\max}} \int_{x_0}^{x} \left[\zeta_0(\chi,y) - \zeta_f(\chi,y)\right] d\chi\,dy, \tag{10}$$

where the variable of integration χ represents the coordinate along the profile, and x and x_0, and y_0, y_{max} and y_P are the limits of integration along the profile and along the coast, respectively. x_0 is the value of the x-coordinate corresponding to the first point of the profile and x takes values from x_0 to x_{max}. Along the beach, y_0 is the value of the y-coordinate corresponding to the southernmost point of the beach, y_{max} the northernmost point of the beach and y_P the value corresponding to the reference profile. The factor represents the average cumulative eroded area of the two sections of the beach along the profile (x). A positive value signifies that the mean volume of material along the section of the beach is reduced compared with the initial situation (erosion).

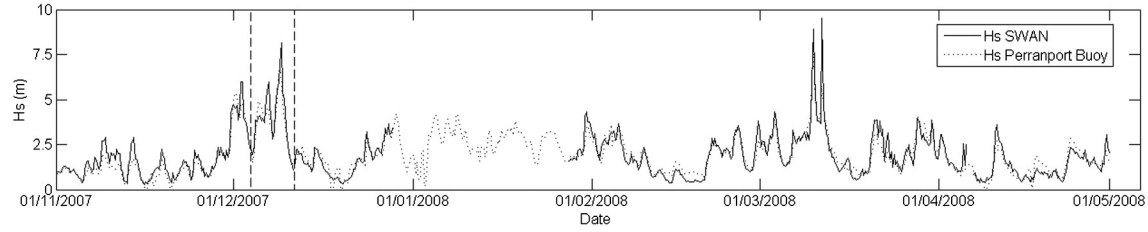

Fig. 5. Time series of simulated (H_s, *SWAN*) and measured (H_s, *buoy*) significant wave height to validate the high resolution wave propagation model. The storm conditions studied (from 5 Dec 2007, 00:00 UTC; to 10 Dec 2007, 18:00 UTC) to assess the impact of the wave farm are highlighted.

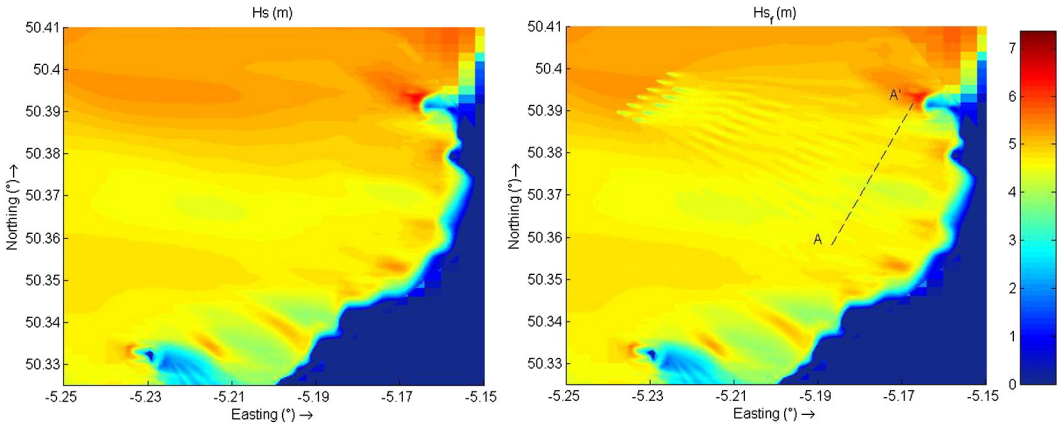

Fig. 6. Significant wave height in the baseline scenario (H_s) and with the wave farm (H_{sf}) at the first peak of the storm studied (5 Dec 2007, 18:00 UTC). [Deep water wave conditions: $H_{s0} = 6.89$ m, $T_p = 15.64$ s, $\theta_p = 268.45°$]. The line AA′ is shown.

4. Results and discussion

The validation of the high-resolution wave propagation model was carried out using the significant wave height (H_s) values from the wave buoy at Perranporth Beach from November 2007 to April 2008 (Abanades et al., 2014). Fig. 5 shows the good fit achieved by the model. The error statistics studied for the validation confirmed that the correlation between the series achieves a Root Mean Square Error (*RMSE*) of 0.46 m and a coefficient of determination (R^2) of 0.84.

The results of the wave propagation model were studied in both scenarios: baseline and in the presence of the wave farm, to observe the impact of the wave farm on the wave conditions. The reduction of the significant wave height in the lee of the farm is shown in Fig. 6, in which the shadow zone downstream of each WEC is apparent.

Using this data, Fig. 7 shows the reduction of the significant wave height between the scenario in the presence of the farm and the baseline scenario. The reduction within the wave farm was greater than 30%, although advancing towards the coastline from the wave farm, the difference decreased due to the wave energy being diffracted from the edges into the shadow of the farm. However, this energy was not enough to mitigate the effect of the wave farm nearshore; indeed the reduction was greater than 10% along the 20 m contour in the northern area of the grid, which was the area most sheltered by the wave farm.

Having investigated the effects of the wave farm on the wave conditions in its lee, the results along the line AA′ (Fig. 6), in approximately 20 m of water depth, were input to the coastal processes model. The significant wave height (H_s) across AA′ in both scenarios is shown in Fig. 8, where the shadow due to the wave energy absorption of each device can be readily observed. The impact of the wave farm was found to be more significant in the northern and middle areas of the beach.

The coastal processes model used the output of the wave propagation model to study how modification of the wave conditions affected the coastal processes and, consequently, the beach morphology during the period studied. The longshore and offshore/onshore sediment transport was studied through a suite of core impact indicators, defined in Section 3.2, to assess the impact of the wave farm.

The sea bed level was studied at the end of the time period studied in both scenarios: in the presence of the farm and in the baseline scenario, through the BLI factor (Fig. 9). The reduction of the erosion was observed mainly in the dune in the back of the beach, reaching values greater than 4 m, a result of the wave energy extraction by the wave farm. A reduction of the erosion was also found along the bar in water depth between 5 and 10 m, especially in the middle area of the beach where the *BLI* parameter reached values of 0.5 m. On the other hand, the material eroded from the dune was moved to the lower section of the profile, between the bar and the dune, which resulted in the *BLI* parameter taking negative values in the region of −0.5 m.

On this basis, the impact of the wave farm on the bed level is shown in Fig. 10 along three profiles: P1 (south), P2 (middle) and P3 (north), shown in Fig. 2. The initial profile (ζ_0) was compared with the profiles at the end of the storm studied in both scenarios: the baseline scenario (ζ_b) and in the presence of the farm (ζ_f). The results show a more significant effect on profiles P3 and P2, in the northern and middle areas of the beach, than on P1, in accordance with the wave conditions shown in Fig. 8. As may be observed in Fig. 9, the effects of the wave farm are

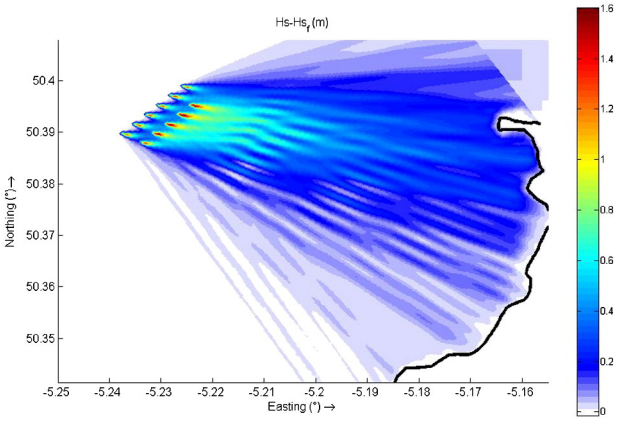

Fig. 7. Significant wave height difference between the baseline scenario (H_s) and with the wave farm (H_{sf}) at the first peak of the storm studied (5 Dec 2007, 18:00 UTC). The black line represents the shoreline [Deep water wave conditions: $H_{s0} = 6.89$ m, $T_p = 15.64$ s, $\theta_p = 268.45°$].

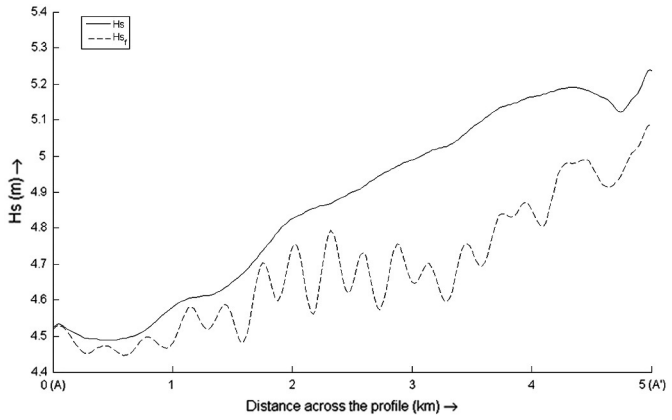

Fig. 8. Significant wave height in the baseline scenario (H_s) and in the presence of the farm (H_{sf}) across the line AA′ at the first peak of the storm studied (5 Dec 2007, 18:00 UTC). [Deep water wave conditions: $H_{s0} = 6.89$ m, $T_p = 15.64$ s, $\theta_p = 268.45°$].

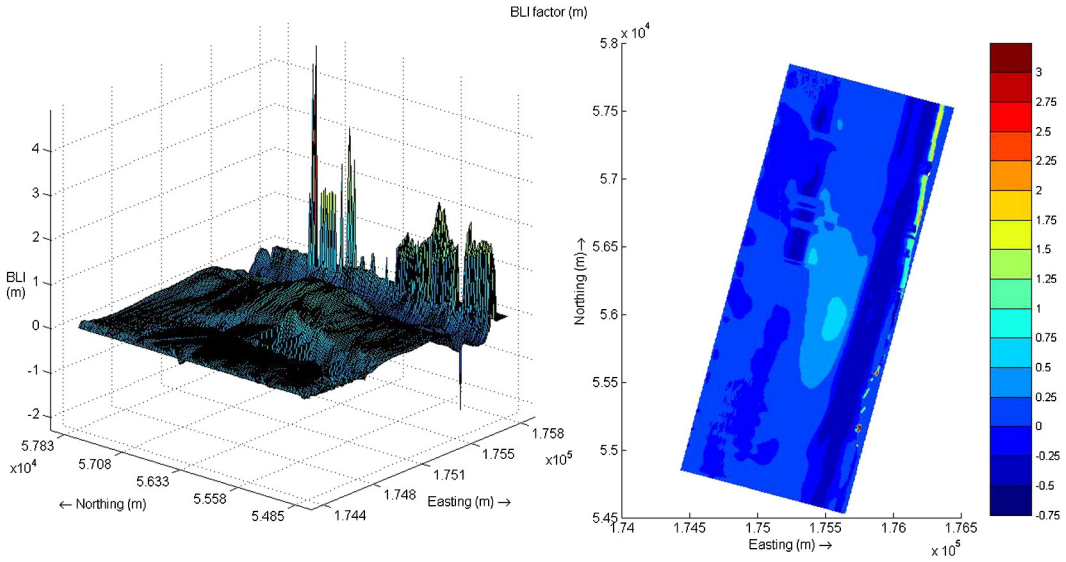

Fig. 9. Bed level impact (*BLI*) at the end of the time period studied [10 Dec 2007, 06:00 UTC].

more pronounced in the intertidal area over the mean water level (at the landward end of the profiles) and over the bar. Furthermore, profile P3 shows that the wave farm not only reduced the eroded area but also altered the sediment transport pattern, moving the initial erosion point up to 30 m towards the shoreline.

The volume of material moved per linear metre along the beach (y) was studied through the mean Cumulative Eroded Area (*CEA*). This indicator showed the difference in material eroded along the profile (x) between the initial and final points of the time period studied in both scenarios: baseline (CEA_b) and with the wave farm (CEA_f). Fig. 11

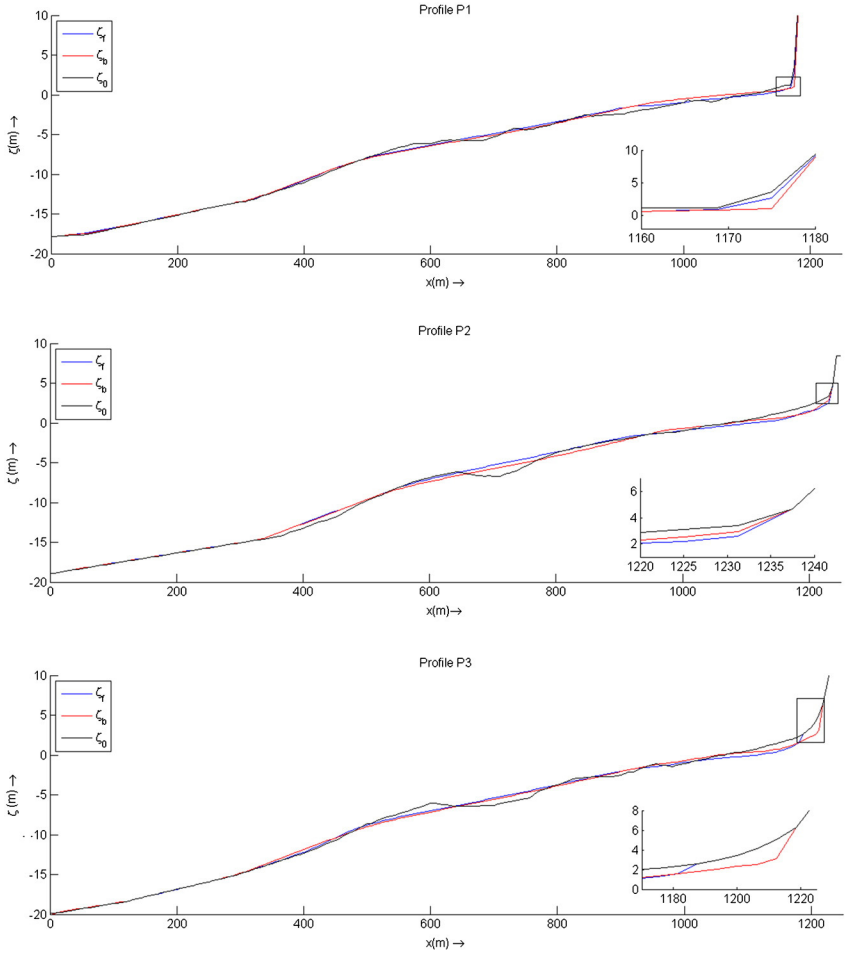

Fig. 10. Bed level at profiles P1, P2 and P3: initial (ζ_0) [05 Dec 2007, 00:00 UTC] and at the end of the simulation in the baseline scenario (ζ_b) and with the wave farm (ζ_f) [10 Dec 2007, 06:00 UTC].

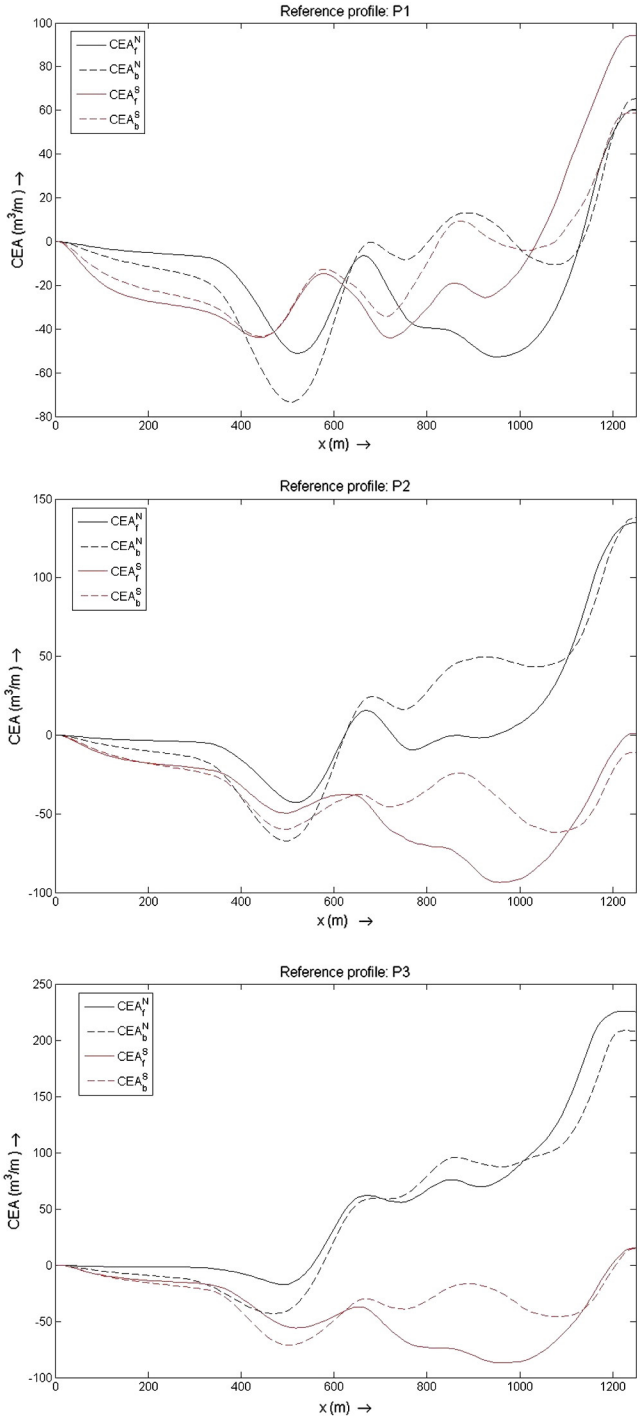

Fig. 11. Mean cumulative eroded area in the baseline scenario (CEA_b) and in the presence of the wave farm (CEA_f) in the southern area (in red) and northern area (in black) across each of the reference profiles P1, P2 and P3, at the end of the time period studied [10 Dec 2007, 06:00 UTC]. The *x*-coordinate represents the distance along the profile, with $x = 0$ the most offshore point.

shows the results in the southern and northern areas across the different reference profiles P1 (south), P2 (middle) and P3 (north). In the case of profile P2, the wave farm modified the sediment transport patterns significantly: whereas erosion was reduced in the northern area of the beach, in the southern area the material eroded increased for water depths below 5 m. As for profile P1, the northern area of the beach presented less sediment transport in the presence of the wave farm for water depths over 7 m, whilst accretion occurred for water depths below 7 m. In the case of profile P3, the sediment transport patterns were hardly affected by the wave farm for water depths over 5 m, but in water depths below 5 m erosion decreased in the southern area of the beach. In summary, in the baseline scenario (without the wave farm) accretion was found to occur in the deeper sections of the profile in the northern area owing to the offshore sediment transport from the beach face and the submarine bar. In the presence of the wave farm, however, the erosion of the beach face and submarine bar was significantly reduced. As a result of this, and of the increase of the southward sediment transport, the accretion of the deeper sections of the profile in the northern area that occurred in the baseline scenario was replaced by accretion in the southern area of the beach for values of the *x* coordinate greater than 600 m (as may be seen on profiles P2 and P3).

Finally, the results of the beach face eroded area (*FEA*) confirmed the contribution of the wave farm to reducing erosion. Fig. 12 shows the evolution of the erosion along Perranporth Beach ($y = 0$ corresponds to the southernmost point of the beach). The most severe erosion took place in the southernmost area of the beach, which is not backed by the dune system, and the northern area, where the waves were higher (Fig. 8). As regards the efficacy of the wave farm for coastal protection, the reduction in erosion was more significant in the northern area of the beach than that in the south and in the middle. In Fig. 13, the non-dimensional erosion reduction (*NER*) is represented on the basis of the results of the eroded area in the beach face, confirming that the wave farm attenuated the erosion in the north of the beach, with values over 50%. As regards the southern area of the beach, 500 m < *y* < 1500 m, the *NER* factor fluctuated strongly, due to isolated responses of different points of the profiles.

The results obtained in this work seem to lend credence to the hypothesis formulated at the outset, namely that a wave farm can serve as a coastal defence measure. It is important to bear in mind, however, that these results, and in particular its quantitative aspects, were derived for a specific case study: a beach with a bar between −5 m and −10 m backed by a well-developed dune system and under the attack of a storm of certain characteristics. Needless to say, these quantitative results may not apply to other situations. Furthermore, the study constitutes a first approximation to the potential of wave farms for coastal defence, a complex question owing to the many processes involved. On open oceanic coasts, such as the present case study, most sediment transport takes place in the surf zone, with wave-induced currents playing the main role. It is well known that on these coasts the fundamental effect of the tide as regards sediment dynamics is a direct result of the variation of the water level, namely the extension of the section of the beach profile on which the energy of the breaking waves is dissipated. This fundamental effect of the tide was taken into account in this work by including the tide in the morphodynamic model. As regards the interaction between the waves and tidal currents in the area,

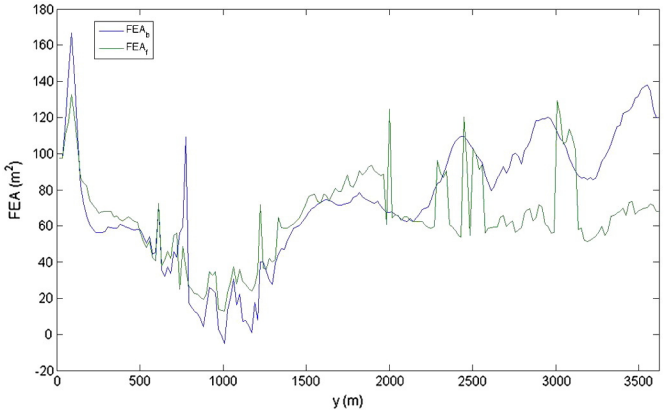

Fig. 12. Beach face eroded area in two scenarios: baseline (FEA_b) and with the wave farm (FEA_f) along Perranporth Beach (*y* — coordinate, with *y* increasing towards the north of the beach) at the end of the time period studied [10 Dec 2007, 06:00 UTC].

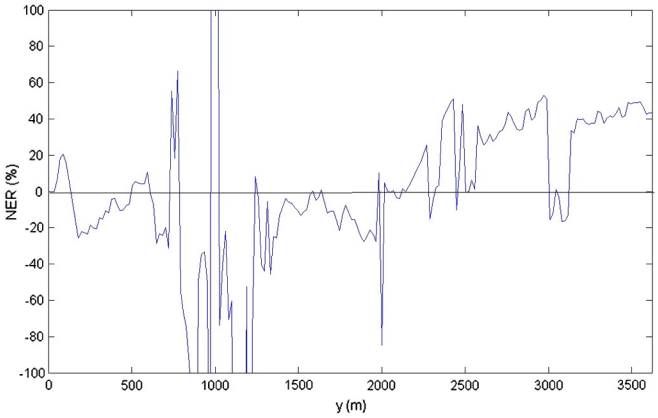

Fig. 13. Non-dimensional erosion reduction (*NER*) at the beach face along Perranporth Beach (y — coordinate, with y increasing towards the north of the beach) at the end of the time period studied [10 Dec 2007, 06:00 UTC].

highlighted in a recent work by Gonzalez-Santamaria et al. (2013), the authors look forward to continuing this line of work in the near future by considering the effects that such interaction could have on wave propagation and, consequently, on the sediment transport patterns at Perranporth. So far this interaction has not been considered, and could be a source of uncertainty in the results. Other sources of uncertainty could be the limitations of the 2DH modelling approach and the operational procedures of the wave farm under storm conditions, which are not easy to establish at this point, when no wave farm is operational yet. As indicated, the investigation of the applicability of wave farms to coastal defence is far from finished, and these uncertainties will hopefully be tackled as wave energy progresses to become a fully-fledged renewable energy source.

5. Conclusions

This paper dealt with the impact of a wave farm on a sandy coast through a case study. A coastal wave model was coupled to a coastal processes model to investigate how the attenuation of wave energy caused by the wave farm affects the morphology of a beach in its lee. The wave propagation model was used to study the interaction of the wave farm with the wave field. It was implemented on a high-resolution computational grid, which enabled to resolve the wakes of the individual WECs forming the farm. Energy extraction by the WECs led to a reduction of the significant wave height, which exceeded 30% of the incident significant wave height immediately in the lee of the farm, decreased towards the shoreline; in a water depth of 20 m this reduction was approximately 10%. The impact of the farm on the nearshore wave conditions was found to be more significant in the northern area of the beach owing to the incoming wave direction and local bathymetry. Based on the results of the wave propagation model, the coastal processes model was applied to assess the response of the beach under storm conditions in two scenarios: without the wave farm (baseline) and with it. By comparing both scenarios the effects of the wave farm on the beach morphology were established.

For this purpose a new suite of core impact indicators was developed: the bed level impact (*BLI*), beach face eroded area (*FEA*), non-dimensional erosion reduction (*NER*) and cumulative eroded area (*CEA*). The bed level impact (*BLI*) evidenced the capacity of the wave farm to significantly reduce erosion in two sections of the beach profile: (i) over the submarine bar, where the seabed drop caused by erosion was reduced by more than 0.5 m (*BLI* greater than 0.5 m); and (ii) at the beach face, where the *BLI* exceeded 4 m at different positions along the beach. The variation along the 3.6 km long beach in the area eroded from the beach face was assessed by means of the *FEA* and *NER* indicators. The wave farm was found to result in a non-dimensional erosion reduction above 50% along a 1.5 km stretch in the north section of the beach. This pronounced impact of wave energy extraction was confirmed with the *CEA* indicator.

For each of the reference profiles P1, P2 and P3, the north and south sections experience different behaviour. In the north sections, in the absence of the farm accretion occurred in the deeper section of the profile at the expense of erosion over the bar and intertidal areas; in contrast, no accretion in the deeper section was observed in the presence of the wave farm —in line with the aforementioned reduction in the erosion over the bar and beach face. In the south sections, whilst there are small differences in the deeper parts of the profile, in the upper parts (intertidal areas) an increase of the accretion was found with the wave farm. This would appear to indicate that, whereas in the baseline scenario substantial offshore sediment transport occurs, in particular in the north sections, leading to accretion in the deeper section of the profile at the expense of the material eroded from the beach face and the bar, the wave farm modifies this pattern by reducing the offshore sediment transport and increasing the southbound longshore sediment transport, resulting in accretion throughout the profile in the southern part of the beach.

To sum up, the nearshore wave farm was found to cause a substantial impact on the beach dynamics. Erosion, especially at the beach face, was significantly reduced, which lends credence to the hypothesis that a wave farm can serve as a coastal defence measure. This synergy between coastal protection and energy production enhances the economic viability of wave energy. Furthermore, the application of wave farms to coastal protection has an advantage from the standpoint of coastal management, at least if floating wave energy converters are considered (as in this work) —the effectiveness of the wave farm as a coastal defence mechanism is not affected by sea level change.

Acknowledgments

This research was carried out in the framework of the Atlantic Power Cluster Project, funded by the Atlantic Arc Programme of the European Commission and the School of Marine Sciences and Engineering of Plymouth University. The authors are grateful to the Coastal Channel Observatory and DIGIMAP for providing the data.

References

Abanades, J., Greaves, D., Iglesias, G., 2014. Wave farm impact on the beach profile: a case study. Coast. Eng. 86, 36–44.
Austin, M., et al., 2010. Temporal observations of rip current circulation on a macro-tidal beach. Cont. Shelf Res. 30 (9), 1149–1165.
Baldock, T.E., et al., 2011. Large-scale experiments on beach profile evolution and surf and swash zone sediment transport induced by long waves, wave groups and random waves. Coast. Eng. 58 (2), 214–227.
Beels, C., Troch, P., De Visch, K., Kofoed, J.P., De Backer, G., 2010. Application of the time-dependent mild-slope equations for the simulation of wake effects in the lee of a farm of wave dragon wave energy converters. Renew. Energy 35 (8), 1644–1661.
Bernhoff, H., Sjöstedt, E., Leijon, M., 2006. Wave energy resources in sheltered sea areas: a case study of the Baltic Sea. Renew. Energy 31 (13), 2164–2170.
Booij, N., Holthuijsen, L., Ris, R., 1996. The"Swan" Wave Model for Shallow Water. Coastal engineering conference, pp. 668–676.
Callaghan, D.P., Ranasinghe, R., Roelvink, D., 2013. Probabilistic estimation of storm erosion using analytical, semi-empirical, and process based storm erosion models. Coast. Eng. 82, 64–75.
Carballo, R., Iglesias, G., 2013. Wave farm impact based on realistic wave–WEC interaction. Energy 51, 216–229.
Defne, Z., Haas, K.A., Fritz, H.M., 2009. Wave power potential along the Atlantic Coast of the southeastern USA. Renew. Energy 34 (10), 2197–2205.
Fernandez, H., et al., 2012. The new wave energy converter WaveCat: concept and laboratory tests. Mar. Struct. 29 (1), 58–70.
Galappatti, G., Vreugdenhil, C., 1985. A depth-integrated model for suspended sediment transport. J. Hydraul. Res. 23 (4), 359–377.
Gonçalves, M., Martinho, P., Guedes Soares, C., 2014. Wave energy conditions in the western French coast. Renew. Energy 62, 155–163.
Gonzalez-Santamaria, R., Zou, Q.-P., Pan, S., 2013. Impacts of a wave farm on waves, currents and coastal morphology in south west England. Estuar. Coasts 1–14.
Iglesias, G., Carballo, R., 2009. Wave energy potential along the Death Coast (Spain). Energy 34 (11), 1963–1975.
Iglesias, G., Carballo, R., 2010a. Offshore and inshore wave energy assessment: Asturias (Spain). Energy 35 (5), 1964–1972.

Iglesias, G., Carballo, R., 2010b. Wave energy and nearshore hot spots: the case of the Bay of Biscay. Renew. Energy 35 (11), 2490–2500.
Iglesias, G., Carballo, R., 2011. Choosing the site for the first wave farm in a region: a case study in the Galician southwest (Spain). Energy 36 (9), 5525–5531.
Iglesias, G., Carballo, R., 2014. Wave farm impact: the role of farm-to-coast distance. Renew. Energy 69, 375–385.
Masselink, G., Evans, D., Hughes, M.G., Russell, P., 2005. Suspended sediment transport in the swash zone of a dissipative beach. Mar. Geol. 216 (3), 169–189.
McCall, R.T., et al., 2010. Two-dimensional time dependent hurricane overwash and erosion modeling at Santa Rosa Island. Coast. Eng. 57 (7), 668–683.
Mendoza, E., et al., 2013. Beach response to wave energy converter farms acting as coastal defence. Coast. Eng. (0).
Millar, D.L., Smith, H.C.M., Reeve, D.E., 2007. Modelling analysis of the sensitivity of shoreline change to a wave farm. Ocean Eng. 34 (5–6), 884–901.
Monk, K., Zou, Q., Conley, D., 2013. An approximate solution for the wave energy shadow in the lee of an array of overtopping type wave energy converters. Coast. Eng. 73, 115–132.
Palha, A., Mendes, L., Fortes, C.J., Brito-Melo, A., Sarmento, A., 2010. The impact of wave energy farms in the shoreline wave climate: Portuguese pilot zone case study using Pelamis energy wave devices. Renew. Energy 35 (1), 62–77.
Pender, D., Karunarathna, H., 2013. A statistical-process based approach for modelling beach profile variability. Coast. Eng. 81, 19–29.
Pontes, M., et al., 1998. The European Wave Energy Resource. 3rd European Wave Energy Conference, Patras, Greece.
Reeve, D.E., et al., 2011. An investigation of the impacts of climate change on wave energy generation: the wave hub, Cornwall, UK. Renew. Energy 36 (9), 2404–2413.
Roelvink, J., et al., 2006. Xbeach Model Description and Manual. UNESCO-IHE Institute for Water Education.
Roelvink, D., et al., 2009. Modelling storm impacts on beaches, dunes and barrier islands. Coast. Eng. 56 (11–12), 1133–1152.
Ruol, P., Zanuttigh, B., Martinelli, L., Kofoed, P., Frigaard, P., 2011. Near-shore Floating Wave Energy Converters: Applications for Coastal Protection. Proceedings of the international conference of Coastal Engineering 2010, Shanghai.
Rusu, L., Guedes Soares, C., 2012. Wave energy assessments in the Azores islands. Renew. Energy 45, 183–196.
Rusu, E., Guedes Soares, C., 2013. Coastal impact induced by a Pelamis wave farm operating in the Portuguese nearshore. Renew. Energy 58, 34–49.
Splinter, K.D., Carley, J.T., Golshani, A., Tomlinson, R., 2014. A relationship to describe the cumulative impact of storm clusters on beach erosion. Coast. Eng. 83, 49–55.
Stopa, J.E., Cheung, K.F., Chen, Y.-L., 2011. Assessment of wave energy resources in Hawaii. Renew. Energy 36 (2), 554–567.
Thorpe, T., 2001. The Wave Energy Programme in the UK and the European Wave Energy Network.
Tolman, H.L., 2002. User Manual and System Documentation of Wavewatch-iii Version 2. 22.
Van Thiel de Vries, J., 2009. Dune Erosion During Storm Surges(PhD Thesis Thesis) Delft University of Technology.
Vicinanza, D., Contestabile, P., Ferrante, V., 2013. Wave energy potential in the north-west of Sardinia (Italy). Renew. Energy 50, 506–521.
Zanuttigh, B., Angelelli, E., 2013. Experimental investigation of floating wave energy converters for coastal protection purpose. Coast. Eng. 80, 148–159.

Renewable Energy 75 (2015) 572–582

Contents lists available at ScienceDirect

Renewable Energy

journal homepage: www.elsevier.com/locate/renene

Coastal defence using wave farms: The role of farm-to-coast distance

J. Abanades*, D. Greaves, G. Iglesias

Plymouth University, School of Marine Science and Engineering, Marine Building, Drake Circus, Plymouth PL4 8AA, UK

ARTICLE INFO

Article history:
Received 5 June 2014
Accepted 20 October 2014
Available online

Keywords:
Wave energy
Wave farm
Nearshore impact
Beach morphology
Erosion
Sediment transport

ABSTRACT

The location of a wave farm and, in particular, its distance to the coast is one of the key aspects in a wave energy project. The effects of the farm on the coast, which can be instrumental in mitigating storm-induced erosion and thus contribute to coastal defence, are sometimes disregarded in selecting its location, possibly due to the inexistence of an *ad hoc* methodology. In this context, the objective of this work is to examine the influence of the farm-to-coast distance through a sensitivity analysis in a case study: Perranporth (UK). The impacts of a wave farm on the beach morphology are examined in four scenarios with different farm-to-coast distances using a high-resolution suite of numerical models. The results show that a wave farm closest to the beach offers the highest degree of coastal protection (up to 20% of beach erosion reduction). The downside of this enhanced coastal protection is that the wave resource available at this location would be slightly smaller (approx. 10%) than in the case of the wave farms further from the coast. More generally, we find that the farm-to-coast distance is a critical variable in determining the effectiveness of a wave farm for coastal defence.

1. Introduction

The importance of wave energy is reflected in the number of very active research lines: the resource characterisation [1–17], the technology development [18–29] or the environmental impacts [30–43]. Conventionally, the main criterion to establish the optimum location for wave farms was the maximisation of wave power [44,45], and other important aspects were often disregarded, such as the effects on the nearshore wave conditions [46,47] and, in particular, the eventual contribution to coastal protection provided by a wave farm. Abanades et al. [48,49], proved that a nearshore wave farm reduced the erosion at the beach face by as much as 35% after storm events due to the extraction of wave energy by Wave Energy Converters (WECs). On this basis, the objective of this work is to establish the dependence of the degree of coastal protection offered by the farm on its distance from the coastline by means of a sensitivity analysis.

To accomplish this objective, four scenarios are compared, corresponding to three locations of the wave farm at different distances from the coast, plus the baseline (no farm) scenario, under different wave conditions. First, the impacts of the wave farm on the wave conditions are examined using a nearshore wave model, SWAN, Simulating Waves Nearshore [50]. This is a phase-averaged spectral model that computes the effects of the wave farm using an energy transmission coefficient, whose values are obtained from the laboratory tests carried out by Fernandez et al. [27]. The wave farm is implemented on a high-resolution grid at different distances from a reference (10 m water depth) contour: (i) 2 km, (ii) 4 km; and (iii) 6 km. Second, based on the results of the aforementioned scenarios a coastal processes model, XBeach [51], is used to compare the effects of the wave farm at the different locations with the baseline scenario. A set of impact indicators is developed, specifically, to quantify these effects and establish the role played by the farm-to-coast distance.

This methodology is applied to a case study at Perranporth Beach (Fig. 1), Cornwall (UK). A 3.5 km long sandy beach facing directly toward the North Atlantic Ocean, Perranporth is in an area with a great potential for marine renewable energy [52] – as corroborated by the Wave Hub pilot test site. The extremely energetic storms of February 2014 proved that Perranporth is subject to increased erosion risks from rising sea level and storminess [53]. In view of these risks, and given that a wave farm consisting of floating WECs adapts naturally to any sea level changes [54], Perranporth constitutes a prime area for using such wave farms for coastal protection.

* Corresponding author. Tel.: +44 (0)7583 544041.
E-mail address: javier.abanadestercero@plymouth.ac.uk (J. Abanades).

http://dx.doi.org/10.1016/j.renene.2014.10.048
0960-1481/

Nomenclature

N	wave action density
c_x and c_y	velocity propagation in the x- and y-space, respectively
c_θ and c_σ	velocity propagation in the direction and σ the relative frequency space, respectively
S	source term
ρ	water density
g	gravity acceleration
h	water depth
H_s	significant wave height
T_p	wave peak period
θ	wave direction
K_t	wave transmission coefficient
t	time
RSH	reduction in the significant wave height
D	distance between the twin bows of a WEC
$H_{s,b}$	significant wave height in the baseline scenario
$H_{s,\mathrm{fi}}$	significant wave height in the i-th wave farm scenario
J	wave power
$E(\sigma,\theta)$	directional spectral density
H_{rms}	root mean square wave height
T_{m01}	mean absolute wave period
θ_m	mean wave direction
s	directional spreading coefficient
C	wave group varying depth averaged
D_h	sediment diffusion coefficient
u^E and v^E	depth-averaged velocities
C_{eq}	equilibrium concentration
MSR	mean spring tide range
LCD	local chart datum
BLI	bed level impact in the i-th wave farm scenario
FEA_b	beach face eroded area in the baseline scenario
FEA_i	beach face eroded area in the i-th wave farm scenario
NER_i	non-dimensional erosion reduction in the i-th wave farm scenario
CEA_b	mean cumulative eroded area in the baseline scenario
CEA_i	mean cumulative eroded area in the i-th wave farm scenario
ζ	seabed level

2. Materials and methods

2.1. Wave model

The wave propagation was computed using SWAN v40.41, a third-generation spectral wave model based on the action balance equation that can be solved in spherical or geographical coordinates [55]:

$$\frac{\partial N}{\partial t}+\frac{\partial(c_x N)}{\partial x}+\frac{\partial(c_y N)}{\partial y}+\frac{\partial(c_\theta N)}{\partial \theta}+\frac{\partial(c_\sigma N)}{\partial \sigma}=\frac{S}{\sigma} \tag{1}$$

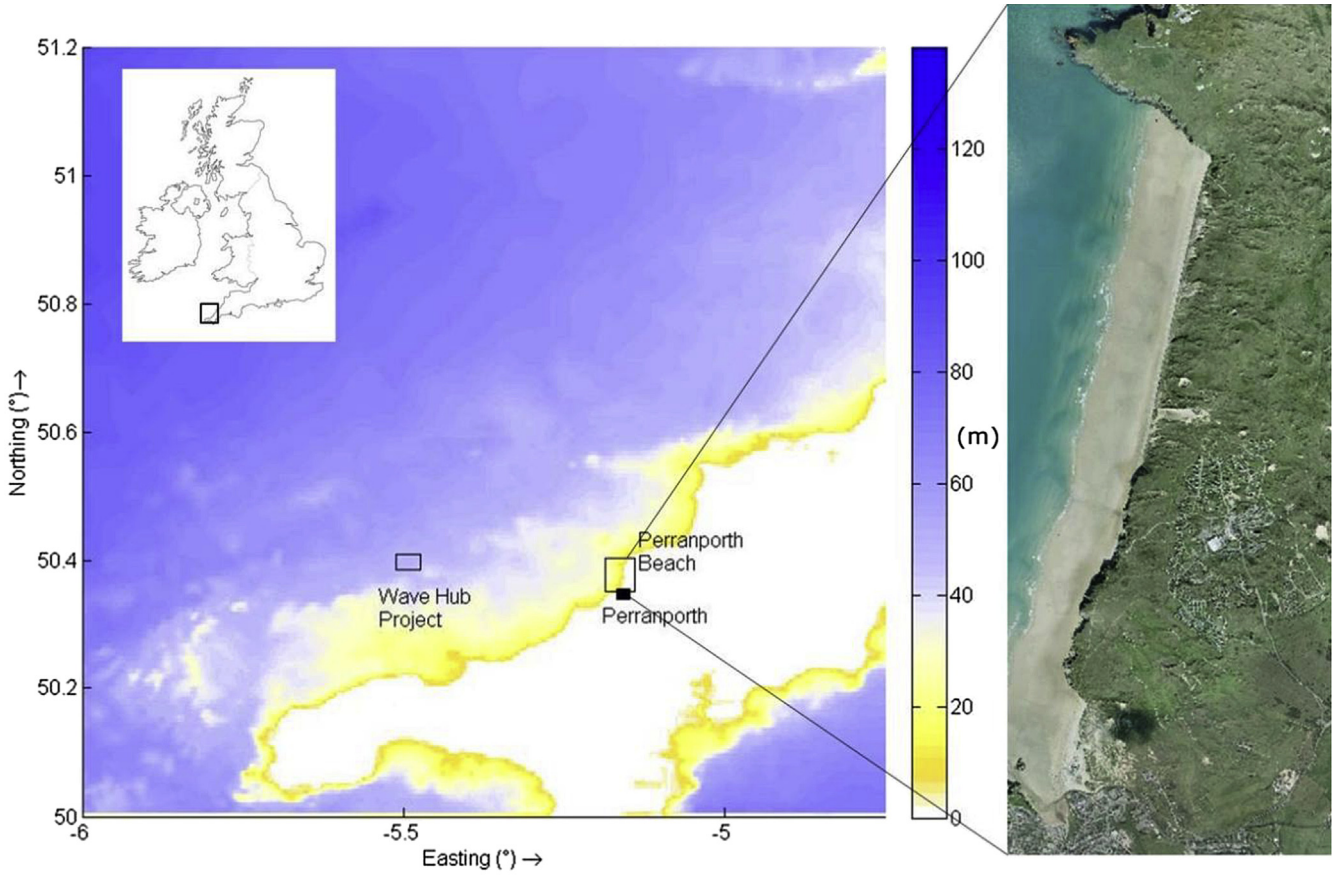

Fig. 1. Bathymetry of SW England [water depths in m] including the location of Perranporth Beach, Wave Hub Project and an aerial photo of Perranporth Beach [source: Coastal Channel Observatory].

in which the first term on the left-hand side of this equation represents the variation of wave action density (N) – the wave energy density divided by the relative frequency – in time (t), the second and third term the velocity propagation in the geographical space (with c_x and c_y the propagation velocity in x- and y-space, respectively) and the fourth and fifth term the propagation velocity in the θ- and σ-space, respectively (where θ represents the direction and σ the relative frequency). On the right-hand side of Equation (1), the source term S represents the effects of generation, dissipation and nonlinear wave–wave interactions.

In the present study the wave model was set up to account the following wave processes: shoaling, refraction due to current and depth, whitecapping, bottom friction and depth induced wave breaking [56]; using two computational grids with different resolutions (Fig. 2): (i) an offshore grid covering an area of approx. 100 km × 50 km with a grid size of 400 × 200 m, and (ii) a high-resolution nearshore (nested) grid covering the study area, with dimensions of approx. 8 km × 6 km and a grid size of 16 m × 12 m. Onto the latter grid was implemented the wave farm, whose layout was chosen based on the sensitivity analysis carried out by Carballo and Iglesias [46]. It consisted of 11 WaveCat WECs [27,57] arranged in two rows, with a spacing between devices of 2.2D, where D = 90 m is the distance between the twin bows of a single device, occupying an area approx. of 1500 m × 350 m. Following Kenney [58] and based on the analysis of the offshore wave climate in the area, two wave conditions (Table 1) were prescribed at the outer (ocean) boundary of the offshore grid. Wave transmission through the wave farm was modelled using the transmission coefficients obtained in the laboratory tests reported by Fernandez et al. [27]. For the purposes of the sensitivity analysis three locations of the wave farm were considered, at distances of 2 km, 4 km and 6 km from the reference (10 m water depth) contour – corresponding to water depths of approx. 25 m, 30 m and 35 m, respectively (Fig. 3).

To measure the impact of the wave farm on the wave conditions in its lee an impact indicator was defined: the Reduction in the Significant wave Height, RSH_i,

$$\mathrm{RSH}_i\left(x,y\right) = H_{s,b}(x,y)^{-1}\left(H_{s,b}\left(x,y\right) - H_{s,f_i}\left(x,y\right)\right), \quad \text{with } i = 2\text{ km},\ 4\text{ km or }6\text{ km}, \tag{2}$$

where the subindex i refers to the position of the wave farm, and $H_{s,b}$ and $H_{s,\mathrm{fi}}$ are the significant wave height in the baseline scenario and with the wave farm, respectively, at a point of the coast designated by its coordinates (x,y), with the x-coordinate referring to the easting and the y-coordinate to the northing. This non-dimensional indicator quantifies the shadow caused by the wave farm in its lee.

Table 1
Wave conditions: significant wave height (H_s), peak period (T_p), direction (θ) and directional spreading (s); and wave transmission coefficient (K_t) for the different case studies.

Case study	H_s (m)	T_p (s)	θ (°)	s (°)	K_t
CS1	3	12	315 (NW)	26.50	0.76
CS2	3.5	11	315 (NW)	26.34	0.78

The performance of the wave farm at the different positions was also analysed by means of the wave power (J, in units of W m^{-1} in the SI), which is computed in SWAN from its x- and y-components:

$$J_x = \int_0^{2\pi}\int_0^{360} \rho g c_x E(\sigma,\theta)\,\mathrm{d}\sigma\,\mathrm{d}\theta \tag{3}$$

$$J_y = \int_0^{2\pi}\int_0^{360} \rho g c_y E(\sigma,\theta)\,\mathrm{d}\sigma\,\mathrm{d}\theta \tag{4}$$

where ρ is the water density, g is the acceleration due to gravity, and $E(\sigma,\theta)$ is the directional spectral density, which specifies how the energy is distributed over frequencies (σ) and directions (θ). The wave power magnitude is then given by

$$J = \left(J_x^2 + J_y^2\right)^{\frac{1}{2}}. \tag{5}$$

2.2. Coastal processes model

Based on the results of the wave model, the coastal processes model, XBeach v1.20.3606, was used to compute the impact of the wave farm on beach morphology. XBeach is a 2DH (two-dimensional horizontal) time-dependent model that solves coupled cross-shore and alongshore equations for wave propagation, flow, sediment transport and bottom changes. The full description of the model can be found in Roelvink et al. [51].

The sediment transport module solves the depth-averaged advection diffusion equation [59] on the time scale of wave groups [60],

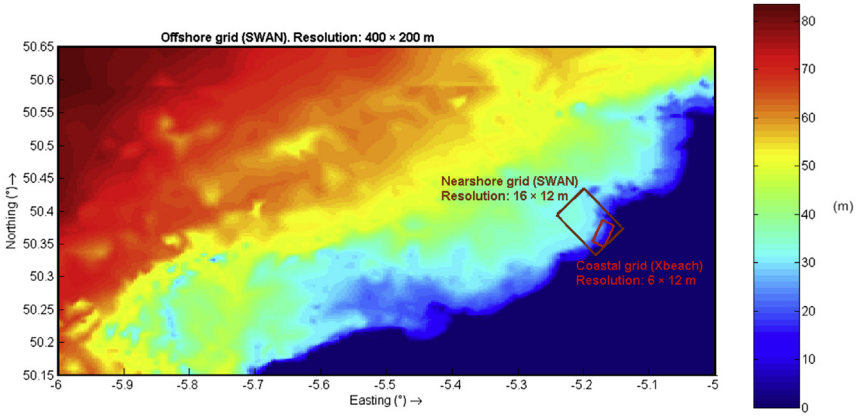

Fig. 2. Computational grids of the wave propagation (SWAN) and coastal processes (XBeach) model [water depths in m].

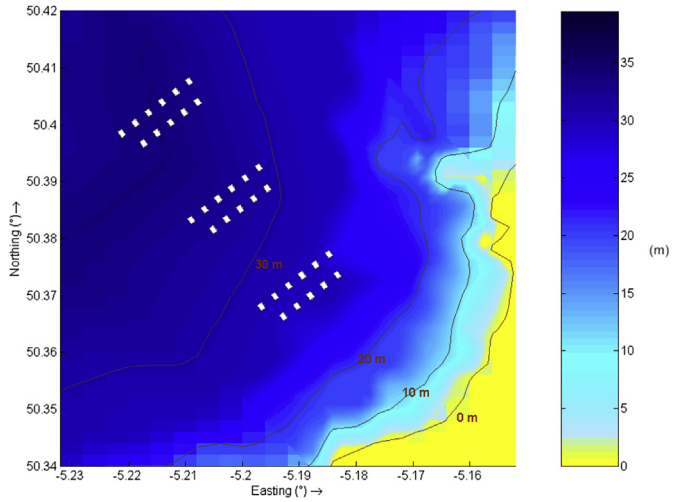

Fig. 3. The three locations considered for the wave farm, at distances of 2 km, 4 km and 6 km from the reference (10 m water depth) contour [water depth in m].

$$\frac{\partial(hC)}{\partial t}+\frac{\partial(hCu^E)}{\partial x}+\frac{\partial(hCv^E)}{\partial y}+\frac{\partial h\left[D_h h\frac{\partial C}{\partial x}\right]}{\partial x}+\frac{\partial h\left[D_h h\frac{\partial C}{\partial y}\right]}{\partial y} = \frac{hC_{eq}-hC}{T_S} \tag{6}$$

where C is the wave group varying depth averaged, sediment concentration, D_h is the sediment diffusion coefficient, which is represented by an adaptation time, T_s, that is based on the local water depth, h, and sediment fall velocity. The terms u^E and v^E represents the depth-averaged velocities and C_{eq} the equilibrium concentration, representing the source term in the right hand side of the equation. The sediment transport formula defined by Van Thiel de Vries [61] was chosen to determine the sediment equilibrium concentration.

XBeach has been widely validated to determine the impact of storms on sandy [62–64] and gravel beaches [65–68] at different locations. In this case, the impact of the wave farm on the beach morphology (3D) was compared to the baseline scenario at Perranporth Beach following the model set up applied by Abanades et al. [48] at the same location to study the evolution of the beach profile (2D). The high-resolution grid implemented on XBeach covered an area of 1.4 km cross-shore and 3.0 km alongshore at Perranporth Beach with a resolution of 6 m and 12.5 m, respectively. The bathymetry data, from the Coastal Channel Observatory, were interpolated onto this grid (Fig. 4), which comprised elevation values from −20 m to more than 30 m with reference to the local chart datum (LCD).

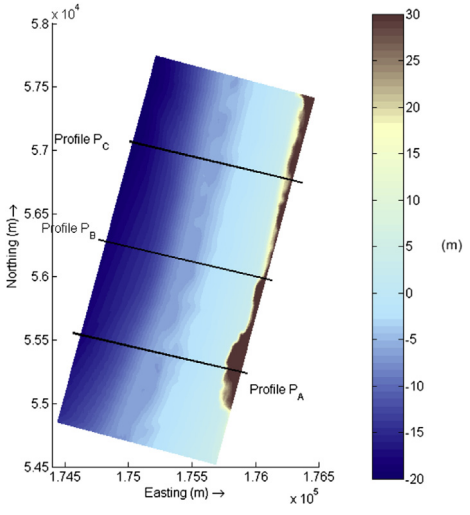

Fig. 4. Bathymetry of Perranporth Beach computed in XBeach. Profiles P1, P2 and P3 included. Water depth in relation to local chart datum [in m].

The following parameters obtained from the wave model along the line A–A′ (Fig. 5) were the input of XBeach for the analysis of the beach response under the storm events: root mean square wave height (H_{rms}), mean absolute wave period (T_{m01}), mean wave direction (θ_m) and directional spreading coefficient (s). As for tidal effects, Perranporth is a macrotidal beach with a Mean Spring tidal Range, MSR, of 6.3 m [69], and consequently their influence on the response of the beach ought to be considered [70]. The MSR was included in the model with a semi-diurnal tidal regime (two low and two high tides each day).

The effects of the wave farm on the beach morphology were determined based on a comparison of the different wave farm scenarios with the baseline (no farm) case. The following impact indicators were defined: (i) bed level impact (BLI_i), (ii) beach face eroded area (FEA_b or FEA_i), (iii) non-dimensional erosion reduction (NER_i), and (iv) mean cumulative eroded area (CEA_b or CEA_i). The indicators corresponding to the baseline and wave farm scenarios were denoted with the subscripts b or i, respectively, with i indicating the farm-to-coast distance (i = 2 km, 4 km or 6 km).

The bed level impact (BLI_i), with units of m in the S.I., was defined as

$$BLI_i(x,y)=\zeta_{f,i}(x,y)-\zeta_b(x,y),\ \text{with } i=2\text{ km},\ 4\text{ km or }6\text{ km}, \tag{7}$$

where $\zeta_{f,i}(x,y)$ and $\zeta_b(x,y)$ are the seabed level in the wave farm and baseline scenarios, respectively, at a generic point of the beach designated by its coordinates (x,y) in the horizontal reference plane. The y-coordinate axis follows the general orientation of the beach, with values increasing towards the northern end of the beach, and the x-coordinate is the horizontal coordinate along the profiles, with values increasing towards the landward end of the profile. Thus, the BLI_i indicator represents the change in bed level in the i-th scenario. A positive value signifies that the seabed level is higher in the presence of the wave farm.

The beach face is the area over the mean water level exposed to the action of the waves. In order to quantify the wave farm effects on this particularly relevant area of the beach, the beach face eroded area (FEA), with units of m^2 in the S.I., was defined in the wave farm ($FEA_{f,i}$) and baseline (FEA_b) scenarios by

$$FEA_b(y)=\int_{x_1}^{x_{max}}[\zeta_0(x,y)-\zeta_b(x,y)]dx, \tag{8}$$

$$FEA_{f,i}(y)=\int_{x_1}^{x_{max}}\left[\zeta_0\left(x,y\right)-\zeta_{f,i}\left(x,y\right)\right]dx,\quad \text{with } i=2\text{ km},\ 4\text{ km or }6\text{ km}, \tag{9}$$

where $\zeta_0(x,y)$ is the initial bed level at the point of coordinates (x,y), and x_1 and x_{max} are the values of the x-coordinate at the seaward end of the beach face and landward end of the profile, respectively. These indicators are profile functions (the profile being designated

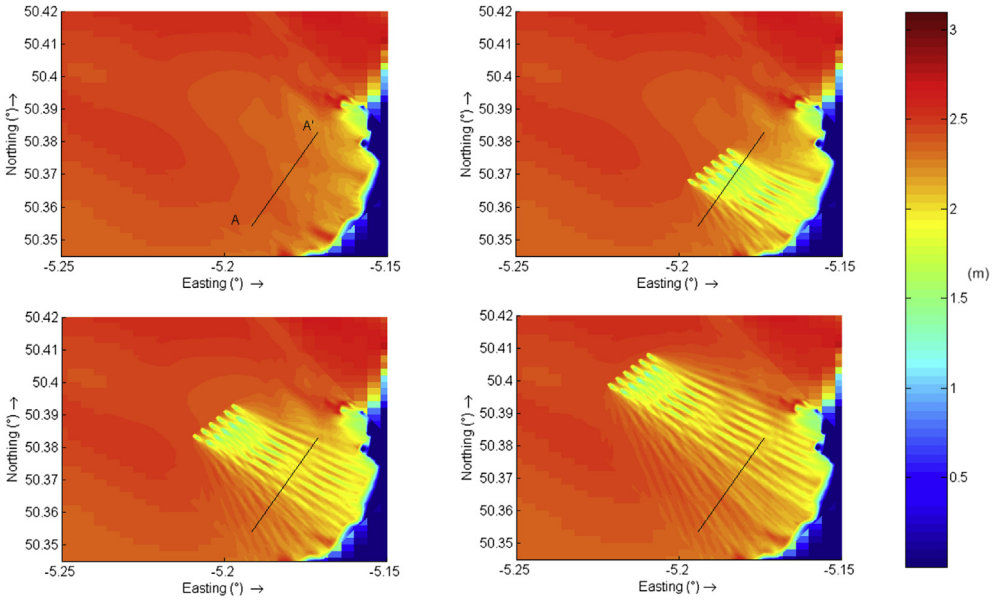

Fig. 5. Significant wave height [m] in the baseline scenario and in the presence of the farm at distances of 2 km, 4 km and 6 km from the reference (10 m water depth) contour in CS1 (clockwise from above left).

by the y-coordinate) that evaluate the erosion caused by the storms at the beach face, thus enabling to compare the reduction of the erosion obtained in each of the three wave farm scenarios relative to the baseline case.

The non-dimensional erosion reduction,

$$\mathrm{NER}_i(y) = 1 - (x_{\max} - x_1)^{-1} \int_{x_1}^{x_{\max}} \left[\zeta_0\left(x,y\right) - \zeta_{f,i}\left(x,y\right)\right] \times \left[\zeta_0(x,y) - \zeta_b(x,y)\right]^{-1} \mathrm{d}x, \tag{10}$$

is also a profile function, in this case non-dimensional, which computes the variation in the eroded area of a generic profile (y) as a fraction of the total eroded area of the same profile brought about by the wave farm. A positive or negative value implies a reduction or increase in the eroded area, respectively, as a result of the wave farm.

Finally, the mean cumulative eroded area (CEA), with units of m^2 (or m^3 per linear metre of beach), was determined as well in the baseline scenario (CEA_b) and with the different wave farms ($\mathrm{CEA}_{f,i}$). For its definition three reference profiles were considered: P_A, P_B and P_C (Fig. 2). For each of these the beach was divided into two parts, to the north (CEA_b^N and$\mathrm{CEA}_{f,i}^N$) and south (CEA_b^S and$\mathrm{CEA}_{f,i}^S$) of the reference profile, and the corresponding indicators were computed from

$$\mathrm{CEA}_b^S(x) = (y_P - y_0)^{-1} \int_{y_0}^{y_P} \int_{x_0}^{x} \left[\zeta_0(\chi,y) - \zeta_b(\chi,y)\right] \mathrm{d}\chi \, \mathrm{d}y, \tag{11}$$

$$\mathrm{CEA}_{f,i}^S(x) = (y_P - y_0)^{-1} \int_{y_0}^{y_P} \int_{x_0}^{x} \left[\zeta_0\left(\chi,y\right) - \zeta_{f,i}\left(\chi,y\right)\right] \mathrm{d}\chi \, \mathrm{d}y, \tag{12}$$

$$\mathrm{CEA}_b^N(x) = (y_{\max} - y_P)^{-1} \int_{y_P}^{y_{\max}} \int_{x_0}^{x} \left[\zeta_0(\chi,y) - \zeta_b(\chi,y)\right] \mathrm{d}\chi \, \mathrm{d}y, \tag{13}$$

$$\mathrm{CEA}_{f,i}^N(x) = (y_{\max} - y_P)^{-1} \int_{y_P}^{y_{\max}} \int_{x_0}^{x} \left[\zeta_0\left(\chi,y\right) - \zeta_{f,i}\left(\chi,y\right)\right] \mathrm{d}\chi \, \mathrm{d}y, \tag{14}$$

where the integration variables χ and y correspond to integration along the profile and the beach, respectively. The integration limits along the profile are: x_0, the value of the x-coordinate corresponding to the first point of the profile (seaward end); $x_{\max}$, the (landward) end of the profile. Along the beach, the integration limits are: y_0 and $y_{\max}$, the values of the y-coordinate corresponding to the southernmost and northernmost points of the beach, and y_P the value corresponding to the reference profile. The CEA indicator represents the average cumulative eroded area of the two sections of the beach along the profile (x). A positive value signifies that the mean volume of material along the section of the beach is reduced compared with the initial situation (erosion).

3. Results and discussion

First, the results obtained from the nearshore wave model were analysed to study the impact of the wave farm on the wave conditions. The nearshore significant wave height (H_s) for the different scenarios (baseline and with the wave farm at distances of 2 km, 4 km and 6 km from the reference contour) is shown in Fig. 5 for CS1 (Table 1). The reduction in the significant wave height in the lee of the farm caused by the energy extraction is apparent. This reduction was assessed by means of the impact indicator RSH_i (Fig. 6) defined in Section 3.1. The maximum value of the indicator was achieved within the second row of WECs with values of up to 50%. At a distance of 1.5 km from the second row of devices, the reduction reached a peak of 40% due to the merging of the shadows caused by the first and the second row of devices. However, this reduction decreased moving towards the coast due to the redistribution of the energy from the edges into the shadow caused by the wave farm. At a water depth of 10 m, the average reduction caused by the wave farm closest to the coast (2 km) was approx. 25%, whereas for the wave farm at 4 and 6 km the average reduction was approx. 15% and 9%, respectively.

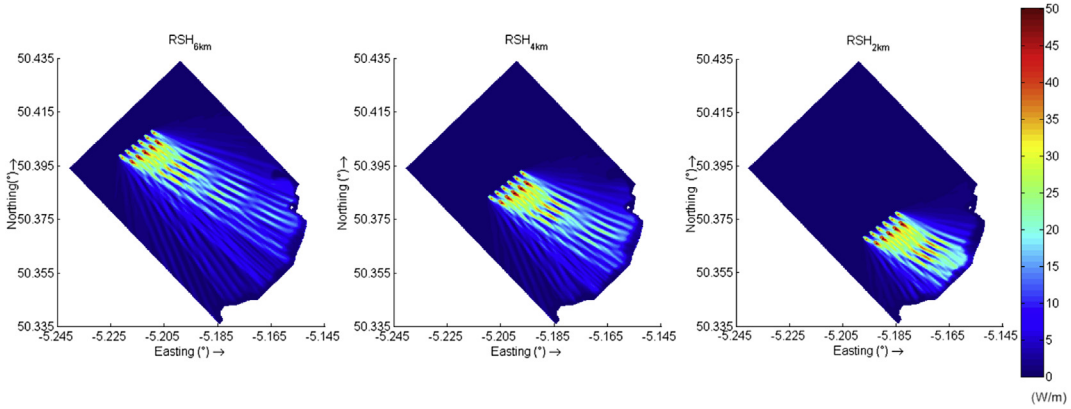

Fig. 6. Reduction of the significant wave height (%) with the wave farm at a distance of: 2 km (RSH2 km), 4 km (RSH4 km) and 6 km (RSH6 km) from the reference (10 m water depth) contour in study CS2 [in m].

The relevance of the farm-to-coast distance may be readily observed in the shadows caused by the wave farm at different distances. The area affected at the coastline by the wave farm furthest to the coast (6 km) was greater than 7 km, however the average reduction of the significant wave height in this area was less than 5%. On the other hand, the wave farm at 2 km affected a smaller area in the coastline, around 4 km, but the reduction exceeded 10%. Fig. 7 shows this reduction for CS1 (above) and CS2 (below) along the line AA′, located in Fig. 5, which corresponded to the area of interest at Perranporth Beach and was used as input for the coastal processes model. This figure confirmed the different shadow pattern brought about by the wave farm at a distance of 4 and 6 km compared with the 2 km. In the latter, the reduction mainly occurred in the central section of the beach, being less significant in the northern area of the beach. However, for the other two scenarios, the reduction was found to be approx. constant along the line AA′.

In terms of wave power, the resource was evaluated using Equations (2)–(4) at the location of each of the WECs in the wave farm. Table 2 shows the overall wave power incident on the wave farm for the different distances, it was found that the closer the wave farm to the coast, the lesser the resource, due to the dissipation caused by the different coastal processes that occur in intermediate and shallow water. For the wave farm closest to the coast the reduction of the wave power compared to the scenario with the wave farm at a distance of 6 km was 10.5% and 8.7% for CS1 and CS2, respectively. In the case of the wave farm at 4 km the reduction compared with the scenario at 6 km is 5.7% and 7.3% for CS1 and CS2, respectively. In summary, on the one hand the wave farm closest to the beach caused the greatest reduction in the significant wave height, but, on the other hand, the resource in that area is lower than in deeper areas, and, therefore, a comparative study of the response of the beach under storm conditions is necessary to determine the best location for a wave farm in terms of wave energy resource and coastal protection.

Second, the coastal processes model used the output of the wave model to study in which manner the modification of the wave patterns affected the coastal processes and, consequently, the beach morphology. To quantify this alteration the results were analysed by means of the impact indicators defined in Section 3.2. The first indicator was the bed level difference, BLI, which represented the difference of the bed level between the baseline and the wave farm scenarios at a point in time. Fig. 8 shows BLI values at the end of the storm for CS1 with the wave farm at a distance of 2 km (left), 4 km (middle) and 6 km (right). It was observed that the main impact caused by the wave farm was located at the beach face, where reductions of the erosion up to 1.5 m were found.

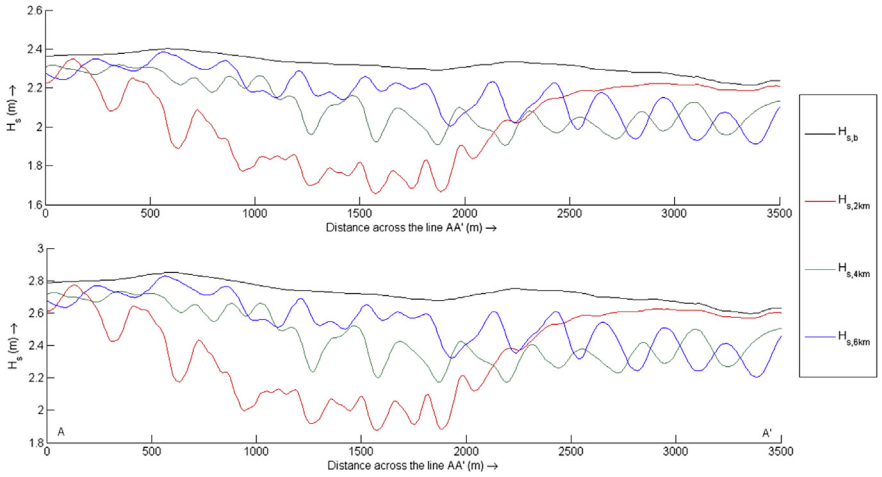

Fig. 7. Significant wave height [in m] in the baseline scenario (Hs, *b*) and in the presence of the farm at a distance of: 2 km (Hs, 2 km), 4 km (Hs, 4 km) and 6 km (Hs, 6 km) from the reference (10 m water depth) contour across the line AA′ in CS1 (above) and CS2 (below).

Table 2
Overall wave power incident in the wave farm [kW/m].

Case study (H_s)	Wave farm scenario		
	2 km	4 km	6 km
CS1: 3 m	197.52	208.02	220.75
CS2: 3.5 m	339.80	345.09	372.13

Fig. 9 illustrates the evolution of three profiles at the end of the storm for CS2, corresponding with three section of the beach that were identified by their different responses under the storms: (i) the southern section of the beach (P1 in Fig. 9) with a smooth slope in the intertidal area; (ii) the area backed by a very steep dune (P2 in Fig. 9) where the mean water level was close to the toe of the dune; and (iii) the northern section of the beach (P_3 in Fig. 9) also backed by the dune, but with a greater distance from the toe of the dune to the mean water level. In the case of P_1 and P_3 the main erosion occurred on the beach face and this material was moved to lower sections of the beach, however in the case of P2 accretion was detected in the intertidal area due to the material eroded in the steep dune for the proximity of the mean water level to it. In the area of P3 were found the greatest values of the BLI indicator, with reductions greater than 1 m, while in the section P1 the reduction took values of approx. 0.5 m.

In the comparison between scenarios, the wave farm at a distance of 2 km caused greater reduction of the erosion along the beach than the other scenarios, in which areas with significant reductions of erosion were combined with negligible values or even accretion. In the lower sections of the beach, accretion occurred due to the amount of material eroded in the beach face. For instance, in the scenario with the wave farm closest to the coast the BLI took negative values of −0.5 m in the southern area of the beach, which meant that the accretion without the farm was bigger than with it, due to the greater erosion produced in the intertidal area in the baseline scenario. This reduction of the accretion with the wave farm at a distance of 4 km and 6 km took place only in a few sections of the beach with BLI values less than 0.3 m.

The impact factor FEA was defined to quantify the erosion in the beach face along the beach (Fig. 10). The greatest values of this indicator along the beach were focussed in the southern area because this section was not backed by the dune. The erosion in the baseline scenario was, in general, greater than the scenarios with the wave farm, especially in the middle and northern area of the beach, y–coordinate (along the beach) > 1250 m. To compare the reduction between the different wave farm scenarios the indicator NER was defined, which showed the variation of the erosion in terms of the eroded area in the baseline scenario (Fig. 11). The NER values fluctuated considerably along the beach, but it was observed that the reduction using a wave farm at a distance of 2 km was greater than the other two scenarios.

In the area of the steep dune (500 m < y–coordinate < 1250 m), the erosion in the beach face was very low (negligible in some sections), and very few profiles presented an isolated response taking the NER factor negative values (greater erosion with the farm than without it). However, in terms of the average reduction of the beach face erosion along the whole beach, it was confirmed that the wave farm at 2 km offered a greater degree of coastal protection, around 15% in both case studies, than the scenario with the wave farm at 4 and 6 km, which presented an approximate reduction of approx. 10%. Considering particular sections of the beach, the impact was much more significant, for instance, the reduction exceeded 20% for the wave farm at 2 km for values of the y − coordinate between 1200 and 2000 m in CS2, which was the area most affected by the reduction of the significant wave height (Fig. 7). The results for the wave farm at 4 and 6 km did not present large differences in terms of the reduction of the erosion along the whole beach; however the average reduction for the farm at 4 km was slightly greater (13%) than the farm at 6 km (11%) in the area backed by the dune (y > 1250 m).

Finally, the CEA indicator computed the volume of material moved per linear metre along the beach between the initial conditions and the last point of the simulation for the different scenarios. This indicator was applied to the northern (CEA^N) and southern (CEA^S) section of the beach taking as reference for each case the following profiles (Fig. 4): P_A (south), P_B (middle) and P_C (north), which allowed the variations in the longshore sediment transport to be studied. Fig. 12 shows the evolution of this factor along the profile (x) for CS1, where the negative values represented an increase in the volume of material with respect to the initial conditions (accretion). In the lowest section of the profile, the volume of material for the scenarios studied was larger than the initial volume due to the material eroded, mainly from the following sections along the profile: (i) the beach face (1200 m < x-coordinate < 1300 m) and (ii) the area that faced the storms in low

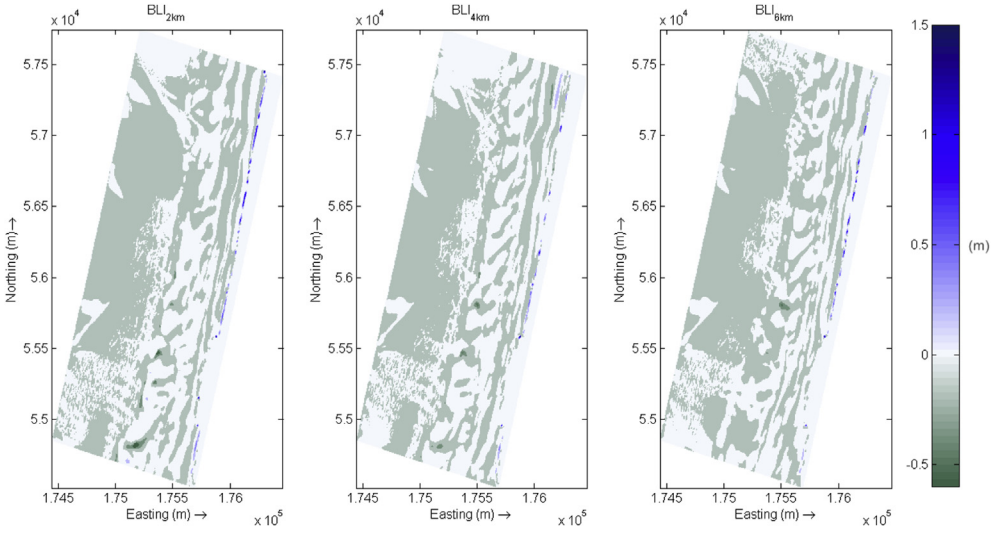

Fig. 8. Bed level impact with the wave farm at a distance of 2 km ($BLI_{2\ km}$), 4 km ($BLI_{4\ km}$) and 6 km ($BLI_{6\ km}$) at the end of the storm in CS1.

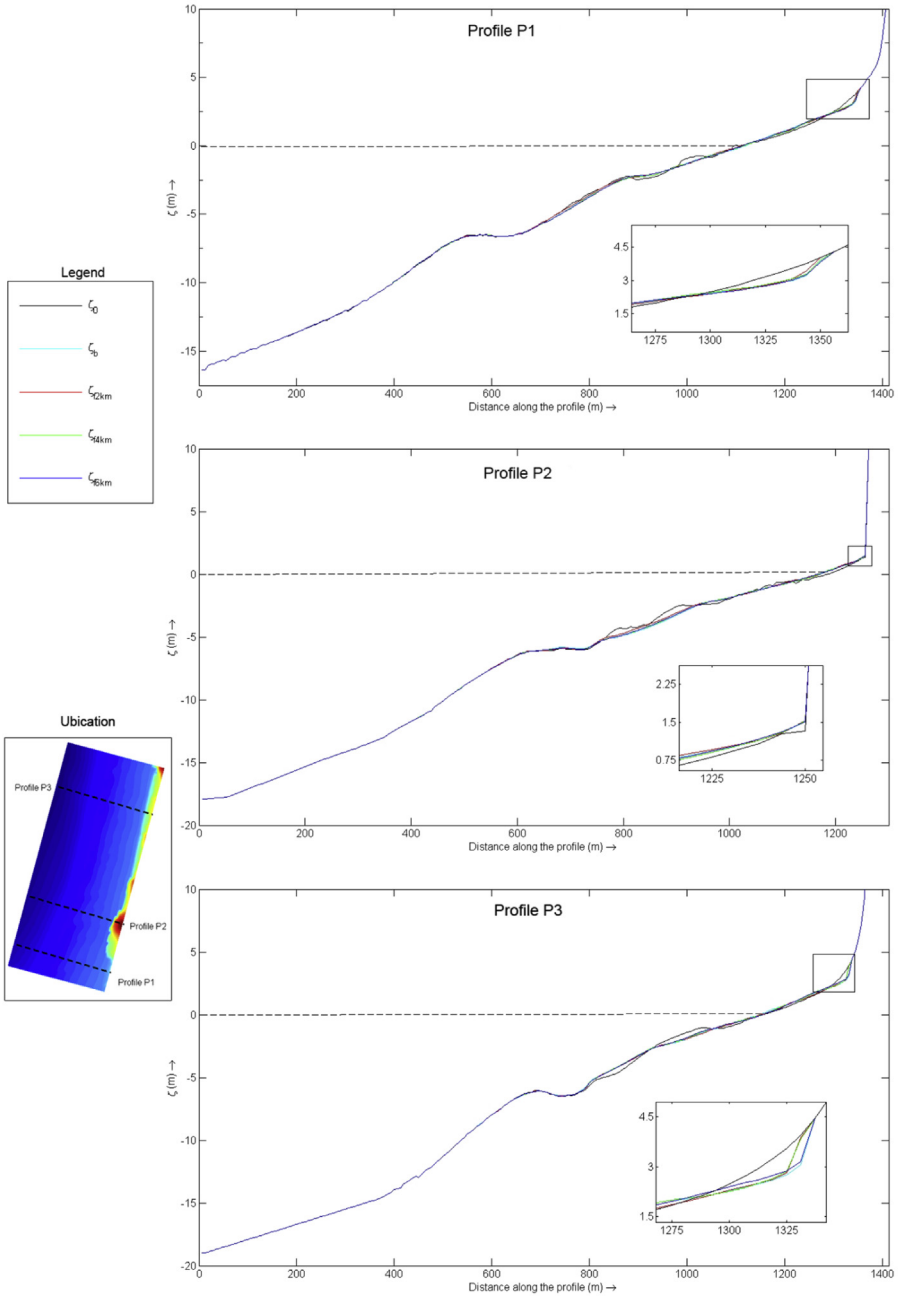

Fig. 9. Bed level at Profiles P_1, P_2 and P_3: initial (ζ_0) and at the end of the storm in CS2 in the baseline scenario (ζ_b) and with the wave farm at a distance of 2 km ($\zeta_{f2\ km}$), 4 km ($\zeta_{f4\ km}$) and 6 km ($\zeta_{f6\ km}$).

tide (800 m < *x*-coordinate < 1000 m), which was more significant in the southern area of the reference profiles. The geomorphological complexity of the southern section of the beach resulted in very different behaviour between the different scenarios.

The wave farm at a distance of 2 km presented a significant rise in the volume of material in the southern area of the beach, especially taking as reference the profiles P_A and P_B. This could be associated to the modification of the wave patterns brought about by the wave farm, given that the main reduction of the significant wave height occurred in the southern and middle area of the beach. Therefore, part of the material eroded in the northern section, where the reduction of the significant wave height was less, could be moved to the southern part of the beach, increasing the volume in this section. As for the wave farm at 4 and 6 km, they did not present significant differences compared with the baseline scenario, nonetheless the erosion caused in the absence of the farm was greater. For instance, in the northern area of the different profiles, it is observed that the greatest accretion at $x = 1250$ m occurred in the baseline scenario due to the largest amount of material eroded at the beach face. In the case of the profile P_A, this was followed by the scenario with the wave farm at a distance of 2 km, associated with the material moved from the north of the beach, but for the profiles P_B and P_C, the greatest values of accretion, after the baseline scenario, occurred with the wave farm at 4 and 6 km given that the farm at these distances reduced the erosion less than the scenario at 2 km. To sum up, a wave farm can alter not just the wave conditions in its lee but also the morphology and the sediment transport of the beach.

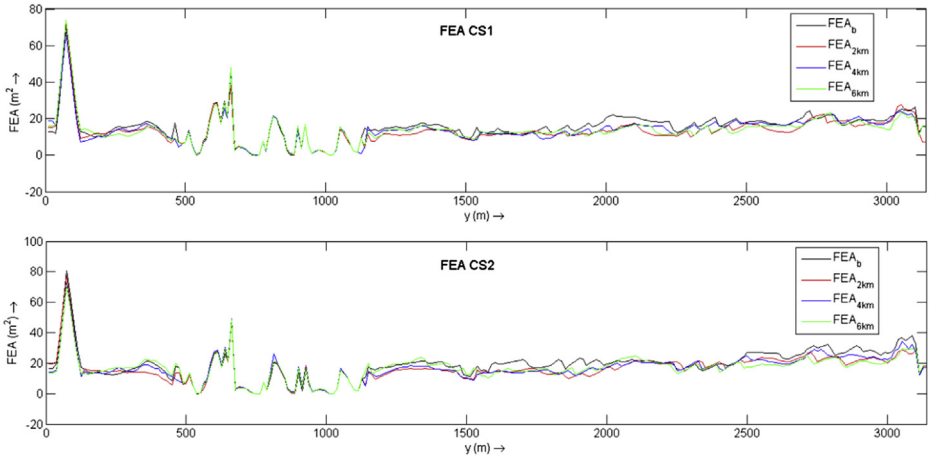

Fig. 10. Beach face eroded area in the following scenarios: baseline (FEA_b) and with the wave farm at a distance of 2 km ($FEA_{2\ km}$), 4 km ($FEA_{4\ km}$) and 6 km ($FEA_{6\ km}$) along Perranporth Beach (y – coordinate, with y increasing towards the north of the beach) at the end of the storm in CS1 (above) and CS2 (below).

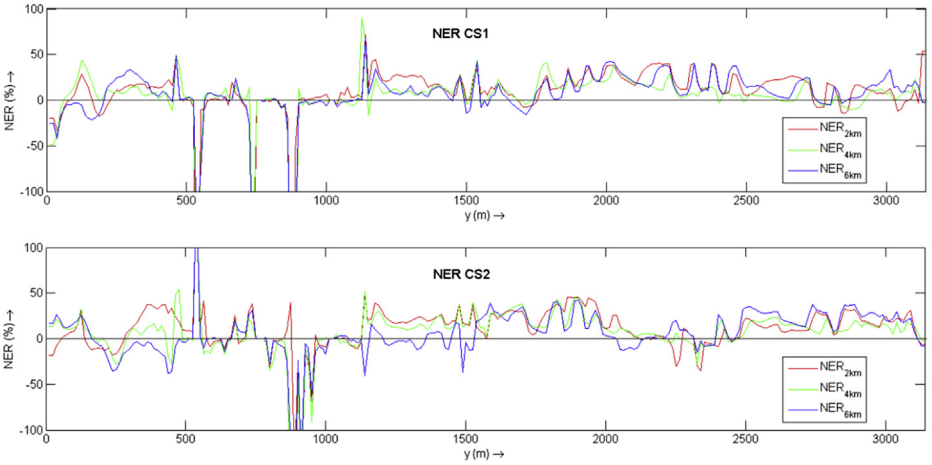

Fig. 11. Non-dimensional erosion reduction (NER) at the beach face in the following scenarios: with the wave farm at a distance of 2 km ($NER_{2\ km}$), 4 km ($NER_{4\ km}$) and 6 km ($NER_{6\ km}$) along Perranporth Beach (y-coordinate, with y increasing towards the north of the beach) at the end of the storm in CS1 (above) and CS2 (below).

A previous study conducted by Abanades et al. [49] analysed the applicability of a wave farm to coastal defence. The present work, while confirming the suitability of wave farms as a coastal defence means, considers for the first time the influence of the farm-to-coast distance. By proving the importance of this parameter and giving quantitative data on the variation of the beach morphodynamics induced by the wave farm at different distances, this work contributes to the applicability of wave farms to coastal defence. Furthermore, wave farms present the following advantages versus traditional measures of coastal protection: (i) the generation of carbon-free electricity – their main purpose, with coastal defence as a secondary benefit; and (ii) in the case of floating WECs such as WaveCat, the effectiveness of the wave farm is not affected by sea level change.

4. Conclusions

The role played by the distance in the impact of a wave farm on the beach morphology was analysed in this paper. To investigate this, a wave farm formed by 11 WECs was located at different distances: 2 km, 4 km and 6 km from a reference (10 m water depth) contour in a high-resolution suite of numerical models. This suite consisted of a nearshore wave model coupled to a coastal processes model, which allowed the impacts of the wave farm on wave conditions and coastal processes to be assessed.

The wave farm extracted energy from the waves, which was characterised by means of wave transmission coefficients that were obtained in laboratory tests. The comparison between the baseline and the wave farm scenarios showed the importance of the farm-to-coast distance, given that, depending on the location, the area affected by the farm and the magnitude of the wave height reduction varied considerably. In the case of the wave farm at a distance of 6 km, the impact of the farm covered an area of 7 km along the coast but the reduction of the significant wave height at a water depth of 10 m was less than 10%; nonetheless, the area affected by the wave farm closest to the farm was 4 km and the reduction approx. 25% due to less energy being diffracted into the shadow of the farm situated closer to the beach.

The impact of the wave farm on the wave conditions resulted in an alteration of the coastal processes nearshore, and therefore, of the beach morphology. To quantify this, a suite of impact indicators was developed and applied to the results of the different scenarios. The reduction of the erosion brought about by the different wave farms was mainly in two areas of the beach: (i) the area at a water depth of approx. 3 m, which faced the storms during the low tide; and (ii) the beach face of the beach. Whereas in the former, the

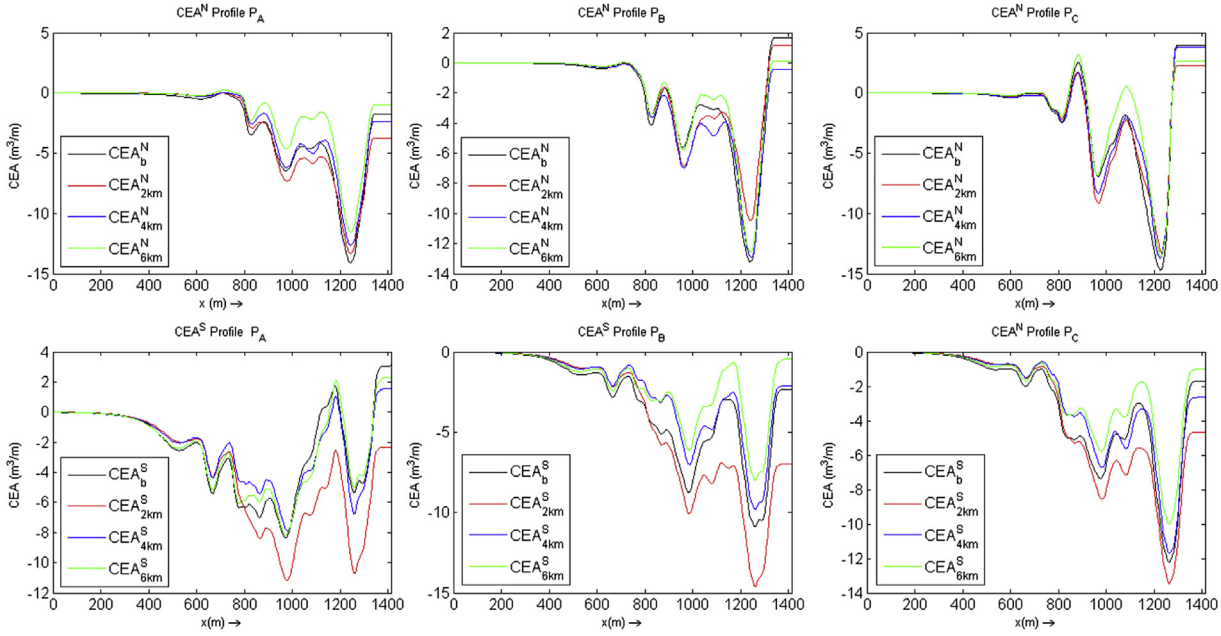

Fig. 12. Mean cumulative eroded area in the baseline scenario (CEA_b) and in presence of the wave farm at a distance of 2 km ($CEA_{2\ km}$), 4 km ($CEA_{4\ km}$) and 6 km ($CEA_{6\ km}$) from the reference (10 m water depth) contour in the northern area (above) and southern (below) across each of the reference profiles P_A, P_B and P_C (Fig. 4) at the end of the storm in CS1. The *x*-coordinate represents the distance along the profile, with $x = 0$ the most offshore point. (For interpretation of the references to colour in this figure legend, the reader is referred to the web version of this article.)

reduction did not exceed 0.5 m, in the latter it reached 1.5 m. In the comparison between scenarios, the wave farm at 2 km offered greater reductions of the erosion than the farm at 4 and 6 km, which presented similar responses. The overall reduction of the erosion on the beach face compared to the baseline scenario was 15% for the closest wave farm and approx. 10% for the other two. These values fluctuated significantly along the beach, and in some sections, especially in the northern area of the beach, exceeded 40%.

Lastly, it was also found that the wave farm may change the distribution of sediment along the beach. The alteration of the wave conditions with the farm at 2 km modified the sediment transport patterns, increasing the volume of material moved to the southern area of the beach. This confirmed that the effects on the beach morphology of the wave farm closest to the coast were more pronounced than in the other scenarios; nevertheless, the overall wave resource in this area was 10% less than with the case with the furthest farm (6 km) due to the attenuation of wave energy caused by the coastal processes that occur in shallow waters. When comparing the scenarios at 4 km and 6 km, the impact on the beach morphology did not present significant differences but there were differences in the overall resource at the wave farm: 8% less at 4 km than at 6 km.

In summary, the selection of the location for a wave farm is not trivial. This work proved that the degree of coastal protection afforded by a wave farm varies significantly as a function of its distance to the coastline. On these grounds, the effects of the wave farm on the coast ought to be one of the main considerations (alongside the energy resource) in this selection, not least in areas subject to erosion risks, where the wave farms can contribute considerably to its mitigation.

Acknowledgements

This research was carried out in the framework of the Atlantic Power Cluster Project, funded by the Atlantic Arc Programme of the European Commission (Atlantic Area Project 2011-1/151, ATLANTICPOWER) and the School of Marine Sciences and Engineering of Plymouth University. The authors are grateful to the Coastal Channel Observatory and DIGIMAP for providing the data.

References

[1] Stoutenburg ED, Jenkins N, Jacobson MZ. Power output variations of co-located offshore wind turbines and wave energy converters in California. Renew Energy 2010;35:2781–91.
[2] Stopa JE, Cheung KF, Chen Y-L. Assessment of wave energy resources in Hawaii. Renew Energy 2011;36:554–67.
[3] Pontes M, Athanassoulis G, Barstow S, Cavaleri L, Holmes B, Mollison D, et al. WERATLAS–Atlas of wave Energy resource in Europe. In: Report to the european commission, JOULE II programme; 1996. p. 96.
[4] Pontes M, Athanassoulis G, Barstow S, Bertotti L, Cavaleri L, Holmes B, et al. The european wave energy resource. In: 3rd european wave energy conference, Patras, Greece; 1998.
[5] Liberti L, Carillo A, Sannino G. Wave energy resource assessment in the Mediterranean, the Italian perspective. Renew Energy 2013;50:938–49.
[6] Gonçalves M, Martinho P, Guedes Soares C. Wave energy conditions in the western French coast. Renew Energy 2014;62:155–63.
[7] Defne Z, Haas KA, Fritz HM. Wave power potential along the Atlantic coast of the southeastern USA. Renew Energy 2009;34:2197–205.
[8] Bernhoff H, Sjöstedt E, Leijon M. Wave energy resources in sheltered sea areas: a case study of the Baltic Sea,. Renew Energy 2006;31:2164–70.
[9] Iglesias G, Carballo R. Wave energy potential along the Death Coast (Spain). Energy 2009;34:1963–75.
[10] Vicinanza D, Contestabile P, Ferrante V. Wave energy potential in the north-west of Sardinia (Italy). Renew Energy 2013;50:506–21.
[11] Rusu L, Guedes Soares C. Wave energy assessments in the Azores islands. Renew Energy 2012;45:183–96.
[12] Veigas M, Ramos V, Iglesias G. A wave farm for an island: detailed effects on the nearshore wave climate. Energy.
[13] Iglesias G, Carballo R. Offshore and inshore wave energy assessment: Asturias (N Spain). Energy 2010;35:1964–72.
[14] Carballo R, Sánchez M, Ramos V, Taveira-Pinto F, Iglesias G. A high resolution geospatial database for wave energy exploitation,. Energy 2014;68:572–83.
[15] Guedes Soares C, Bento AR, Gonçalves M, Silva D, Martinho P. Numerical evaluation of the wave energy resource along the Atlantic European coast. Comput Geosci 2014:7137–49.
[16] Gonçalves M, Martinho P, Guedes Soares C. Assessment of wave energy in the Canary Islands. Renew Energy 2014;68:774–84.
[17] Folley M, Whittaker T. Analysis of the nearshore wave energy resource. Renew Energy 2009;34:1709–15.

[18] Wolgamot HA, Taylor PH, Eatock Taylor R. The interaction factor and directionality in wave energy arrays. Ocean Eng 2012;47:65–73.
[19] Thorpe TW. A brief review of wave energy,. Harwell Laboratory, Energy Technology Support Unit; 1999.
[20] Tedd J, Kofoed JP. Measurements of overtopping flow time series on the wave dragon, wave energy converter. Renew Energy 2009;34:711–7.
[21] Pelc R, Fujita RM. Renewable energy from the ocean. Mar Policy 2002;26:471–9.
[22] Drew B, Plummer A, Sahinkaya MN. A review of wave energy converter technology, Proc Inst Mech Eng Part A: J Power Energy 2009;223:887–902.
[23] Kofoed JP, Frigaard P, Friis-Madsen E, Sørensen HC. Prototype testing of the wave energy converter wave dragon. Renew Energy 2006;31:181–9.
[24] Falcão AFO, Justino PAP. OWC wave energy devices with air flow control. Ocean Eng 1999;26:1275–95.
[25] Falcão AFO. Wave-power absorption by a periodic linear array of oscillating water columns. Ocean Eng 2002;29:1163–86.
[26] El Marjani A, Castro Ruiz F, Rodriguez MA, Parra Santos MT. Numerical modelling in wave energy conversion systems. Energy 2008;33:1246–53.
[27] Fernandez H, Iglesias G, Carballo R, Castro A, Fraguela JA, Taveira-Pinto F, et al. The new wave energy converter WaveCat: concept and laboratory tests,. Mar Struct 2012;29:58–70.
[28] López I, Pereiras B, Castro F, Iglesias G. Optimisation of turbine-induced damping for an OWC wave energy converter using a RANS–VOF numerical model. Appl Energy 2014;127:105–14.
[29] López I, Iglesias G. Efficiency of OWC wave energy converters: a virtual laboratory,. Appl Ocean Res 2014;44:63–70.
[30] Rusu E, Guedes Soares C. Coastal impact induced by a Pelamis wave farm operating in the Portuguese nearshore. Renew Energy 2013;58:34–49.
[31] Palha A, Mendes L, Fortes CJ, Brito-Melo A, Sarmento A. The impact of wave energy farms in the shoreline wave climate: Portuguese pilot zone case study using Pelamis energy wave devices,. Renew Energy 2010;35:62–77.
[32] Reeve DE, Chen Y, Pan S, Magar V, Simmonds DJ, Zacharioudaki A. An investigation of the impacts of climate change on wave energy generation: the Wave Hub, Cornwall, UK,. Renew Energy 2011;36:2404–13.
[33] Beels C, Troch P, De Backer G, Vantorre M, De Rouck J. Numerical implementation and sensitivity analysis of a wave energy converter in a time-dependent mild-slope equation model. Coast Eng 2010;57:471–92.
[34] Monk K, Zou Q, Conley D. An approximate solution for the wave energy shadow in the lee of an array of overtopping type wave energy converters. Coast Eng 2013;73:115–32.
[35] Smith HCM, Pearce C, Millar DL. Further analysis of change in nearshore wave climate due to an offshore wave farm: an enhanced case study for the Wave Hub site. Renew Energy 2012;40:51–64.
[36] Millar DL, Smith HCM, Reeve DE. Modelling analysis of the sensitivity of shoreline change to a wave farm. Ocean Eng 2007;34:884–901.
[37] Mendoza E, Silva R, Zanuttigh B, Angelelli E, Lykke Andersen T, Martinelli L, et al. Beach response to wave energy converter farms acting as coastal defence. Coast Eng 2013.
[38] Zanuttigh B, Angelelli E. Experimental investigation of floating wave energy converters for coastal protection purpose. Coast Eng 2013;80:148–59.
[39] Bento AR, Rusu E, Martinho P, Guedes Soares C. Assessment of the changes induced by a wave energy farm in the nearshore wave conditions. Comput Geosci 2014;71(0):50–61.
[40] Boehlert GW, Gill AB. Environmental and ecological effects of ocean renewable energy development: a current synthesis. 2010.
[41] Babarit A. Impact of long separating distances on the energy production of two interacting wave energy converters. Ocean Eng 2010;37:718–29.
[42] Babarit A. On the park effect in arrays of oscillating wave energy converters. Renew Energy 2013;58:68–78.
[43] Vidal C, Méndez Fernando J, Díaz G, Legaz R. Impact of Santoña WEC installation on the littoral processes. In: Proceedings of the 7th European wave and tidal energy conference, Porto, Portugal; 2007.
[44] Iglesias G, Carballo R. Choosing the site for the first wave farm in a region: a case study in the Galician Southwest (Spain). Energy 2011;36:5525–31.
[45] Iglesias G, Carballo R. Wave energy and nearshore hot spots: the case of the SE Bay of Biscay,. Renew Energy 2010;35:2490–500.
[46] Carballo R, Iglesias G. Wave farm impact based on realistic wave-WEC interaction. Energy 2013.
[47] Iglesias G, Carballo R. Wave farm impact: the role of farm-to-coast distance,. Renew Energy 2014;69:375–85.
[48] Abanades J, Greaves D, Iglesias G. Wave farm impact on the beach profile: a case study,. Coast Eng 2014;86:36–44.
[49] Abanades J, Greaves D, Iglesias G. Coastal defence through wave farms. Coast Eng 2014;91:299–307.
[50] Booij N, Holthuijsen L, Ris R. The "SWAN" wave model for shallow water, in: coastal engineering conference. ASCE Am Soc Civ Eng 1996:668–76.
[51] Roelvink J, Reniers A, Van Dongeren A, Van Thiel de Vries J, Lescinski J, McCall R. XBeach model description and manual. In: UNESCO-IHE Institute for Water Education; 2006.
[52] Thorpe T. The wave energy programme in the UK and the European wave energy network. 2001.
[53] CISCAG, Shoreline. Management Plan in, Cornwall and Isles of Scilly coastal Advisory group. 2011.
[54] Martinelli L, Ruol P, Zanuttigh B. Wave basin experiments on floating breakwaters with different layouts. Appl Ocean Res 2008;30:199–207.
[55] Holthuijsen LH. Waves in oceanic and coastal waters. Cambridge University Press; 2007.
[56] Rusu E, Gonçalves M, Guedes Soares C. Evaluation of the wave transformation in an open bay with two spectral models. Ocean Eng 2011;38:1763–81.
[57] Iglesias G, Carballo R, Castro A, Fraga B. Development and design of the WaveCat™ energy converter. Coast Eng 2008:3970–82.
[58] Kenney J. SW Wave Hub metocean design basis. SWRDA. (Online). Available from: 2009.
[59] Galappatti G, Vreugdenhil C. A depth-integrated model for suspended sediment transport,. J Hydraul Res 1985;23:359–77.
[60] Baldock TE, Alsina JA, Caceres I, Vicinanza D, Contestabile P, Power H, et al. Large-scale experiments on beach profile evolution and surf and swash zone sediment transport induced by long waves, wave groups and random waves. Coast Eng 2011;58:214–27.
[61] Van Thiel de Vries J. Dune erosion during storm surges. Delft University of Technology; 2009.
[62] Roelvink D, Reniers A, van Dongeren A, van Thiel de Vries J, McCall R, Lescinski J. Modelling storm impacts on beaches, dunes and barrier islands. Coast Eng 2009;56:1133–52.
[63] McCall RT, Van Thiel de Vries JSM, Plant NG, Van Dongeren AR, Roelvink JA, Thompson DM, et al. Two-dimensional time dependent hurricane overwash and erosion modeling at Santa Rosa Island. Coast Eng 2010;57:668–83.
[64] Pender D, Karunarathna H. A statistical-process based approach for modelling beach profile variability,. Coast Eng 2013;81:19–29.
[65] Williams JJ, de Alegría-Arzaburu AR, McCall RT, Van Dongeren A. Modelling gravel barrier profile response to combined waves and tides using XBeach: laboratory and field results. Coast Eng 2012;63:62–80.
[66] McCall RT, Masselink G, Roelvink D, Russell P, Davidson M, Poate T. Modelling overwash and infiltration on gravel barriers. 2012.
[67] McCall R, Masselink G, Poate T, Bradbury A, Russell P, Davidson M. Predicting overwash on gravel barriers. 2013.
[68] Jamal MH, Simmonds DJ, Magar V. Modelling gravel beach dynamics with XBeach. Coast Eng 2014;89:20–9.
[69] Austin M, Scott T, Brown J, Brown J, MacMahan J, Masselink G, et al. Temporal observations of rip current circulation on a macro-tidal beach. Cont Shelf Res 2010;30:1149–65.
[70] Masselink G, Short AD. The effect of tide range on beach morphodynamics and morphology: a conceptual beach model. J Coast Res 1993:785–800.

Marine Geology 361 (2015) 126–135

Contents lists available at ScienceDirect

Marine Geology

journal homepage: www.elsevier.com/locate/margeo

Wave farm impact on beach modal state

J. Abanades *, D. Greaves, G. Iglesias

Plymouth University, School of Marine Science and Engineering, Marine Building, Drake Circus, Plymouth PL4 8AA, UK

ARTICLE INFO

Article history:
Received 16 October 2014
Received in revised form 14 January 2015
Accepted 24 January 2015
Available online 28 January 2015

Keywords:
wave energy
wave farm
nearshore impact
beach morphology
conceptual beach model
sediment transport

ABSTRACT

The extraction of wave energy by the Wave Energy Converters (WECs) forming a wave farm results in a milder wave climate in its lee, which can have an impact on coastal processes. The objective of this work is to determine whether the beach morphology can be altered by the operation of the wave farm, and if so, to quantify this alteration. For this purpose, we examine how the farm affects the modal state of the beach with reference to a baseline (no farm) scenario. The modal state is defined based on an empirical classification that accounts for wave conditions, tidal regime and sediment size. As a beach typically goes through different modal states, we determine the percentages of time in an average year corresponding to each state in the baseline scenario, and how these percentages are altered by a wave farm as a function of its distance from the coast. This methodology is illustrated through a case study: Perranporth Beach (UK), an area of great potential for wave energy development. High-resolution numerical modelling is used, with two levels of grid refinement. We find that the wave farm has a relevant impact on the modal state of the system, which passes from wave-dominated to tide-dominated during significant periods of time. The sensitivity analysis, involving three cases with the farm at distances of 2 km, 4 km and 6 km from the beach, showed that the farm-to-coast distance plays a major role. Thus, the shift from a wave- to a tide-dominated beach is exacerbated in the case of the wave farm closest to the coastline, with the submarine bar vanishing over long periods of time. We conclude that the presence of the wave farm drastically alters the morphological response of the beach, and that this alteration is strongly dependent on the farm-to-coast distance.

1. Introduction

Wave energy is poised to become one of the major renewable energies in a number of coastal regions around the world (Bernhoff et al., 2006; Carballo et al., 2014; Cornett, 2008; Defne et al., 2009; Gonçalves et al., 2014; Iglesias and Carballo, 2010a; Iglesias et al., 2009c; Lenee-Bluhm et al., 2011; Liberti et al., 2013; Stopa et al., 2011; Veigas et al., 2014a; Veigas and Iglesias, 2013, 2014; Vicinanza et al., 2013). The influence of wave energy extraction by the Wave Energy Converters (WECs) forming a wave farm on the nearshore wave conditions was recently shown by different authors (Carballo and Iglesias, 2013; Iglesias and Carballo, 2014; Mendoza et al., 2014; Millar et al., 2007; Palha et al., 2010; Ruol et al., 2011; Smith et al., 2012; Veigas et al., 2014b,c; Vidal et al., 2007; Zanuttigh and Angelelli, 2013). Abanades et al. (2014b) proved that this extraction resulted in a medium-term reduction of the erosion exceeding 20% in some sections of the beach profile (2D). In further studies, Abanades et al. (2014a, 2015) considered the 3D response of the beach under storm conditions in order to establish the applicability of wave farms to coastal defence. Erosion was found to decrease by more than 50% in certain areas of the beach. In the wake of these studies, which evidence the impact of wave farms on beach morphology, the question arises as to whether a wave farm can modify the modal state of a beach, and, if so, in what manner.

The objective of the present study is to answer this fundamental question by means of a case study: Perranporth Beach (UK). To quantify the effects of the wave farm on the modal state of the beach, scenarios with and without the farm were compared and the percentage of time corresponding to the different modal states during the period from 1st of November 2007 to 31st of October 2008 was determined. In addition, the seasonal variability: "winter" (Nov–Apr) vs "summer" (May–Oct) was also examined. The modal states were established following the empirical classification presented by Masselink and Short (1993), based on Wright and Short (1984). The modal states vary as a function of the wave climate (breaking wave height and peak period), the beach sediment characteristics (sediment fall velocity) and the tidal regime (mean spring tidal range).

The effects of the wave farm on the coast are characterised using a wave propagation model, SWAN (Booij et al., 1996). The wave farm, which consists of eleven WaveCat WECs arranged in two rows, is implemented on a high-resolution grid so as to accurately resolve the wakes of the individual WECs, and hence that of the wave farm as a whole. Four scenarios are examined: three with the wave farm at different distances from a reference contour (10 m water depth): 2 km, 4 km and 6 km, following Abanades et al. (2015), plus the baseline scenario (without the wave farm). Thanks to the three distances considered it

* Corresponding author.
E-mail address: javier.abanadestercero@plymouth.ac.uk (J. Abanades).

http://dx.doi.org/10.1016/j.margeo.2015.01.008
0025-3227/

is possible to analyse the role of the farm-to-coast distance in the impact on the beach morphology. The WEC–wave field interaction is modelled by means of the wave transmission coefficient, obtained through laboratory tests as reported by Fernandez et al. (2012). The numerical model, successfully validated with wave buoy data, is used to calculate the wave conditions and on this ground establish the modal state of the beach.

The understanding and modelling of beaches are essential to coastal management (Budillon et al., 2006; Cowell et al., 1995; De Vriend et al., 1993; Hughes et al., 2014; Iglesias et al., 2009a,b; Ortega-Sánchez et al., 2014; Ortega Sanchez et al., 2003; Poate et al., 2014). In the case of Perranporth, the beach was described as dissipative (Butt et al., 2001; Masselink et al., 2005) and as a low-tide bar rip system (Scott et al., 2007, 2011), with Austin et al. (2010) indicating that it is at the transition between the low tide bar/rip and dissipative beach. In this context, the characterisation obtained in the present work contributes to understanding the behaviour of Perranporth by providing quantitative estimates of its morphodynamical variability throughout a year.

2. Material and methods

2.1. Conceptual beach model

The conceptual beach classifications are empirical models based on the relationships between the characteristics of different types of beaches (wave climate, sediment size and tidal regime) and field observations. Therefore, these models allow the evolution of beach dynamics as a function of the beach features to be predicted, and also, the quantification of the potential changes induced by a modification of these, such as the reduction of wave energy brought about by a wave farm.

The classification presented by Wright and Short (1984), also called the Australian beach model, is based on the field observations collected in Australia for microtidal beaches. This classification indicates the prevailing conditions in the surf zone: dissipative, intermediate or reflective, as a function of the dimensionless fall velocity parameter (Ω), also known as the Dean's number (Dean, 1973),

$$\Omega = \frac{H_b}{w_s T} \tag{1}$$

where H_b is the breaking wave height, T is the wave peak period corresponding to the breaking conditions and w_s is the sediment fall velocity, which is defined for the present paper according the Shore Protection Manual (US Army Corps Of Engineers, 1984),

$$B = \left(\frac{\gamma_s}{\gamma_w} - 1\right)\frac{gD_{50}^3}{\nu^2} \tag{2}$$

$$w_s = \begin{cases} \left(\frac{\gamma_s}{\gamma_w} - 1\right)\frac{gD_{50}^2}{18\nu}; & B < 39, \\ \left(\frac{\gamma_s}{\gamma_w} - 1\right)^{0.7}\frac{g^{0.7}D_{50}^{1.1}}{6\nu^{0.4}}; & 39 < B < 10^4 \\ \left[\left(\frac{\gamma_s}{\gamma_w} - 1\right)\frac{gD_{50}}{0.91}\right]^{0.5}; & B > 10^4 \end{cases} \tag{3}$$

where γ_s and γ_w are the densities of the sediment and water, respectively, g the gravitational acceleration, D_{50} the sediment grain size and ν the fluid kinematic viscosity.

This model represents the evolution of microtidal beaches well; however, it does not account for the influence of the tide on the swash, surf zone and shoaling wave processes (Davis and Hayes, 1984). This was corrected with the introduction of a new parameter: the relative tide range (RTR), which allows the characterisation of all wave-dominated beaches in all tidal ranges (Masselink and Short, 1993):

$$RTR = \frac{MSR}{H_b}, \tag{4}$$

where MSR is the mean spring tidal range.

Fig. 1 shows the relationships between the dimensionless fall velocity and the relative tide range parameters that are used to establish the modal beach state. As the RTR parameter increases the beach evolves from a classic reflective state through the formation of a low tide terrace at the toe of the beach face and low tide rips to a steep beach face fronted by a dissipative low tide terrace. In the case of an intermediate barred beach, the increase in the tidal range moves the bar down to the low tide level generating a low tide bar and rips. Finally, for barred dissipative beaches characterised by multiple subdued bars at different water depths, the increase of RTR results in the disappearance of these bars. The latter two groups shift to ultra-dissipative beaches with values of RTR between 7 and 15. For values of RTR greater than 15 the resulting beach is fully tide-dominated.

2.2. Case study: Perranporth Beach

The characterisation of the changes induced by a wave farm in the morphodynamical behaviour of a beach is conducted at Perranporth Beach (Fig. 2), a prospective site for wave energy exploitation for its prime location on the Atlantic façade of Europe, which has been highlighted for its wave energy resource (Guedes Soares et al., 2014; Iglesias and Carballo, 2009, 2010b, 2011; Pontes et al., 1996). An example of this potential is the Wave Hub project (Gonzalez-Santamaria et al., 2013; Reeve et al., 2011), a grid-connected offshore facility for sea tests of WECs, located in SW England. In addition to its wave energy potential, a further reason for choosing Perranporth is that this beach, facing directly the North Atlantic Ocean, has experienced increased erosion due to rising sea level and storminess — as corroborated by the extremely energetic storms of February 2014. Therefore, this would be a prime area for using a wave farm to control the storm-induced erosion (Abanades et al., 2014a,b, 2015).

Perranporth is an approx. 4 km beach composed by a medium sand size, $D_{50} = 0.27$–0.29 mm, and characterised by a low intertidal slope, $\tan\beta = 0.015$–0.025. In the present study, the offshore bathymetric data, from the UK data centre Digimap, and the beach profile data, obtained through field survey by the Coastal Channel Observatory, are implemented onto the wave propagation model. In the three beach profiles selected to determine the beach modal state the relevant features can be readily observed (Fig. 3): a submarine bar at a water depth between 5 and 10 m and a well-developed dune system that backs the landward end of the beach. The latter aspect does not play a role in the modal state, which only considers the intertidal area, but the bar system does — and is indicative of a dissipative or intermediate state. In the case of profile P3, two submarine bars are distinct — typical of a barred dissipative state.

As regards the wave conditions, wave buoy data are used in conjunction with hindcast data to force the wave propagation model. Hindcast data from WaveWatch III, a third-generation offshore wave model consisting of global and regional nested grids with a resolution of 100 km (Tolman, 2002), are used to prescribe the offshore boundary conditions. The validation is carried out with the wave buoy located off Perranporth Beach at a water depth of approx. 10 m. The average values of the significant wave height, peak period and direction from November 2007 to October 2008 were 1.60 m, 10.37 s and 282.59°, respectively. Dividing this period into "winter" (Nov–Apr) and "summer" (May–Oct) to analyse the seasonal variability of the beach, the values in "winter" of the significant wave height, peak period and direction were 1.98 m, 11.30 s and 285.23°, respectively, and in "summer" 1.32 m, 9.62 s and 279.95°.

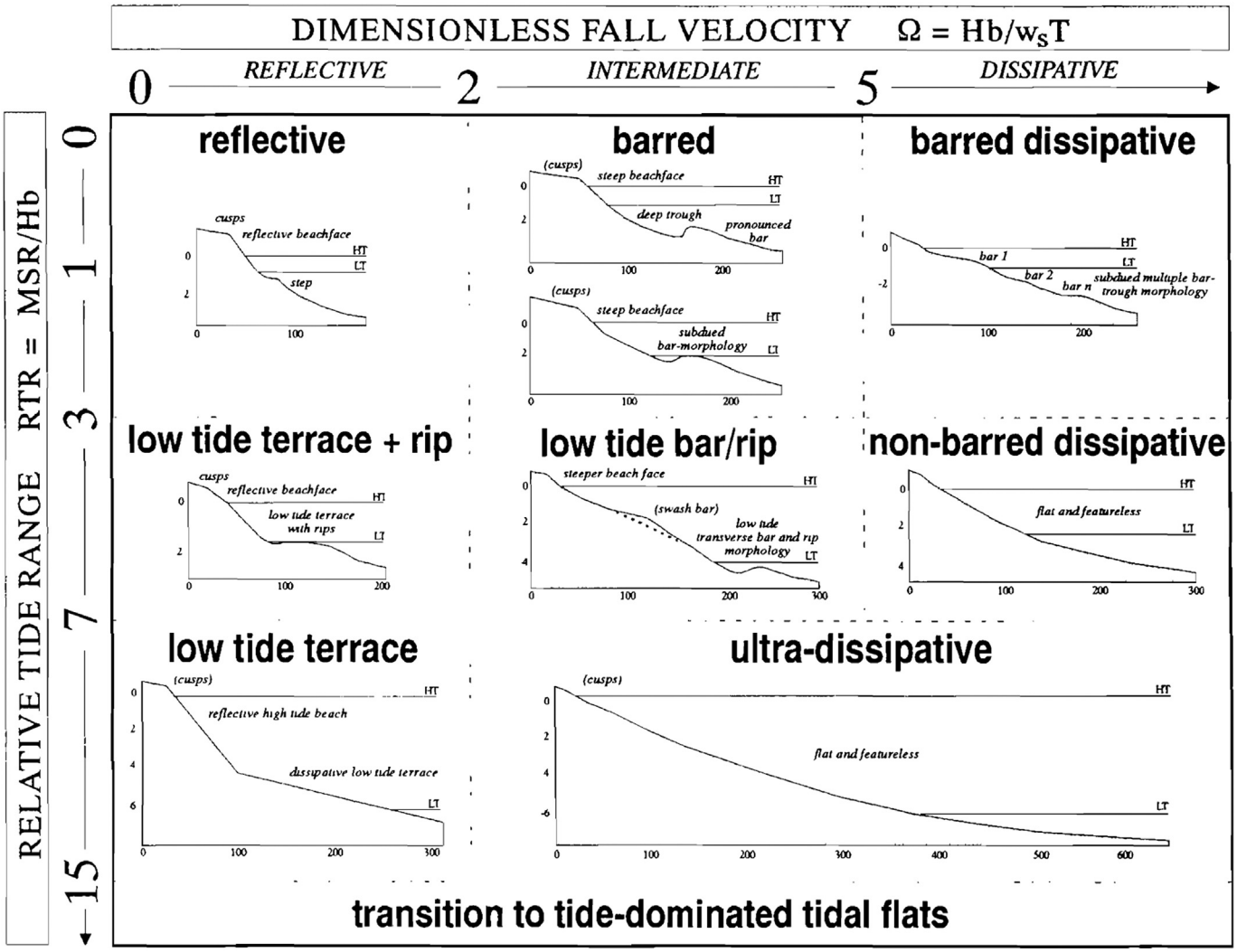

Fig. 1. Conceptual beach model (Masselink and Short, 1993).

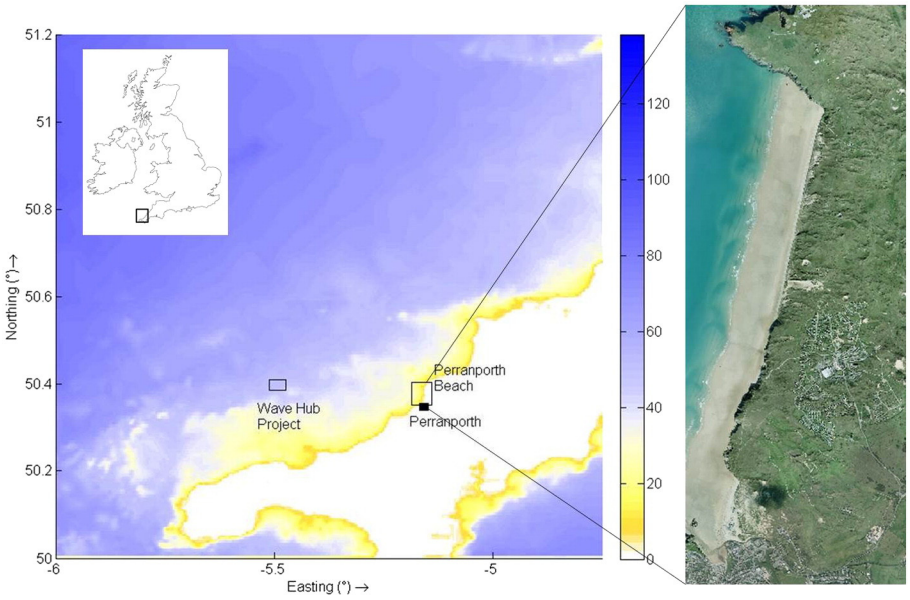

Fig. 2. Bathymetry of SW England [water depths in m] including the location of Perranporth Beach, the WaveHub Project and an aerial photo of Perranporth Beach. Source: Coastal Channel Observatory.

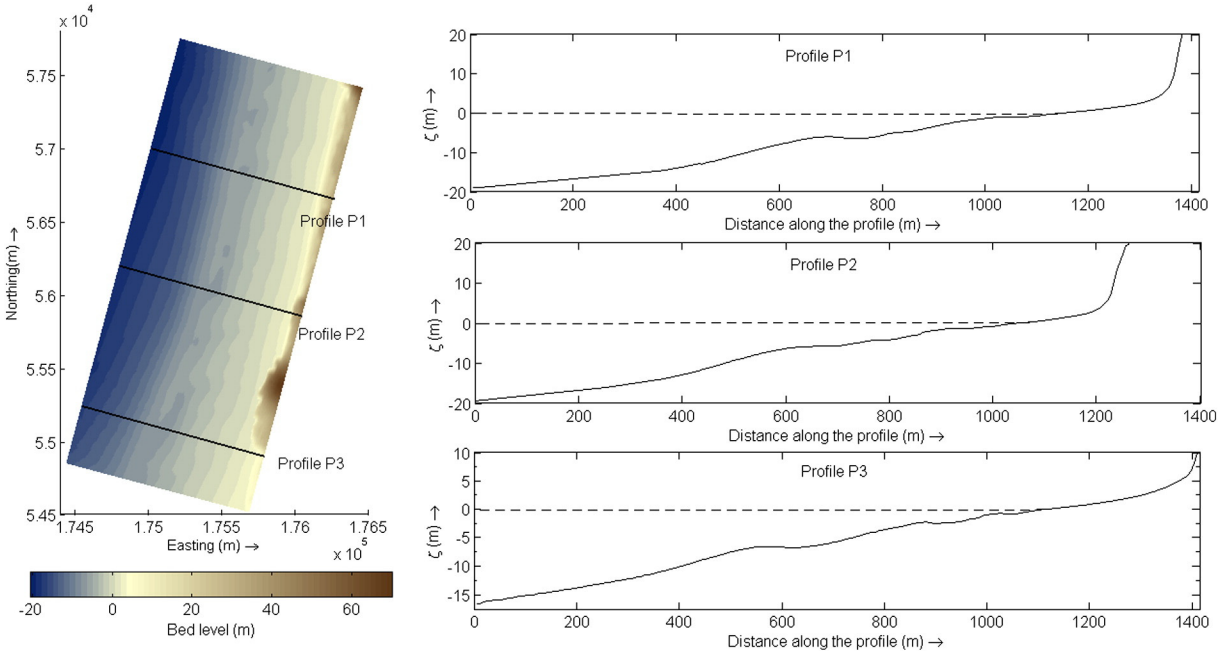

Fig. 3. Three different profiles at Perranporth Beach and their respective localisation. Water depth in relation to local chart datum [in m].

Wind data from the Global Forecast System (GFS) weather model are also used as input of the wave model. In the period covered in the study the mean wind velocity magnitude at a height of 10 m above the sea surface (u_{10}) was 8.46 ms^{-1}. Strictly speaking there is no prevailing direction for the wind but the strongest winds, with velocities over 20 ms^{-1} come from the quarter between NE to NW.

Finally, the tide is also included in the model. As mentioned in the Introduction section, the large tidal range typical of SW England has a considerable effect on the beach morphodynamics. Perranporth is a macrotidal beach ($MSR = 6.3$ m) characterised by a semidiurnal regime.

2.3. Wave propagation model

The wave propagation is carried out using SWAN, a third-generation phase-averaged wave model for the simulation of waves in waters of deep, intermediate and shallow depth. SWAN computes the evolution of the wave spectrum based on the spectral wave action balance equation,

$$\frac{\partial N}{\partial t} + \nabla \cdot \left(\vec{c} N\right) + \frac{\partial (c_\theta N)}{\partial \theta} + \frac{\partial (c_\sigma N)}{\partial \sigma} = \frac{S}{\sigma} \tag{5}$$

where N is the wave action density, t the time, $\vec{c}$ the propagation velocity in the geographical space, θ the wave direction, σ the relative frequency, and c_θ and c_σ the propagation velocity in the θ- and σ-space, respectively. The rate of change of wave action in time is given by the first term of Eq. (1), the second term represents the spatial propagation of wave action and the third and fourth terms stand for the refraction and changes in the relative frequencies respectively induced by depth and currents. Finally, on the right-hand side, S is the source term and represents the generation and dissipation of energy density by the different processes involved.

A high-resolution grid is essential in this work in order to: (i) implement the WECs that formed the wave farm in their exact position, (ii) represent accurately the impact of the wave farm on the wave conditions in its lee, and (iii) determine the wave conditions to establish the morphodynamical state of the beach. On this basis, two computational grids are defined (Fig. 4): (i) an offshore grid covering approx. 100 km × 50 km with a grid size of 400 × 200 m, and (ii) a high-resolution nearshore (nested) grid covering the study area, with dimensions of approx. 8 km × 6 km and a grid size of 16 m × 12 m.

The wave farm consists of 11 WaveCat WECs arranged in two rows, with a spacing between devices equal to 2.2D, where $D = 90$ m is the distance between the twin bows of a single WaveCat WEC. The farm was located at distances of 2 km, 4 km, and 6 km (Fig. 5) from a reference contour (10 m water depth), which corresponds to water depths of approx. 25 m, 30 m and 35 m, respectively (Carballo and Iglesias, 2013; Iglesias and Carballo, 2014). The WEC–wave field interaction is modelled by means of the results obtained for the wave transmission coefficient in the lee of the device in the laboratory tests carried out by Fernandez et al. (2012). Compared with wave transmission, diffraction plays a minor role in analysing the effects of the WECs on the beach — the distance between the WECs and the reference 10 m contour (2000 m, 4000 m and 6000 m) being one order of magnitude larger than the width of the WECs (90 m). Therefore, the approximate solution of diffraction implemented on SWAN is sufficient for our purposes in this work.

The resource available is compared between the different scenarios through the average wave power of the wave farm, $\overline{J}$, in units of Wm^{-1} in the SI,

$$\overline{J} = \frac{\sum_{n=1}^{N} \sum_{t=1}^{T} (J_n)_t}{T}, \tag{6}$$

where the index n represents a generic WEC of the wave farm, N is the total number of WECs (11), t a point in time, T the total number of time points studied (1 year) and $(J_n)_t$ the wave power at the n-WEC location at the t point of time, which is computed in SWAN as

$$J = \int_0^{2\pi} \int_0^{360} \rho g c E(\sigma, \theta)\, d\sigma\, d\theta, \tag{7}$$

where ρ is the water density, g is the acceleration due to gravity, and $E(\sigma, \theta)$ is the directional spectral density, which specifies how the energy is distributed over frequencies (σ) and directions (θ).

The effects caused by the farm in the different scenarios are assessed by means of the average relative nearshore impact, $\overline{RNI}$

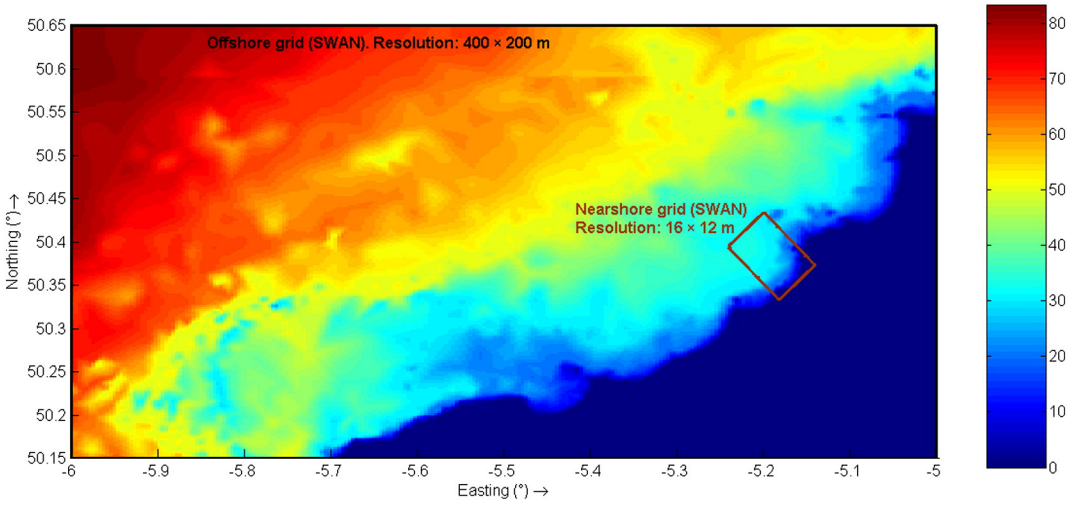

Fig. 4. Computational grids of the wave propagation and the coastal processes model [water depths in m].

(Iglesias and Carballo, 2014), a non-dimensional impact indicator defined by

$$\overline{RNI}_i = \frac{1}{T}\frac{1}{S}\sum_{t=1}^{T}\sum_{s=1}^{S}\frac{J^{20}{}_b(s,t) - J^{20}{}_{f,i}(s,t)}{J^{20}{}_b(s,t)}, \tag{8}$$

where $J^{20}{}_{f,i}(s,t)$ is the wave power in the presence of the farm at a generic point (s) of the 20 m contour at a point of time (t), with the subindex i indicating the farm-to-coast distance ($i = 2$ km, 4 km or 6 km) and $J^{20}{}_b(s,t)$ is the baseline wave power (without the farm) at the same point, with S and T the total number of points along the contour and in time, respectively.

Finally, the wave conditions necessary to establish the morphological beach state – breaking wave height (H_b) and peak period (T_p) – are determined coupling the results from SWAN to the Kamphuis' formulae (Kamphuis, 1991), a breaking criterion for irregular waves based on the following expressions:

$$H_{sb} = 0.095 e^{4m} L_{bp} \tanh\left(\frac{2\Pi d_b}{L_{bp}}\right) \quad , \text{ and} \tag{9}$$

$$\frac{H_{sb}}{d_b} = 0.56 e^{3.5m} \quad , \tag{10}$$

where H_{sb} represents the breaking significant wave height, m the beach slope, L_{bp} the breaking wave length and d_b the breaking water depth. Once the breaking wave height was determined, the corresponding period was selected.

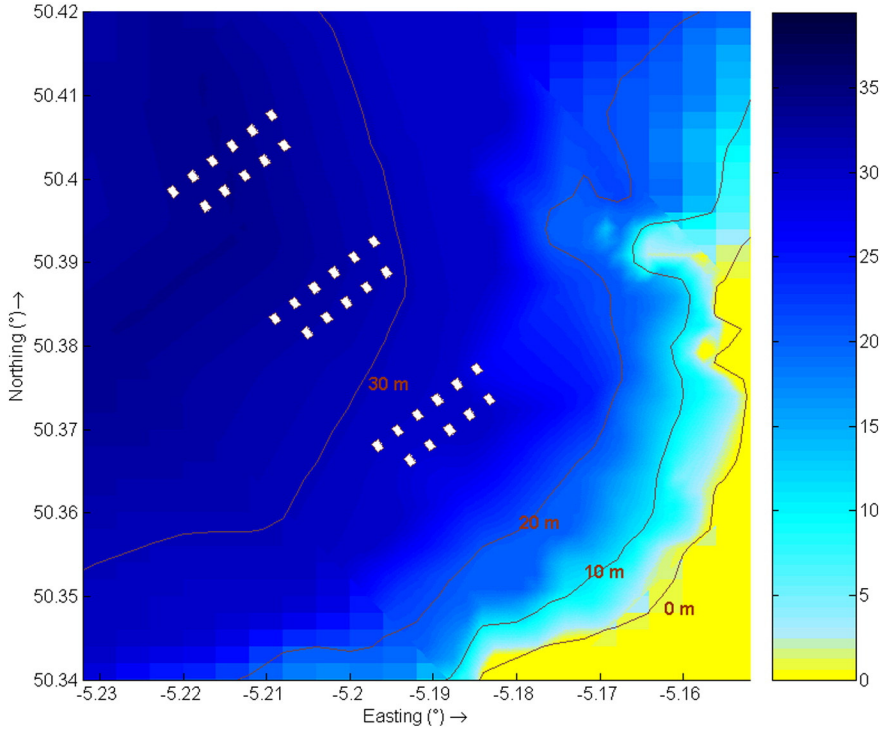

Fig. 5. Wave farm located at different distances: 2 km, 4 km and 6 km to the 10 m water depth contour at Perranporth Beach [water depth in m].

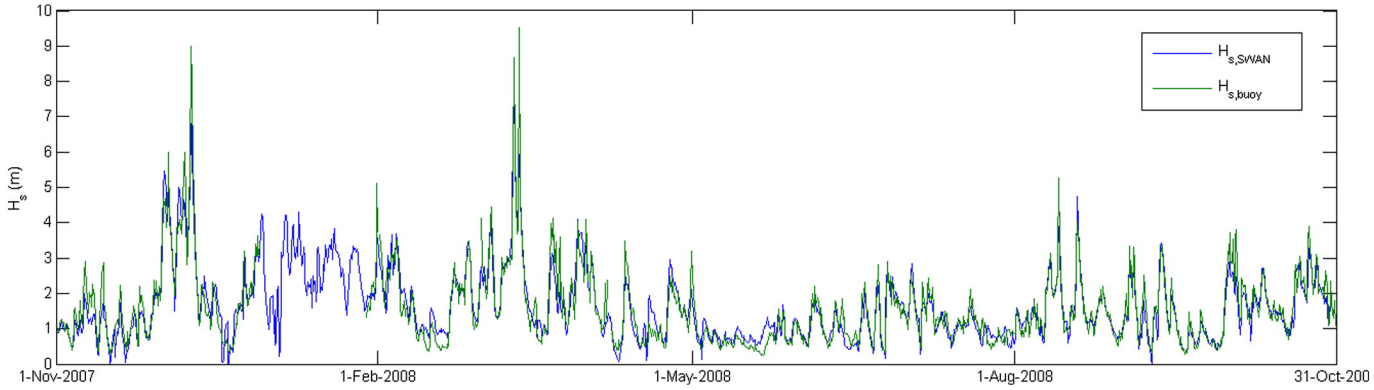

Fig. 6. Time series of simulated ($H_{s,\,SWAN}$) and measured ($H_{s,\,buoy}$) significant wave height.

3. Results and discussion

First, the model is validated using the wave buoy data at Perranporth Beach from November 2007 to October 2008, missing out January 2008 owing to the lack of data. Fig. 6 and Fig. 7 shows the good fit achieved between the significant wave height computed by SWAN and the values from the wave buoy. The coefficient of determination, R^2, and the root mean square error, *RMSE*, confirm the goodness of the fit: $R^2 = 0.94$ and $RMSE = 0.38$ m.

Second, the effects on the wave conditions of the wave farm scenarios are analysed and compared to the baseline scenario. Fig. 8 shows the reduction of the significant wave height in the lee of the farm at a point in time. The greatest values of the reduction are found behind the second row of devices with values of approx. 40%, although these decrease towards the coast due to the wave energy diffracted from the sides into the wake of the farm. In the case of the wave farm at a distance of 2 km from the shoreline the reduction of the significant wave height at a water depth of 10 m at this point in time is 25%, whilst for the farm at 4 and 6 km the values are 12% and 5%, respectively. (See Fig. 7.)

As regards the shadow caused by the wave farm, the area affected varies according to the wave direction, especially in the cases with a farm-to-coast distance of 4 and 6 km. The impact with waves coming from the east (Fig. 8) is mainly focussed on the north area of the beach, whilst with waves from the NW the impact covers practically all the beach. In contrast, the impact of the wave farm closest to the beach does not vary with the wave conditions due to its proximity to the coast. Fig. 9 illustrates the modification of the significant wave height in the different scenarios along the 20 m contour. It is observed that the greater the farm-to-coast distance, the larger the extension of the shadow; in the cases of the furthest and closest farm the shadow covers over 8 km and 3 km, respectively. However, the greatest impact of the furthest farm is outside of the beach limits for these offshore wave conditions.

In terms of wave power reduction, the relative nearshore impact indicator, $\overline{RNI}_i$, was defined to assess the average impact at a water depth contour of 20 m. The values for the different farm-to-coast distances are: $\overline{RNI}_{2\text{ km}} = 25.59\%$, $\overline{RNI}_{4\text{ km}} = 7.34\%$ and $\overline{RNI}_{6\text{ km}} = 2.66\%$. The reduction in wave energy is much more significant for the wave farm at 2 km, however, the overall resource for the wave farm at 2 km is 15% lower than that for the farm at 6 km (Table 1). The difference in terms of the available resource is less between the farm at 4 km and 6 km (5%). The results are also divided into "winter" (1st November–31st April) and "summer" (1st May–31st October) to assess the seasonal variability of wave power (approx. 70%), which, will be shown to affect the modal state of the beach.

Based on the results of the wave propagation model the modal state of the beach is determined. In order to investigate the spatial variability of the impact along with its seasonal variability, three profiles (Fig. 3) are selected: profiles P1, P2 and P3 corresponded with the south, middle and north section of the beach.

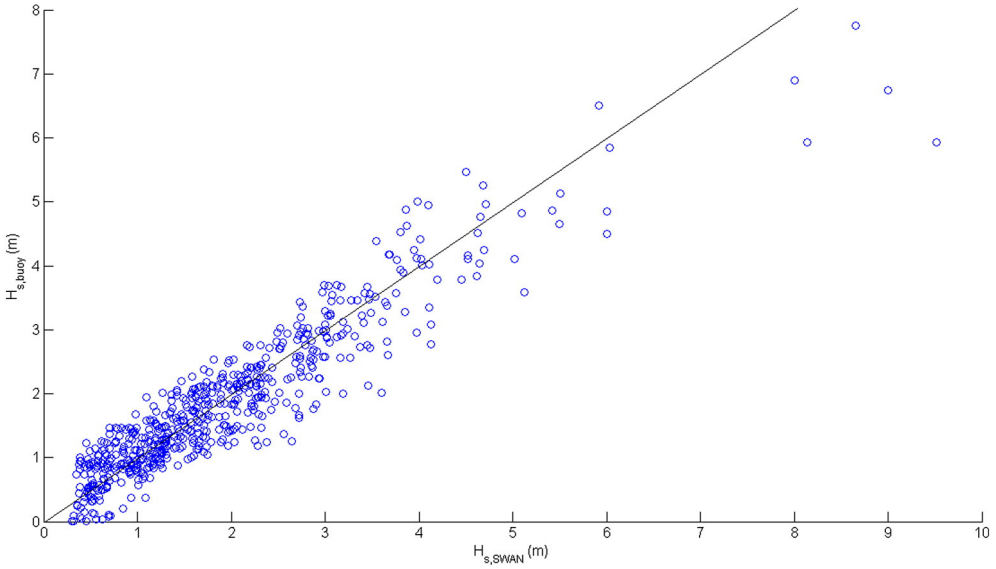

Fig. 7. Scatter diagram: simulated ($H_{s,\,SWAN}$) vs. measured ($H_{s,\,buoy}$) significant wave height.

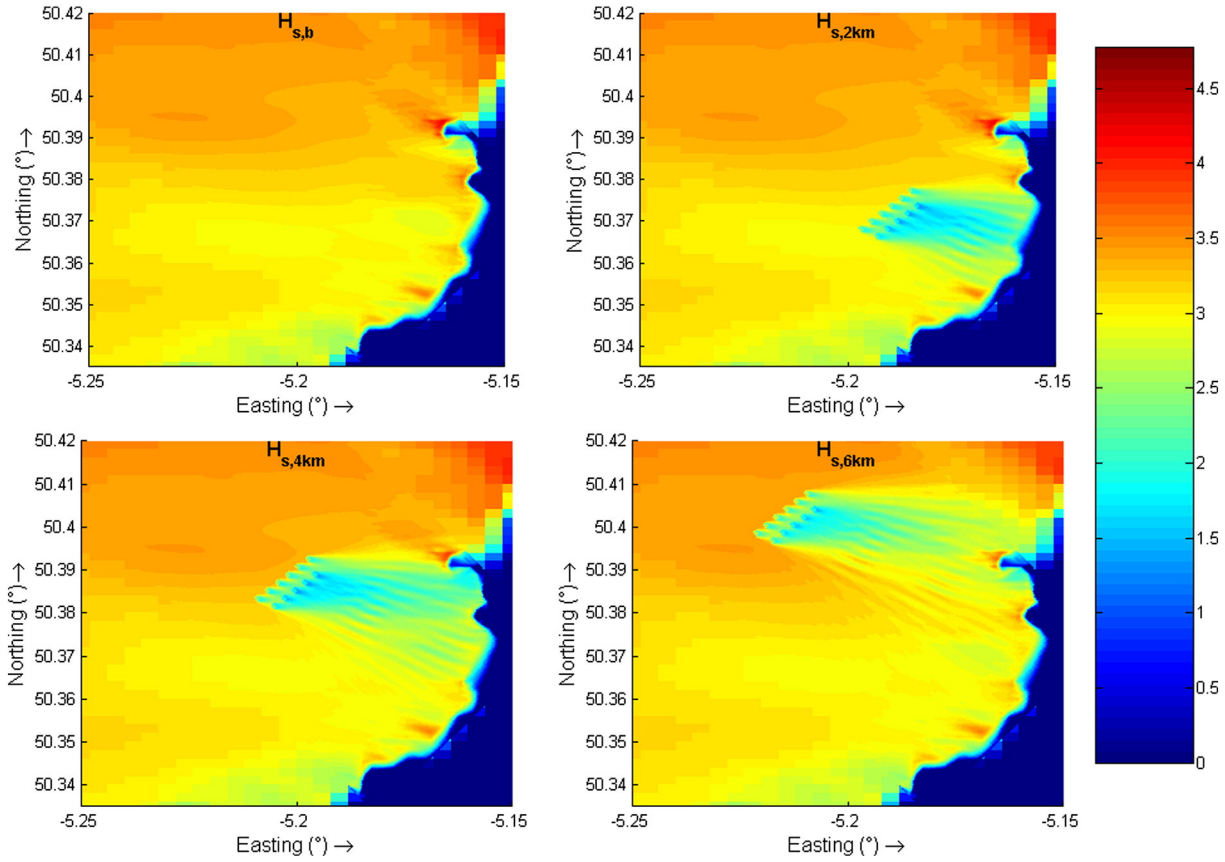

Fig. 8. Significant wave height [m] in the baseline scenario ($H_{s,\,b}$) and in the presence of the farm at distances of 2 km ($H_{s,\,2\,km}$), 4 km ($H_{s,\,4\,km}$) and 6 km ($H_{s,\,6\,km}$) from the reference (10 m water depth) contour at 19th January 2014, 18:00 UTC [deep water wave conditions: $H_s = 4.69$ m, $T_p = 11.86$ s and $\theta = 252.41°$].

First, the results for the south section of the beach are shown in Table 2. This section of the beach is predominantly dissipative (third column in the table), although the percentage that the beach is found to be intermediate (second column) is far from negligible. Indeed, in the case with the farm at a distance of 2 km, the low tide bar/rip becomes the most frequent state. The comparison between the baseline and farm scenarios reflects a slight modification of the modal state of the beach owing to the low impact of the wave farm on the wave conditions in this area. The maximum difference between the baseline and the farm scenarios is the case of the non-barred dissipative state, in which the reduction does not exceed 1%. In any case, the trends due to the reduction of the significant wave height are shown in the results; for instance, the percentage of low tide bar/rip state increases as the wave farm become closer, because the relative range tidal parameter

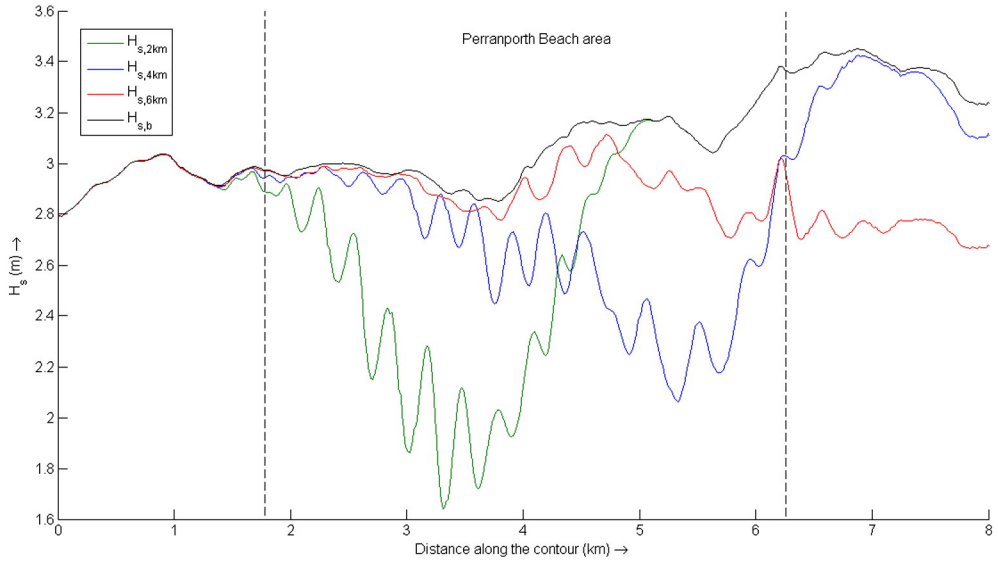

Fig. 9. Significant wave height [m] in the baseline scenario ($H_{s,\,b}$) and in the presence of the farm at distances of 2 km ($H_{s,\,2\,km}$), 4 km ($H_{s,\,4\,km}$) and 6 km ($H_{s,\,6\,km}$) along the 20 m water depth contour at 19th January 2014, 18:00 UTC [deep water wave conditions: $H_s = 4.69$ m, $T_p = 11.86$ s and $\theta = 252.41°$].

Table 1
Average resource available in the wave farm for the different scenarios divided into "summer" (1st May–31st October) and "winter" (1st November–31st April).

Scenario	$\bar{J}$ (kW/m)		
	"Winter"	"Summer"	Average
2 km	239.98	78.15	159.01
4 km	275.72	86.07	180.83
6 km	288.28	91.49	189.82

(*RTR*) is inversely proportional to the breaking wave height. On the other hand, the dimensionless fall velocity parameter (Ω) is directly proportional to the breaking wave height, and, therefore the barred dissipative state occurred more frequently in the baseline scenario than in the cases with the farm.

Second, in the case of the middle of the beach (Table 3), the results were slightly different compared with the south section, due to the morphological differences between them (see Fig. 3). In this area, the wave farm impacts are greater compared to the south section. Whereas the wave farm at 4 km and 6 km does not present significant differences compared with the baseline scenario, the wave farm at 2 km changes the behaviour of the beach significantly, reducing the barred dissipative state by more than 5% or 20 days per year, and increasing the ultradissipative state by more than 15 days. Overall, with the wave farm at 2 km the most frequent state shifted from non-barred dissipative (baseline) to ultra-dissipative due to the reduction of breaking wave height.

Third, the north section of the beach is the area that presented the greatest differences between the baseline and the farm scenarios (Table 4). The trends mentioned in previous paragraphs are accentuated in this area, the reduction in the barred and non-barred dissipative states results in a greater occurrence of the ultra-dissipative beach, from 5 days to 36 days per year in the case of the farm at 6 and 2 km, respectively — a very substantial change in the morphological behaviour of the beach. As regards the Ω parameter, it is observed that the closest wave farm makes the low tide terrace and the low tide bar and rip states more frequent by 10 and 12 days per year, respectively, compared with the baseline scenario.

Table 3
Percentages of the beach modal state for the middle section of the beach (Profile P2) from 1st November 2007 to 31st October 2008.

Profile P2: Middle section					
Reflective		Barred		Barred dissipative	
Baseline	0.00%	Baseline	0.07%	Baseline	21.73%
6 km	0.00%	6 km	0.07%	6 km	20.90%
4 km	0.00%	4 km	0.07%	4 km	20.29%
2 km	0.00%	2 km	0.00%	2 km	16.04%
Low tide Terrace + rip		Low tide bar/rip		Non-barred dissipative	
Baseline	0.00%	Baseline	22.76%	Baseline	26.11%
6 km	0.00%	6 km	22.69%	6 km	25.63%
4 km	0.00%	4 km	22.62%	4 km	25.29%
2 km	0.07%	2 km	23.85%	2 km	25.29%
Low tide terrace		Ultra-dissipative			
Baseline	2.06%	Baseline	22.69%		
6 km	2.19%	6 km	23.85%		
4 km	2.19%	4 km	24.81%		
2 km	3.29%	2 km	26.32%		
Transition to tide-dominated tidal flat					
Baseline			4.59%		
6 km			4.66%		
4 km			4.73%		
2 km			5.14%		

Finally, regarding the seasonal variability, significant differences between "summer" and "winter" are found. These differences are analysed with reference to the north section (Table 5) for the sake of space — similar trends were found in the other sections. The main feature that distinguishes the winter from the summer is the presence of the bar in the baseline scenario. In winter, the beach is predominantly barred dissipative, what is usually called a "winter" or "storm" profile. The more energetic conditions increase the erosion, and lower the beach face as sand is moved offshore and deposited on submarine bars, which help protect the beach by causing the waves to break further offshore. In summer,

Table 2
Percentages of the beach modal state for the south section of the beach (Profile P1) from 1st November 2007 to 31st October 2008.

Profile P1: South section					
Reflective		Barred		Barred dissipative	
Baseline	0.00%	Baseline	0.07%	Baseline	16.04%
6 km	0.00%	6 km	0.07%	6 km	15.96%
4 km	0.00%	4 km	0.07%	4 km	15.90%
2 km	0.00%	2 km	0.07%	2 km	15.70%
Low tide Terrace + rip		Low tide bar/rip		Non-barred dissipative	
Baseline	0.00%	Baseline	25.50%	Baseline	26.59%
6 km	0.00%	6 km	25.70%	6 km	26.39%
4 km	0.00%	4 km	25.98%	4 km	26.18%
2 km	0.00%	2 km	26.18%	2 km	25.77%
Low tide terrace		Ultra-dissipative			
Baseline	3.36%	Baseline	22.89%		
6 km	3.36%	6 km	22.89%		
4 km	3.43%	4 km	22.82%		
2 km	3.36%	2 km	23.24%		
Transition to tide-dominated tidal flat					
Baseline			5.55%		
6 km			5.63%		
4 km			5.62%		
2 km			5.69%		

Table 4
Percentages of the beach modal state for the north section of the beach (Profile P3) from 1st November 2007 to 31st October 2008.

Profile P3: North section					
Reflective		Barred		Barred dissipative	
Baseline	0.00%	Baseline	0.14%	Baseline	16.59%
6 km	0.00%	6 km	0.07%	6 km	15.49%
4 km	0.00%	4 km	0.07%	4 km	14.39%
2 km	0.00%	2 km	0.07%	2 km	6.18%
Low tide Terrace + rip		Low tide bar/rip		Non-barred dissipative	
Baseline	0.00%	Baseline	28.10%	Baseline	28.71%
6 km	0.00%	6 km	27.55%	6 km	28.92%
4 km	0.00%	4 km	28.24%	4 km	28.71%
2 km	0.00%	2 km	31.11%	2 km	22.62%
Low tide terrace		Ultra-dissipative			
Baseline	0.89%	Baseline	22.68%		
6 km	0.96%	6 km	23.99%		
4 km	1.03%	4 km	24.40%		
2 km	3.49%	2 km	32.28%		
Transition to tide-dominated tidal flat					
Baseline			2.89%		
6 km			3.02%		
4 km			3.16%		
2 km			4.25%		

Table 5
Percentages of the beach modal state for the north section of the beach (Profile P3) in "summer" (1st November 2007 - 31st April 2008) and "winter" (1st May 2008 - 31st October 2008).

Profile P3: North section								
Reflective			Barred			Barred dissipative		
Scenario	Summer	Winter	Scenario	Summer	Winter	Scenario	Summer	Winter
Baseline	0.00%	0.00%	Baseline	0.00%	0.27%	Baseline	4.66%	28.53%
6 km	0.00%	0.00%	6 km	0.00%	0.14%	6 km	4.11%	26.89%
4 km	0.00%	0.00%	4 km	0.00%	0.14%	4 km	3.42%	25.38%
2 km	0.00%	0.00%	2 km	0.00%	0.14%	2 km	0.68%	11.66%
Low tide Terrace + rip			Low tide bar/rip			Non-barred dissipative		
Scenario	Summer	Winter	Scenario	Summer	Winter	Scenario	Summer	Winter
Baseline	0.00%	0.00%	Baseline	29.86%	26.34%	Baseline	29.59%	27.85%
6 km	0.00%	0.00%	6 km	29.59%	25.51%	6 km	29.18%	28.67%
4 km	0.00%	0.00%	4 km	30.00%	26.48%	4 km	28.63%	28.81%
2 km	0.00%	0.00%	2 km	27.67%	34.57%	2 km	18.77%	26.47%
Low tide terrace			Ultra-dissipative					
Scenario	Summer	Winter	Scenario	Summer		Winter		
Baseline	0.27%	1.51%	Baseline	33.15%		12.21%		
6 km	0.27%	1.65%	6 km	34.25%		13.72%		
4 km	0.41%	1.65%	4 km	34.79%		13.99%		
2 km	4.66%	2.33%	2 km	44.66%		19.89%		
Transition to tide-dominated tidal flat								
Scenario			Summer			Winter		
Baseline			3.29%			2.47%		
6 km			3.43%			2.60%		
4 km			3.57%			2.74%		
2 km			4.94%			3.56%		

the state of the beach shifts from barred to non-barred – non-barred dissipative or ultra-dissipative – due to the milder wave conditions, and, therefore, the reduction of offshore sediment transport.

In the scenarios with the farm this seasonal behaviour changes specially with the farm at 2 km. In winter, the barred dissipative state becomes less frequent in favour of ultra-dissipative and low tide bar/rip states. In the latter, the beach keeps the bar system but enlarges the intertidal flat, with the result that the system behaves as an intermediate beach at mid tide, reflective at high tide and dissipative at low tide. By contrast, in summer, the increase of the occurrence of ultra-dissipative state is very significant given that the beach behaves according this state during almost half of the summer.

In summary, Perranporth beach is found to be at the transition between the low tide bar/rip and dissipative beach states in the scenario without the farm. Despite the spatial variations between the different profiles, the greatest differences are observed in the seasonal study. The absence of the bar distinguished the behaviour of the beach during summer from winter. However, the presence of the wave farm affects the modal state of the beach drastically, decreasing the occurrence of wave-dominated states (barred and non-barred dissipative states) in the favour of tide-dominated (low tide bar and rip in winter and ultra-dissipative in summer). The reduction of the breaking wave height brought about by the wave farm (~18%, comparing the baseline scenario with the nearest farm) results in a significant modification of the morphological response of the beach. The reduction of the wave-dominated states would seem to lead to an increase in the onshore sediment transport and the removal of the offshore bar, the materials of which would cause accretion on the beach — in line with the findings by Abanades et al. (2014a,b).

4. Conclusions

In view of the accelerated pace of development of wave energy, a thorough understanding of the effects of nearshore wave farms on beach morphodynamics will soon be fundamental to coastal management. This paper examines these effects with reference to the modal state of the beach using an empirical classification based on wave conditions, sediment size and tidal regime. The spatial and temporal changes to the modal state of the beach induced by the wave farm are investigated. To resolve accurately the wake of the individual WECs in the farm, a state-of-the-art wave propagation model is implemented on a high-resolution grid. To assess the influence of the farm-to-coast distance, a sensitivity analysis is carried out with a wave farm located at different distances from the coast.

We find that the farm-to-coast distance plays a major role, and that the wave farm closest to the shoreline (2 km) substantially alters the nearshore wave conditions. For instance, the reduction of wave power along the 20 m contour exceeds 25% over a 3 km stretch of coastline. In contrast, the reduction in the case of the furthest wave farm is under 10%, extending over 8 km of coastline. This milder nearshore wave climate, brought about by the wave farm, is shown to modify the morphological behaviour of the beach. In the baseline scenario, Perranporth Beach is at the transition between the low tide bar/rip and dissipative states. The modal state varies along the beach, although large spatial differences are not observed concurrently. However, the seasonal variability is far more pronounced. In winter the beach is wave-dominated, the energetic wave conditions increasing offshore sediment transport and forming a submarine bar. In summer, under milder wave conditions, the beach is tide-dominated.

We also find that the wave farm modify the morphological behaviour of the beach significantly, especially in its north and middle section, where the wave height reduction is more apparent. The predominant character of the beach is transformed from wave- to tide-dominated. For instance, in the north section the predominant state is a low tide bar/rip in the baseline scenario, which turns into an ultra-dissipative system in the case of the nearest (2 km) wave farm. In this case the wave-dominated states are reduced by over 10%, or over 36 days per

year. This modification also occurs in the cases with farm-to-coast distances of 4 km and 6 km, albeit to a lesser extent: the barred dissipative states become less frequent (by up to 10 days per year) and accordingly, the tide-dominated states, e.g., ultra-dissipative or transition to tide-dominated tidal flat, occur more often. The reduction in the occurrence of the barred states corresponds to an increase of the onshore sediment transport and the removal of the offshore bar, which would in turn lead to accretion of the beach.

In sum, this work showed that a wave farm can alter the behaviour of a beach in its lee considerably. This in itself need not be regarded as a negative impact; on the contrary, the wave farm can lead to beach accretion and thus serve to counter erosional trends. Moreover, the effects of the wave farm on the beach can be controlled by locating the farm closer to, or further from, the shoreline.

Acknowledgements

This research was carried out in the framework of the Atlantic Power Cluster Project, funded by the Atlantic Arc Programme of the European Commission (2011-1/151) and the School of Marine Sciences and Engineering of Plymouth University. The authors are grateful to the Coastal Channel Observatory and DIGIMAP for providing the data.

References

Abanades, J., Greaves, D., Iglesias, G., 2014a. Coastal defence through wave farms. Coast. Eng. 91, 299–307.
Abanades, J., Greaves, D., Iglesias, G., 2014b. Wave farm impact on the beach profile: a case study. Coast. Eng. 86, 36–44.
Abanades, J., Greaves, D., Iglesias, G., 2015. Coastal defence using wave farms: the role of farm-to-coast distance. Renew. Energy 75, 572–582.
Austin, M., et al., 2010. Temporal observations of rip current circulation on a macro-tidal beach. Cont. Shelf Res. 30 (9), 1149–1165.
Bernhoff, H., Sjöstedt, E., Leijon, M., 2006. Wave energy resources in sheltered sea areas: a case study of the Baltic Sea. Renew. Energy 31 (13), 2164–2170.
Booij, N., Holthuijsen, L., Ris, R., 1996. The "swan" wave model for shallow water. Coastal Engineering Conference, pp. 668–676.
Budillon, F., Vicinanza, D., Ferrante, V., Iorio, M., 2006. Sediment transport and deposition during extreme sea storm events at the Salerno Bay (Tyrrhenian Sea): comparison of field data with numerical model results. Nat. Hazards Earth Syst. Sci. 6 (5), 839–852.
Butt, T., Russell, P., Turner, I., 2001. The influence of swash infiltration–exfiltration on beach face sediment transport: onshore or offshore? Coast. Eng. 42 (1), 35–52.
Carballo, R., Iglesias, G., 2013. Wave farm impact based on realistic wave–WEC interaction. Energy 51, 216–229.
Carballo, R., Sánchez, M., Ramos, V., Taveira-Pinto, F., Iglesias, G., 2014. A high resolution geospatial database for wave energy exploitation. Energy 68, 572–583.
Cornett, A.M., 2008. A Global Wave Energy Resource, Assessment (ISOPE-579).
Cowell, P., Roy, P., Jones, R., 1995. Simulation of large-scale coastal change using a morphological behaviour model. Mar. Geol. 126 (1), 45–61.
Davis, R.A., Hayes, M.O., 1984. What is a wave-dominated coast? Mar. Geol. 60 (1), 313–329.
De Vriend, H., et al., 1993. Approaches to long-term modelling of coastal morphology: a review. Coast. Eng. 21 (1), 225–269.
Dean, R.G., 1973. Heuristic models of sand transport in the surf zone. First Australian Conference on Coastal Engineering, 1973: Engineering Dynamics of the Coastal Zonep. 215.
Defne, Z., Haas, K.A., Fritz, H.M., 2009. Wave power potential along the Atlantic coast of the southeastern USA. Renew. Energy 34 (10), 2197–2205.
Fernandez, H., et al., 2012. The new wave energy converter WaveCat: concept and laboratory tests. Mar. Struct. 29 (1), 58–70.
Gonçalves, M., Martinho, P., Guedes Soares, C., 2014. Assessment of wave energy in the canary islands. Renew. Energy 68, 774–784.
Gonzalez-Santamaria, R., Zou, Q.-P., Pan, S., 2013. Impacts of a wave farm on waves, currents and coastal morphology in south west England. Estuar. Coasts 1–14.
Guedes Soares, C., Bento, A.R., Gonçalves, M., Silva, D., Martinho, P., 2014. Numerical evaluation of the wave energy resource along the Atlantic European coast. Comput. Geosci. 71, 37–49.
Hughes, M.G., Aagaard, T., Baldock, T.E., Power, H.E., 2014. Spectral signatures for swash on reflective, intermediate and dissipative beaches. Mar. Geol. 355, 88–97.
Iglesias, G., Carballo, R., 2009. Wave energy potential along the death coast (Spain). Energy 34 (11), 1963–1975.
Iglesias, G., Carballo, R., 2010a. Offshore and inshore wave energy assessment: Asturias (N Spain). Energy 35 (5), 1964–1972.
Iglesias, G., Carballo, R., 2010b. Wave energy and nearshore hot spots: the case of the SE Bay of Biscay. Renew. Energy 35 (11), 2490–2500.
Iglesias, G., Carballo, R., 2011. Choosing the site for the first wave farm in a region: a case study in the Galician Southwest (Spain). Energy 36 (9), 5525–5531.
Iglesias, G., Carballo, R., 2014. Wave farm impact: the role of farm-to-coast distance. Renew. Energy 69, 375–385.
Iglesias, G., López, I., Carballo, R., Castro, A., 2009a. Headland-bay beach planform and tidal range: a neural network model. Geomorphology 112 (1–2), 135–143.
Iglesias, G., López, I., Castro, A., Carballo, R., 2009b. Neural network modelling of planform geometry of headland-bay beaches. Geomorphology 103 (4), 577–587.
Iglesias, G., et al., 2009c. Wave energy potential in Galicia (NW Spain). Renew. Energy 34 (11), 2323–2333.
Kamphuis, J., 1991. Wave transformation. Coast. Eng. 15 (3), 173–184.
Lenee-Bluhm, P., Paasch, R., Özkan-Haller, H.T., 2011. Characterizing the wave energy resource of the US Pacific Northwest. Renew. Energy 36 (8), 2106–2119.
Liberti, L., Carillo, A., Sannino, G., 2013. Wave energy resource assessment in the Mediterranean, the Italian perspective. Renew. Energy 50, 938–949.
Masselink, G., Short, A.D., 1993. The effect of tide range on beach morphodynamics and morphology: a conceptual beach model. J. Coast. Res. 785–800.
Masselink, G., Evans, D., Hughes, M.G., Russell, P., 2005. Suspended sediment transport in the swash zone of a dissipative beach. Mar. Geol. 216 (3), 169–189.
Mendoza, E., et al., 2014. Beach response to wave energy converter farms acting as coastal defence. Coast. Eng. 87 (0), 97–111.
Millar, D.L., Smith, H.C.M., Reeve, D.E., 2007. Modelling analysis of the sensitivity of shoreline change to a wave farm. Ocean Eng. 34 (5–6), 884–901.
Ortega Sanchez, M., Losada, M., Baquerizo, A., 2003. On the development of large-scale cuspate features on a semi-reflective beach: Carchuna beach, Southern Spain. Mar. Geol. 198 (3), 209–223.
Ortega-Sánchez, M., Lobo, F.J., López-Ruiz, A., Losada, M.A., Fernández-Salas, L.M., 2014. The influence of shelf-indenting canyons and infralittoral prograding wedges on coastal morphology: the Carchuna system in Southern Spain. Mar. Geol. 347, 107–122.
Palha, A., Mendes, L., Fortes, C.J., Brito-Melo, A., Sarmento, A., 2010. The impact of wave energy farms in the shoreline wave climate: Portuguese pilot zone case study using Pelamis energy wave devices. Renew. Energy 35 (1), 62–77.
Poate, T., Masselink, G., Russell, P., Austin, M., 2014. Morphodynamic variability of high-energy macrotidal beaches, Cornwall, UK. Mar. Geol. 350, 97–111.
Pontes, M., et al., 1996. Weratlas—atlas of wave energy resource in Europe. Report to the European Commission, JOULE II Programme (96 pp.).
Reeve, D.E., et al., 2011. An investigation of the impacts of climate change on wave energy generation: the Wave Hub, Cornwall, UK. Renew. Energy 36 (9), 2404–2413.
Ruol, P., Zanuttigh, B., Martinelli, L., Kofoed, P., Frigaard, P., 2011. Near-shore floating wave energy converters: applications for coastal protection. Proceedings of the International Conference of Coastal Engineering 2010, Shanghai.
Scott, T., Russell, P., Masselink, G., Wooler, A., Short, A., 2007. Beach rescue statistics and their relation to nearshore morphology and hazards: a case study for southwest England. J. Coast. Res. 50, 1–6.
Scott, T., Masselink, G., Russell, P., 2011. Morphodynamic characteristics and classification of beaches in England and Wales. Mar. Geol. 286 (1–4), 1–20.
Smith, H.C.M., Pearce, C., Millar, D.L., 2012. Further analysis of change in nearshore wave climate due to an offshore wave farm: an enhanced case study for the wave hub site. Renew. Energy 40 (1), 51–64.
Stopa, J.E., Cheung, K.F., Chen, Y.-L., 2011. Assessment of wave energy resources in Hawaii. Renew. Energy 36 (2), 554–567.
Tolman, H., 2002. Validation of WaveWatch III version 1.15 for a global domain. Tech. Note (213), 33.
US Army Corps Of Engineers, 1984. Shore Protection Manual 2v. Army Engineer Waterways Experiment Station, Vicksburg, MS, pp. 37–53.
Veigas, M., Iglesias, G., 2013. Wave and offshore wind potential for the island of Tenerife. Energy Convers. Manag. 76, 738–745.
Veigas, M., Iglesias, G., 2014. Potentials of a hybrid offshore farm for the island of Fuerteventura. Energy Convers. Manag. 86, 300–308.
Veigas, M., Carballo, R., Iglesias, G., 2014a. Wave and offshore wind energy on an island. Energy Sustain. Dev. 22, 57–65.
Veigas, M., López, M., Iglesias, G., 2014b. Assessing the optimal location for a shoreline wave energy converter. Appl. Energy 132, 404–411.
Veigas, M., Ramos, V., Iglesias, G., 2014c. A wave farm for an island: detailed effects on the nearshore wave climate. Energy 69, 801–812.
Vicinanza, D., Contestabile, P., Ferrante, V., 2013. Wave energy potential in the north-west of Sardinia (Italy). Renew. Energy 50, 506–521.
Vidal, C., Méndez Fernando, J., Díaz, G., Legaz, R., 2007. Impact of Santoña WEC installation on the littoral processes. Proceedings of the 7th European Wave and Tidal Energy Conference, Porto, Portugal.
Wright, L., Short, A.D., 1984. Morphodynamic variability of surf zones and beaches: a synthesis. Mar. Geol. 56 (1), 93–118.
Zanuttigh, B., Angelelli, E., 2013. Experimental investigation of floating wave energy converters for coastal protection purpose. Coast. Eng. 80, 148–159.